
UNIVERSIDAD MICHOACANA DE
SAN NICOLÁS DE HIDALGO

Facultad de Ingeniería Eléctrica
División de Estudios de Posgrado

# *"CO-OPTIMIZATION OF ELECTRICITY AND GAS NETWORKS: IMPACT OF WIND POWER PENETRATION AND UNCERTAINTY"*

by

ALBERTO MARTINEZ MARES

THESIS

REQUIREMENT FOR THE DEGREE OF
**DOCTOR OF SCIENCE**
**IN ELECTRICAL ENGINEERING**

ADVISOR:
CLAUDIO RUBÉN FUERTE ESQUIVEL, PhD.


MORELIA, MICHOACÁN FEBRUARY 2014

# CO-OPTIMIZATION OF ELECTRICITY AND GAS NETWORKS: IMPACT OF WIND POWER PENETRATION AND UNCERTAINTY

Los Miembros del Jurado de Examen de Grado aprueban
la **Tesis de Doctorado en Ciencias en Ingeniería Eléctrica Opción en Sistemas Eléctricos**
de ***Alberto Martínez Mares***

Dr. Juan José Flores Romero
*Presidente del Jurado*

Dr. Claudio Rubén Fuerte Esquivel
*Director de Tesis*

Dr. J. Jesús Rico Melgoza
*Vocal*

J. Jesús Rico Melgoza

Dra. Elisa Espinosa Juárez
*Vocal*

Dr. Marcelino Madrigal Martínez
*Revisor Externo*

Dr. J. Aurelio Medina Rios
*Jefe de la División de Estudios de Posgrado*
*de la Facultad de Ingeniería Eléctrica. UMSNH*
*(Por reconocimiento de firmas)*

UNIVERSIDAD MICHOACANA DE SAN NICOLÁS DE HIDALGO
Febrero 2014

# Abstract

The current focus on the reduction of the environmental footprint from the energy sector throughout the world has motivated energy policy incentives promoting the optimal use of energy resources in the electricity production to satisfy the rising power demand requirements. Besides, the increasing participation of non-conventional renewable energies, which unlike fossil-based power plants where the rate of energy output is controllable, in the renewable power it is variable, uncertain, and therefore non-dispatchable. This creates new challenges for both system planners and operators not only in the electricity system, but also the fossil fuel industry.

These challenges in electric power systems have made evident the necessity of analysis techniques and methodologies that include the effect of the interactions between the different primary energy systems: electricity, coal, gas, etc. In this research work, the modeling of these energy networks is performed under the same frame of reference, and the analysis is focused on the interdependencies between primary energy networks, departing from steady-state formulations, toward optimization models, in which the negative impacts of the non-dispatchable energies can be minimized or controlled attaining a fossil fuel-based generation management.

A multi-energy load flow formulation is proposed which permits the assessment of the interdependencies between primary energy networks based on the concept of distributed slack nodes, overcoming the drawback of only adjusting the active power of a single slack generator for any unmet system load and for system losses, representing more realistically the interdependency between networks. The effect of gas temperature has also been included as a state variable in order to assess the compressors' energy

consumption and to identify operating conditions that could lead to harmful hydrate formation in pipelines.

A single-time multi-energy optimal flow approach, focused on the wind power randomness, which has not already been tackled. In this context, the proposed approach is based on the robust optimization concept and allows us to fully understand and analyze how the variability in wind power generation affects the steady-state infrastructure interdependencies in a real-time, multi-energy operation environment.

A multi-energy day-ahead optimal flow approach is proposed in order to assess the impact of wind power variability and its prediction error on the fossil fuel generation management. In this formulation, the interdependency between electricity and primary energy infrastructures is considered more realistically because the power dispatch of generation units is adjusted according to the variability of the wind power outputs in order to achieve the total power balance in the electric power system. Lastly, the interactions between primary energy networks have been analyzed in a Unit Commitment context with the aim of assess the impact of turning on/off generators in their corresponding energy system.

Keywords: Natural Gas, Optimal Power Flow, Unit Commitment, Multi-Energy, Primary Energies.

# Resumen

El enfoque actual en la reducción del impacto ecológico del sector energético en el mundo ha motivado la creación de incentivos y políticas energéticas promoviendo el uso óptimo de los recursos energéticos utilizados en la producción de electricidad para satisfacer los crecientes requerimientos en demanda de potencia. Además, la creciente participación de energías renovables no-convencionales, las cuales a diferencia de las plantas de generación basadas en combustibles fósiles donde la cantidad de energía suministrada al sistema de potencia es controlables, en la plantas de generación basadas en energías renovables es variable, con incertidumbre y por lo tanto no despachable. Esta condición causa nuevos retos para los departamentos de planeación y operación no únicamente en los sistemas eléctricos de potencia, sino además en la industria de los combustibles fósiles.

Estos retos en los sistemas eléctricos de potencia han evidenciado la necesidad de nuevas técnicas de análisis y metodologías que incluyan el efecto de las interacciones entre los diferentes sistemas de energía primarias: electricidad, carbón, gas natural, etc. En este proyecto de investigación, el modelado de estas redes de energía se desarrolla bajo un mismo marco de referencia, y el análisis se concentra en las interdependencias existentes entre diferentes infraestructuras de energía primaria, iniciando con formulaciones en estado estable hacia modelos de optimización en los cuales los impactos negativos de las fuentes de energías no despachables pueden ser minimizados o controlados obteniendo una manejo organizado del consumo de combustibles fósiles en la generación de energía eléctrica.

El modelo multi-energético de flujos de carga propuesto permite evaluar las interde-

pendencias entre redes de energía primaria basados en el concepto de nodo compensador distribuido, superando la limitante de ajustar la potencia activa de un solo generador compensador para cualquier desbalance de carga y pérdidas en el sistema, representando más realísticamente la interdependencia entre redes. El efecto de la temperatura del gas ha sido incluido como una variable de estado con la finalidad de determinar el consumo de energía en los compresores e identificar condicione de operación que pudieran llevar a una formación de hidratos en los gasoductos.

Se propone un modelo multi-energético de flujos óptimos para un solo instante de tiempo, enfocado en la aleatoriedad de la producción de energía eólica, el cual no ha sido abordado. En este contexto, el modelo propuesto se basa en el concepto de optimización robusta y nos permite comprender completamente y analizar como la variabilidad en la generación eólica afecta las interdependencias de los sistemas en estado estable en un tiempo real y multi-energético ambiente de operación.

Una formulación multi-energética para un día en adelanto es propuesta con la finalidad de evaluar el impacto de la variabilidad de la generación eólica y el error asociado a su pronóstico, en la administración de la generación basada en combustibles fósiles. En esta formulación, la interdependencia entre la red eléctrica y los sistemas de energía primaria se considera más realista debido a que el despacho de generación de potencia activa se ajusta de acuerdo con la variabilidad de la producción de energía eólica con la finalidad de obtener un balance total de potencia activa en el sistema eléctrico de potencia.

Finalmente, las interacciones entre redes de energía primaria han sido analizadas en un contexto de asignación de unidades con el objetivo de evaluar el impacto de encender/apagar unidades de generación en su correspondiente red de energía primaria.

Palabras Clave: Gas Natural, Flujos Óptimos de Potencia, Asignación de Unidades, Multi-Energía, Energías Primarias.

# Acknowledgments

The completion of this doctoral research has been possible with the direct or indirect help and support of several people. I would like to express my sincere gratitude to all of them.

First of all, I am deeply grateful to my research advisor, PhD. Claudio Rubén Fuerte Esquivel for giving me the opportunity and confidence to work with him throughout this research. It´s been four years of continuous learning and professional growth under his supervision. I thank him for encouraging me to improve every day and become a better professional with his guidance and unconditional friendship.

Also, I would like to thank the faculty and teaching staff of the UMSNH who took part in the completion of my doctoral studies. Likewise, I express my gratitude to the Electrical Department in the University of Clarkson for accepting me in my research internship which played a crucial role and guidance during this research work.

The National Council for Science and Technology (CONACYT) also deserves my recognition and acknowledgment for the financial support received, which facilitated the accomplishment of my doctoral degree.

I thank all my colleges and friends from the UMSNH, ITM, UANL, U. of Clarkson, CFE and GE for their all-important encouraging words and friendship.

I want to express my most profound gratitude to my parents, Don Beto and Doña Martha for their support, guidance and for all their love during these hard years, besides my siblings, Tita, Oly, Ame and Moy who are the example of constant effort and overcoming, also to Monse, Dessi, Pancho and Mayo for his friendship and enjoyable moments, to all of you thanks for be who you are and all the good things I have learned

from you, I can not be always present, but you are always in my mind and heart.

Lastly but not least, to my wife Suhail who has become my accomplice and partner of my dreams, thanks for your unconditional love and support during these years, also a special mention for Betin, the person who made the most important contribution during my doctoral studies, thanks a lot for all your love and patience, finally We will share more time together with the cherry of the cake in our family, Leo, both of you represent the highest inspiration required during my doctoral research. To all of you, I would like to live enough time to compensate you.

"... touch my world with your fingertips and we can have forever, and we can love forever ....", F. Mercury.

# Contents

# List of Figures

# List of Tables

# Nomenclature

## Constants

| | |
|---|---|
| $C$ | 77.54, for natural gas flow units conversion. |
| $c_k$ | 0.24, Specific heat ration for natural gas, (dimensionless). |
| $g$ | 9.81, gravity constant acceleration, ($m/s^2$). |
| $MW_{air}$ | 28.96, air molecular weight, kg/kmol. |
| $R_G$ | 10.7316, gas constant, (PSI $ft^3$/lbmol $^oR$). |
| $\gamma_G$ | Gas specific gravity, (dimensionless). |
| $\eta_{JT}$ | Joule-Thompson coefficient, ($^oR$/PSI). |

## Parameters

| | |
|---|---|
| $A_{km}$ | Cross section area of pipeline from node $k$ to node $m$, ($m^2$). |
| $B_{ij}$ | Susceptance of the nodal admittance matrix, (pu). |
| $c_p$ | Gas heat capacity at constant pressure, (dimensionless). |
| $D_{km}$ | Inner diameter of pipeline from node $k$ to node $m$, (inches). |
| $E_c$ | Compressors parasitic efficiency, (dimensionless). |

| | |
|---|---|
| $E_p^{km}$ | Efficiency of pipeline from node $k$ to node $m$, (dimensionless). |
| $G_{ij}$ | Conductance of the nodal admittance matrix, (pu). |
| $G_{lk}$ | Gas load extracted to the node $k$, (MMSCF). |
| $G_{sk}$ | Gas source injected to the node $k$, (MMSCF). |
| $GHV_{co}$ | Gross heating value for the coal, 27.5 (MBTU/Ton). |
| $GHV_d$ | Gross heating value for the diesel, 33.4 (MJ/liter). |
| $GHV_{ng}$ | Gross heating value for the natural gas, 1015 (BTU/SCF). |
| $H_k$, $H_m$ | Elevation over the sea level of nodes $k$ and $m$, (ft). |
| $L^{km}$ | Length of pipeline from node $k$ to node $m$, (Mi). |
| $N_c^k$ | Number of compressors conected to the $k^{th}$ node. |
| $N_{co}$ | Number of nodes in the coal supply network. |
| $N_e$ | Number of nodes in the electrical network. |
| $N_{ng}$ | Number of nodes in the natural gas network. |
| $N_p^k$ | Number of pipelines conected to the $k^{th}$ node. |
| $N_{PV}$ | Number of controlled voltage nodes in the electrical network. |
| $p_s$ | Probability of ocurrence for the scenario s, (%). |
| $R^{km}$ | Compression ratio between nodes $k$ and $m$, (dimensionless). |
| $T_b$ | Temperature base for the natural gas network, ($^o$R). |
| $V_r^{km}$ | Average speed of train in the railroad from the node $k$ to node $m$, (Mi/hr). |
| $w_s$ | Wind speed, (m/s). |
| $z_0$ | Compressibility factor of gas at base conditions, (dimensionless). |

$Z_a$ Compressibility factor of the gas, (dimensionless).

$\rho_0$ Gas density at base conditions, (dimensionless).

$\rho_k$ Gas specific heat ratio, (dimensionless).

$\rho_{air}$ Air density, (kg/m$^3$).

$\lambda_{fr}^{km}$ Friction coefficient for pipeline from node $k$ to node $m$, (dimensionless).

$\Pi_b$ Pressure base for the natural gas network, (PSI).

$\eta_c$ Compression process efficiency, (dimensionless).

$\eta_r^{km}$ Efficiency of train in railroad from node $k$ to node $m$, (dimensionless).

# Variables

$BHP^{km}$ Energy consumption in compressor from node $k$ to node $m$, (HP).

$G_c^{km}$ Natural gas flow in the compressor from the node $k$ to $m$, (MMSCF).

$G_p^{km}$ Natural gas flow in the pipeline from the node $k$ to $m$, (MMSCF).

$G_p^{km,in}$ Natural gas flow at the inlet node of pipeline from the node $k$ to $m$, (MMSCF).

$G_p^{km,out}$ Natural gas flow at the outlet node of pipeline from the node $k$ to $m$, (MMSCF).

$H_p^{km}$ Slope pipeline correction from node $k$ to node $m$, (PSI$^2$)

$L_c^{km,i}$ Active power extracted from $i^{th}$ electrical node by the compressor from node $k$ to node $m$, (pu).

$P_{load}^i$ Active power load extracted at the $i^{th}$ node, (pu).

$P_{gen}^i$ Generated active power injected at the $i^{th}$ node, (pu).

| | |
|---|---|
| $Q^i_{load}$ | Reactive power load extracted at the $i^{th}$ node, (pu). |
| $Q^i_{gen}$ | Generated reactive power injected at the $i^{th}$ node, (pu). |
| $T^{km}_a$ | Average temperature of gas flowing in pipeline from node $k$ to node $m$, ($^{o}$R). |
| $T_k$, $T_m$ | Gas temperature at nodes $k$ and $m$, ($^{o}$R). |
| $T^{km}_s$ | Temperature of soil surrounding pipelines from node $k$ to node $m$, ($^{o}$R). |
| $V^t_i$ | Magnitude voltage in the $i^{th}$ node of the electrical network at the subperiod $t$, (pu). |
| $Z_a$ | Compressibility factor, (dimensionless). |
| $\triangle f$ | Frequency deviation, (hz). |
| $\theta_i$, $\theta_j$ | Nodal voltage angle for nodes $i$ and $j$, (radians). |
| $\Pi^t_k$, $\Pi^t_m$ | Nodal pressure at the $k^{th}$ and $m^{th}$ nodes of the natural gas network at the subperiod $t$, (PSI). |
| $\Pi^{km}_a$ | Average pressure of gas flowing in pipeline from node $k$ to node $m$, (PSI). |
| $\tau^{km}_c$ | Natural gas extracted by the compressor from node $k$ to node $m$, (MMSCF). |
| $\xi_s$ | Objective function corresponding to the scenario $s$. |

# Chapter 1

# Introduction

## 1.1 Introduction

The secure and reliable operation of an electric power system depends not only on the availability and performance of the electric generation and transmission facilities but also on its interdependency with those networks used to produce, transport and store the various forms of primary energy that is transformed into electricity. Traditionally, all these networks have been designed and operated separately from each other. The restructuring of energy systems in several parts of the world, however, has increased the interest in evaluating in a coordinated manner the interdependency existing between the individual primary energy and electricity sectors in order to determine how the state of each network affects the economic and secure operation of the overall energy grid.

The primary energy used in renewable electric sources depends entirely on natural phenomena; however, planning the procurement of fossil fuels in a safe and timely manner is possible while considering the transportation from the primary source to the power plants.

From the fossil fuels used for electric power generation, natural gas has the major projection in the plans for generation expansions in the next 30 years; in the Mexican case, an increment of 50% with respect to 2010 is expected. One of the main reasons for

the development of technologies based on natural gas for electric generation is its use through combined cycle power plants, which have benefits with respect to other fossil fuels' technologies: higher efficiencies, lower levels of pollutant emissions, construction time and reliability, among others.

The reliability in gas-fired power plants is based on the availability of the primary energy resource, delivered through a natural gas network (composed of pipelines, compressors, nodes, etc.) or through liquified gas containers, which are mainly transported in barges. With respect to the coal-fired generators, the expansion of this technology has been delimited recently by the increasingly environmental restrictions; however, it is important to take into account that the diversity of sourcing has a direct impact on the fuel's prices volatility.

In Mexico, the expansion in the natural gas network, which currently has an average age of 32 years, is strongly related to the requirements of natural gas for new power plants. In this context, in 2010, 52% of the electricity for public service was generated with natural gas as the primary resource, and the prediction for 2025 is that the share of natural gas technologies will be increased to 58%.

Considering that natural gas and coal are vital fossil fuels that are responsible for the 58% and 11% of the total electricity net generation in the Mexican Interconnected System, respectively for the year 2025, as well as the above-mentioned information, studies associated with the existing interdependency between the electricity, natural gas and coal supply networks must be realized under a integral frame of reference that helps build a better understanding of the complex interdependencies between those networks.

## 1.2 Background and Motivation

The restructuring of energy systems in several parts of the world has increased the interest in evaluating in a coordinated manner the interdependency existing between the individual primary energy and electricity sectors in order to determine how the

state of each network affects the economic and secure operation of the overall energy grid. Among all types of primary energy systems, electric power generation relies increasingly on the natural gas supply system as additional natural gas-fired power plants are installed in power systems because of their low cost and environmental impact [Kaplan 2010]; as a consequence, electric power and natural gas systems are becoming increasingly interdependent.

There are several proposals for modeling the combined natural gas and electricity networks with a single integrated formulation to achieve an optimal operation of the coupled energy system. In [Shahidehpour 2005], the interdependency of both structures is evaluated in terms of the impact of the gas market prices on the unit commitment and dispatch. Hence, the gas network is not modeled directly, and the interdependency is only considered through the production cost of natural gas-fired plants given by the gas market price times the plant's gas consumption. In [Quelhas 2006], both networks are represented as networks composed of nodes and arcs that possess capacity and efficiency constraints. The economic efficiencies of the energy flows in the integrated energy system are then evaluated. Appropriately chosen multipliers on the arcs represent energy losses, such that the technical operating parameters of the networks are omitted in the model. Other proposals concerned with optimal power flow studies in combined natural gas and electricity networks explicitly take into account the former network [An 2003, Munoz 2003, Geidl 2007, Chaudry 2008, Liu 2009]. These proposals consider equality constraints associated with the balance of the injected power and injected gas, which must be satisfied at each node in the electrical and natural gas systems, respectively, considering the nodal voltages and nodal pressures as state variables. The static security constraints associated with the operation of both networks are related to nodal voltage magnitudes, thermal limits in transmission lines, generation limits of active and reactive powers, nodal pressures and compression rates, as well as the injection and consumption of gas. Other constraints have also been considered: the maximum flow rate in natural gas pipes [Munoz 2003], natural gas contracts and reserves [Chaudry 2008] and the linepack of a pipeline [Liu 2009]. In [Geidl 2007], the

coupling of both networks is explicitly studied via an energy hub that represents the energy interaction through coupling matrices whose elements correspond to efficiency and conversion factors; no other quantities are used. The maximum amount of energy that can be provided from the natural gas system to each gas-fired electric generator is computed in [Munoz 2003] by modeling these generators as natural gas loads; thus the electric transmission network is not considered in the study. On the other hand, the electricity network is represented by a direct current model in [Chaudry 2008] and [Liu 2009]. Several assumptions are adopted in all above-mentioned references to simplify the gas flow calculations by using Weymouth's formula which neglects changes in the altitude over the pipeline, in the compressibility factor and the gas temperature along the pipeline among others [Abdolahi 2007], [Mokhatab 2006]. The gas temperature, however, must be determined in combination with nodal pressure profiles to define suitable operational conditions that avoid the hydrate formation in the inner wall of a pipeline, natural gas fluctuations, the excessive energy consumption in compression stations and the condensation of gas [Mokhatab 2006], [Coelho 2007], as well as assuring the quality of the natural gas supplied at each gas-fired generator in order to maximize the efficiency in the energy conversion cycle [Kehlhofer 2009]. Hence, the gas temperature must be considered a variable in the gas flow equation. In the context of electricity networks, their daily operation relies on extensive power flow studies to indicate whether or not the nodal voltage magnitudes and power flows in transmission components are within prescribed operating limits. The power flow solution is obtained, though, without considering either the availability of primary energy supply or the primary energy network operating condition, i.e. the natural gas network. Thus, apart from optimal power flow studies, a crucial study to quantify the interdependency of energy networks is related to the computation of an equilibrium point by using an energy flow algorithm, with results that will provide the initial operating condition to perform a higher hierarchy level of power system studies. Therefore, in order to address the challenge of analyzing the steady-state interdependency between natural gas and electricity networks, while considering power flow analysis to be the

cornerstone of power system studies, we propose a integrated approach for the solution of the gas and power flow problem in both networks for a time horizon corresponding to a single time period (snapshot). In the context of the secure operation of power systems, primary frequency regulation analyzes are performed to determine the spinning reserve allocation that is required to withstand a set of predefined contingencies. There are several proposals to evaluate the primary frequency regulation effect on power generation dispatch [Shahidehpour 2005, Quelhas 2006, An 2003, Munoz 2003] which also consider load models with dependence of frequency and voltage; nevertheless none of these formulations perform an integral analysis that permits the understanding of how this primary regulation control affects the mass flow in the natural gas network under contingencies in the electrical system. The proposed gas and power flow algorithm reported in this thesis considers both primary frequency regulation and the load dependency on voltage magnitude and frequency to assess their effect on the existing interdependency between both energy networks. In the formulation context, the gas and electricity networks have similar structure characteristics which are condensated in the following Table.

Table 1.1: Gas and electricity structures.

| Function | Natural Gas System | Electric Power System |
|---|---|---|
| Source | Gas injected | Active power injected |
| Load | Gas extracted | Active power extracted |
| Transmission | Pipelines | Lines |
| Transformation | Compressors | Transformer |
| Interconnection | Nodes | Nodes |

On the other hand, renewable energy resources are receiving considerable attention in the continued growth and development of electric power systems, with wind power production being the production the fastest growing type of renewable energy [Thresher 2007]. Unlike fossil- and hydro-based power plants, however, where the rate of generation is controllable, the ability to control the output of wind turbines is limited, and the capacity of a wind farm changes according to wind speeds [Sorensen 2007] such that the wind energy converted into electric power has to be consumed imme-

diately and is not dispatchable. In this context, as wind power becomes an important portion of generation portfolios, evaluating how the wind power uncertainty impacts the economic generation dispatch of conventional power plants becomes necessary [Sadanandan 1983, Wang 2008], as well as the existing interdependency between the electricity network and those networks used to transport the various forms of primary energy that are converted into electric energy [Rinaldi 2001]. Only two publications report the impact of wind generation on the existing interdependency between energy networks [Martinez-Mares 2012A], [Qadrdan 2010]. The impact of wind generation on a multi-energy system composed of electricity, coal and natural gas supply networks is reported in [Martinez-Mares 2012A] for a multi-time period of study, while a direct current model of the electrical network is assumed in [Qadrdan 2010] to assess the impact of wind generation on the British gas network for a multi-time period of analysis. Despite the contributions of all these proposals in the understanding of how the operation of each network influences or is correlated to the state of the other, their mathematical formulations are based on the assumption that all the data, which include wind power generation, are precisely known at the time when the solution must be determined: the uncertainties are ignored. The data uncertainty is invariably present in the analysis of multi-energy systems so that a small perturbation in the data values assumed for the analysis may lead to non-optimality or even infeasibility of the current solution. The latter may occur when critical constraints are violated in such a way that the current solution is completely meaningless from a practical viewpoint. Therefore, the next natural step in the study of multi-energy networks consists of developing a mathematical optimization model considering the effect of data uncertainties on the optimality and feasibility of the solution. In this context, one contribution of this thesis is a mathematical formulation to deal with the problem of wind power uncertainty in the study of interdependencies between the natural gas, coal and electricity networks, considering their corresponding network and operating parameters, which has not already been tackled. The problem of contemplating uncertainties can be addressed by sensitivity analysis or stochastic programming [Mulvey 1995, Erdogan 2006]. The objective of the

former approach consists of understanding the effect of small data perturbations on a solution obtained by an optimization approach that ignores the data uncertainty and finds the interval of data values in which the current solution remains optimal [Mulvey 1995]. When a large number of data uncertainties or large perturbations, however, are present in the model, this analysis may be rendered impractical. On the other hand, the goal of the stochastic optimization is to find the feasibility of the solution, with at least some specified probability, in terms of probabilistic constraints assuming that the distributions of uncertain data are known. A fundamental problem associated with this approach, though, is the difficulty in accurately estimating these distributions, and that can destroy the convexity properties of the model [Erdogan 2006]. In view of the difficulties of the aforementioned approaches, a new framework to explore data uncertainty in optimization, referred to as the robust optimization (RO) approach, has been proposed by several authors [Mulvey 1995, Malcom 1994, Ben-Tal 2009, Hajimiragha 2007]. In proposals [Ben-Tal 2009] and [Hajimiragha 2007], a set-based robust optimization is formulated assuming that uncertain parameters belong to a bounded uncertainty set, and a robust solution is one that is feasible for the worst-case value of the parameters within that uncertainty set. Robust optimization considering ellipsoidal uncertainty sets has been investigated in [Ben-Tal 2009], while Bertsimas and Sim have investigated the case where the uncertainty set is a polyhedron [Hajimiragha 2007]. On the other hand, the key idea of [Mulvey 1995] and [Malcom 1994] is to define the problem data by a finite set of scenarios, assuming that the values of uncertainty parameters are known for each scenario, and a RO model is then formulated in order to find an uncertainty-immunized solution that remains feasible and nearly optimal for all scenarios. A critical point of this approach is that a significant gain in the model's robustness, over the given set of possible uncertainties, is achieved at the expense of losing optimality with respect to the objective value; this shortcoming has been overcome, though, by introducing a function that embodies a trade-off between the objective function value and its variability over the given set of scenarios. In addition, a feasibility penalty function is used to relax some constraints under some of the scenarios [Mulvey 1995, Malcom 1994]. The

need for robustness in several problems associated with the planning and operation of electric power systems has been recognized. For example, the RO approach has been applied to the power capacity expansion problem [Malcom 1994], and more recently to the optimization of the penetration levels of plug-in hybrid electric vehicles into the transportation sector [Hajimiragha 2007] and to the optimal scheduling problem of an energy hub [Parisio 2012]. As a follow-up to this analysis, this research proposes a robust optimization (RO) model to assess how uncertainties associated with wind speed forecasts affect the economic and secure operation of a multi-energy system composed of natural gas, coal and electricity networks, which are coupled at multiple nodes of the electricity network through thermal power plants.

The fact that the wind power is variable, uncertain and therefore non-dispatchable has created new challenges for both system planners and operators in not only the electricity system, but also the fossil fuel industry [Wang 2008, Liu 2009, Monteiro 2009, Kaplan 2007]. Among these challenges has been the need to ensure a suitable generation dispatch strategy. Due to the intermittent nature of the wind itself, wind speed and/or wind power generation forecasts for short-, medium- and long-term models have been proposed to provide compliance with power system reliability standards. A relevant number of recent works propose the combined modeling of natural gas, coal and electricity networks for a integral analysis of energy flows and the coordinated optimization of the coupled energy systems [Giebel 2002, Brown 2004, Drud 1995, Brooke 1998, Breeze 2005, Hickman 1999, Quelhas 2006, Zammerilli 2010]. The only proposal that analyzes interdependencies between coal, natural gas and electricity subsystems, however considers the networks' modeling based on nodes and arcs where the technical operating parameters are omitted [Quelhas 2006]. To avoid this drawback, a multi-energy day-ahead nonlinear optimal power flow (OPF) approach is proposed in this thesis in order to assess how the wind energy penetration impacts on the fossil fuel-based generation management of multiple primary energy systems, while considering the network's topology and operating parameters.

Short-term operation planning for electric power systems is performed over a time

horizon ranging from 12 hours to one week ahead of time, usually divided into discrete periods of one hour, with the aim of scheduling the hourly on/off status and power contributions of generating units to satisfy the forecast demand at minimum operating cost. This scheduling process, termed short-term unit commitment (UC), considers generation and transmission limits, as well as intertemporal technical restrictions associated with the generation status of dispatchable units at different time periods, [Murillo 2000]. Several formulations have been proposed to deal with this scheduling problem considering different models for thermal and hydraulic units, different types of network constraints and different optimization techniques [Beltran 2001]. Lagrangian relaxation, subgradient and dynamic programming methods are now among the most widely used approaches for solving the UC problem. Two types of constraints are considered in the optimization of the UC problem: the constraints dependent on the set variables belonging to only one single discrete subperiod, referred to as static constraints, and the constraints that are functions of variables from several discrete subperiods, termed dynamic or intertemporal constraints. Examples of these intertemporal constraints are the physical restrictions associated with the operation of thermal generators such as the minimum shut-down time, which is the number of subperiods that the generator must remain *offline* before it can be switched to an *online* status; the counterpart minimum start-up time is the time that the unit must be *online* before it can be turned *off*; up and down ramps, which represent the maximum changed allowed in power generation between consecutive subperiods; banking generator units, which are switched off to attain the most economical operation state, but a certain amount of fuel is supplied to the boiler of these units in order to keep a certain temperature in the steam in case that the units must be turned on in subsequent subperiods; and lastly the cold start and hot start restrictions, which represent the effect of the boiler temperature at the time that the generator is switched *online*, if the boiler has completely lost its temperature the start-up cost will be higher for the generator.

In the conventional UC study, the operative restrictions for the primary energy networks are modeled by the limit operative constraints of each electric generator

[Wood 1984], and there is not more information about the operation conditions of the primary energy network from an optimal or security point of view. Some proposals have included a steady-state formulation of natural gas system into the UC problem under the assumption that the discretization of the study term is long enough to disregard the gas flow transient behavior [Liu 2009, Mohtashami 2009]. For short-term planning studies, however, and considering that the gas flows through the networks at speeds typically around 60-90 km/hr, the slow dynamic behavior shall be duly modeled. This challenging problem is addressed in this thesis along with the development of a unit commitment approach that explicitly considers electricity, natural gas and coal networks. Note that the interdependencies between primary energy networks are affected by the status of each thermal generator. Hence, the integral formulation allows the representation of all the networks with their respective security constraints in such a way that if a given generator has a *online* or *offline* status, the integral formulation ensures that no security or operative constraints have been violated in all the networks involved in the analysis.

## 1.3 Hypothesis

An integral mathematical model of the electric power system and the primary energy networks can provide a better understanding of the interaction between the different energy networks, identify challenges and quantify risks, as well as propose and assess integral solutions for the multi-energy system.

## 1.4 General Objective

The major motivation for this research is the lack of a general model where all networks involved in the integrated energy system are fully represented. Hence, the general objective of this research is to develop a general mathematical modeling of energy networks in a integral frame of reference. Such a model allows a scientist/engineer assessment of the existing interdependency between these networks in terms of the

most common studies performed in the operation of electric power systems: power flows, optimal power flows and unit commitment studies.

The particular objectives are:

- To understand the natural gas networks from an operative point of view.
- To develop algotihms for the analysis of gas systems considering static and dynamic models.
- To assess the interaction between gas and electric networks considering small disturbances in the electric power system.
- To explore a robust optimization methodology to evaluate the impact of wind power uncertainty in the fossil fuel management.
- To assess the interdependencies of primary energy networks through an optimization multi-period formulation.
- To assess the interdependencies of primary energy networks under the Unit Commitment methodology.

## 1.5 Contributions and Scientific Methodology

The work in this thesis proposes a integral approach for the solution of the gas and power flow problem in both networks for a time horizon corresponding to a single time period (snapshot). This problem is individually formulated for each system based on the balance of nodal flows, representing the gas flow equations of the natural gas system in a consistent manner with regards to their counterparts in the electrical system, and a generic framework is then proposed to execute the flow analysis in conjunction with both systems. In this context, the gas temperature is viewed as a variable in the gas flow equation based on the proposal detailed in [Coutler 1979] in order to identify operating conditions with the risk of hydrate formation and to assess its effect on the energy consumed by compressors. The conventional electric power flow formulation

assumes the existence of a slack generator that supplies the entire imbalance of active power in the system, even when a sufficient spinning reserve exists in other generators; however, as pointed out in [Guoyu 1985], "a slack bus is something artificial which has no relation to the physical system since no such distinction exists among generators." In order to overcome this shortcoming, the concept of distributed slack nodes is used in the proposed approach; thus, the active power output of an arbitrary number of generators is adjusted to achieve a total active power balance in the electric power system. The use of this concept justifies the integral model proposed to assess the equilibrium point of the overall energy grid. In addition, it also increases the value of the proposed approach because the adjustments of active power generation as a function of the gas supply and the electric energy consumed by moto-compressor are computed during the solution process in a closed-loop computation, more realistically representing the interdependency between both networks. Additionally, the primary frequency regulation is contemplated in the power system modeling. Lastly, the set of nonlinear algebraic equations representing both systems is solved by using Newton's method in order to assess the values of state variables that provide the steady-state of the overall energy grid under a pre-specified operating condition. A robust optimization (RO) model is proposed in this thesis to assess how uncertainties associated with wind speed forecasts affect the economic and safe operation of a multi-energy system composed of natural gas, coal and electricity networks, which are coupled at multiple nodes of the electricity network through thermal power plants. An analytical RO framework is then formulated as an integrated, generalized, single period network flow model, capable of simulating the economic and secure operation of the overall energy system taking directly into account the uncertainty of wind power generation. In this case, the interdependency between the electricity and primary energy networks is considered more realistically because the power dispatch of generation units is adjusted according to the variability and uncertainty of the wind power output in order to achieve the total power balance in the electric power system. In accordance to the idea reported in [Mulvey 1995] and [Malcom 1994], both deterministic and uncertain problem data are defined by a finite

set of scenarios, each of which is a deterministic set containing some of the possible values that may be realized for the uncertain data. In this case, the approach assumes that the values of wind speed uncertainty are known for a limited number of scenarios and that the total sum of the probabilities of occurrence of each scenario is equal to one. Therefore, the discrete probability distribution for the limited number of scenarios is known. A RO model is then formulated in order to find an uncertainty-immunized solution that remains feasible and nearly optimal for all scenarios that the uncertain data could define: the RO is a "methodology capable of detecting cases when data uncertainty can heavily affect the quality of the nominal solution, and in these cases to generate a robust solution, one that is immunized against the effect of data uncertainty" [Ben-Tal 2009]. In order to assess how the wind energy penetration and wind power forecast error impact on the fossil fuel-based generation management of multiple primary energy networks, a multi-period nonlinear optimal power flow (OPF) approach is also proposed considering multiple primary energy networks (coal, natural gas and hydraulic resources) and the safe operation associated with each energy system. The approach is formulated and analyzed utilizing CONOPT [Drud 1995], which is a nonlinear optimization solver for GAMS® [Brooke 1998].

Lastly, a UC formulation where all networks involved in the integrated energy system are fully represented in an integrated fashion, where considering that the coal and natural gas represent more than 95% of the fossil fuels consumption for electric power production in US ["Electric Power Monthly", Data for November 2013, http://www.eia.gov/electricity/monthly/], for the purposes of this work only these non-renewable primary energies are modeled in the proposed approach. A contribution of this approach is the modeling of the slow dynamic behavior of gas flows considering a two-port model of pipelines. On the other hand, the UC is performed based on the variable duplication method, discussed in [Beltran 2001] and [Murillo 2000], where a combination of one dynamic programming (DP) and one optimal power flow (OPF) modules is performed to economically determine a schedule of what generation units, involving the turn-on and turn-off times and power production set-points for each gener-

ator, will be used in each time subperiod while ensuring that no operational constraints are violated in the energy networks during the whole time period of study.

## 1.6 Publications

*Journal Papers*

- Martinez-Mares A. and Fuerte-Esquivel C.R., "A robust optimization approach for the interdependency analysis of integrated energy systems considering wind power uncertainty," IEEE Transactions on Power Systems, ISSN 0885-8950, vol. 28, no.4, November 2013, pp. 3964-3976.

- Martínez-Mares A. and Fuerte-Esquivel C.R., "A unified gas and power flow analysis in natural gas and electricity coupled networks," IEEE Transactions on Power Systems, ISSN 0885-8950, vol. 27, no. 4, November 2012, pp.2156-2166.

*Conference papers*

- Martinez-Mares A., Fuerte-Esquivel C.R., Wu L., and Ortmeyer T., "Wind energy impact in fossil fuel management: A multi-energy OPF approach," IEEE Power Engineering Society General Meeting, ISSN: 1944-9925, 22-26, July, 2012, San Diego, California, U.S.A., 8 pages.

- Martinez-Mares A. and Fuerte-Esquivel C.R., "Integrated energy flow analysis in natural gas and electricity coupled systems," 43rd North American Power Symposium 2011, NAPS 2011, ISBN: 978-1-4577-0418-5, August 4-6, 2011, Boston, MA, 7 pages.

## 1.7 Thesis Content

To the best of the author's knowledge, the proposed ideas reported in Chapter 1 had not been explored before this work was developed; and they are described in detail in the rest of the thesis as follows.

Chapter 2 presents the static and dynamic models of the natural gas network based on detailed mass flow and thermal balance formulations. Algorithms to perform steady-state and dynamic gas flow analyzes with nonlinear models are also proposed and implemented.

Chapter 3 describes the electric power system modeling for steady-state analysis including the concept of distributed slack bus, the primary frequency response in each generator and the nonlinear load behavior. The formulation to integrate both natural gas and electricity networks, as well as the unified solution of the resulting set of nonlinear equations by Newton's approach, are also presented. Lastly, the application of the proposed approach to two coupled energy systems is numerically demonstrated.

Chapter 4 presents the static models associated with the coal subsystem as well as the hydraulic and wind energy resources. The nonlinear RO model of the integrated multi-energy system, composed of the natural gas, coal and electricity subsystems, is detailed considering the uncertainty of wind speed forecast. The application of the proposed model is also presented, where the impact of uncertainties on the economic and safe operation of the overall system is discussed.

Chapter 5 presents a brief description of the wind generators, their main characteristics and operational constraints. In addition, the effect of wind-speed forecast errors on the management of primary energy resources in power systems with a high penetration of wind energy generators has been studied based on a multi-energy networks, multi-period OPF formulation.

Chapter 6 proposes a unit commitment (UC) formulation to perform a multi-period analysis considering the interdependencies between primary energy networks, as well as the impact that the intertemporal constraints inherent to the physical operation to thermal power plants have in the commitment of each generator. Furthermore, the

mathematical model representing the transient behavior of the natural gas traveling in pipelines has been included.

Chapter 7 provides the general conclusions of this research work and presents suggestions for future related areas that require further investigation.

Table 1.2: Summary of mathematical models used in this thesis for each energy system.

| Chapter | Natural Gas | Coal | Hydro | Wind | Electric Power System |
|---|---|---|---|---|---|
| 2 | Nonlinear: Steady and Dynamic State | — | — | — | — |
| 3 | Nonlinear: Steady State | — | — | — | Nonlinear: Steady State |
| 4 | Nonlinear: Steady State | Linear: Steady State | Nonlinear: Steady State | Nonlinear: Steady State | Nonlinear: Steady State |
| 5 | Nonlinear: Steady State | Linear: Steady State | Nonlinear: Steady State | Nonlinear: Steady State | Nonlinear: Steady State |
| 6 | Nonlinear: Dynamic State | Linear: Steady State | Nonlinear: Steady State | Nonlinear: Steady State | Nonlinear: Steady State |

# Chapter 2

# Natural Gas Systems

## 2.1 Introduction

This chapter describes the three most basic elements of the natural gas networks, their mathematical models and the manner in which these components are integrated in a single framework to assess the steady-state and dynamic performance of the gas flow. These elements are *pipelines, compressors and nodes. Pipelines* are the means of transportation that frequently cover long distances to take the natural gas from the gas surface deposits to the consumption centers. Since the natural gas flow is driven by pressure through pipelines and the natural gas flowing in pipelines loses pressure because of the pipeline's physical characteristics, the *compressors* installed in the network permit the maintenance of the nodal pressure profile along the gas network under secure operative limits. Lastly, the third element corresponds to the *nodes* representing the interconnection points between pipelines, compressors, gas sources and gas loads, as well as the location where the natural gas balance must be satisfied at every instant of time.

The mathematical modeling of those components depends on the study requirements, a *steady-state* model can determine the operative conditions of the network for a single-shot of time, which is a very important tool for real-time and daily operation of the natural gas networks [An 2003]. On the other hand, a multi-period time-based

study is necessary for short- and medium-term operation planning, so that the discretization of the time period at which the required study will be performed could require most complex mathematical models in order to represent the dynamic behavior of the gas flow through the pipeline. This dynamic behavior is a function of both the time and space coordinates, and it is frequently represented by a set of partial differential equations [Osiadacz 1990, Liu 2011].

The corresponding steady-state and dynamic models of the natural gas network composed of gas sources, pipelines, compressor stations and gas load's models (steady-state and dynamic) are reported in this chapter considering their corresponding physical characteristics and the manner in which these components interact.

## 2.2 Pipeline Modeling

### 2.2.1 Steady-State Modeling

The quantity of gas transmitted through each pipeline is a function of the pipeline's *physical parameters* and the *operation conditions* of the natural gas network. Several mathematical models have been proposed to compute the mass flow of natural gas through pipelines; in [Coelho 2007, Olajumoke 2010] a detailed analysis of the most common formulations used in the natural gas industry has been examined, with the main difference between them being the way in which the friction coefficient term and natural gas characteristics are considered in the formulation. In this context, and as reported in [Mokhatab 2006, Schroeder 2000, An 2003], the most commonly used model corresponds to the Weymouth Equation, which is expressed in a pipeline connecting gas nodes $k$ and $m$ as follows :

$$G_p^{km} = C \left(\frac{T_b}{\Pi_b}\right) D_{km}^{2.5} \left(\frac{\mid \Pi_k^2 - \Pi_m^2 - H_p^{km} \mid}{L^{km}\gamma_G T_a^{km} Z_a \lambda_{fr}^{km}}\right)^{0.5} E_p^{km} \tag{2.1}$$

where $C$ is a constant whose magnitude is 77.54, $T_b$ and $\Pi_b$ are the temperature and pressure of the natural gas at base conditions, respectively, the parameter $D_{km}$ repre-

sents the inner diameter of the pipeline, $\Pi_k$ and $\Pi_m$ correspond to the nodal pressure at both ends of the pipeline, $H_p^{km}$ is a correction factor which considers the effect of changes in the altitude over the pipeline, and it is calculated by (2.4); $L^{km}$ is the pipeline's length, $\gamma_G$ is the constant natural gas specific gravity, $T_a^{km}$ is the gas average temperature along the pipeline, and it is computed by (2.6), $Z_a$ is the compressibility factor of the natural gas, $\lambda_{fr}^{km}$ is the friction coefficient and finally the parameter $E_p$ represents the efficiency of the pipeline which is used for calibration purposes according to [Schroeder 2000].

In Equation (2.1), the direction of the flow is determined by the following relations: if $\left(\Pi_k^2 - \Pi_m^2 - H_p^{km}\right) > 0$, then the natural gas is flowing from the node $k$ to the node $m$, and if $\left(\Pi_k^2 - \Pi_m^2 - H_p^{km}\right) < 0$, then the natural gas flows from the node $m$ to the node $k$.

Based on the knowledge of the network and the experience of engineers that operate the gas network, the physical characteristics of each pipeline and the gas composition in Equation (2.1) can be expressed by a single constant $C_{km}$ given by

$$C_{km} = C\left(\frac{T_b}{\Pi_b}\right) D_{km}^{2.5}\left(\frac{1}{L^{km}\gamma_G T_a^{km} Z_a \lambda_{fr}^{km}}\right)^{0.5}. \tag{2.2}$$

This leads to a simpler equation for the natural gas flowing in a pipeline connecting nodes $k$ and $m$

$$G_p^{km} = C_{km}\left(\mid \Pi_k^2 - \Pi_m^2 - H_p^{km} \mid\right)^{0.5}. \tag{2.3}$$

From Equation (2.1), clearly the quantity of flowing natural gas is a function of its physical parameters $\left(D_{km},\, H_C,\, \lambda_{fr}^{km},\, E_p^{km}\, and\, L^{km}\right)$, the operation conditions of the gas network ($\Pi_k$, $\Pi_m$, $T_a$) and the physical composition of the gas ($Z_a$). Note that (2.1) indicates that pipelines with greater diameters, shorter lengths, higher efficiencies and lower friction factors, which transport lighter gases and operate at lower temperatures, are able to transport larger quantities of natural gas with fewer extreme operation conditions (i.e. a lower difference of nodal pressures). One very important characteristics

of this steady-state model is that the amount of gas flowing at the inlet node $k$ equals the gas flowing at the outlet node $m$ of the pipeline.

The term $H_p^{km}$ considers the effect of the changes in the altitude over the pipeline [Mokhatab 2006], and it is calculated by the following expression:

$$H_p^{km} = \frac{0.0375\, g\, (H_m - H_k) \left(\Pi_a^{km}\right)^2}{Z_a\, T_a^{km}}. \tag{2.4}$$

Note that the Equation (2.4) considers the difference of elevation over the sea level between the inlet and outlet nodes of the pipeline ($H_m$ and $H_k$) and is also a function of the average pressure along the pipeline $\Pi_a^{km}$; furthermore, the parameter $g$ corresponds to the acceleration of gravity. The following expression has been proposed to compute this average pressure considering the nonlinear pressure drop with distance [Mokhatab 2006]:

$$\Pi_a^{km} = \frac{2}{3}\left[(\Pi_k + \Pi_m) - \left(\frac{\Pi_k\, \Pi_m}{\Pi_k + \Pi_m}\right)\right]. \tag{2.5}$$

The average temperature $T_a$ in Equations (2.4) and (2.5) can be computed as an arithmetic average of the gas temperatures at the inlet $T_k$ and outlet $T_m$ nodes of the pipeline [Schroeder 2000], which is the approach typically utilized in buried natural gas networks where the pipelines are not exposed directly to the environment temperature $T_s^{km}$. Nevertheless, the following equations are used in natural gas networks where the nonlinear effect must be included, as well as the weather to which pipelines are exposed [Mokhatab 2006]:

$$T_a^{km} = \frac{T_k - T_m}{\ln \frac{T_k - T_s^{km}}{T_m - T_s^{km}}} + T_s^{km}. \tag{2.6}$$

Lastly, the friction factor for pipelines composing high pressure networks working in the fully turbulent flow region is strictly dependent on the inner diameter of the pipeline [An 2003] and is given by Equation (2.7):

$$\lambda_{fr}^{km} = \frac{0.032}{D^{1/3}}. \tag{2.7}$$

### 2.2.2 Dynamic Modeling

The aim of this section is to describe a suitable model to represent the dynamic behavior of the natural gas flowing in pipelines, which can be applied to studies involving the evolution of state variables over the time. In short- and medium-term operation planning studies of energy systems, the evolution of the system is analyzed for a specified period of time ranging from a few hours up to one day in advance.

Typically, the multi-period time based studies are performed through the decomposition of the whole time period into subperiods, often subperiods of one hour. Unlike the electric power system, however, where the electricity travels at the speed of light and the network's transient response has completely disappeared in a subperiod of time of one hour because the time constants associated with the network's variables are extremely small, dynamics are much slower in high pressure natural gas systems because the network's time constants are much larger, and the natural gas travels typically at a velocity around 60 to 90 km/hour. This implies that the amount of gas flowing at the inlet node of a pipeline is different than the amount of gas flowing at its outlet node for any instant of time, so that an amount of gas is stored inside the pipeline. Therefore, the dynamics in the gas network cannot be neglected without gross errors for study periods of one hour [Liu 2011].

Transients in gas systems are generally associated with the time variant nature of loads at distribution points and from adjustments made by the system operator in order to achieve the gas balance at each node of the network. In this context, the transient flow of gas in pipelines is mathematically represented by a set of four nonlinear partial differential Equations (2.8) to (2.11). Furthermore, one of the biggest complexities of this model is the use of a distributed-parameter model for the pipeline which is time- and space-dependent [Osiadacz 1990]:

$$\frac{\partial G}{\partial x} + A\frac{\partial \rho}{\partial t} = 0 \tag{2.8}$$

$$\frac{\partial \Pi}{\partial x} + g\rho\frac{\partial h}{\partial x} + \frac{\lambda_{fr}\,|\nu|\,\nu}{2D}\rho + \frac{1}{A}\frac{\partial G}{\partial t} + \frac{\partial\left(\rho\nu^2\right)}{\partial x} = 0 \tag{2.9}$$

$$\begin{aligned} W\left(\rho A\,dx\right) &= \frac{\partial}{\partial t}\left[\left(\rho A\,dx\right)\left(c_\nu T + \frac{v^2}{2} + g\,dh\right)\right] \\ &+ \frac{\partial}{\partial x}\left[\left(\rho A\,dx\right)\left(c_\nu T + \frac{\Pi}{\rho} + \frac{v^2}{2} + g\,dh\right)\right] \end{aligned} \tag{2.10}$$

$$\rho = \frac{\rho_0 z_0 T_0}{\Pi_0}\frac{\Pi}{z\,T} \tag{2.11}$$

where $G$ is the mass flow with a density $\rho$, temperature $T$ and specific heat $c_v$ traveling at a velocity $\nu$ in a pipeline with length $x$ and cross section area $A$ at the time $t$. The parameter $h$ represents the change in elevation with respect to the sea level between the inlet and outlet node, and lastly, the parameters with the suffix "0" represent the base conditions of the gas (pressure, temperature, compressibility and density).

Equation (2.8) is known as the *continuity equation* and simply states that mass may neither be created nor destroyed, such that the changes of the gas flow is commensurate with the alteration of the gas density: the rate of change of the gas density $\rho$ in the time corresponds to the mass flow out of or into the pipe across its boundaries. Therefore, the gas density inside the pipeline increases if the amount of gas entering the pipe is greater than the one leaving the pipe. Equation (2.9) is the known form of Newton's second law and is referred to as the *momentum equation,* which describes the sum of all forces acting on the gas particles. From a physical background, this equation states that "the force acting on a gas particle or system particles of fixed mass at a certain time is equal to the rate of change of momentum of the particle (system of particles) at that instant" [Osiadacz 1990]. The first term of this equation describes the forces acting on the element of fluid in the direction of motion at a certain instant and corresponds to the variation of the pressure force with the pipe's length. The second term corresponds to the gravitational force working on the gas, which is influenced by the slope of the

pipeline. The third term is associated with the shear force due to the friction with the pipe wall. The fourth and fifth terms represent the referred rated of change of momentum and correspond to the gas inertia or the change of flow rate in time and the flowing gas dynamic pressure, also called impact pressure, respectively. The equation of *conservation of energy* (2.10) deals with the connection of the inner energy of gas and the heat exchange with the soil. In this case, the gas very slowly emits energy to the soil, such that (2.10) is used to represent the heat transfer that takes place during the dynamic process in the gas, where changes of temperature within the gas are due to heat conduction between the pipe and the soil. Lastly, (2.11) relates the pressure, temperature and the density of the gas and is known as the *gas state equation* [Osiadacz 1990, Moritz 2007].

Several formulations have been proposed to solve (2.8) to (2.11). By way of example, this set of equations has been solved using a finite difference method in which the size of discretization step on both time and space coordinates for each pipeline are critical parameters for the computation time and accuracy [Liu 2011, Chaudry 2008, Tao 1998]. Other works have proposed the representation of pipelines through a transfer function model; these models have shown higher computational efficiency at the expense of accuracy [Behbahani-Nejad 2008, Aalto 2008, Kralik 2008].

Recently, a model to represent the dynamic behavior of gas inside a pipeline has been proposed in [Moritz 2007], which consists of the simplification of the Equations (2.8) through (2.11) by two discretized algebraic equations based on the implicit Euler's method. The discretization of (2.8) and (2.9) are performed in both space and time coordinates. The former discretization is carried out considering the pipeline as a two-port network having only two nodes representing the beginning and ending of the pipe, which are referred to as *in* and *out* nodes, respectively. On the other hand, the time discretization consists of decomposing the entire time period of study into equidistant subperiods, which have been considered in hourly time steps.

The Moritz's model neglects the heat exchange between the gas inside the pipeline

and the soil; furthermore, it considers a constant temperature for the gas flow, so that (2.10) is neglected in the model. Lastly, the *gas state equation* (2.11) is set in the remaining Equations (2.8) and (2.9) to obtain a set of two differential equations, which is discretized as described above. This procedure results in the following set of two nonlinear equations for each pipeline in the natural gas system:

$$\frac{G_p^{km,\,out} - G_p^{km,\,in}}{L^{km}} + A\frac{z_0 T_0}{\Pi_0 T}\frac{\frac{\Pi_m(t)}{z(\Pi_m(t))} - \frac{\Pi_m(t-\Delta t)}{z(\Pi_m(t-\Delta t))}}{\Delta t} = 0 \qquad (2.12)$$

$$\begin{aligned} &\frac{\Pi_m(t) - \Pi_k(t)}{L^{km}} + g\frac{\rho_0 z_0 T_0}{\Pi_0 T}\frac{\partial h}{\partial x}\frac{\Pi_m(t)}{z(\Pi_m(t))} \\ &\quad + \frac{\lambda_{fr}}{2D}\frac{\rho_0 \Pi_0 T}{A^2 z_0 T_0}\frac{G_p^{km,\,out}(t)^2\, z(\Pi_m(t))}{\Pi_m(t)} \\ &\quad + \frac{\rho_0}{A}\frac{G_p^{km,\,out}(t) - G_p^{km,\,out}(t-\Delta t)}{\Delta t} \\ &+ \frac{\rho_0 \Pi_0 T}{A^2 z_0 T_0}\frac{\frac{G_p^{km,\,out}(t)^2 z(\Pi_m(t))}{\Pi_m(t)} - \frac{G_p^{km,\,in}(t)^2 z(\Pi_k(t))}{\Pi_k(t)}}{L^{km}} \;=\; 0. \end{aligned} \qquad (2.13)$$

Figure 2.1 shows the transient behavior for nodal pressures at nodes 2 and 3 of the three nodes benchmark gas network reported in [Tao 1998], whose corresponding parameters are presented in Appendix A. These results correspond to a numeric solution for the set of PDE's equations presented in [Osiadacz 1990], the solution through a finite differences method [Tao 1998], the transfer function model proposed in [Kralik 2008], and finally the two-port network modeling from [Moritz 2007]. A comparison of these results clearly shows the numerical validity of the latter proposal, which will be the one used in this thesis.

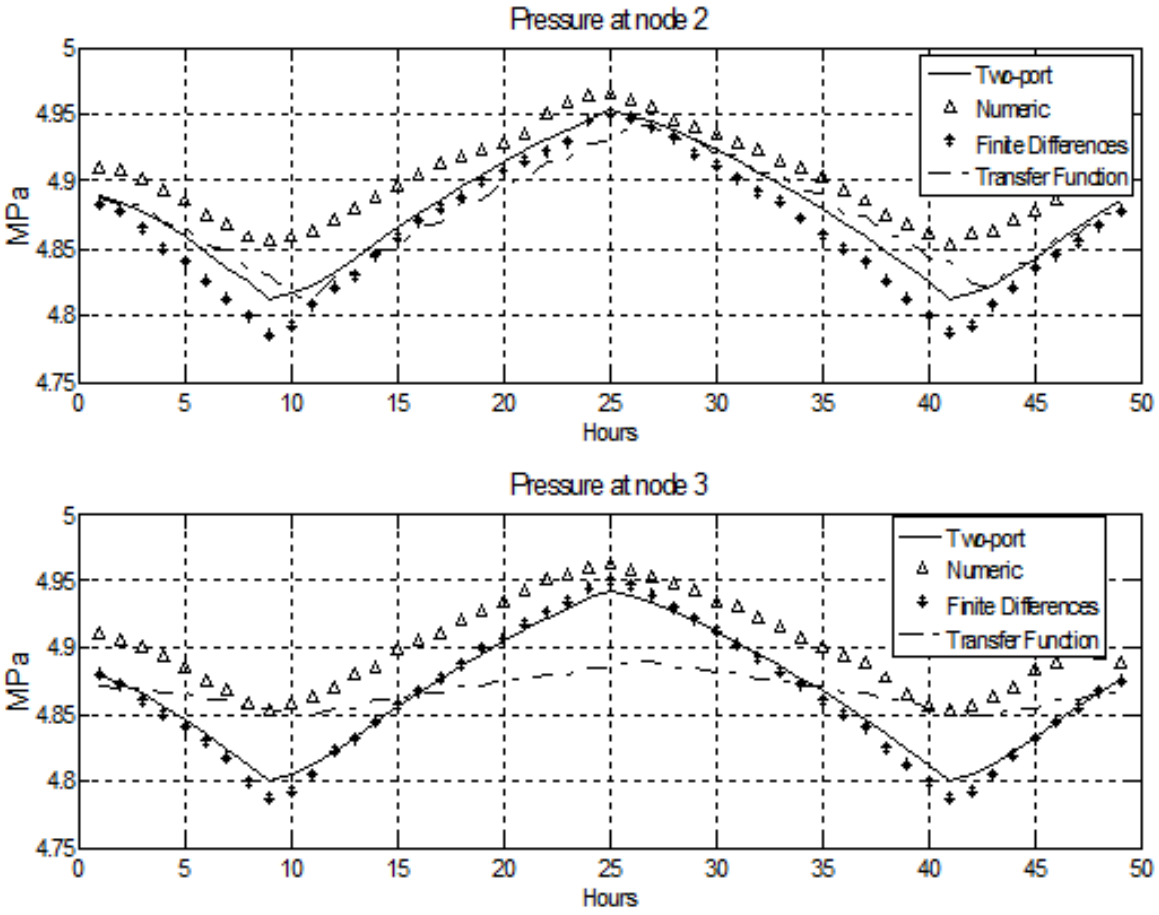


Figure 2.1: Natural gas dynamic models.

Since the electricity and natural gas travel at the speed of light and 40-60 miles/hr, respectively, and the natural gas pipeline has storage capacity, steady-state gas flows cannot be assumed strictly for multi-period simulations with time steps shorter than several hours. This implies that pipelines with distributed parameters and time-varying state variables must be considered for multi-period analysis. In this case, the dynamic modeling of the gas flowing inside the pipeline is necessary to obtain an accurate assessment of the influence of disturbances in the electric power systems on the gas system performance under multi-period analysis. Note that the use of steady state or dynamic models of the gas flow is also defined by the gas pressure at which the gas network is operating: in low (resp. high) pressure networks the dynamics are very rapid (resp. much slower) and can be ignored (resp. cannot be neglected) for must practical

purpose. Lastly, Table 2.1 report different time frames of power systems control actions/phenomena and pair them with time frames of gas network phenomena in order to help in the decision for the application of the static or dynamic models of the gas pipelines.

Table 2.1: Disturbances range of time for electric and gas networks, [Soder 2011].

| Range of Time | Phenomena | |
|---|---|---|
| | Electric System | Gas System |
| $< 10\,ms$ | Electromagnetic Transients | — |
| $\leq 1\,s$ | Saturation and Resonances | — |
| $\leq 10\,s$ | Transients and Linear Stability | Plant Startup Dynamic Analysis |
| $\leq 1\,min$ | Secondary Frequency and Voltage Regulation | Multi-phase Pipes Dynamic Analysis |
| $< 1\,hour$ | Hierarchical Voltage Control and Operative Dispatch | Control Operation Dynamic Analysis |
| $> 1\,hour$ | Operation Control / Dispatch | Sales and Security Static Analysis |

## 2.3 Compression Stations

The requirements for the transmission of large volumes of gas over long distances have increased the necessity of higher operation pressures in the natural gas networks. When gas is circulating inside a pipeline, there exists a loss of pressure caused mainly by the friction of the fluid in the pipeline's walls and the heat transfer between the flowing gas and the environment surrounding the pipeline. Hence, compression stations are required to control the pressure profile along the network in order to maintain the natural gas flowing from the deposits to the consumption centers [Mokhatab 2006]. The compression stations are represented mathematically by a simple linear equation relating the pressure value at the inner node and at the outer node of the compression station by the ratio $R^{km}$

$$\Pi_k R^{km} = \Pi_m. \tag{2.14}$$

The energy consumption by each compression station is a nonlinear function of the compression ratio and is computed by the following expression [An 2003, Mokhatab 2006]:

$$BHP^{km} = 0.0854\, Z_a \left[\frac{G_c^{km}\, T_k}{E_c\, \eta_c}\right] \left[\frac{c_k}{c_k - 1}\right] \left[\left(\frac{\Pi_m}{\Pi_k}\right)^{\frac{c_k - 1}{c_k}} - 1\right] \tag{2.15}$$

where $T_k$ is the gas temperature at the compressor's inlet node. In addition, $G_c^{km}$ corresponds to the state variable of the gas flowing through the compressor; this variable is calculated iteratively during the solution of the set of nonlinear equations modeling the natural gas network. The parameters $E_c$ and $\eta_c$ represent the parasitic and compression process efficiencies respectively; $c_k$ is the specific heat ratio for the natural gas. Lastly $\Pi_m$ and $\Pi_k$ represent the nodal pressure at the outlet and inlet nodes of the pipeline respectively.

This energy required by the compressor to increase the pressure level is supplied from the electric power system in the case of *moto-compressors* and is calculated by (2.16) or from the natural gas system, where a quantity of gas is extracted from the network in the case of *turbo-compressors* according to Equation (2.17) [Mokhatab 2006]. The former type is commonly used in urban areas, whereas the latter is preferably used in sub-urban areas or when an electric power network is not available:

$$L_c^{km,i} = BHP^{km} \left(\frac{7.457x10^{-6}}{3600}\right) \tag{2.16}$$

$$\tau_c^{km} = \alpha_c^{km} + \beta_c^{km}\, BHP^{km} + \gamma_c^{km}\, BHP^{km\,2}. \tag{2.17}$$

The expression (2.16) computes the instant active power load in per unit (100 MVA base), which shall be supplied from the node $i$ of the electric power system to deliver the energy required by the compressor connected between nodes $k$ and $m$ of the natural gas network. The Equation (2.17) computes the quantity of gas required by the *turbo-compressor* which is typically extracted from the inlet node; in addition, the parameters $\alpha_c$, $\beta_c$ and $\gamma_c$ define the efficiency in the energy conversion process from the chemical

energy contained in the gas to the mechanical energy required by the compressor station.

The compression station model described by the Equations (2.14) to (2.17) is valid for both steady-state and dynamic analyzes because the short time constants involved in the transient behavior of the compression process.

## 2.4 Natural Gas Nodes

The nodes of the natural gas system represent the interconnection points between the different elements of the network: *pipelines, compressors, loads and sources.* The most conventional type of sources in the natural gas industry are gas fields, gas extracted from oil fields, coal bed methane and, most recently, shale gas deposits in which the natural gas is frequently processed through a liquefaction/regasification procedure to be injected in some specific nodes in the natural gas system [Mokhatab 2006]. All these natural gas sources can be modeled as *constant gas injection* sources at uncontrolled nodal pressure or as *constant nodal pressure* sources which means no controlled natural gas injection. Regarding the variety of gas loads, these could be categorized as industrial load, residential load and load for electric power generation; the first and second type of gas loads are included in the formulation as constant gas extractions, whilst the last one is modeled as a function of the active power generated at each power plant [Martinez-Mares 2011].

The mass flow balance at each node must be satisfied at every instant of time to assure that the sum of gas injected at each node must be equal to zero, as given by considering the $k^{th}$ node

$$\Delta G^k = \sum_{i=1}^{N_{ng}} G_p^{ki} + \sum_{j=1}^{N_{ng}} G_c^{kj} + \sum_{x=1}^{N_c^k} \tau_k^{xi} - \sum_{y=1}^{N_s^k} G_{sk}^{y} + \sum_{z=1}^{N_l^k} G_{lk}^{z} = 0, \qquad (2.18)$$
$$\forall\, i \in N_p^k;\ \forall\, j \in N_c^k;\ \forall\, k \in (N_{ng} - 1)$$

where the first two terms of this equation correspond to the total gas injected at the $k^{th}$ node through the pipelines and compressors, respectively. The third term is the total gas extracted from the $k^{th}$ node by all compressors embedded at this node. On the other hand, the fourth and fifth terms correspond to the total gas injected at and extracted from the $k^{th}$ node by the gas sources and gas loads connected at this node, respectively. Note that the nodal gas supplied and extracted by sources and loads, respectively, must remain between operation limits as defined by the following expressions:

$$G_{sk}^{y-min} \leq G_{sk}^{y} \leq G_{sk}^{y-max} \tag{2.19}$$

$$G_{lk}^{z-min} \leq G_{lk}^{z} \leq G_{lk}^{z-max} \tag{2.20}$$

Lastly, note that at least one nodal pressure must be specified (controlled pressure node, which means uncontrolled gas injection) in order to attain the equilibrium in the whole natural gas network; this node has the same function of the slack bus in the load flow formulations for electrical power systems. Therefore, this known nodal pressure is taken as a reference to compute all other unknown nodal pressures, and the gas injection computed at this node will provide the gas flow balance in the network by compensating for the gas consumed by compressors. In this case, the corresponding gas balance equation associated with this slack node is not included in the mathematical formulation, but is solved separately by finding the gas injected at this node once the steady-state of the overall gas network has been computed [An 2003, Martinez-Mares 2011].

## 2.5 Temperature Effect in Gas Flows

The temperature of the gas inside the pipeline is a variable that shall be controlled to avoid critical operation conditions of the gas composition [Carroll 2003, Mokhatab 2006].

The knowledge of gas temperature at each node of the network permits the defi-

nition of heater's location to prevent hydrate[1] formation or gas condensation, the gas inlet temperature for compressors and the minimum gas flow values in the network [Mokhatab 2006]. The gas condensation and hydrates formation can cause critical operating problems, because they could be deposited in the inner wall of a pipeline and block the gas flow; the solution to these problems in the natural gas industry represents great technical difficulties and high maintenance costs [Mokhatab 2006, Carroll 2003]. Several methods to evaluate the hydrates formation have been reported in the literature, with one of the most used approaches being the chart proposed in [Carroll 2003] and shown in Figure 2.2.

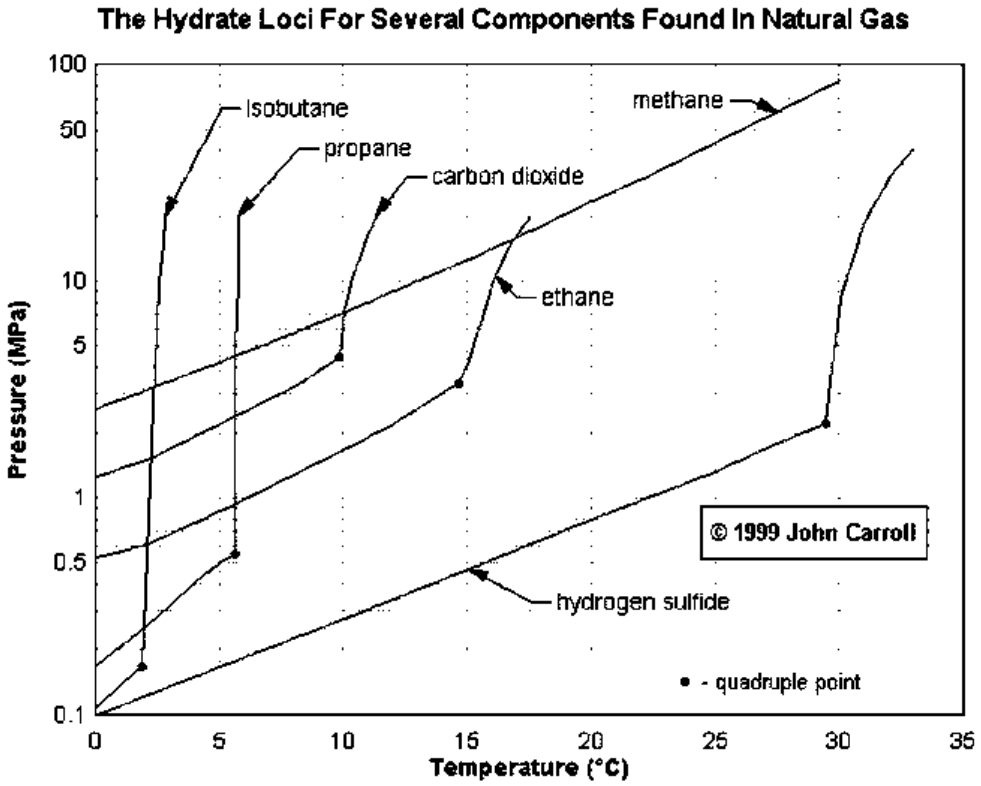


Figure 2.2: Hydrate formation chart [Carroll 2003].

Natural gas is composed mainly of methane, and as reported in this chart, higher

[1]These are solid mixtures formed by the presence of hydrogen bonds and gas compounds [Carroll 2003]

operation pressures require higher gas temperature conditions in order to keep the gas composition in a safety zone (the right-hand side of the curve) to avoid hydrates formation. By way of example, the risk of hydrates formation increases for gas temperatures below 14$^{o}$C considering an operation pressure of 10 MPa.

The temperature at node $k$ of gas flowing in a pipeline connecting nodes $k$ to $m$ is computed by (2.21), based on the proposal in [Coutler 1979], which considers that the gas temperature starts at the inlet pipe's temperature and tends to the surrounding pipe's temperature as the gas flows through the pipeline:

$$\begin{aligned} T_k^{km} &= \left\{ T_k - \left[ T_s^{km} + \left(\frac{\eta_{JT}}{a}\right)\left(\frac{\Pi_k - \Pi_m}{L^{km}}\right)\right]\right\} e^{-aL^{km}} + \\ &+ \left[ T_s^{km} + \left(\frac{\eta_{JT}}{a}\right)\left(\frac{\Pi_k - \Pi_m}{L^{km}}\right)\right] \end{aligned} \tag{2.21}$$

where

$$a = \frac{\pi\, D^{km}\, U^{km}}{m_G\, C_P} \tag{2.22}$$

$$m_G = G_p^{km}\left(\frac{\Pi_b}{\Pi_k}\right)\left(\frac{T_k}{T_0}\right) Z_a \left(\frac{1}{86400}\right)\rho_G^{km}$$

$$\rho_G^{km} = \frac{\Pi_k\, \gamma_G\, MW_{air}}{Z_a\, R_G\, T_k}. \tag{2.23}$$

In this case $\eta_{JT}$ and $U^{km}$ correspond to the Joule-Thompson and heat transfer coefficients, $C_p$ is the heat capacity of the gas at constant pressure, $\gamma_G$ is the gas specific gravity and $MW_{air}$ the air molecular weight.

When gas injections with different temperatures arrive to a given node from different pipelines and compressors, a calculation of the thermal equilibrium of the nodal gas

mixture based on the heat transfer theory is necessary [Coulson 1999]. Therefore, the thermal equilibrium at the $k^{th}$ node is given by the following expression:

$$T_k = \sum_{m \epsilon k} \frac{G_p^{mk}}{G_{total}^k} T_k^{mk} + \sum_{j \epsilon k} \frac{G_c^{jk}}{G_{total}^k} T_k^{jk}, \ \forall \, k = 1, \cdots, \ N_{ng}. \tag{2.24}$$

In this case, the same temperature value at both ends of the compression stations is assumed.

## 2.6 Steady-State Formulation of the Gas Network

Once the mathematical models for steady state and dynamic behavior of the natural gas elements have been described, this section presents an energy balance nodal formulation suitable to perform a gas flow study for the whole gas network. The derivation of this formulation results in a set of nonlinear algebraic equations that is solved through the Newton-Raphson method. The formulation is based on the law of the conservation of energy, such that the sum of all the mass flow injections to a certain node must be equal to zero (or below a certain tolerance). Under this premise, one energy balance equation must be obtained for each node in the natural gas network, as given by Equation (2.18), while the temperature of gas at each node is determined by Equation (2.24). The set of state variables that define how the natural gas network is operating is given by

$$x_{ng} = \begin{bmatrix} \Pi_{1 \rightarrow (N_{ng}-1)} \\ T_{1 \rightarrow N_{ng}} \\ BHP^{1 \rightarrow N_c} \\ \tau^{1 \rightarrow N_c} \\ G_c^{1 \rightarrow N_c} \end{bmatrix} \tag{2.25}$$

where the first and second elements correspond to the set of pressures and gas temperatures at each node of the natural gas network. The rest of the elements in the vector $x_{ng}$ are associated with the compressor's mathematical model: the consumed energy, the gas extracted from the gas system when a turbo-compressor is employed and the gas flowing through the compressor.

The natural gas extracted in the case of turbo-compressors expressed by (2.17) can be included directly in the Equation (2.18) as a function of the state variable $BHP^{km}$; this permits removing one state variable and one state equation from the nonlinear set of equations modeling the natural gas network.

The set of algebraic nonlinear equations representing the equilibrium condition that must exist at each node of the network are given by

$$\Delta G^k = 0, \; \forall \, k \; \in \; (N_{ng} - 1) \tag{2.26}$$

$$\Delta T_k = -T_k + \sum_{m \, \epsilon \, k} \frac{G_p^{mk}}{G_{total}^k} T_k^{mk} + \sum_{j \, \epsilon \, k} \frac{G_c^{jk}}{G_{total}^k} T_k^{jk} = 0, \; \forall \, k \; \in \; N_{ng} \tag{2.27}$$

$$\Delta R^{km} = -\Pi_k R^{km} + \Pi_m = 0, \; \forall \, km \; \in \; N_c \tag{2.28}$$

$$\begin{aligned} \Delta BHP^{km} \quad &= \quad -BHP^{km} + \\ &+ \quad 0.0854 \, Z_a \left[ \frac{G_c^{km} \, T_k}{E_c \, \eta_c} \right] \left[ \frac{c_k}{c_k - 1} \right] \left[ \left( \frac{\Pi_m}{\Pi_k} \right)^{\frac{c_k - 1}{c_k}} - 1 \right] \\ &= 0, \quad \forall \, km \; \in \; N_c \end{aligned} \tag{2.29}$$

$$\Delta \tau^{km} = -\tau_c^{km} + \alpha_c^{km} + \beta_c^{km} \, BHP^{km} + \gamma_c^{km} \, BHP^{km \, 2} = 0, \; \forall \, km \; \in \; N_c. \tag{2.30}$$

Note that the Equation (2.30) and the state variable corresponding to the gas ex-

tracted from the system only exist for cases where *turbo-compressors* are embedded in the network. These nonlinear equations representing the equilibrium point or steady-state operation of the natural gas network are grouped in the following expression:

$$f_{ng} = \begin{bmatrix} \Delta G^k \\ \Delta T_k \\ \Delta R^{km} \\ \Delta BHP^{km} \\ \Delta \tau^{km} \end{bmatrix} = 0 \, \forall k \in (N_{ng} - 1) \, ; \forall km \in N_c. \tag{2.31}$$

The set of nonlinear equations above is defined for all nodes $N_{ng}$ in the natural gas system except the slack and for all the compressor's installed $N_c$.

The equilibrium point of the natural gas system is obtained by solving the Equation (2.31) for the state variables $x_{ng}$ and by assuming that gas sources and gas loads are known in the system. Newton's method is applied to provide a solution for (2.31) by approximating $f_{ng}$ by its first-order Taylor's expansion, which results in $f_{ng}\left(x_{ng}^0\right) + J_{ng}\left(x_{ng}^0\right) \triangle x_{ng} = 0$. This linearized equation, with the Jacobian matrix $J_{ng}$ given by (2.32), is solved for $\triangle x_{ng}$ to get a new approximation value $x_{ng}^1 = x_{ng}^0 + \triangle x_{ng}$. This process is repeated to get a sequence of values $x_{ng}^2$, $x_{ng}^3$, .... $x_{ng}^p$ with the corresponding initial conditions $x_{ng}^1$, $x_{ng}^2$, .... $x_{ng}^{(p-1)}$which, under certain conditions, converges to the solution $x_{ng}^*$ where $f_{ng}\left(x_{ng}^*\right) = 0$ or the maximum number of iterations has been exceeded.

$$J_{ng} = \begin{bmatrix} \frac{\partial \Delta G}{\partial \Pi} & \frac{\partial \Delta G}{\partial T} & \frac{\partial \Delta G}{\partial BHP} & \frac{\partial \Delta G}{\partial \tau} & \frac{\partial \Delta G}{\partial G_c} \\ \frac{\partial \Delta T}{\partial \Pi} & \frac{\partial \Delta T}{\partial T} & \frac{\partial \Delta T}{\partial BHP} & \frac{\partial \Delta T}{\partial \tau} & \frac{\partial \Delta T}{\partial G_c} \\ \frac{\partial \Delta R}{\partial \Pi} & \frac{\partial \Delta R}{\partial T} & \frac{\partial \Delta R}{\partial BHP} & \frac{\partial \Delta R}{\partial \tau} & \frac{\partial \Delta R}{\partial G_c} \\ \frac{\partial \Delta BHP}{\partial \Pi} & \frac{\partial \Delta BHP}{\partial T} & \frac{\partial \Delta BHP}{\partial BHP} & \frac{\partial \Delta BHP}{\partial \tau} & \frac{\partial \Delta BHP}{\partial G_c} \\ \frac{\partial \Delta \tau}{\partial \Pi} & \frac{\partial \Delta \tau}{\partial T} & \frac{\partial \Delta \tau}{\partial BHP} & \frac{\partial \Delta \tau}{\partial \tau} & \frac{\partial \Delta \tau}{\partial G_c} \end{bmatrix}. \quad (2.32)$$

As is commonly known, if an accurate initial estimation for the state variables can be made and if $f_{ng}$ is sufficiently smooth, Newton´s method converges quickly. In this context, special caution should be taken to initialize the state variables of the gas network. By way of example, the gas flow through the gas network is a function of the difference of pressures at the pipeline's ends such that initialization of pressures gives rise to an ill-conditioned Jacobian matrix if a flat initialization is adopted when changes in the pipeline's altitude are not contemplated. In such a situation, the linearized mass flow equation yields a null diagonal element in the Jacobian.

The strategy adopted to remedy this situation consists of selecting the initial values for nodal pressures at the pipeline's ends considering a difference of pressures of 5 to 10 % between the receiving and sending nodes, taking as a reference value the specified pressure at the slack node. This initialization process is adopted independently of how the changes in the pipeline's altitude are being considered.

### 2.6.1 Study Case

In this section the steady-state nodal formulation is applied to the 15 nodes natural gas system shown in Figure 2.3 and previously reported in [An 2003]. This system consists of five loads, two sources, 12 pipelines and four compressors, with the data information

detailed in Appendix A.

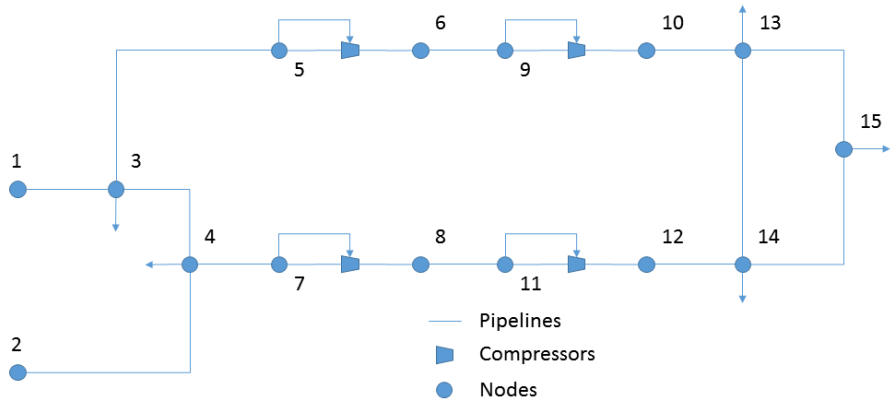


Figure 2.3: 15 Nodes natural gas benchmark system.

In this case of study the network contains four turbo-compressors, and the gas required by the compression stations is extracted from the natural gas system at the inlet node. Node 1 is assumed as the slack node of the system with a controlled pressure of 1000 PSI (6.9 MPa). For illustrative purposes, the following two scenarios are simulated: *a)* supposing a constant gas temperature at all nodes of the network at 550$^{o}$R (approximately 32.4$^{o}$C), and *b)* considering the gas temperature as a state variable to be computed during the iterative solution with an environmental temperature of 500$^{o}$R (approximately 4.6$^{o}$C), except at nodes of compressors and gas sources where a constant gas temperature is set at 550$^{o}$R. The compression ratios are 1.8, 1.9, 1.3 and 1.3 for the compressor 1 to 4, respectively.

Table 2.2: Nodal pressures and temperatures for study case 2.1

| Node | Case a) | | Case b) | |
|---|---|---|---|---|
| | Pressure (PSI) | Temperature ($^{o}$R) | Pressure (PSI) | Temperature ($^{o}$R) |
| 1 | 1000.0 | 550 | 1000 | 550.0 |
| 2 | 974.9 | 550 | 976.4 | 550.0 |
| 3 | 706.7 | 550 | 717.9 | 519.6 |
| 4 | 714.7 | 550 | 725.3 | 522.6 |
| 5 | 534.7 | 550 | 555.6 | 550.0 |
| 6 | 962.5 | 550 | 1000.0 | 550.0 |
| 7 | 568.1 | 550 | 586.0 | 550.0 |
| 8 | 1079.3 | 550 | 1113.4 | 550.0 |
| 9 | 826.7 | 550 | 870.2 | 550.0 |
| 10 | 1074.7 | 550 | 1131.2 | 550.0 |
| 11 | 816.7 | 550 | 861.2 | 550.0 |
| 12 | 1061.7 | 550 | 1119.6 | 550.0 |
| 13 | 763.5 | 550 | 852.0 | 519.5 |
| 14 | 763.0 | 550 | 851.5 | 520.6 |
| 15 | 762.3 | 550 | 851.0 | 519.9 |

Table 2.3: Energy, gas consumption and flow through compression stations for study case 2.1

| Compressor | Energy Consumption (HP) | | Gas extracted (MSCF) | | Gas flow (MMSCF) | |
|---|---|---|---|---|---|---|
| | Case a) | Case b) | Case a) | Case b) | Case a) | Case b) |
| 1 | 3907 | 3907 | 32.5 | 32.5 | 4.77 | 4.77 |
| 2 | 3823 | 3823 | 31.9 | 31.8 | 4.30 | 4.30 |
| 3 | 1670 | 1670 | 13.9 | 13.9 | 4.75 | 4.75 |
| 4 | 1487 | 1487 | 12.4 | 12.4 | 4.28 | 4.28 |

Table 2.2 reports the nodal pressures and temperatures for both scenarios of the study case. As mentioned in Section 2.2.1, those natural gas networks operating with gases at lower temperatures have lower pressures losses. This statement is verified by observing that higher nodal pressures are obtained for the case *b)* at those nodes where the nodal gas temperature is affected by the environment, while in case *a)* the temperature of gas remains constant independently of environmental temperature. On the other hand, from the computed nodal pressures one can verify that the ratio of compression has been satisfied in all the compression stations. Lastly, Table 2.3 reports the operation conditions in the compression stations.

The following step in the analysis of this natural gas network is the localization of the operation condition (pressure/temperature) of each node of the system using the chart proposed by Carroll [Carroll 2003] in Figure 2.2 to determine if any node of the system is in risk of hydrates formation. This study is presented in the next chapter.

## 2.7 Dynamic Formulation of the Gas Network

The energy balance model presented in the previous section is modified to include the equations representing the dynamic behavior of the natural gas flowing through the pipelines. First, instead of using the Equation (2.1) to compute the nodal injections and extractions of gas by the pipelines in the natural gas network, the Equation (2.12) is incorporated to calculated the nodal gas balance in Equation (2.18). In this equation there are two new unknown variables: $G_p^{km,out}$ and $G_p^{km,in}$, solving the Equation (2.12) for $G_p^{km,in}$, however, permits having an expression for the gas injected at both ends of the pipeline with a single variable. In this case, the variable $G_p^{km,out}$ is expressed as follows:

$$G_p^{km,in} = G_p^{km,out} + L^{km} A \frac{z_0 T_0}{\Pi_0 T_g} \frac{\frac{\Pi_m(t)}{z\Pi_m(t)} - \frac{\Pi_m(t-\Delta t)}{z\Pi_m(t-\Delta t)}}{\Delta t}. \tag{2.33}$$

This allows only one additional variable in the natural gas modeling; this imbalance in state variables and equations is overcome with the addition of the Equation (2.13) in

the $f_{ng}$ nonlinear equations set for a single subperiod of time, which is now expressed in the following form:

$$f_{ng} = \begin{bmatrix} \Delta G^k \\ \Delta G_d^{km} \\ \Delta R^{ij} \\ \Delta BHP^{ij} \\ \Delta \tau^{ij} \end{bmatrix} = 0 \, \forall k \in (N_{ng} - 1) \, ; \forall ij \in N_c; \forall km \in N_p. \tag{2.34}$$

The set of nonlinear equations described above is defined for all the nodes $N_{ng}$ except the slack, as well as for all the compressor $N_c$ and pipelines $N_p$ in the gas network, where $\triangle G_d^{km}$ corresponds to the dynamic homogeneous Equation (2.13) which is a function of $x_{ng}^{t-1}$, to obtain the initial values $x^t$. If these values are not available for the initialization, they can be obtained through the steady-state formulation presented in the previous section; this strategy has been used during the development of this thesis. Lastly, this set of nonlinear equations is solved through the Newton-Rapshon's method as described in the last section, but with the Jacobian matrix for the dynamic formulation given by the Equation (2.35) and the vector of states (2.36)

$$J_{ng} = \begin{bmatrix} \frac{\partial \triangle G}{\partial \Pi} & \frac{\partial \triangle G}{\partial G_p^{out}} & \frac{\partial \triangle G}{\partial BHP} & \frac{\partial \triangle G}{\partial \tau} & \frac{\partial \triangle G}{\partial G_c} \\ \frac{\partial \triangle G_d}{\partial \Pi} & \frac{\partial \triangle G_d}{\partial G_p^{out}} & \frac{\partial \triangle G_d}{\partial BHP} & \frac{\partial \triangle G_d}{\partial \tau} & \frac{\partial \triangle G_d}{\partial G_c} \\ \frac{\partial \triangle R}{\partial \Pi} & \frac{\partial \triangle R}{\partial G_p^{out}} & \frac{\partial \triangle R}{\partial BHP} & \frac{\partial \triangle R}{\partial \tau} & \frac{\partial \triangle R}{\partial G_c} \\ \frac{\partial \triangle BHP}{\partial \Pi} & \frac{\partial \triangle BHP}{\partial G_p^{out}} & \frac{\partial \triangle BHP}{\partial BHP} & \frac{\partial \triangle BHP}{\partial \tau} & \frac{\partial \triangle BHP}{\partial G_c} \\ \frac{\partial \triangle \tau}{\partial \Pi} & \frac{\partial \triangle \tau}{\partial G_p^{out}} & \frac{\partial \triangle \tau}{\partial BHP} & \frac{\partial \triangle \tau}{\partial \tau} & \frac{\partial \triangle \tau}{\partial G_c} \end{bmatrix} \tag{2.35}$$

$$x_{ng} = \begin{bmatrix} \Pi_{1\rightarrow(N_{ng}-1)} \\ G_d^{out\ 1\rightarrow N_p} \\ BHP^{1\rightarrow N_c} \\ \tau^{1\rightarrow N_c} \\ G_c^{1\rightarrow N_c} \end{bmatrix}. \tag{2.36}$$

The iterative process is performed until the mismatch is reduced below a certain tolerance, and in such a case the final value of the vector $x_{ng}^*$ represents the solution for the natural gas network for the corresponding subperiod of analysis. The operation conditions for loads and sources in the next subperiod of analysis are then included, and the process is repeated to obtain the solution for the $t+1$ subperiod. Finally, this process is repeated for the entire period of study.

### 2.7.1 Study Case

In this section the nodal formulation is applied to the three nodes benchmark system presented in [Tao 1998], which consists of three pipelines, two loads and one source. The detailed information of this gas network is described in Appendix A, and the one-line diagram of this gas network is presented in Figure 2.4.

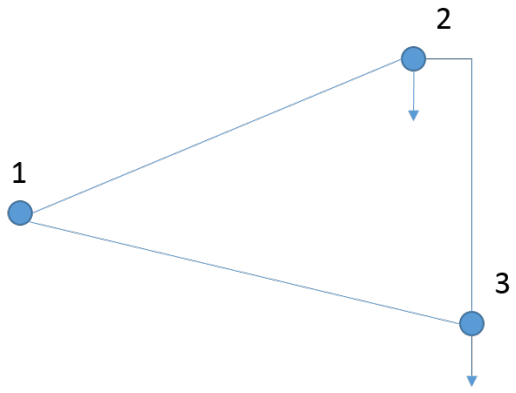


Figure 2.4: Three nodes natural gas benchmark system.

In this study case, node 1 is considered as the slack node with a reference pressure

of 5 MPa, while loads at nodes 2 and 3 have the cyclic load shown on Figure 2.5. The results of nodal pressure in nodes 2 and 3 calculated by the static and the dynamic models presented in Sections 2.6 and 2.7, respectively, are reported in Figure (2.6).

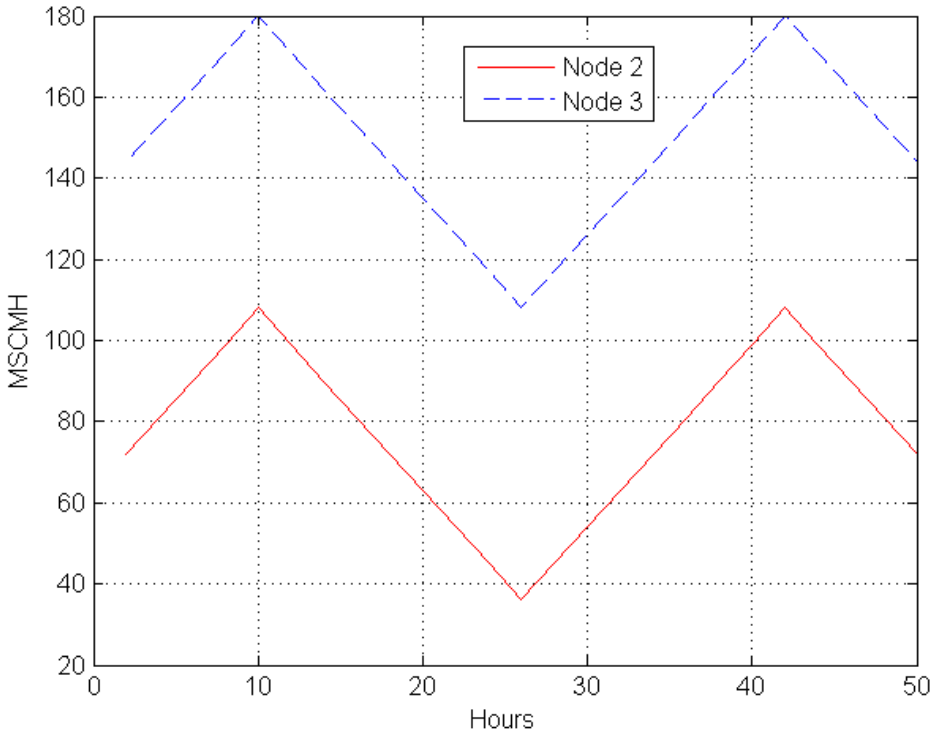


Figure 2.5: Load in the three nodes benchmark system.

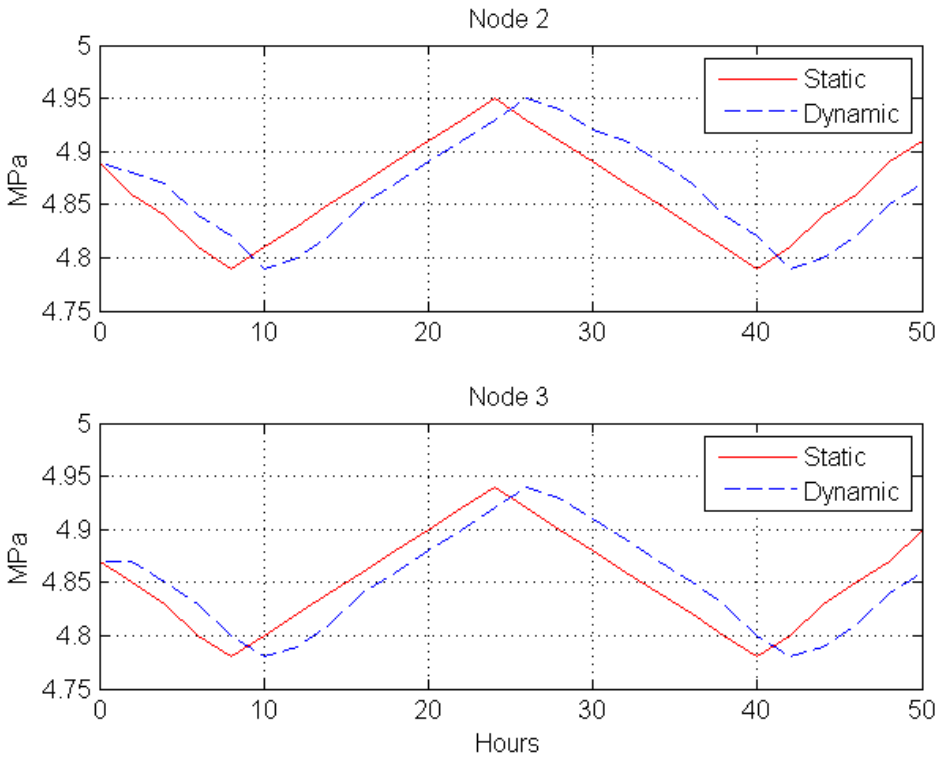


Figure 2.6: Nodal pressure static and dynamic models.

Clearly from Figure 2.6, a slower change in nodal pressure in the dynamic model takes place with respect to the static formulation. This effect is associated with the physical characteristics of the pipelines and gas flowing in the system: the longer the pipelines, the slower the dynamic behavior.

## 2.8 Conclusions and Remarks

The strategies and techniques employed for the analysis of electric power systems have been applied to the modeling and analysis of natural gas networks operating in either steady or dynamic states. The importance of the environmental temperature in the gas network design and operation has been presented in this chapter, examining its effect in the efficiency of the natural gas network and the assessment of hydrates formation inside the pipelines. The two different models for pipelines presented in this chapter have different applications which basically relies on the analysis of a single time-shot

gas flow analysis or the evolution of the state variables of the system for a specific time period of study.

In this chapter the basic configuration of natural gas infrastructures has been described as well as the static and dynamic models with their corresponding applications, the function of each component in the network and the assessment of gas loads and sources, these characteristics of the gas system will be analyzed deeply during the analysis of the interaction between primary energy networks in the following chapters of this work.

# Chapter 3

# A Steady-State Interdependency Analysis of Natural Gas and Electricity Coupled Networks

## 3.1 Introduction

The restructuring of energy markets has increased the concern about the existing interdependency between the primary energy supply and electricity networks, which are analyzed traditionally as independent systems. The aim of this chapter is focused on an integrated formulation for the steady-state analysis of electricity and natural gas coupled systems considering the effect of temperature in the natural gas system operation and a distributed slack node technique in the electricity network. A general approach is described to execute a single gas and power flow analysis in a integral framework based on the Newton-Raphson's formulation.

## 3.2 Electricity System Formulation

The AC power flow model is used to represent the electricity network, which is already well documented in [Acha 2004]. The steady-state operation of a power system is for-

mulated by stipulating that at each system's node the power injected by generators, the power demanded by loads and powers exchanged through the transmission elements connected to the node must add up to zero. This applies for both active and reactive powers and the mathematical expressions representing this balance are termed *mismatch power flow equations*. These equations take the following form at the $i^{th}$ node of the network, [Acha 2004].

$$\triangle P_i = P^i_{gen} - P^i_{load} - P^i_{cal} = 0, \qquad \forall\, i \in N_e \tag{3.1}$$

$$\triangle Q_i = Q^i_{gen} - Q^i_{load} - Q^i_{cal} = 0, \qquad \forall\, i \in (N_e - N_{PV}) \tag{3.2}$$

where:

$$P^i_{cal} = \sum_{j \in i} \left\{ V_i^2 G_{ii} + V_i V_j \left[ G_{ij} cos\left(\theta_i - \theta_j\right) + B_{ij} sin\left(\theta_i - \theta_j\right) \right] \right\} \tag{3.3}$$

$$Q^i_{cal} = \sum_{j \in i} \left\{ -V_i^2 B_{ii} + V_i V_j \left[ G_{ij} sin\left(\theta_i - \theta_j\right) - B_{ij} cos\left(\theta_i - \theta_j\right) \right] \right\} \tag{3.4}$$

The equilibrium point of the power system is obtained by solving the set of Equations (3.1) and (3.2) for the voltage magnitudes and phase angles at all nodes in the network, $[x_e] = [V,\, \theta]$, by knowing the generations and loads injected in the system.

The active and reactive power flows throughout the transmission elements embedded at the $i^{th}$ node are then determined in accordance to Equations (3.3) and (3.4). Besides, since the power transmission losses cannot be calculated without knowing the power flow through the transmission elements, one of the generator nodes is designated to pick up this slack in power generation, which is referred as the *slack node*, with its voltage magnitude and phase angle assumed to be known. Since the value of the phase angle at the slack node remains constant, this value becomes the reference against which all other voltage phase angles in the system are measured.

In the real operation of the electric power systems, the losses associated with the transmission elements are distributed over all the online generators. Hence, in order to overcome the shortcoming of only adjusting the active power of a single slack generator to achieve a total active power balance, the concept of distributed slack nodes is used in this work, [Guoyu 1985]. In this case, the active power output of a selected number of generators is regulated during the power flow solution, based on their assigned participation factors, to supply the generation required to satisfy the entire active power imbalance in the system. Hence, the variable active power of regulating generators is defined as:

$$P^{i}_{gen} = P^{i0}_{gen} + k^{i}_{gen} \triangle P_{gen}, \qquad \forall\, i \in N_e \tag{3.5}$$

$$\sum_{i \in N_{rg}} k^{i}_{gen} = 1 \tag{3.6}$$

where $\triangle P_{gen}$ is the unknown additional generation of active power required to satisfy the existing imbalance between the set-point system generation and the total active power demand plus the transmission losses. On the other hand, all the corresponding participation factor must add up to one in order to distribute the existing imbalance between the specified regulating generators, as expressed in Equation (3.6).

In this approach [Guoyu 1985], the slack node is considered as any of the other system's nodes with corresponding active and reactive power mismatch equations, and the reference voltage phase angle can be arbitrarily selected at any of the system's nodes. In addition to the standard classification of system nodes into: generator voltage-controlled *(PV)*, generator voltage-uncontrolled *(PQ)* and load *(PQ)* nodes [Acha 2004], two new nodes types are defined: a generator *(PV)* node with variable active power generation and a generator *(PQ)* node with variable power generation. It is important to take into account that in these nodes, the active power output constraints imposed on

each generator correspond to the generator's own operational limit and to the amount of primary energy available for power generation. If any regulating generators reaches one of its active power generation limits, its active power output is fixed at the offended limit for the remaining of the power flow solution process, and the active power balance of the system is provided by the rest of online regulating generators. On the other hand, even though the reactive power mismatch Equation (3.2) of a *(PV)* node is not considered in the formulation, it is solved at each iterative step to assess whether or not the generator reactive power is within limits. If the generator cannot provide the necessary reactive power support to constraint the voltage magnitude at the specified value, then the reactive power is fixed at the violated limit and the voltage magnitude is freed. Lastly, the unknown vector of state variables that determine the power system's equilibrium point is now given by $[x_e] = [V, \theta, \triangle P_{gen}]$, where $V \in \mathbb{R}^{(N_e - N_{pv})}$, $\theta \in \mathbb{R}^{(N_e - 1)}$ and $\triangle P_{gen} \in \mathbb{R}$.

## 3.3 Heat Rate Curves

The energy conversion process on thermal-generators is characterized by the efficiency of the process, which corresponds to 40~45% for coal-fired generators and 50~55% for gas-fired generators considering that the most advanced technologies are used in these fossil fuel power plants, [Breeze 2005]. The efficiency of the process is associated with how much fuel is necessary to produce a certain amount of electric power, and is given by the relation of the energy output over the energy input. On the other hand, the heat rate curve corresponds to the ratio of values of fuel to values of generation: is the ration of the input energy to the output energy scaled by MWs. Figure 3.1 shows the relationship between the heat rate and efficiency curves of a typical combined cycle plant. In this context, all generators are designed to reach their maximum efficiency at their corresponding rated capacity.

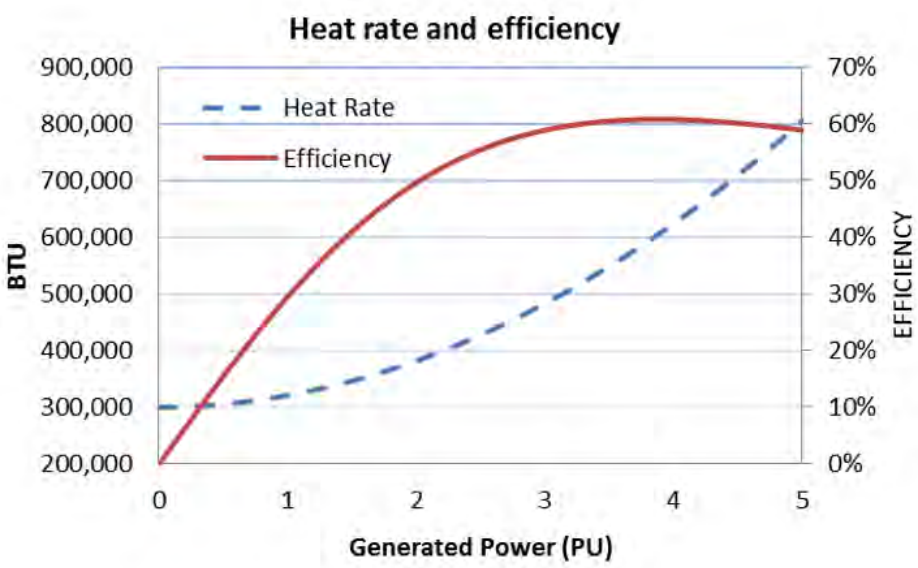


Figure 3.1: Heat rate curve.

The heat rate curve is typically represented by a polynomial expression of second order, which is a function of active power output in the electrical generator as given by

$$HR^i = \alpha_g^i + \beta_g^i P_{gen}^i + \gamma_g^i \left(P_{gen}^i\right)^2 \tag{3.7}$$

The use of Equation (3.7) permits to determine the amount of calorific power necessary to produce the active power output of each generator, which in turn is used to determine the amount of natural gas or coal required to provide this calorific power. This amount is computed by Equation (3.8), and represents the quantity of fossil-fuel extracted from the $k^{th}$ node in the primary energy network by the electric generator to deliver active output power to the $i^{th}$ node of the electric system

$$G_{lk}^i = \frac{HR^i}{GHV} \tag{3.8}$$

The parameter $GHV$ in (3.8) represents the gross heating value per volume unit of the corresponding primary energy, and for purposes of this work the values of 1150 BTU/ft3 and 12500 BTU/lb have been considered for natural gas and coal, respectively.

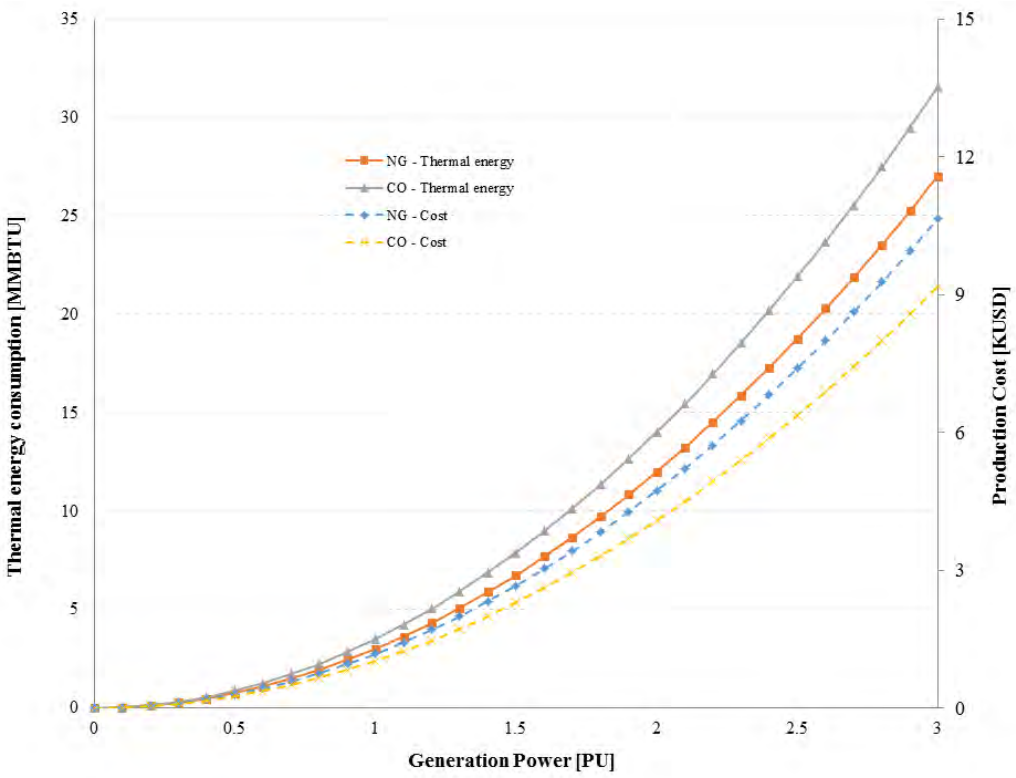


Figure 3.2: Heat rate vs. cost curves.

In the context of this chapter, the relationship between the natural gas and electricity systems is provided by the gas-fired turbines' generators, which act as energy converters. This coupling is mathematically formulated by Equation (3.7), which represents the efficiency conversion of the energy contained in natural gas at the $k^{th}$ node into electrical energy injected at the $i^{th}$ node of the electrical network.

Additionally, the gas flow required for the energy demanded by the heat rate curve is computed by Equation (3.8). Note that the gas consumed by a gas-fired turbine is a function of the active power generated by the unit and the natural gas available at the extraction node.

## 3.4 Unified Gas and Power Flow Solution Considering Distributed Slack Generators.

The integrated gas and power flow formulation of the natural gas and electricity systems is obtained by combining the stated flow models considering the link between both networks through gas-fired power plants connected to gas pipelines and compressors using electrical energy. Hence, the set of nonlinear equations that has to be solved for the state variables of both networks is given by

$$f = \begin{bmatrix} \Delta G \\ \Delta T \\ \Delta BHP \\ \Delta R \\ \Delta \tau \\ \triangle P \\ \triangle Q \end{bmatrix} = 0 \tag{3.9}$$

where $\triangle G$ corresponds to the gas nodal balance according to the Equation (2.26) defined for $\mathbb{R}^{(N_{ng}-1)}$, $\triangle T$ the nodal gas temperature by (2.27) for $\mathbb{R}^{(N_{ng}-1)}$; $\triangle BHP$, $\triangle R$ and $\triangle \tau$ from Equations (2.28) - (2.30) for energy consumption, compression ratio and gas extracted by compressors employed in the natural gas network, respectively, and defined for $\mathbb{R}^{N_c}$. As mentioned in section 2.6, the term $\tau$ associated with the gas extracted by compressors in Equation (2.26) can be expressed as a function of the state variable $BHP$, reducing the set of nonlinear equations to the following expression:

$$f = \begin{bmatrix} \triangle G \\ \triangle T \\ \triangle BHP \\ \triangle R \\ \triangle P \\ \triangle Q \end{bmatrix} = 0 \tag{3.10}$$

Besides, $\triangle P$ and $\triangle Q$ defined by Equations (3.1) and (3.2) with a domain of $\mathbb{R}^{N_e}$ and $\mathbb{R}^{(N_e - N_{PV})}$, respectively, represent the active and reactive power balance in the electric power system. Note that an active power balance for every node in the electric network is required considering the slack distributed formulation; in this case the term $P^i_{gen}$ in Equation (3.1) is substituted by the following expression:

$$P^i_{gen} = P^{i0}_{gen} + k^i_{gen} \triangle P_{gen} \; \forall i \in N_e \tag{3.11}$$

where $P^{i0}_{gen}$ correspond to the base case condition of the $i^{th}$ electric generator, and $\triangle P_{gen}$ describes the total imbalance existent in the electric network that must be distributed between the electric generators in accordance to their participation factor defined by the parameter $k^i_{gen}$. It is important that in order to distribute totally the imbalance the following expression must be satisfied:

$$\sum_{i \in N_e} k^i_{gen} = 1 \tag{3.12}$$

The vector of total state variables is defined by $[x] = [x_{ng}, x_e]^t = [\Pi, T, BHP, G_c, \theta, V, \triangle P_{gen}]^t$ with their corresponding domains: $\mathbb{R}^{(N_{ng}-1)}$, $\mathbb{R}^{(N_{ng}-1)}$, $\mathbb{R}^{(N_c)}$, $\mathbb{R}^{(N_c)}$, $\mathbb{R}^{(N_e-1)}$, $\mathbb{R}^{(N_e - N_{PV})}$, $\mathbb{R}^1$.

The proposed integral solution approach consists of applying the Newton's method to provide an approximate solution to the total set of equality constraints defined in Equation (3.10), by solving for $\triangle x$ in the linear problem $J^l \triangle x^l = -f\left(x^l\right)$, where $J$ is known as the Jacobian matrix and is given in expanded form by (3.13). For given initial values of $\left[x^l\right] = \left[x^l_{ng}, x^l_e\right]^t$, the method updates the solution, $\left[x^{l+1}\right] = \left[x^{l+1}_{ng} = x^l_{ng} + \triangle x^l_{ng},\; x^{l+1}_e = x^l_e + \triangle x^l_e\right]$, at each iteration until a pre-defined tolerance is satisfied or a maximum number of iterations is reached.

$$J = \left[\begin{array}{cccc|ccc} \frac{\partial \triangle G}{\partial \Pi} & \frac{\partial \triangle G}{\partial T} & \frac{\partial \triangle G}{\partial BHP} & \frac{\partial \triangle G}{\partial G_c} & 0 & 0 & \frac{\partial \triangle G}{\partial \triangle P_{gen}} \\ \frac{\partial \triangle T}{\partial \Pi} & \frac{\partial \triangle T}{\partial T} & 0 & \frac{\partial \triangle T}{\partial G_c} & 0 & 0 & 0 \\ \frac{\partial \triangle BHP}{\partial \Pi} & \frac{\partial \triangle BHP}{\partial T} & \frac{\partial \triangle BHP}{\partial BHP} & \frac{\partial \triangle BHP}{\partial G_c} & 0 & 0 & 0 \\ \frac{\partial \triangle R}{\partial \Pi} & 0 & 0 & 0 & 0 & 0 & 0 \\ \hline 0 & 0 & \frac{\partial \triangle P}{\partial BHP} & 0 & \frac{\partial \triangle P}{\partial \theta} & \frac{\partial \triangle P}{\partial V} & \frac{\partial \triangle P}{\partial \triangle P_g} \\ 0 & 0 & 0 & 0 & \frac{\partial \triangle Q}{\partial \theta} & \frac{\partial \triangle Q}{\partial V} & 0 \end{array}\right] \tag{3.13}$$

The coupling terms between the natural gas and electric nonlinear equations correspond to the change of nodal active power balance due the electricity extraction by moto-compressors $\frac{\partial \triangle P}{\partial BHP}$ and the nodal gas balance due the gas extracted by gas-fired generators $\frac{\partial \triangle G}{\partial \triangle P_{gen}}$, which is a function of the active power imbalance existing in the electric network.

The attractiveness of using Newton's method is that it arrives at the solution with local quadratic convergence regardless of the network size if all state variables involved in the study are suitably initialized and the Jacobian matrix is non singular at the solution point [Ortega 2000].

For the electric power system, the voltage magnitudes are initialized at 1 p.u. at all uncontrolled voltage magnitude nodes, while the controlled $PV$ nodes are initialized at specified values that remain constant throughout the iterative solution if no generator reactive power limits are violated. The initial voltage phase angles are selected to be 0 at all buses [Sttot 1971]. The unknown additional generation of active power $\triangle P_{gen}$ is initialized in zero. Finally, guides for initial conditions for the state variables of the natural gas system are given in Section 2.6.

## 3.5 Case Studies Considering Distributed Slack Generators

The suitability of the proposed approach for conducting steady-state flow studies of an electric power system coupled with a natural gas network is reported in this section.

### 3.5.1 Belgian Gas Network Coupled with the IEEE-14 Bus System

The proposed approach is applied to analyze an integrated gas-electricity network composed by the Belgian gas network [Wolf 2000], shown in Figure 3.3, and by the IEEE-14 bus test system ["Power Systems Test Case Archive", http://www.ee.washington.edu/research/pstca/]. The 20-nodes natural gas network is composed of eight gas non-electric loads, seven sources, 24 pipelines and two compressors driven by an external energy source, as shown in Tables 3.1 and 3.2. The pipelines' constants are calculated according to the Equation (2.2) and are given in Table 3.1. The node referred to as Zeebugge in Table 3.2 is considered the slack node. On the other hand, the electricity network has the electric energy demand reported in Table 3.3, and it is assumed there are two gas-fired generators at nodes 2 and 3 which are supplied from nodes 4 and 12 of the gas network, respectively. For the purpose of analysis, the gas and power flow solution was firstly obtained considering the gas temperature constant at 506.7 °R at all natural gas nodes and assuming the following two cases of slack nodes in the electricity network: 1.a) a single slack node and 1.b) distributed slack nodes. In the former, generator 2 is selected as the single slack generator to produce sufficient power for any unmet system load and for system losses, while holding all other active power generation at the set values reported in [Unsihuay 2007]. This single slack node option is simply obtained by setting $k^2_{gen} = 1$ with all other participation factors $k^i_{gen} = 0$, $\forall\, i = 1,\ 3,\ 6$, as indicated in the second row of Table 3.4. In the latter, all generators regulate their active power according to the assigned participation factors reported in the third row of Table 3.4. A second set of flow analyzes in both networks

is also performed considering the slack node options mentioned above but supposing a constant gas temperature of 515.0 °R only at those nodes where compressors and gas sources are connected, while for the rest of nodes the temperature is considered a state variable to be computed during the iterative solution process assuming an environmental temperature of 500°R and a heat transfer coefficient of 0.025 $BTU/ft^2$ for every pipeline of the network. These cases of studies are referred to as 1.c) and 1.d) for the single slack node and distributed slack nodes, respectively.

The state variables were initialized according to the guidelines given in Section (2.6) for all case of studies, performing two simulations for each case to consider the initialization of $BHP$ at null values and at values computed by (2.14) and (2.15).

For each case, the same gas flow solutions were obtained independently of the $BHP$ initialization. For cases 1.a, 1.b, 1.c and 1.d the solutions were obtained in 7, 10, 7 and 10 iterations, respectively, to a mismatch tolerance of $10^{-6}$ in the gas network and a $10^{-12}$ in the electricity network. From a physical point of view and according to the proposed formulation, a tolerance of $10^{-6}$ in the natural gas state variables represents a nodal mismatch balance of mSCF, and in order to set a comparable framework, a tolerance of $10^{-12}$ in the electrical state variables corresponds to a nodal mismatch balance of 100 mVA.

The results obtained for all cases are reported in Tables 3.1 and 3.2 for natural gas flow in pipelines and natural gas nodal variables, respectively; the electric network results are shown in Table 3.3. For purposes of validation of the proposed approach, the results obtained in case 1.a are compared with the optimal equilibrium point reported in [Unsihuay 2007], both being practically the same results. Note that in the formulation proposed in [Unsihuay 2007] both networks are solved sequentially, compressors are not included explicitly in the mathematical formulation and the gas temperature is always considered constant. In the sequential solution, Newton's method is used to solve the power flow equations of the electric power system, and an interior-point linear programing approach is used to solve the gas flow problem.

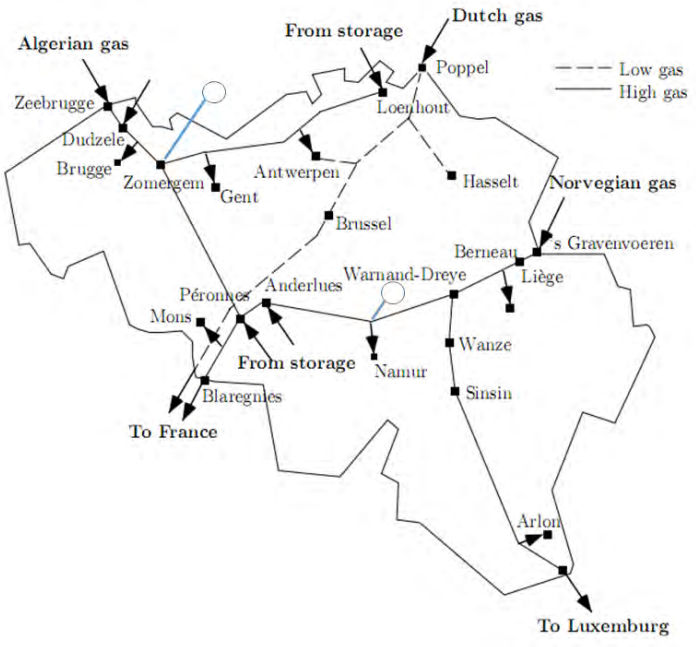


Figure 3.3: Belgium natural gas transmission system.

Table 3.1: Natural gas flows at pipelines.

| Pipeline | $C_{km}$ (SCF/PSIA) | From | To | Gas flow ($SCF/hour$) | | | |
|---|---|---|---|---|---|---|---|
| | | | | *1.a)* | *1.b)* | *1.c)* | *1.d)* |
| 1 | 6566436 | 1 | 2 | 10.80 | 10.81 | 10.80 | 10.81 |
| 2 | 6566436 | 1 | 2 | 10.80 | 10.81 | 10.80 | 10.81 |
| 3 | 4912482 | 2 | 3 | 15.62 | 15.62 | 15.62 | 15.62 |
| 4 | 4912482 | 2 | 3 | 15.62 | 15.62 | 15.62 | 15.62 |
| 5 | 4326324 | 3 | 4 | 25.47 | 25.49 | 25.47 | 25.49 |
| 6 | 240319 | 5 | 6 | 0.562 | 0.561 | 0.562 | 0.562 |
| 7 | 1175149 | 6 | 7 | -5.373 | -5.373 | -5.373 | -5.373 |
| 8 | 764054 | 7 | 4 | -13.10 | -13.10 | -13.10 | -13.10 |
| 9 | 1728699 | 4 | 14 | 11.67 | 11.67 | 11.67 | 11.67 |
| 10 | 1144991 | 8 | 9 | 26.76 | 26.76 | 26.76 | 26.76 |
| 11 | 123179 | 8 | 9 | 2.879 | 2.879 | 2.879 | 2.879 |
| 12 | 4907626 | 9 | 10 | 19.75 | 19.75 | 19.75 | 19.75 |
| 13 | 2457651 | 9 | 10 | 9.892 | 9.892 | 9.892 | 9.892 |
| 14 | 3641178 | 10 | 11 | 12.45 | 12.45 | 12.45 | 12.45 |
| 15 | 2285681 | 10 | 11 | 7.820 | 7.820 | 7.820 | 7.820 |
| 16 | 2869666 | 11 | 12 | 17.75 | 17.75 | 17.75 | 17.75 |
| 17 | 3497039 | 12 | 13 | 14.028 | 14.022 | 14.028 | 14.022 |
| 18 | 5874893 | 13 | 14 | 19.31 | 19.30 | 19.31 | 19.30 |
| 19 | 3500118 | 14 | 15 | 33.05 | 33.05 | 33.05 | 33.05 |
| 20 | 2491576 | 15 | 16 | 22.97 | 22.97 | 22.97 | 22.97 |
| 21 | 109941 | 11 | 17 | 2.522 | 2.522 | 2.522 | 2.522 |
| 22 | 160430 | 17 | 18 | 2.522 | 2.522 | 2.522 | 2.522 |
| 23 | 304984 | 18 | 19 | 2.522 | 2.522 | 2.522 | 2.522 |
| 24 | 204329 | 19 | 20 | 2.823 | 2.823 | 2.823 | 2.823 |

Table 3.2: Natural gas supply, demand and nodal pressures.

| Node | Name | Source | | Demand | Electric | | 1.a) | 1.b) | 1.c) | | 1.d | |
|---|---|---|---|---|---|---|---|---|---|---|---|---|
| | | (*MSCF/hr*) | | (*MSCF/hr*) | (*MSCF/hr*) | | Press | Press | Press | Temp | Press | Temp |
| | | *1.a) / 1.c)* | *1.b) / 1.d)* | | *1.a) / 1.c)* | *1.b) / 1.d)* | *(PSIA)* | *(PSIA)* | *(PSIA)* | $^{\circ}R$ | *(PSIA)* | $^{\circ}R$ |
| 1 | Zeebugge | 21.613 | 21. 6256 | 0.000 | 0.000 | 0.000 | 942.7 | 942.7 | 942.7 | 515 | 942.7 | 515 |
| 2 | Dudzele | 9.632 | 9.632 | 0.000 | 0.000 | 0.000 | 942.0 | 942.0 | 942.0 | 515 | 942.0 | 515 |
| 3 | Brugge | 0.000 | 0.000 | 5.7666 | 0.000 | 0.000 | 939.2 | 939.2 | 939.2 | 514.69 | 939.2 | 514.69 |
| 4 | Zomergem | 0.000 | 0.000 | 0.000 | 0.6973 | 0.7037 | 929.8 | 929.8 | 929.7 | 513.65 | 929.6 | 513.65 |
| 5 | Loenhout | 0.5620 | 0.5620 | 0.000 | 0.000 | 0.000 | 841.2 | 841.2 | 840.8 | 515 | 840.8 | 515 |
| 6 | Antwerpen | 0.000 | 0.000 | 5.9358 | 0.000 | 0.000 | 839.6 | 839.6 | 839.1 | 504.80 | 839.1 | 504.80 |
| 7 | Gent | 0.000 | 0.000 | 7.7339 | 0.000 | 0.000 | 845.9 | 845.9 | 845.4 | 504.44 | 845.4 | 504.44 |
| 8 | Voeren | 29.6466 | 29.6466 | 0.000 | 0.000 | 0.000 | 782.2 | 782.1 | 785.1 | 515 | 785.0 | 515 |
| 9 | Berneau | 0.000 | 0.000 | 0.000 | 0.000 | 0.000 | 942.7 | 942.7 | 942.7 | 515 | 942.7 | 515 |
| 10 | Liege | 0.000 | 0.000 | 9.3672 | 0.000 | 0.000 | 938.3 | 938.3 | 938.3 | 514.51 | 938.2 | 514.51 |
| 11 | Warnand | 0.000 | 0.000 | 0.000 | 0.000 | 0.000 | 935.2 | 935.1 | 935.0 | 514.16 | 935.0 | 514.16 |
| 12 | Namur | 0.000 | 0.000 | 3.1194 | 0.6094 | 0.6159 | 924.7 | 924.7 | 924.5 | 513.00 | 924.4 | 513.00 |
| 13 | Anderlues | 5.2824 | 5.2824 | 0.000 | 0.000 | 0.000 | 920.3 | 920.3 | 920.0 | 515 | 920.0 | 515 |
| 14 | Peronnes | 2.0703 | 2.0703 | 0.000 | 0.000 | 0.000 | 917.3 | 917.3 | 917.0 | 515 | 916.9 | 515 |
| 15 | Mons | 0.000 | 0.000 | 10.0764 | 0.000 | 0.000 | 892.4 | 892.3 | 891.6 | 512.23 | 891.6 | 512.23 |
| 16 | Blaregnies | 0.000 | 0.000 | 22.978 | 0.000 | 0.000 | 867.9 | 867.9 | 866.9 | 509.53 | 866.9 | 509.53 |
| 17 | Wanze | 0.000 | 0.000 | 0.000 | 0.000 | 0.000 | 779.7 | 779.6 | 781.0 | 497.33 | 781.0 | 497.33 |
| 18 | Sinsin | 0.000 | 0.000 | 0.000 | 0.000 | 0.000 | 856.2 | 856.2 | 859.0 | 515 | 859.0 | 515 |
| 19 | Arlon | 0.3016 | 0.3016 | 0.000 | 0.000 | 0.000 | 835.7 | 835.7 | 838.3 | 515 | 838.2 | 515 |
| 20 | Petange | 0.000 | 0.000 | 2.8237 | 0.000 | 0.000 | 775.7 | 775.6 | 777.9 | 508.39 | 777.8 | 508.39 |
| TOTAL | | 69.108 | 69.121 | 67.801 | 1.306 | 1.319 | | | | | | |

Table 3.3: Electricity supply and demand.

| Node | *Generation (MW/MVAR)* | | | | *Demand* | |
|---|---|---|---|---|---|---|
| | *1.a) / 1.c)* | | *1.b) / 1.d)* | | *(MW/MVAR)* | |
| | *P* | *Q* | *P* | *Q* | *P* | *Q* |
| 1 | 63.43 | 21.89 | 61.19 | 22.49 | 0 | 0 |
| 2 | 94.79 | 4.29 | 95.66 | 3.84 | 21.7 | 12.7 |
| 3 | 82.84 | -6.44 | 83.71 | -6.73 | 94.2 | 19 |
| 4 | 0 | 0 | 0 | 0 | 47.8 | -3.9 |
| 5 | 0 | 0 | 0 | 0 | 7.6 | 1.6 |
| 6 | 21.64 | 7.84 | 22.07 | 7.76 | 11.2 | 7.5 |
| 7 | 0 | 0 | 0 | 0 | 0 | 0 |
| 8 | 0 | 17.35 | 0 | 17.35 | 0 | 0 |
| 9 | 0 | 0 | 0 | 0 | 29.5 | 16.6 |
| 10 | 0 | 0 | 0 | 0 | 9 | 5.8 |
| 11 | 0 | 0 | 0 | 0 | 3.5 | 1.8 |
| 12 | 0 | 0 | 0 | 0 | 6.1 | 1.6 |
| 13 | 0 | 0 | 0 | 0 | 13.5 | 5.8 |
| 14 | 0 | 0 | 0 | 0 | 14.9 | 5 |
| TOTAL | 262.71 | 44.94 | 262.67 | 44.72 | 259.0 | 73.5 |

In Figure 3.4, the Belgium natural gas networks has been represented with the gas flow values corresponding to the scenario *1.a* of this study case.

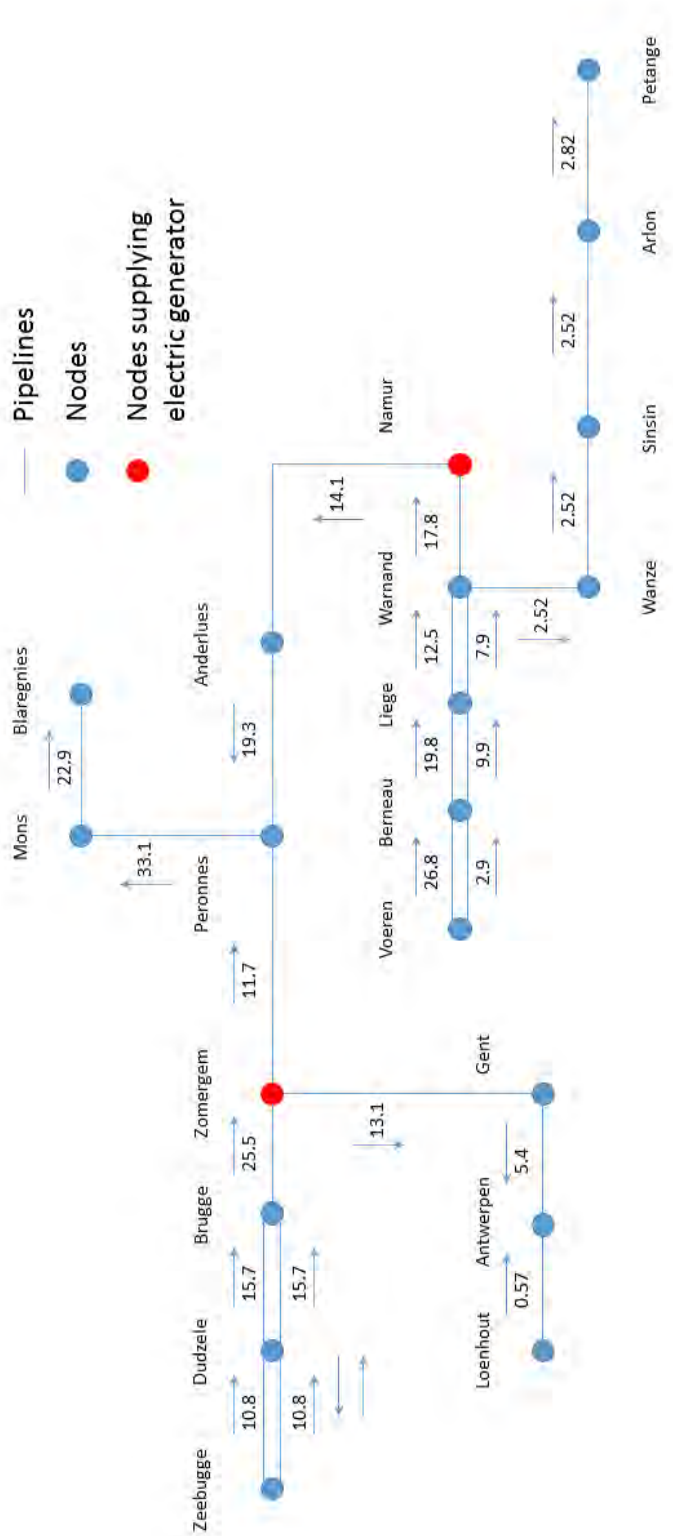


Figure 3.4: Belgium natural gas network, representation of case *1.a*

Table 3.4: Participation factors of electric generators.

| Nodes | 1 | 2 | 3 | 6 |
|---|---|---|---|---|
| Single slack node | 0.0 | 1.0 | 0.0 | 0.0 |
| Distributed slack node | 0.5 | 0.2 | 0.2 | 0.1 |

Lastly, the use of the chart proposed by Carroll [Carroll 2003] shows that for cases *1c* and *1d*, three nodes (6, 7, and 17) of the gas network have a relation of nodal pressure and temperature within the unsafe operating zone with a risk of hydrate formation in the inner-wall of pipelines, as shown in Figure 3.5. Based on these observations and in accordance to section 2.5, reducing the level of pressure along the network in order to operate in the feasibility region free of hydrate formation is necessary.

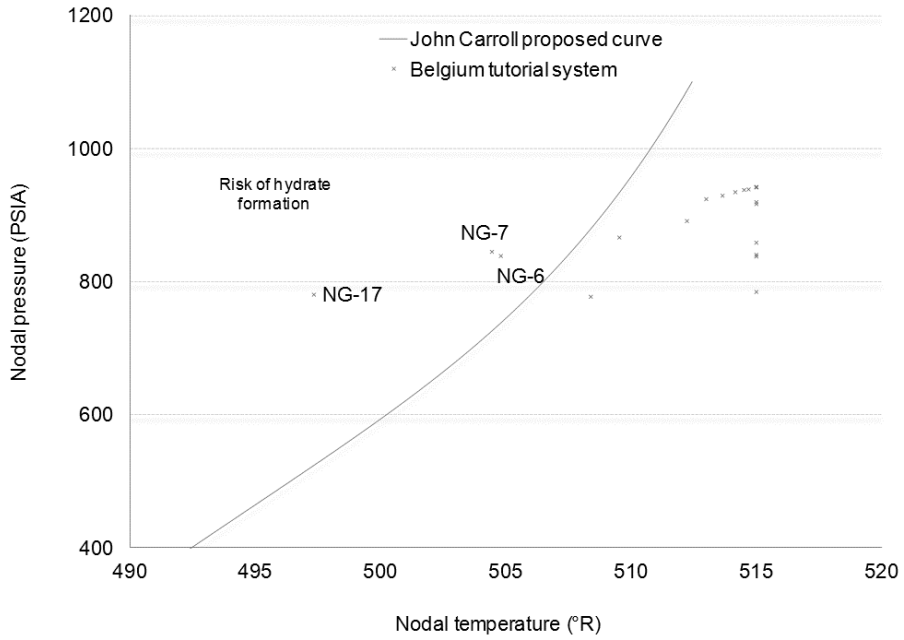


Figure 3.5: Operation condition of the natural gas network for case *1.c*.

Figure 3.6 shows the convergence process for each energy network in the case *1.a*, in this figure the faster convergence in the electric networkwith respect to the gas system is observed.

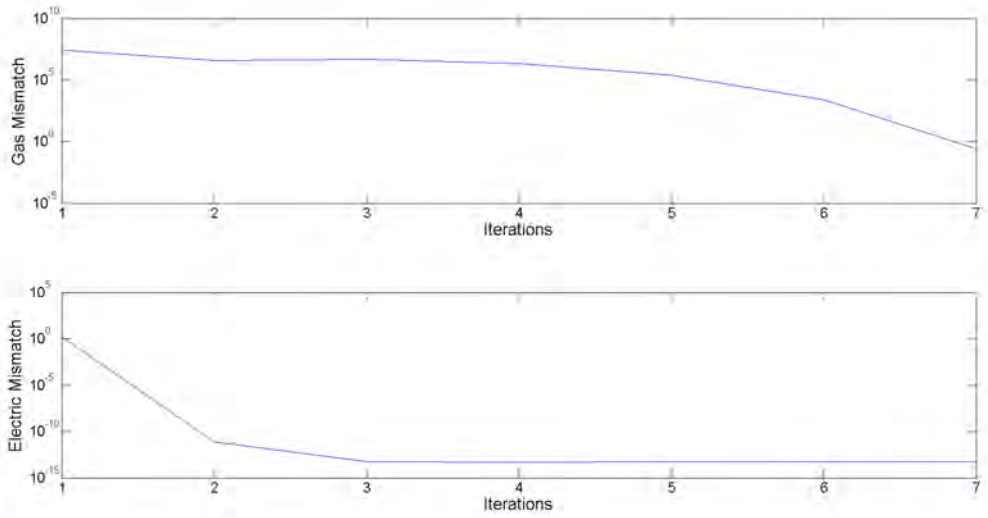


Figure 3.6: Convergence process in energy network for case *1.a*.

### 3.5.2 15-Nodes Natural Gas and IEEE-118 Bus Test Systems

The analyzed energy network consists of the 54-machine, 118-bus IEEE electric power system ["Power Systems Test Case Archive", http://www.ee.washington.edu/research/pstca/] and a 15-nodes natural gas network [An 2003]. The networks are coupled via eight gas-fired generators as shown in Figure 3.7. The gas network has five gas non-electric loads, two sources and four compressors. Two compressors are driven by gas turbines, and the gas is tapped from the inlet node of the compressor station, while the other two compressors are driven by electric motors supplied from the electric network. The node NG-1 serves as the slack node in the gas network. The parameters of the heat rate curves are given in Table 3.5, while the pipelines' and compressors' data are reported in Appendix A.

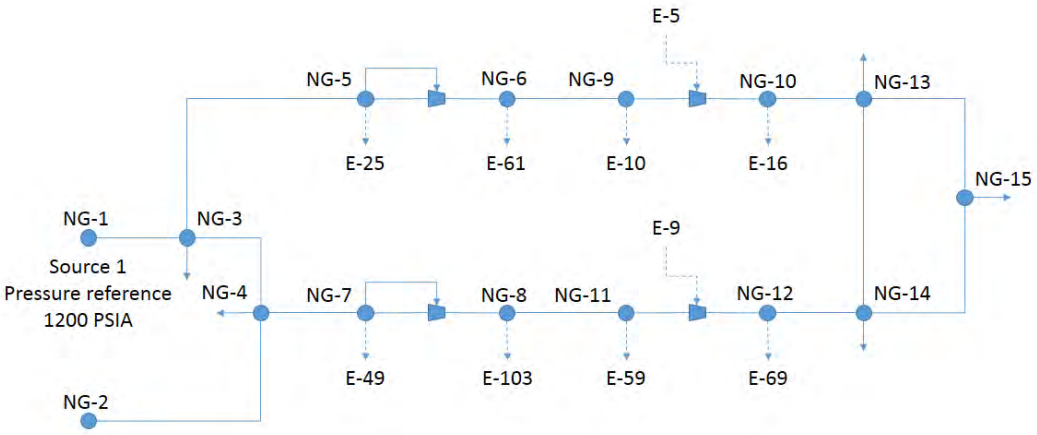


Figure 3.7: Natural gas and electricity coupled networks.

In order to assess the temperature effect on the equilibrium point associated with the natural gas network, the following two scenarios were simulated: i) The first scenario assumes a constant temperature of 550°R at all natural gas nodes and considers two types of slack nodes in the electrical network, 2.a) a single slack node as defined in the second row of Table 3.6 and 2.b) distributed slack nodes with participation factors as reported in the third row of Table 3.6; ii) The gas temperature is considered as a state variable to be computed during the iterative solution, except at nodes of compressors and gas sources where a constant gas temperature is set at 550°R. In this second scenario, an environmental temperature of 500°R and a heat transfer coefficient of 0.025 $BTU/ft^2$ for every pipeline of the network are assumed. Similarly to the first scenario, a single slack node and distributed slack nodes have been considered in the electricity network, as reported in Table 3.6, to perform the steady-state analysis of the overall energy grid. These study cases are referred to as 2.c) and 2.d), respectively.

Table 3.5: Gas-fired generator's heat rate curves.

| Nodes | | Heat rate parameters | | |
|---|---|---|---|---|
| Electric | Gas Natural | $\alpha_g^i$ | $\beta_g^i$ | $\gamma_g^i$ |
| 10 | 9 | 350000 | 10 | 2 |
| 16 | 10 | 16000 | 10 | 2 |
| 25 | 5 | 255000 | 10 | 2 |
| 49 | 7 | 240000 | 10 | 2 |
| 59 | 11 | 195000 | 10 | 2 |
| 61 | 6 | 200000 | 10 | 2 |
| 69 | 12 | 300000 | 10 | 2 |
| 103 | 8 | 60000 | 10 | 2 |

Table 3.6: Participation factors of electric generators.

| Nodes | 10 | 16 | 25 | 49 | 59 | 61 | 69 | 103 |
|---|---|---|---|---|---|---|---|---|
| Single slack node | 0.0 | 0.0 | 0.0 | 0.0 | 0.0 | 0.0 | 1.0 | 0.0 |
| Distributed slack node | 0.25 | 0.02 | 0.1 | 0.1 | 0.07 | 0.08 | 0.35 | 0.03 |

Table 3.7 summarizes the results for the natural gas network associated with the natural gas supply, gas demanded by gas-fired plants, nodal pressures and nodal temperatures. The last two set of results are reported in order to identify the operating conditions with risk of hydrate formation according to the chart proposed by Carroll [Carroll 2003], Figure 2.2. The equilibrium point obtained for each case is located within the safety zone of operation. Furthermore, these results provide information about how far the equilibrium point is from the boundary of this safety zone. By way of example, the pressure at node NG-4 has a value close to 1040 PSIA, such that the risk of hydrate formation occurs for temperatures below $511^{o}$R. As the data from columns 5 and 6 of this table show, the gas consumed by electric generators is reduced when distributed slack nodes are considered in the electrical system. However, this observation cannot be considered as a general rule because the gas consumed by fired-gas plants depends on the online regulating generators and their assigned participation factors.

Table 3.7: Natural gas supply, demand and nodal pressures.

| Node | Source | | Demand | Electric | | 2.a) | 2.b) | 2.c) | | 2.d) | |
|---|---|---|---|---|---|---|---|---|---|---|---|
| | | | (*MSCF/hr*) | | | Press | Press | Press | Temp | Press | Temp |
| | *2.a) / 2.c)* | *2.b) / 2.d)* | | *2.a) / 2.c)* | *2.b) / 2.d)* | *(PSIA)* | *(PSIA)* | *(PSIA)* | *(ºR)* | *(PSIA)* | *(ºR)* |
| 1 | 6.2494 | 6.1805 | 0 | 0 | 0 | 1200.0 | 1200.0 | 1200.0 | 550.0 | 1200.0 | 550.0 |
| 2 | 8.0000 | 8.0000 | 0 | 0 | 0 | 1298.3 | 1301.6 | 1294.0 | 550.0 | 1297.3 | 550.0 |
| 3 | 0 | 0 | 0.838 | 0 | 0 | 1034.4 | 1038.3 | 1037.8 | 530.6 | 1041.6 | 530.9 |
| 4 | 0 | 0 | 0.218 | 0 | 0 | 1039.6 | 1043.7 | 1042.5 | 522.5 | 1046.4 | 522.6 |
| 5 | 0 | 0 | 0 | 1.2556 | 1.2617 | 806.3 | 814.5 | 817.9 | 550.0 | 825.7 | 550.0 |
| 6 | 0 | 0 | 0 | 0.8966 | 0.9002 | 1451.3 | 1466.1 | 1472.3 | 550.0 | 1486.3 | 550.0 |
| 7 | 0 | 0 | 0 | 1.1537 | 1.1594 | 806.1 | 813.6 | 814.9 | 550.0 | 822.1 | 550.0 |
| 8 | 0 | 0 | 0 | 0.2256 | 0.2259 | 1531.6 | 1545.9 | 1548.3 | 550.0 | 1561.9 | 550.0 |
| 9 | 0 | 0 | 0 | 2.6938 | 2.7253 | 1372.5 | 1389.9 | 1396.5 | 540.0 | 1413.0 | 540.0 |
| 10 | 0 | 0 | 0 | 0.0578 | 0.0578 | 1372.5 | 1389.9 | 1396.5 | 540.0 | 1413.0 | 540.0 |
| 11 | 0 | 0 | 0 | 0.8675 | 0.8706 | 1275.6 | 1296.3 | 1301.0 | 520.0 | 1320.6 | 520.0 |
| 12 | 0 | 0 | 0 | 4.0416 | 3.9220 | 1339.3 | 1361.1 | 1366.1 | 520.0 | 1386.6 | 520.0 |
| 13 | 0 | 0 | 0.223 | 0 | 0 | 1342.4 | 1363.1 | 1368.7 | 537.0 | 1388.1 | 537.3 |
| 14 | 0 | 0 | 0.274 | 0 | 0 | 1338.8 | 1360.1 | 1365.4 | 531.8 | 1385.5 | 530.6 |
| 15 | 0 | 0 | 1.501 | 0 | 0 | 1335.5 | 1356.6 | 1362.2 | 534.4 | 1382.1 | 534.0 |
| TOTAL | 14.2494 | 14.1805 | 3.054 | 11.1921 | 11.1233 | | | | | | |

The natural gas flows through pipelines and compressors as well as the energy consumption of compressors are reported in Tables 3.8 and 3.9, respectively. The former set of results numerically demonstrates that the selection of the type of the slack node in the electrical network affects the flow through the gas network, which clearly shows the interdependency between both networks. Lastly, the algorithm convergence for this solutions are seven, six, nine and eight iterations for scenarios 2.a, 2.b, 2.c and 2.d, respectively, to a mismatch tolerance of $10^{-6}$ and of $10^{-12}$ for the natural gas and electricity systems, respectively.

Table 3.8: Natural gas flows at pipelines and compressors.

| Pipeline | $C_{km}$ | From | To | Gas flow ($SCF^3/hr$) | | | |
|---|---|---|---|---|---|---|---|
| | ($SCF/PSIA$) | | | *2.a)* | *2.b)* | *2.c)* | *2.d)* |
| 1 | 240932.8 | 1 | 3 | 6.24 | 6.18 | 6.24 | 6.18 |
| 2 | 241232.7 | 2 | 4 | 8.00 | 8.00 | 8.00 | 8.00 |
| 3 | 289126.6 | 3 | 4 | -1.27 | -1.30 | -1.24 | -1.27 |
| 4 | 242008.5 | 3 | 5 | 6.68 | 6.65 | 6.66 | 6.61 |
| 5 | 232459.1 | 4 | 7 | 6.50 | 6.48 | 6.54 | 6.51 |
| 6 | 225390.3 | 6 | 9 | 4.53 | 4.48 | 4.50 | 4.45 |
| 7 | 141801.1 | 8 | 11 | 5.12 | 5.09 | 5.16 | 5.12 |
| 8 | 146427.1 | 10 | 13 | 1.78 | 1.70 | 1.75 | 1.67 |
| 9 | 135148.8 | 12 | 14 | 0.216 | 0.30 | 0.25 | 0.33 |
| 10 | 152148.7 | 13 | 14 | 0.640 | 0.58 | 0.62 | 0.56 |
| 11 | 158598.1 | 13 | 15 | 0.918 | 0.89 | 0.91 | 0.88 |
| 12 | 146339.1 | 14 | 15 | 0.582 | 0.61 | 0.59 | 0.62 |
| Compressor | | From | To | *2.a)* | *2.b)* | *2.c)* | *2.d)* |
| 1 | | 5 | 6 | 5.429 | 5.381 | 5.398 | 5.350 |
| 2 | | 7 | 8 | 5.351 | 5.318 | 5.382 | 5.349 |
| 3 | | 9 | 10 | 1.839 | 1.756 | 1.808 | 1.724 |
| 4 | | 11 | 12 | 4.257 | 4.221 | 4.289 | 4.253 |

Table 3.9: Energy consumption by compressors.

| Compressor | From | To | Horse Power (HP) | | | |
|---|---|---|---|---|---|---|
| | | | *2.a)* | *2.b)* | *2.c)* | *2.d)* |
| 1 | 5 | 6 | 184.89 | 183.26 | 183.83 | 182.19 |
| 2 | 7 | 8 | 197.88 | 196.66 | 199.04 | 197.82 |
| 3 | 9 | 10 | 0.00 | 0.00 | 0.00 | 0.00 |
| 4 | 11 | 12 | 11.16 | 11.06 | 10.63 | 10.54 |

On the other hand, the results reported in Table 3.9 demonstrate that the energy consumed by compressors is affected by the gas temperature along the network. In these study cases, compressors consume more energy when a constant gas temperature of $550^{o}$R is assumed at all nodes of the gas network. These results are in accordance to Equation (2.15), i.e. a higher gas temperature along the network, the higher the energy consumption in compression stations. Lastly, the power supplied by gas-fired generators is reported in Table 3.10.

Table 3.10: Electricity supplied by gas fired generators.

| Electric node | NG node | *Generation (MW/MVAR)* | | | |
|---|---|---|---|---|---|
| | | *2.a) / 2.c)* | | *2.b) / 2.d)* | |
| | | P | Q | P | Q |
| 10 | 9 | 450 | - | 454.89 | - |
| 16 | 10 | 10 | 18.34 | 10.39 | 18.25 |
| 25 | 5 | 220 | - | 221.96 | - |
| 49 | 7 | 204 | 8.72 | 205.96 | 7.55 |
| 59 | 11 | 155 | 99.66 | 156.37 | 99.36 |
| 61 | 6 | 160 | - | 161.57 | - |
| 69 | 12 | 645.38 | - | 632.25 | - |
| 103 | 8 | 40 | 17.04 | 40.59 | 16.84 |
| TOTAL | | 1884.3 | - | 1883.9 | - |

## 3.6 Unified Gas and Power Flow Solution Considering Primary Frequency Regulation.

In the formulation presented in the last section a random participation factor has been assigned to each gas-fired power plant in order to contribute to reduce the active power imbalance in the electric network. Another way to assign these participation factors is considering the primary frequency regulation characteristic, which permits to determine the spinning reserve allocation that is required to withstand a set of pre-defined load variations. There are several proposals to evaluate the primary frequency regulation effect on power generations dispatch, [Restrepo 2005, Okamura 1975, Ping 1998, Kremens 2000]; which also consider load models with dependence of frequency and voltage. Nevertheless none of these formulations perform an integral analysis that permits the understanding of how this primary regulation control affects the mass flow in the natural gas network under load variations in the electrical system.

In order to address the challenge of analyzing the steady-state interdependency between natural gas and electricity networks considering the primary frequency regulation as well as the voltage magnitude and frequency dependence of electric loads, the Equations (3.1) and (3.2) are modified as follows,

$$\begin{aligned} \triangle P_i &= \left( P^i_{g\,set} - \frac{P_{Ri}}{R_i} \triangle f \right) \\ &- \left\{ P^i_{l\,set} \left(1 + K_{pi} \triangle f\right) \left( p_{pi} + p_{ci} \left( \frac{V_i}{V_{LBi}} \right) + p_{zi} \left( \frac{V_i}{V_{LBi}} \right)^2 \right) \right\} \\ &- P^i_{cal} = 0, \qquad \forall\, i \in N_e \end{aligned} \tag{3.14}$$

$$
\begin{aligned}
\triangle Q_i &= \left( Q^i_{g\,set} - a_{Qi}\frac{P_{Ri}}{R_i}\triangle f - b_{Qi}\left(\frac{P_{Ri}}{R_i}\triangle f\right)^2\right) \\
&- \left\{ Q^i_{l\,set}\,(1 + K_{qi}\triangle f)\left(q_{pi} + q_{ci}\left(\frac{V_i}{V_{LBi}}\right) + q_{zi}\left(\frac{V_i}{V_{LBi}}\right)^2\right)\right\} \\
&- Q^i_{cal} = 0, \qquad \forall\, i \in (N_e - N_{PV})
\end{aligned}
\tag{3.15}
$$

where $P^i_{g\,set}$ is the active scheduled output of generator, $P_{Ri}$ is the rated output, $R_i$ is the speed regulation, and $\triangle f$ is the system's frequency deviation. Similarly, $Q^i_{g\,set}$ is the reactive scheduled output of generator whilst $a_{Qi}$ and $b_{Qi}$ are the coefficients of reactive power generation control characteristics.

Regarding the load model, $P^i_{l\,set}$ and $Q^i_{l\,set}$ are the rated power of load. In addition, $K_{pi}$ and $K_{qi}$ are frequency characteristic coefficients and $p_{zi}$ and $q_{zi}$ are the portion of total load proportional to constant impedance load. Furthermore, $p_{ci}$ and $q_{ci}$ are the portion of total load proportional to constant current load, while $p_{pi}$ and $q_{pi}$ are the portion of total load proportional to constant power load. Lastly, $V_{LBi}$ and $V_i$ are the nominal and actual voltage magnitude at load node, respectively.

For both power mismatch Equations (3.14) and (3.15), the first term corresponds to the power modulation according to the system frequency deviation; the second term considers the consumption of power as a nonlinear function of nodal voltage magnitude and of system frequency deviation. The last term is associated with the power injected at the terminals of the transmission elements. Note that an increment of the frequency value due to a load shedding will produce an increment in the energy demanded by those loads that remains embedded in the network, which in turn reduces the disturbance impact on the electric power system behavior.

In this new formulation the state variable $\triangle f$ replaces the former state variable $\triangle P_g$, such that the new vector of the state variables to be computed in the electricity system is $[x] = [x_{ng},\, x_e]^t = [\Pi,\, T,\, BHP,\, G_c,\, \theta,\, V,\, \triangle f]^t$ with their corresponding domains: $\mathbb{R}^{(N_{ng}-1)}$, $\mathbb{R}^{(N_{ng}-1)}$, $\mathbb{R}^{(N_c)}$, $\mathbb{R}^{(N_c)}$, $\mathbb{R}^{(N_e-1)}$, $\mathbb{R}^{(N_e-N_{PV})}$, $\mathbb{R}^1$.

Besides, it is important to consider the modification to the Equation (3.7), which is the link between the electric network and the natural gas network, as follows

$$HR^i = \alpha_g^i + \beta_g^i \left( P_{gset}^i - \frac{P_{Ri}}{R_i} \triangle f \right) + \gamma_g^i \left( P_{gset}^i - \frac{P_{Ri}}{R_i} \triangle f \right)^2 . \tag{3.16}$$

The set of coupled nonlinear mismatch equations is now defined by

$$f = \begin{bmatrix} \triangle G \\ \triangle T \\ \triangle BHP \\ \triangle R \\ \triangle \tau \\ \triangle P \\ \triangle Q \end{bmatrix} = 0 \tag{3.17}$$

where $\triangle G$ corresponds to the gas nodal balance according to the Equation (2.26) defined for $\mathbb{R}^{(N_{ng}-1)}$, $\triangle T$ is the nodal gas temperature balance given by (2.27) for $\mathbb{R}^{(N_{ng}-1)}$; $\triangle BHP$, $\triangle R$ and $\triangle \tau$ are defined by Equations (2.28) - (2.30) for energy consumption, compression ratio and gas extracted by compressors employed in the natural gas network, respectively, and defined for $\mathbb{R}^{N_c}$. Finally, if the term $\tau$ associated to the gas extracted by compressors in Equation (2.26) is expressed as a function of the state variable $BHP$, the set of nonlinear mismatch equations are reduced to:

$$f = \begin{bmatrix} \triangle G \\ \triangle T \\ \triangle BHP \\ \triangle R \\ \triangle P \\ \triangle Q \end{bmatrix} = 0 \tag{3.18}$$

Besides, $\triangle P$ and $\triangle Q$ are now defined by Equations (3.14) and (3.15) with a domain of $\mathbb{R}^{N_e}$ and $\mathbb{R}^{(N_e - N_{PV})}$, respectively, and represent the active and reactive power balance in the electric power system considering primary frequency regulation.

The vector of state variables is defined by $[x] = [x_{ng}, x_e]^t = [\Pi, T, BHP, G_c, \theta, V, \triangle f]^t$ with their corresponding domains: $\mathbb{R}^{(N_{ng}-1)}$, $\mathbb{R}^{(N_{ng}-1)}$, $\mathbb{R}^{(N_c)}$, $\mathbb{R}^{(N_c)}$, $\mathbb{R}^{(N_e-1)}$, $\mathbb{R}^{(N_e-N_{PV})}$, $\mathbb{R}^1$.

Lastly, the new Jacobian matrix for this new formulation is given by

$$J = \left[\begin{array}{cccc|ccc} \frac{\partial \triangle G}{\partial \Pi} & \frac{\partial \triangle G}{\partial T} & \frac{\partial \triangle G}{\partial BHP} & \frac{\partial \triangle G}{\partial G_c} & 0 & 0 & \frac{\partial \triangle G}{\partial \triangle f} \\ \frac{\partial \triangle T}{\partial \Pi} & \frac{\partial \triangle T}{\partial T} & 0 & \frac{\partial \triangle T}{\partial G_c} & 0 & 0 & 0 \\ \frac{\partial \triangle BHP}{\partial \Pi} & \frac{\partial \triangle BHP}{\partial T} & \frac{\partial \triangle BHP}{\partial BHP} & \frac{\partial \triangle BHP}{\partial G_c} & 0 & 0 & 0 \\ \frac{\partial \triangle R}{\partial \Pi} & 0 & 0 & 0 & 0 & 0 & 0 \\ \hline 0 & 0 & \frac{\partial \triangle P}{\partial BHP} & 0 & \frac{\partial \triangle P}{\partial \theta} & \frac{\partial \triangle P}{\partial V} & \frac{\partial \triangle P}{\partial \triangle f} \\ 0 & 0 & 0 & 0 & \frac{\partial \triangle Q}{\partial \theta} & \frac{\partial \triangle Q}{\partial V} & \frac{\partial \triangle Q}{\partial \triangle f} \end{array}\right] \tag{3.19}$$

The coupling terms between the natural gas and electric nonlinear equations correspond to the change of nodal active power balance due the electricity extraction by moto-compressors $\frac{\partial \triangle P}{\partial BHP}$ and the nodal gas balance due the gas extracted by gas-fired generators $\frac{\partial \triangle G}{\partial \triangle f}$, which is a function of the frequency deviation.

### 3.6.1 Study Case

The proposed methodology is applied to assess the steady-state operation of the interconnected natural gas and electricity systems shown in Figure 3.8. The former system consists of four nodes connecting two pipelines and one compressor, while the power system consists of 14 nodes (IEEE 14-bus test system) and has two gas-fired generators at nodes 1 and 2. The compressor maintains the pressure at 4.0 MPa at node 4. The natural gas network data are given in Appendix A. In order to assess how the primary frequency control affects the natural gas operation condition, the active power load is modified at different nodes of the electrical system with respect to the base case. A summary of the results associated with the gas and power flow solutions are reported in Table 3.11 for the following cases: 1.a) Load reduction of $\triangle P_{load} = -100\,MW$ in nodes 3 and 4; 1.b) Base case; 1.c) Load increment of $\triangle P_{load} = +100\,MW$ at node 10; and 1.d) Load increment of $\triangle P_{load} = +200\,MW$ at node 10.

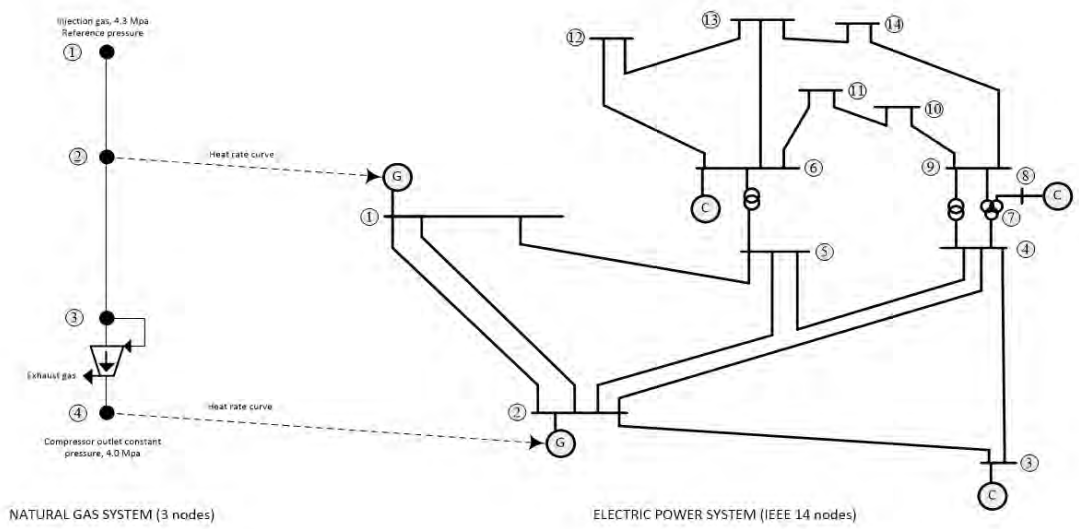


Figure 3.8: Natural gas and electricity coupled systems.

Table 3.11 shows how the increment in the load demand by the electric system modifies the gas system operation condition because of the change in active power produced by gas-fired generators. From these results is clear the reduction of the gas temperature at node 4 as well as the energy consumption by the compression station in accordance to the increments in electric load. Please note that the proposed approach only permits to assess the existing interdependence between the electricity and gas systems for a time horizon corresponding to a single time period. Hence, it is not posible to determine the rate of change of gas temperature with respect to a normal electric load variation.

As a final remark, de-watering the gas and methanol injection can be beneficial in the problem of the formation of hydrates. As reported in [Carroll 2003], the elimination of one of the following three conditions prevents hydrate formation: a) The right combination of temperature and pressure, b) A hydrate former: methane, ethane, carbon dioxide, etc. and c) Water. The hydrate former are not removed from gas because they are the desired product [Carroll 2003], such that the other two considerations have to be addressed in order to reduce the risk of hydrate formation. The gas quality that

the purchaser will accept, in terms of the amount of water contained in the gas, is commonly defined in the commercial arrangements, which implies that the operating conditions that could lead to harmful hydrate formation in pipelines can be identified by the combination of temperature and pressure, as presented in this Chapter. On the other hand, in the natural gas industry methanol and other glycols are used to inhibit hydrate formation. However, as indicated in [Carroll 2003], "It is important to note that they do not prevent hydrate formation, they inhibit it. That is, they reduce the temperature or increase the pressure at which a hydrate will form. The mere presence of an inhibitor does not mean that a hydrate will not form." Hence, the proposed approach will allow us to identify operating conditions that could lead to harmful hydrate formation in pipelines once the inhibitor has been injected in some concentration.

Table 3.11: Resume of energy flow solution.

| Case of study | Natural gas network | | Electrical system | | |
|---|---|---|---|---|---|
| | Node 4 | Gas consumption (MSCF/hr) | Power generation (MW) | | Δf |
| | Temperature ($^{o}$C) | | Gen 1 | Gen 2 | (Hz) |
| *1.a)* | 4.883 | 3.078 | 77.6 | 84.6 | +1.32 |
| *1.b)* | 4.871 | 3.125 | 130.4 | 137.4 | 0 |
| *1.c)* | 4.853 | 3.188 | 179.3 | 186.3 | -1.11 |
| *1.d)* | 4.830 | 3.259 | 222.1 | 229.4 | -2.14 |

## 3.7 Conclusions and Remarks

In this chapter an integrated energy flow analysis of natural gas and electric power systems has been proposed. In the latter, it is assumed that an arbitrary number of gas-fired generators have variable active power as a function of gas supply to better represent the interaction between both networks. Since the environmental temperature has an important impact on the design of pipelines and the operation of the natural gas network, the conventional modeling of this network has been expanded to consider the gas temperature as a state variable in order to assess the compressors' energy consumption and to identify operating conditions that could lead to harmful hydrate

formation in pipelines. The set of nonlinear equations representing the combined natural gas and electricity systems have been obtained based on the nodal balance of gas and power flows, respectively. This set of equations has been linearized and solved using the Newton-Raphson's technique. Numerical examples have been presented to demonstrate the prowess of the proposed approach to analyze the interdependency between both energy networks, where the generation of gas-fired plants as a function of the gas supply and the electric energy consumed by compressor motors are computed automatically together with both gas and electric state variables in a integral frame of reference.

# Chapter 4

# Optimal Flow in Power and Gas Networks Considering Wind Uncertainty

## 4.1 Introduction

As power generation plants, which use wind energy are increasingly integrated into existing electric power systems, it becomes important to evaluate how the wind power uncertainties affect the power system's operation as well as its interdependency with those networks utilized to transport the various forms of primary energy that is converted into electric energy. Currently the operation conditions of the electric power systems is determined considering the best available forecast for the uncertain parameter, this means, the operation is based on the scenario with the highest probability of ocurrence. This chapter proposes a robust optimization model for analyzing the interdependency between natural gas, coal, and electricity networks considering their operation constraints and wind power uncertainties. The optimization model obtains an uncertainty-immunized solution in a integral framework based on the balance of nodal energy flows, which remains feasible and nearly optimal for all values of uncertain data. Since the models of natural gas and electricity networks have been reported

in Chapters 2 and 3, respectively, only the mathematical models adopted for the coal supply network, hydraulic energy system, and wind power generation are reported in detail.

Cases of study are presented to verify the effectiveness of the proposed solution for a multi-energy system composed by the IEEE-118 test system coupled to a 15-nodes natural gas network and a 4-nodes coal distribution system as well as for the real life Belgian natural gas and electricity systems.

## 4.2 Coal Network Model

The coal is transported from the mine-mouth to the electric power plant over long distances and in large quantities, with diesel locomotives as the dominant transportation mode [Kaplan 2007]. For the purposes of this work, the coal transportation system is modeled by a linear network composed of nodes and railways.

Nodes are used to represent the system's facilities such as coal mines, coal piles and/or coal-based thermal power plants which are connected through railways. The steady-state operating point of the coal network is formulated by the coal flow balance equation that must be satisfied at each node of the system: the total amount of coal transported by the rails connected to a nodal point must be equal to the total coal demanded at that node. The balance equation is then given by the following expression.

$$\triangle MC_k = \sum_{m \epsilon k} MC_r^{km} + MC_{source}^k - MC_l^k - MC_l^{k,i} = 0; \qquad \forall\, k \,\epsilon\, N_{co} \tag{4.1}$$

It is important to take into account the physical limits associated with the coal extraction at the mine-mouth, which are determined by the available resources, the storage facilities or railroad transport:

$$MC_{k,min}^{source} \leq MC_{source}^{k} \leq MC_{k,max}^{source} \tag{4.2}$$

Based on the coal flow computed by 4.1, calculating the locomotive's energy consumption is possible, which also permits to assign a cost to the coal transportation. Several formulations have been proposed for calculating the energy consumed by locomotives based on the distance, weight and average train speed in which both geographic and driving aspects are assumed constants, [Hickman 1999]. On the other hand, the methodology presented in [Network Rail 2008] recommends estimating the energy consumption on each railway based on statistical data, considering that the driving conditions, type of locomotive and average speed among other parameters for a given railway are practically the same. Lastly, an efficiency weight is used to penalize the coal freight in such a way that the energy at the inlet node of the railway is different to the energy on the outlet node, [Quelhas 2006]. The computation of energy consumption proposed in [Hickman 1999] is also used in this work and is given by

$$EC_r^{km} = l_r^{km} MC_r^{km} \left[ C_r^{km} + K_r^{km} \frac{\left(V_r^{km}\right)^2}{ln\left(l_r^{km}\right)} \right] \frac{1}{\eta_r^{km}} \tag{4.3}$$

where $l_r^{km}$ represents the railway length running from the $k^{th}$ to the $m^{th}$, $MC_r^{km}$ is the coal amount transported by the railway, $V_r^{km}$ is the average speed of the locomotive, $\eta_r^{km}$ corresponds to an efficiency in the coal transportation by the locomotive; and lastly the parameters $C_r^{km}$ and $K_r^{km}$ characterize the energy consumption of this railway.

This consumed energy is expressed in joules in such a way that the diesel required by the locomotive is computed by

$$DR_r^{km} = \frac{EC_r^{km}}{GHV_d} \tag{4.4}$$

where $GHV_d$ represents the energy contained in one gallon of diesel. Finally, the cost related to the coal freight at each railway of the transportation network is obtained based on cost of diesel in the fuel's market.

Even when the speed of coal transport has not an important impact in the short-

term operation of the electric power systems or real-timer dispatch, it is important to be considered in order to ensure its availability in time and quality, and to determine the storage capacity.

## 4.3 Hydraulic Reservoir Model

Hydro-power plants consist of water reservoirs located at different elevations; when the water is released, the potential energy in the water is converted to electricity in the hydro-plant. For purposes of this chapter, the available hydrological resource is considered known, and the elevation of the surface of the reservoir is assumed constant. This last assumption is regarded as correct because the study is performed for a single time period (snapshot); however, this becomes an important issue in multi-time analysis [Wood 1984]. The coupling between the water reservoir and the electric power system is given by the water rate Equation (4.5); which relates the amount of water needed to generate a specified active power, and whose coefficients $\alpha$, $\beta$ and $\gamma$ define the efficiency in the energy conversion process from the potential energy contained in the water volume to the electrical energy generated by the group turbine-generator:

$$WR_i = \frac{h^i_{rate}}{h_i}\left[\alpha^i + \beta^i P^i_{gen,\,hy} + \gamma^i \left(P^i_{gen,\,hy}\right)^2\right] \tag{4.5}$$

where $h^i_{rate}$ is the nominal height of the level surface for the $i^{th}$ reservoir, $h_i$ is the current height of this level surface; the parameters $\alpha^i$, $\beta^i$ and $\gamma^i$ describe the efficiency in the energy conversion process for the hydro-electric generators.

The water resources available in each basin are delimited by

$$WR_i^{min} \leq WR_i \leq WR_i^{max} \tag{4.6}$$

## 4.4 Wind Generator Model

The increasing level of wind penetration has augmented the concern about its impact on the power system's performance and the effect on the economic dispatch of generators due to the variability of wind [Hetzer 2008]. The power output of a wind turbine is given by (4.7), which indicates that large fluctuations of wind power may occur because of wind speed variations [Castro 2012] :

$$P_{wind} = \frac{1}{2} C_p \, \rho \, A \, ws^2 \tag{4.7}$$

where $C_p$ is the wind-power turbine coefficient, $\rho$ corresponds to the air density, $A$ is the wind-rotor swept area and $ws$ the wind speed impacting the wind-generator.

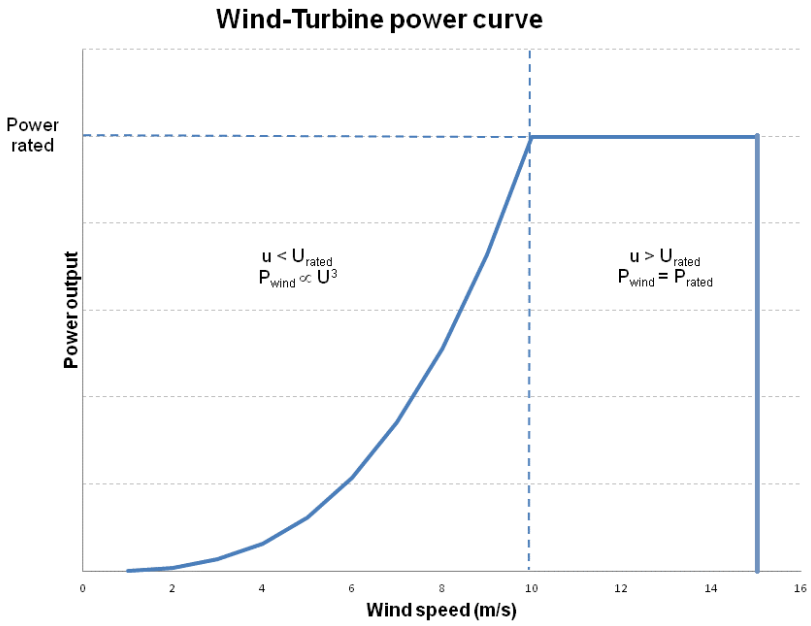


Figure 4.1: Typical power curve for a wind turbine.

Figure 4.1 shows a typical wind power curve as a function of the wind speed $ws$, which can be used to express the output power obtained from the wind generator by the following polynomial function

$$P_{wind} = a_w + b_w\, ws + c_w\, ws^2 + d_w\, ws^3 + e_w\, ws^4 + f_w\, ws^5 + g_w\, ws^6 + h_w\, ws^7 + i_w\, ws^8 \quad (4.8)$$

The expression (4.8) provides the active power in per unit of the generator's rated power, in order to convert this per unit power in MW we use the following equation.

$$P^{i}_{gen,w} = P^{i,rate}_{gen,w}\, P_{wind} \quad (4.9)$$

where $P^{i,rate}_{gen,w}$ corresponds to the rate capacity of the $i^{th}$ wind-generator.

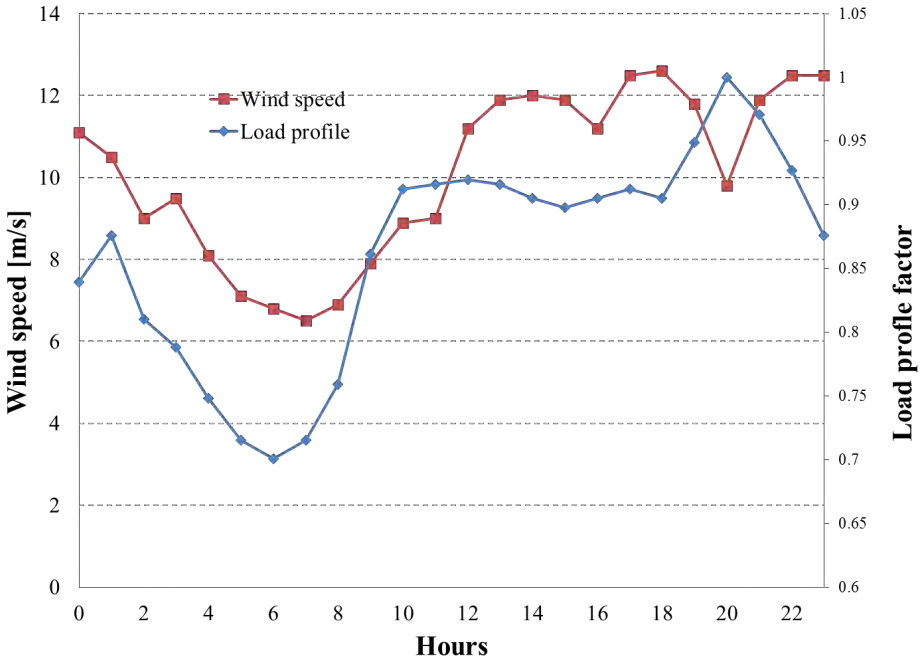


Figure 4.2: Wind speed forecast 24 hours in advance.

From Figure 4.2 it is possible to identify the importance in the wind-speed prediction, this high variability in the wind energy is likely the major challenge in the assessment and integration of wind power to the electric power systems; currently some studies indicate that the mean absolute error could be around 16.8% for 24 hours in advance forecasts, which obviously has bigger impacts in systems with higher wind power penetration, [Zack 2006].

## 4.5 Robust Optimization Model

Mathematically, the single-period, deterministic multi-energy OPF is stated by the following constrained nonlinear optimization problem:

$$\begin{aligned} & min\ f(x,\, \beta) \\ s.t. \quad & h(x,\, \beta) = 0; \quad \underline{x} \leq x \leq \bar{x} \end{aligned} \tag{4.10}$$

where the mapping $f(x,\, \beta) : \mathbb{R}^{q_1} \rightarrow \mathbb{R}$ is the objective function to be optimized, $q_1 = \left(\mathbb{R}^{co} + \mathbb{R}^{ng} + \mathbb{R}^{e} + \mathbb{R}^{\beta}\right)$, where $\mathbb{R}^{co}$, $\mathbb{R}^{ng}$, $\mathbb{R}^{e}$ *and* $\mathbb{R}^{\beta}$ represent the dimension of the state vector corresponding to the coal, gas and electricity as well as the set of uncertain parameters respectively. The set of equality constraints $h(x,\, \beta) : \mathbb{R}^{q_1} \rightarrow \mathbb{R}^{q_2}$ corresponds to the nodal energy balance in the primary energy and electricity networks, $q_2 = N_{co} + N_{ng} + 3N_c + 2N_e - N_{PV}$; the set of inequality constraints $x \in S_{space} \subseteq \mathbb{R}^{q_1}$ corresponds to decision variables with lower and upper limits given by $\underline{x}$ and $\bar{x}$, respectively; and the parameter vector $\beta$ is only composed of deterministic data. The point $x$ in the search space $S_{space}$ that satisfies all constraints is defined as the feasible point $x$. When data take values different than the nominal or expected values, the computed optimal solution considering the nominal data may no longer be optimal or even feasible. Hence, the goal of robust optimization is to provide a solution that remains feasible and near optimal when data changes within a prescribed uncertainty set. The robust optimization (RO) counterpart of (4.10) is formulated by introducing a set of scenarios $\varsigma = \{1,\, 2,\, 3, \cdots,\, S\}$, where each scenario is modeled and solved deterministically with a probability of occurrence $p_s$, where $\sum p_s = 1$, and composed of the values that uncertain data take in the analyzed scenario as well as by the fixed values of deterministic data $s = \{\beta_d,\, \beta_u^s\}\ \forall\ s \in \varsigma$. Note that the values of $p_s$ such that $\sum p_s = 1$ imply that a discrete probability distribution for the selected number of scenarios is known.

The optimal solution of (4.10) is robust with respect to optimality if it remains

close to the optimal solution of any scenario of the input data, and it is robust in terms of feasibility if all constraints are satisfied for all possible values that may be realized for the uncertain parameters. However, it is unlikely that the solution remains near optimal and feasible for all possible scenarios, such that a trade-off between solution and model robustness could be achieved by introducing a function to control the variability in the optimal solution for all realizations of $s$, and/or by relaxing the constraints in a controlled way to permit a certain degree of infeasibility [Malcom 1994]. This latter option is not considered in this chapter: all equality constraints are regarded as active at any solution since they must be satisfied unconditionally at any operating point. Furthermore, the active set of inequality constraints consists of those variables to be explicitly enforced to specified values in a particular feasible solution.

Therefore, the robust optimization model is formulated as:

$$\begin{aligned} min \quad & \sum_{s\in\varsigma} p_s\xi_s + \lambda \sum_{s\in\varsigma} p_s \left(\xi_s - \sum_{s'\in\varsigma} p_{s'}\xi_{s'}\right)^2 \\ s.t. \quad & h_s\left(x,\, \beta_d,\, \beta_u^s\right) = 0;\ \underline{x} \le x \le \bar{x} \qquad \forall\, s \in \varsigma \end{aligned} \tag{4.11}$$

where $\xi_s$ corresponds to the conventional objective function for each scenario analyzed, and the suffix $s'$ is utilized to indicate the term belonging to the weighted summation in the variance calculation. Then, the objective function is composed of the expected optimal solution $\xi_s = f\left(x,\, \beta_d,\, \beta_u^s\right)$ weighted over all possible scenarios plus a constant $\lambda$ times the variance of $\xi_s$, this variance represent the dispersion of the solutions for the different scenarios. In addition, the sets of equality and inequality constraints of the multi-energy system, which must be simultaneously satisfied for all scenarios $s \in \varsigma$, are given by the following equations,

$$\triangle MC_k^s = 0; \qquad \forall\, k \in N_{co} \tag{4.12}$$

$$\triangle G_k^s = 0; \qquad \forall\, k \in N_{ng} \tag{4.13}$$

$$\begin{aligned} \triangle HP_c^{s,\,km} &= BHP^{s,\,km} - 0.0854\, Z_a \left[\frac{G_c^{s,\,km} T_k}{E_c \eta_c}\right] \left[\frac{c_k}{c_k - 1}\right] \left[\left(\frac{\Pi_m^s}{\Pi_k^s}\right)^{\frac{c_k - 1}{c_k}} - 1\right] = 0 \\ &\forall\, c \in N_c;\ \forall\, k \wedge m \in N_{ng};\ k \neq m \end{aligned} \tag{4.14}$$

$$\triangle R_c^{s,\,km} = \frac{\Pi_m^s}{\Pi_k^s} - R_{km} = 0; \qquad \forall\, c \in N_c;\ \forall\, k \wedge m \in N_{ng};\ k \neq m \tag{4.15}$$

$$\triangle P_k^s = 0; \qquad \forall\, k \in N_e \tag{4.16}$$

$$\triangle Q_k^s = 0; \qquad \forall\, k \in (N_e - N_{PV}) \tag{4.17}$$

$$MC_{k,\,min}^{s,\,source} \leq MC_{source}^{s,\,k} \leq MC_{k,\,max}^{s,\,source}; \qquad \forall\, k \in N_{co}^{sources} \tag{4.18}$$

$$G_{sk}^{s,\,min} \leq G_{sk}^s \leq G_{sk}^{s,\,max}; \qquad \forall\, k \in N_{ng}^{sources} \tag{4.19}$$

$$\Pi_k^{min} \leq \Pi_k^s \leq \Pi_k^{max}; \qquad \forall\, k \in N_{ng} \tag{4.20}$$

$$WR_k^{min} \leq WR_k^s \leq WR_k^{max}; \qquad \forall\, k \in N_{hy}^{sources} \tag{4.21}$$

$$P_{gen}^{i,\,min} \leq P_{gen}^{i,\,s} \leq P_{gen}^{i,\,max}; \qquad \forall\, P_{gen}^i \in \left\{P_{gen,\,ng}^i,\, P_{gen,\,co}^i,\, P_{gen,\,hy}^i,\, P_{gen,\,w}^i\right\} \tag{4.22}$$

$$Q_{gen}^{i,min} \leq Q_{gen}^{i,s} \leq Q_{gen}^{i,max}; \qquad \forall\, Q_{gen}^{i} \in \left\{Q_{gen,ng}^{i},\, Q_{gen,co}^{i},\, Q_{gen,hy}^{i},\, Q_{gen,w}^{i}\right\} \tag{4.23}$$

$$V_{k}^{min} \leq V_{k}^{s} \leq V_{k}^{max}; \qquad \forall\, k \in (N_e - N_{PV}) \tag{4.24}$$

The set of decision variables for the RO problem is given as follows: for the gas system, $x_{ng} \in \left\{\Pi \in \mathbb{R}^{s\,(N_{ng}-N_{ng}^{sources})},\, BHP \in \mathbb{R}^{s\,N_c},\, G_c \in \mathbb{R}^{s\,N_c}\right\}$ which corresponds to nodal pressures, energy consumption by compressors, and gas flow through compressors; for the coal system, $x_{co} \in \{MC_r \in \mathbb{R}^{s\,r}\}$ which corresponds to the coal flow in each railroad; and finally $x_e \in \left\{P_{gen} \in \mathbb{R}^{s\,(N_{gen}-N_{gen\,w})},\, V \in \mathbb{R}^{s\,(N_e-N_{PV})},\, \theta \in \mathbb{R}^{s\,(N_e-1)}\right\}$ for the electric power system, which corresponds to the active power output, nodal voltage magnitude and nodal voltage angle. In this set of equations $s$ represents the set of scenarios, $r$ the set of railways in the coal transportation network, $N_{ng}$ and $N_{ng}^{sources}$ correspond to the number of nodes without and with a constant pressure, respectively, for the natural gas system.

In addition, $N_c$ is the number of compressors online in the natural gas system, $N_{gen}$ is the number of generator nodes in the electrical system in which $N_{gen\,w}$ correspond to the wind-energy generators, and $N_e$ is the set of nodes in the electrical network in which there are $N_{PV}$ nodes with constant voltage magnitude.

Lastly, the value of $\lambda$ penalizes the variability of the cost values associated to each scenario, which has a direct effect on the robustness, with respect to optimality. The null or low value of this parameter results in a high variance of the optimal value of the objective function over all possible scenarios. On the other hand, a high value of the penalization factor provides a low dispersion of the optimal values of the objective function associated with the set of scenarios for wind speed.

## 4.6 Study Case of a Multi-Energy Network

The robust optimization model described in the last section is applied to the analysis of a multi-energy system in order to assess the impact of wind power uncertainties on the cost associated with the production of coal and natural gas, which directly affects the existing interdependency between primary energy networks and the electricity system. Furthermore, a RO model is formulated and solved to achieve an *"almost"* constant active power generation from gas-fired plants, over all wind power scenarios, in order to maintain invariant the operating conditions in the natural gas network. The energy system is composed of gas, coal and electricity systems, the first two networks are depicted in Figures 2.3 and 4.3, while their data are reported in Appendix A. The four compressors in the natural gas system are driven by gas turbines, and the gas is tapped from the inlet node of the compressor station. The electrical network corresponds to the IEEE 118-bus system ["Power Systems Test Case Archive", http://www.ee.washington.edu/research/pstca/], which is coupled to the other primary energy networks through thermal, hydro, and wind power generators at those nodes reported in Table 4.1. The parameters for heat rate curves in thermal units and water curves for hydraulic units have been chosen to reflect the typical efficiency behavior in each unit. The generation limits for the thermal and hydro generators are $0.2 \leq P^i_{gen} \leq 4$ pu and $0 \leq P^i_{gen} \leq 4$ pu, respectively, with a base of 100 MVA. Finally, the water available for each hydroelectric generator is computed by Equation (4.5) considering the coefficients and rate powers given in Table 4.1, and a constant gross head for all hydro plants is considered. In accordance with the rated power reported in Table 4.1 the wind power capacity represents approximately 22% of the total installed capacity for this study case.

Based on the idea reported in [Outcalt 2009], we only consider five different wind speed scenarios of 5, 8, 10, 12 and 15 m/s to represent the wind-speed forecast uncertainty. For purposes of this case of study, the probability of each chosen scenario is hypothetically selected as 10, 10, 20, 50 and 10%, respectively. Note that our assumption of five wind speed scenarios with hypothetical probabilities of occurrences

do not affect the proposed RO formulation since these data are considered as input parameters in the proposed formulation; i.e. our proposal does not lose its generality. The same wind power curve characteristic is assumed for all wind generators, which is approximated by the eighth-degree polynomial function (4.8), whose coefficients are reported in Table 4.1. Therefore, each wind generator produces an active power defined by Equation (4.9). In this study case to different variances are considered for the penalization term in Equation (4.11); for the examples A to C the variance of the total operation cost is considered to attain a suitable and robust solution for the fossil fuel management, which determines the quantity of gas and coal required for the operation at which the total cost could be independent of the wind speed scenario for large $\lambda$ values. On the other hand, in the example D, the penalization is realized for the variance of the gas consumption. This solution leads to an invariant active power generated by the gas-fired generators, this means that the operation conditions in the natural gas infrastructure remains constant independently of the wind speed scenario for large $\lambda$ values.

Table 4.1: IEEE-118 Test system, generators.

| Electric Node | Type | Primary energy bus | Rated power | $\alpha$ | $\beta$ | $\gamma$ |
|---|---|---|---|---|---|---|
| E-10 | Gas | NG-4 | 197.0 | 150000 | 12 | 4 |
| E-12 | Gas | NG-5 | 204.4 | 150000 | 12 | 4 |
| E-16 | Gas | NG-8 | 179.2 | 140000 | 14 | 5 |
| E-25 | Gas | NG-12 | 183.1 | 140000 | 14 | 5 |
| E-26 | Gas | NG-13 | 187.0 | 140000 | 14 | 5 |
| E-31 | Gas | NG-15 | 169.9 | 140000 | 14 | 5 |
| E-40 | Coal | C-1 | 199.1 | 150000 | 120 | 7 |
| E-46 | Coal | C-2 | 186.5 | 150000 | 120 | 7 |
| E-49 | Coal | C-3 | 211.2 | 150000 | 120 | 7 |
| E-54 | Coal | C-3 | 225.9 | 150000 | 120 | 7 |
| E-59 | Coal | C-4 | 222.4 | 150000 | 120 | 7 |
| E-87 | Hydro | — | 138.7 | 4000 | 480 | 0.2 |
| E-89 | Hydro | — | 231.6 | 9000 | 450 | 0.2 |
| E100 | Hydro | — | 218.2 | 9000 | 450 | 0.2 |
| E-103 | Hydro | — | 201.9 | 9000 | 450 | 0.2 |
| E-111 | Hydro | — | 159.9 | 4000 | 480 | 0.2 |
| E-61 | Wind | — | 217.0 | $a_w = 1.07$ | $b_w = -0.806$ | $c_w = 0.245$ |
| E-65 | Wind | — | 217.1 | | | |
| E-66 | Wind | | 212.7 | $d_w = -0.043$ | $e_w = 5.09e-3$ | $f_w = 3.8e-4$ |
| E-69 | Wind | | 220.9 | | | |
| E-80 | Wind | — | 231.1 | $g_w = 1.66e-5$ | $h_w = -3.85e-7$ | $i_w = 3.65e-9$ |

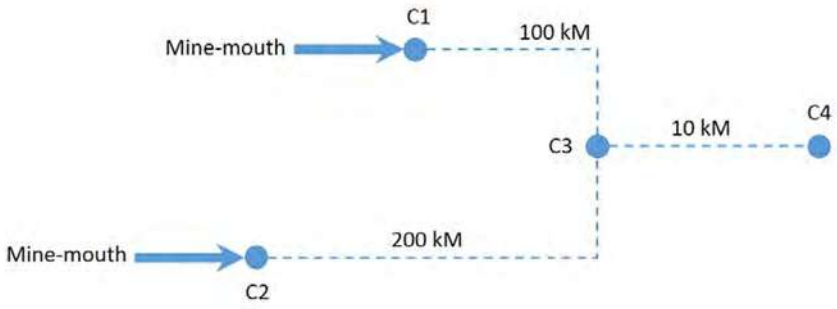


Figure 4.3: Coal transportation system

The RO model (4.11) associated with this multi-energy system is composed by 303 variables, 306 equality constraints and 298 inequality constraints per wind scenario, Equations (4.12) to (4.24), and is numerically solved using the software GAMS/MINOS ["GAMS/MINOS", http://www.gams.com/solvers/solvers.htm#MINOS] for the following three study cases detailed below:

A. A base case for the cost of fossil fuel production considering no penalization in the variance between scenarios, i.e. $\lambda = 0$;

B. Similar to Case A but considering $0 \leq \lambda \leq 1$ to penalize the variance of the total cost of fossil fuel production between scenarios;

C. Similar to the case B considering a reduction of 20% in hydroelectric resources;

D. A case that minimizes the fossil fuel consumed by thermal power plants considering a penalty factor in the range of $0 \leq \lambda \leq 10$ to penalize the cost variance of natural gas used to generate electricity.

The following reference prices are considered for all study cases: Diesel is 1 USD/liter ["Gasoline and Diesel Fuel Update", February 2014, http://www.eia.gov/petroleum/gasdiesel/], natural gas

is 4 USD/MSCF ["Natural Gas Prices", January 31st, 2014, http://www.eia.gov/dnav/ng/ng_pri_sum_dcu_nus_m.htm] and coal is 80.15 USD/Ton ["Coal", December 12, 2013, http://www.eia.gov/coal/data.cfm#prices]. A coal heating value of 12,500 Btu/lb has also been considered for all studies, which corresponds to the category of sub-bituminous coal ["Coal", December 12, 2013, http://www.eia.gov/coal/data.cfm#prices].

The objective function for each scenario is defined as the total cost of primary resources of fossil fuels injected by all natural gas and coal sources:

$$\begin{aligned} \xi &= \sum_{k_1=1}^{NG_{sources}} \left(NG^{k_1}_{cost\,x\,SCFH}\, G^{k_1}_{s}\right) + \sum_{k_2=1}^{CO_{sources}} \left(CO^{k_2}_{cost\,x\,Ton}\, MC^{k_2}_{s}\right) \\ &+ DI_{cost\,x\,liter} \sum_{k_3=1}^{N_{railways}} \left(DR^{k_3}_{r}\right) \end{aligned} \tag{4.25}$$

### 4.6.1 Case A

For the case of study, the results of the cost of primary resources and the active power generation dispatch are summarized in Figure 4.4 for each wind speed scenario. The CPU time for this simulation was 1.6 s. The cost and generation dispatch are indicated by bars and solid lines, respectively. Note that the increment of active power produced by wind generators has a major impact on the total generation associated with coal-fired power plants, which is reduced by approximately 10 pu; meanwhile the generation due to natural gas plants is only reduced by less than 2 pu. These results are caused by the efficient energy conversion process, fossil fuel prices, and gross heating value of each generation technology. As expected, the optimization solution provides no immunization to the wind speed forecast uncertainty, $\lambda = 0$; there then exists a variance of the operation costs between scenarios, which is about 30 KUSD between the first and last scenarios.

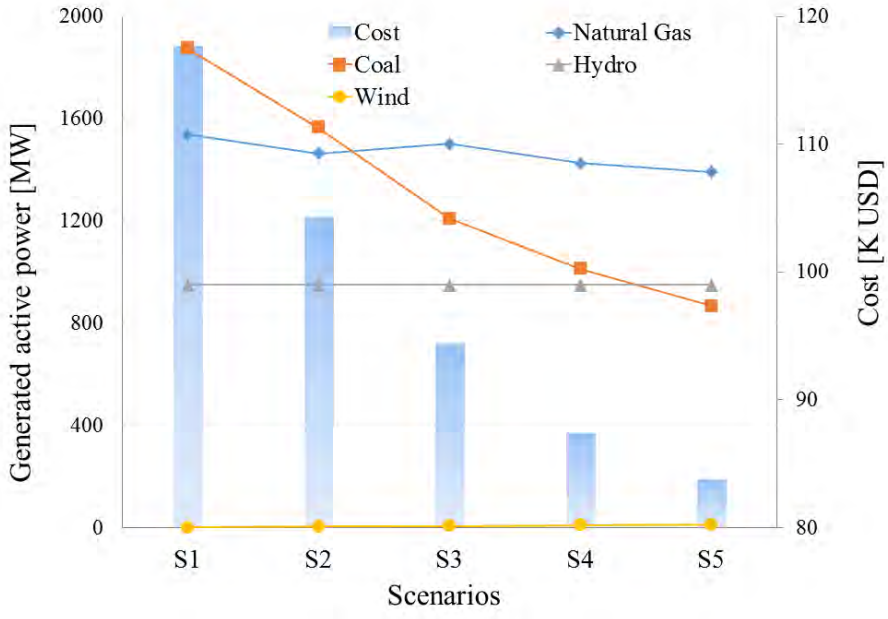


Figure 4.4: Generation dispatch and operation cost, Case A

Table 4.2: Energy Balance, Case A

| Scenario | Gas System, MMSCF | | | Coal System, Ton | | | Electric System, MW | | |
|---|---|---|---|---|---|---|---|---|---|
| | Supply | Industrial Load | Generator's Load | Supply | Industrial Load | Generators' Load | Supply | Load | Losses |
| $S_1$ | 15.725 | 6.000 | 9.640 | 560.9 | 0 | 560.9 | 4396.8 | 4173.1 | 223.7 |
| $S_2$ | 15.237 | 6.000 | 9.150 | 446.4 | 0 | 446.4 | 4352.1 | 4173.1 | 179.0 |
| $S_3$ | 15.405 | 6.000 | 9.319 | 337.3 | 0 | 337.3 | 4335.9 | 4173.1 | 161.9 |
| $S_4$ | 14.755 | 6.000 | 8.755 | 288.2 | 0 | 288.2 | 4315.5 | 4173.1 | 142.4 |
| $S_5$ | 14.600 | 6.000 | 8.600 | 256.8 | 0 | 256.8 | 4307.5 | 4173.1 | 134.4 |

In Table 4.2, the energy balance of each energy network has been presented, for the case of the natural gas system, the difference between gas supplied and the total gas required by industrial and generators corresponds to the gas extracted by turbo-compressors installed in the system.

### 4.6.2 Case B

Study case A is repeated but considering different penalty factors, $0 \leq \lambda \leq 1$, on the operation cost variance. This penalization allows an uncertainty-immunized solution

for all wind speed scenarios but at a suboptimal operation cost as demonstrated in Figure 4.5. The total operating cost of each scenario tends to the same value, which is the most expensive one as the penalty factor is increased. In this case, the same robust optimal operation cost $\xi_s$ is obtained for scenarios 2 to 5 from a penalty factor of $\lambda = 10^{-3}$; at this value of $\lambda$ the operation cost is 112.4 KUSD. On the other hand, all scenarios have the cost of 118.8 KUSD for a penalty factor of $\lambda = 1$, which corresponds to worst-case RO solution. The execution time for each simulation was 25 s of CPU time, except for the case where $\lambda = 0$. The standard deviation of the robust operating costs is also shown in Figure 4.5, which is calculated from the existing variance between the costs of a set of scenarios related to the same value of $\lambda$.

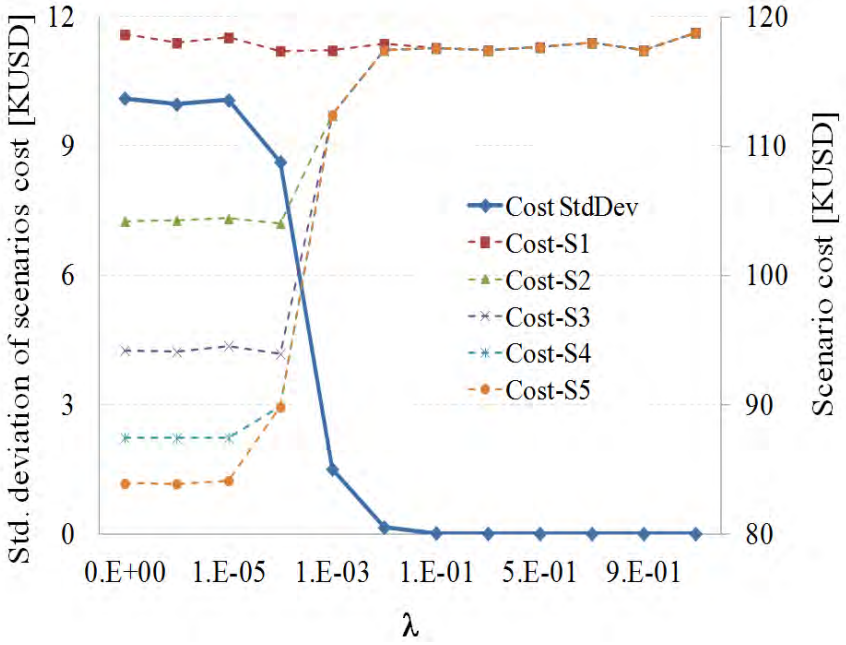


Figure 4.5: Standard deviation and operating costs by scenario, Case B

Table 4.3: Energy Balance for $\lambda = 0.1$, Case B

| Scenario | Gas System, MMSCF | | | Coal System, Ton | | | Electric System, MW | | |
|---|---|---|---|---|---|---|---|---|---|
| | Supply | Industrial Load | Generator's Load | Supply | Industrial Load | Generators' Load | Supply | Load | Losses |
| $S_1$ | 15.696 | 6.000 | 9.606 | 560.9 | 0 | 560.9 | 4392.9 | 4173.1 | 219.9 |
| $S_2$ | 14.567 | 6.000 | 8.476 | 554.6 | 0 | 554.6 | 4366.9 | 4173.1 | 193.8 |
| $S_3$ | 14.369 | 6.000 | 8.277 | 550.9 | 0 | 550.9 | 4389.7 | 4173.1 | 216.6 |
| $S_4$ | 14.306 | 6.000 | 8.214 | 517.8 | 0 | 517.8 | 4365.9 | 4173.1 | 192.8 |
| $S_5$ | 14.536 | 6.000 | 8.444 | 602.5 | 0 | 602.5 | 4548.6 | 4173.1 | 375.5 |

In Table 4.3, the energy balance of each energy network has been presented, for the case of the natural gas system, the difference between gas supplied and the total gas required by industrial and generators corresponds to the gas extracted by turbo-compressors installed in the system.. The standard deviation of active power dispatches over all possible scenarios are shown in Figure 4.6, as a function of the penalty value $\lambda$. A close relation between the variance of the total operation cost shown in Figure 4.5 and the total power dispatched by coal-fired plants shown in Figure 4.6 is observed: the higher penalty factor, the smaller variance in the operation cost and total coal-based power generation associated with the set of scenarios for wind speed. This smaller variance is because of the coal-fired power rises with increments in the values of the penalization factor, as shown in Figure 4.7. This increment in the participation of coal-fired units causes a reduction in the amount of active power supplied by the hydro and gas-fired units in order to meet the electric demand and transmission losses, as shown in Figures 4.8 and 4.9, respectively. In this context, if hydro resources are reduced, or even eliminated, the deficit in active power will be compensated by the natural gas-fired generators. In this case, the profile of both the standard deviation of gas dispatch and the nodal gas pressures along the gas network will be a function of the active power supplied by the gas-fired units at each wind speed scenario. If this power differs between scenarios, the nodal gas pressures do not remain constant and the standard deviation of gas dispatch increases in value.

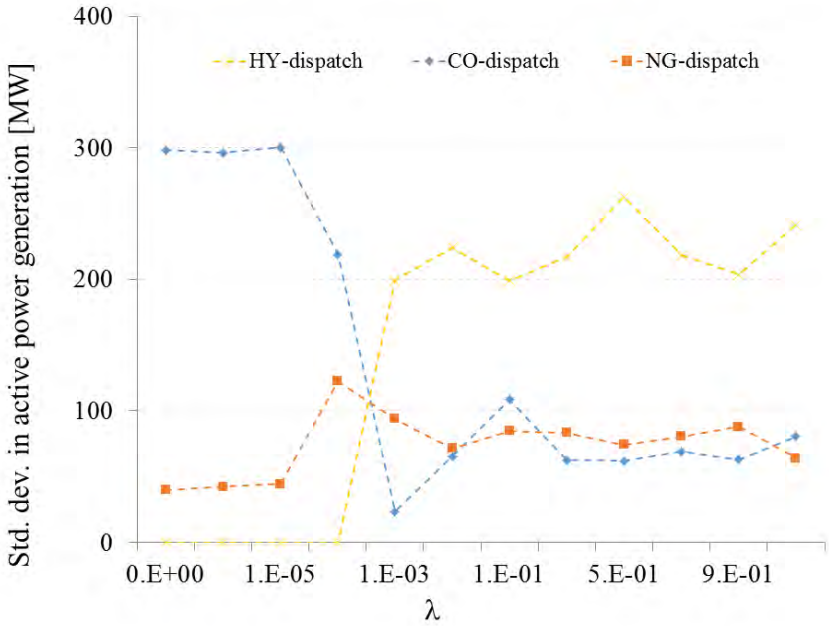


Figure 4.6: Standard deviation for power dispatch between scenarios, Case B

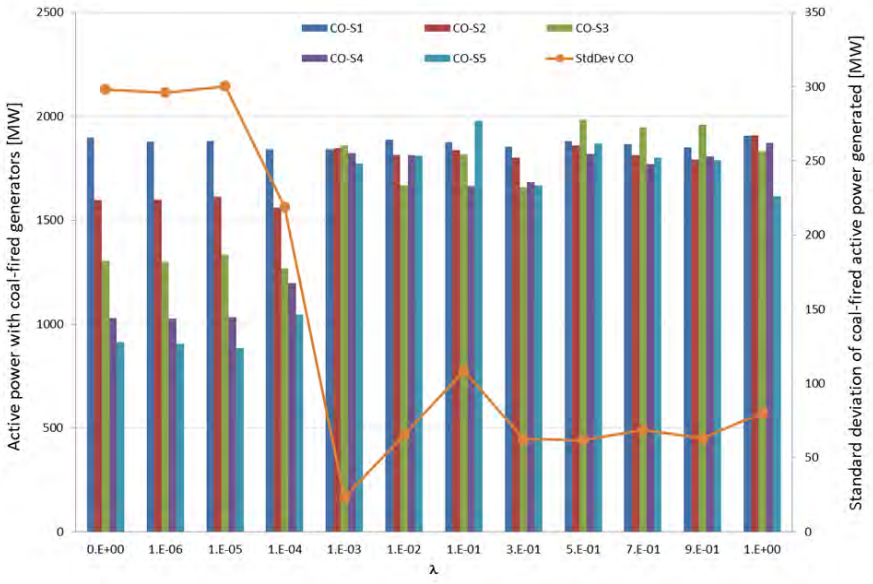


Figure 4.7: Active power and standard deviation of coal-fired units, Case B

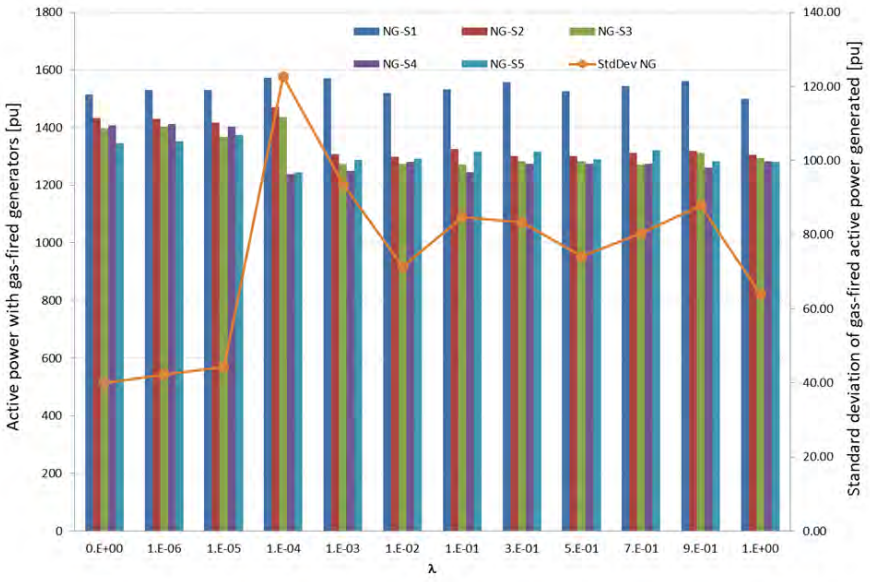


Figure 4.8: Active power and standard deviation of gas-fired units, Case B

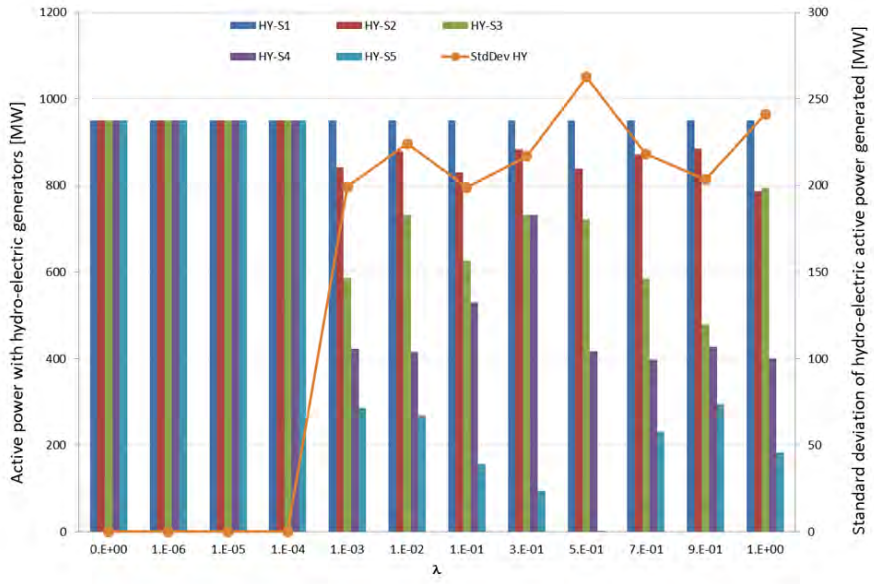


Figure 4.9: Active power and standard deviation of hydro-electric units, Case B

The optimal costs obtained by the proposed approach and the expected cost value are numerically reported in Tables 4.4 and 4.5, respectively. The latter was computed by performing an optimal power flow study for each wind speed scenario considering as an objective function the minimization of the total cost of primary resources of fossil fuels given by Equation (4.25), and the expected cost value was then calculated considering the result of each scenario and its corresponding probability of occurrence. Since the objective function (4.11) of the RO approach includes a weighted penalization term of the cost variance; if this term is set to zero, the total RO cost is similar to the expected cost.

On the other hand, the robust operation cost of each scenario $\xi_s$ and the total RO cost tend to the same value as the penalization factor increases its value, such that the optimal solutions are not affected by the volatility of wind power: an uncertainty-immunized solution is obtained for all scenarios of wind speeds.

Table 4.4: Costs obtained by the RO approach, Case B

| $\lambda$ | Robust cost per scenario $\xi_s$ | | | | | Total RO cost |
|---|---|---|---|---|---|---|
| | $S_1$ | $S_2$ | $S_3$ | $S_4$ | $S_5$ | |
| 0 | 118632.1 | 104189.8 | 94194.1 | 87435.9 | 83886.1 | 93227.0 |
| 0.001 | 117400.6 | 112400.6 | 112400.6 | 112400.6 | 112400.6 | 115150 |
| 0.01 | 117919.9 | 117420.4 | 117420.3 | 117420.2 | 117420.4 | 117690 |
| 0.1 | 117608.8 | 117558.8 | 117558.8 | 117558.8 | 117558.8 | 117590 |
| 0.3 | 117427.9 | 117411.2 | 117411.2 | 117411.2 | 117411.2 | 117420 |
| 0.5 | 117650.4 | 117640.4 | 117640.4 | 117640.4 | 117640.4 | 117650 |
| 0.7 | 117994.9 | 117987.8 | 117987.8 | 117987.8 | 117987.8 | 117990 |
| 0.9 | 117409.5 | 117403.9 | 117403.9 | 117403.9 | 117403.9 | 117410 |
| 1.0 | 118779.1 | 118774.1 | 118774.1 | 118774.1 | 118774.1 | 118780 |

Table 4.5: Costs obtained by the expected value approach, Case B

| Cost per scenario $\xi_s$ | | | | | Expected value cost |
|---|---|---|---|---|---|
| $S_1$ | $S_2$ | $S_3$ | $S_4$ | $S_5$ | |
| 117730.0 | 104260.0 | 94390.7 | 87410.6 | 83781.5 | 93160.1 |

Lastly, since the optimization is performed over the cost of primary energy sources, large industrial loads embedded at the natural gas and coal networks can have an undesirable effect on the amount of fossil fuel that can be supplied to the thermal power plants, constraining their power dispatch. This statement is illustrated in Table 4.6 which reports the active power dispatched by gas-fired generators for two different values of natural gas industrial demands. As expected, a decrement in the active power dispatched by these plants occurs when the industrial demand of natural gas increases. Future research work in which these industrial loads participate in the gas consumption "bidding" can represent this problem from a energy market point of view.

Table 4.6: Electric power generated by gas-fired plants (pu), $\lambda = 0$

| NG industrial load | $S_1$ | $S_2$ | $S_3$ | $S_4$ | $S_5$ |
|---|---|---|---|---|---|
| 6 MMSCF | 15.1 | 14.3 | 13.9 | 14.0 | 13.4 |
| 4 MMSCF | 17.2 | 16.8 | 16.5 | 16.1 | 15.8 |

### 4.6.3 Case C

When hydroelectric resources are reduced, or even eliminated, the deficit in active power will be compensated by the natural gas- and coal-fired generators. In order to show this interdependency between the primary energy networks, the case of study reported in the last section has been repeated considering a reduction of 20% in the hydraulic resources. The active power generated from each type of primary energy is shown in Figures 4.10 to 4.12 together with the profile of the corresponding standard deviations; an increase in the active power dispatched from thermal units is observed in Figures 4.10 and 4.11, as a result of the decrement in the participation of the hydroelectric plants shown in Figure 4.12. Furthermore, the active power generated by gas-fired plants differs between wind speed scenarios and values of the penalization factor, such that the standard deviation of these active power increases in value. These interdependencies also cause the nodal gas pressures along the gas network to not remain constant for the different conditions of generation dispatches.

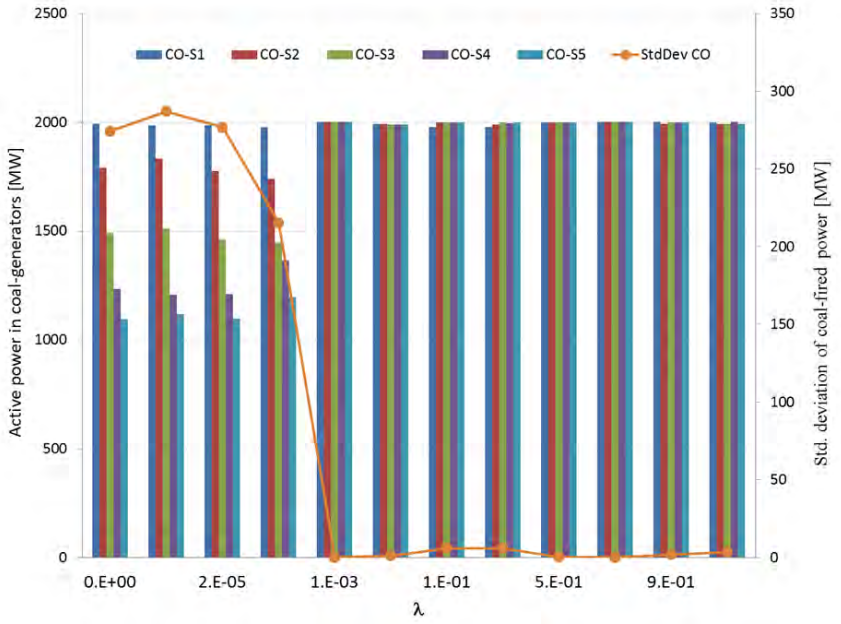


Figure 4.10: Active power and standard deviation of coal-fired units, Case C

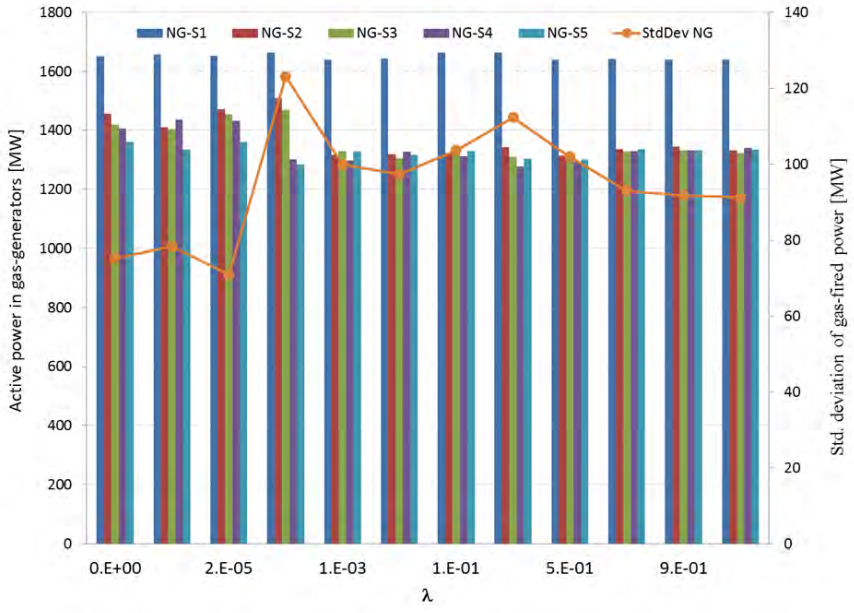


Figure 4.11: Active power and standard deviation of gas-fired units, Case C

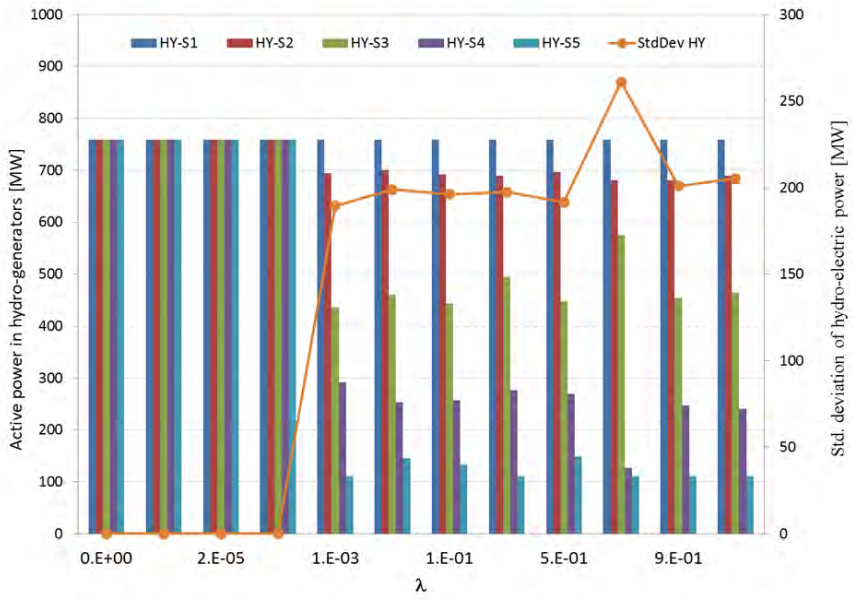


Figure 4.12: Active power and standard deviation of hydro-electric units, Case C

Table 4.7: Energy Balance for $\lambda = 0.001$, Case C

| Scenario | Gas System, MMSCF | | | Coal System, Ton | | | Electric System, MW | | |
|---|---|---|---|---|---|---|---|---|---|
| | Supply | Industrial Load | Generator's Load | Supply | Industrial Load | Generators' Load | Supply | Load | Losses |
| $S_1$ | 16.617 | 6.000 | 10.527 | 612.5 | 0 | 612.5 | 4433.2 | 4173.1 | 260.1 |
| $S_2$ | 14.509 | 6.000 | 8.417 | 612.6 | 0 | 612.6 | 4385.4 | 4173.1 | 212.3 |
| $S_3$ | 14.580 | 6.000 | 8.489 | 612.6 | 0 | 612.6 | 4438.9 | 4173.1 | 265.8 |
| $S_4$ | 14.430 | 6.000 | 8.338 | 612.6 | 0 | 612.6 | 4515.3 | 4173.1 | 342.2 |
| $S_5$ | 14.456 | 6.000 | 8.472 | 612.6 | 0 | 612.6 | 4536.8 | 4173.1 | 363.7 |

In Table 4.7, the energy balance of each energy network has been presented, for the case of the natural gas system, the difference between gas supplied and the total gas required by industrial and generators corresponds to the gas extracted by turbo-compressors installed in the system.

### 4.6.4 Case D

The cost minimization of fossil-fuel consumption by thermal power plants is considered as the objective function in this study case as given by

$$\psi = \sum_{i \in P_{gen,\,ng}} \left( NG^{k}_{cost\,x\,SCFH}\, MG^{k,i}_{l} \right) + \sum_{i \in P_{gen,\,co}} \left( CO^{k}_{cost\,x\,Ton}\, MC^{k,i}_{l} \right) \tag{4.26}$$

In addition, the cost variance of natural gas consumed by each gas-fired plant is penalized in order to set a similar operation condition in the natural gas network for all wind speed scenarios. Therefore, the objective function of the robust model is now given by expression (4.27) to achieve both goals.

$$min \qquad \sum_{s \in \varsigma} p_s \psi_s + \tag{4.27}$$

$$\sum_{i \in P^{i}_{gen,\,ng}} \sum_{s \in \varsigma} p_s \left( NG^{k}_{cost\,x\,SCFH}\, MG^{s,k,i}_{load} - \sum_{s' \in \varsigma} p_{s'} NG^{k}_{cost\,x\,SCFH}\, MG^{s,k,i}_{load} \right)^2$$

The results obtained are reported in Table 4.8 for the nodal pressures in the natural gas network and for the active power dispatched by gas-fired plants considering all wind speed scenarios and three different values of the penalty factor. These results illustrate how the robust optimization solution steer the multi-energy system to an equilibrium point where the operation in the natural gas network is immune to the uncertainties in wind speed forecast, as the penalty factor is increased. This immunity is achieved because each gas-fired plant has a similar power dispatch; in such a way that their gas consumption remains constant over all wind speed scenarios, as also indicated in that table.

Table 4.8: Natural gas nodal pressure and active power generated by gas-fired plants, Case D

| Nodal Pressure (PSI) | | | | | | | | | | | | | | | | | | | | | |
|---|---|---|---|---|---|---|---|---|---|---|---|---|---|---|---|---|---|---|---|---|---|
| | $\lambda = 0$ | | | | | $\lambda = 0.001$ | | | | | | | | $\lambda = 10$ | | | | | | | |
| Node | $S_1$ | $S_2$ | $S_3$ | $S_4$ | $S_5$ | $S_1$ | $S_2$ | $S_3$ | $S_4$ | $S_5$ | $S_1$ | $S_2$ | $S_3$ | $S_4$ | $S_5$ | $S_1$ | $S_2$ | $S_3$ | $S_4$ | $S_5$ |
| 1 | 1200.0 | 1200.0 | 1200.0 | 1200.0 | 1200.0 | 1200.0 | 1200.0 | 1200.0 | 1200.0 | 1200.0 | 1200.0 | 1200.0 | 1200.0 | 1200.0 | 1200.0 | 1200.0 | 1200.0 | 1200.0 | 1200.0 | 1200.0 | 1200.0 |
| 2 | 1200.0 | 1200.0 | 1200.0 | 1200.0 | 1200.0 | 1200.0 | 1200.0 | 1200.0 | 1200.0 | 1200.0 | 1200.0 | 1200.0 | 1200.0 | 1200.0 | 1200.0 | 1200.0 | 1200.0 | 1200.0 | 1200.0 | 1200.0 | 1200.0 |
| 3 | 950.8 | 965.8 | 984.5 | 984.5 | 989.0 | 974.3 | 976.0 | 977.8 | 978.2 | 978.6 | 980.9 | 983.6 | 983.6 | 983.6 | 983.6 | 980.9 | 983.6 | 983.6 | 983.6 | 983.6 | 983.6 |
| 4 | 950.9 | 966.3 | 984.7 | 984.7 | 989.3 | 974.5 | 976.2 | 978.1 | 978.5 | 978.9 | 980.9 | 983.6 | 983.6 | 983.6 | 983.6 | 980.9 | 983.6 | 983.6 | 983.6 | 983.6 | 983.6 |
| 5 | 588.5 | 616.8 | 687.8 | 686.8 | 696.1 | 655.1 | 659.1 | 663.6 | 665.1 | 664.2 | 688.0 | 694.3 | 694.3 | 694.3 | 694.3 | 688.0 | 694.3 | 694.3 | 694.3 | 694.3 | 694.3 |
| 6 | 882.8 | 925.2 | 1031.8 | 1030.2 | 1044.2 | 982.6 | 988.6 | 995.4 | 997.7 | 996.2 | 1032.0 | 1041.4 | 1041.4 | 1041.4 | 1041.4 | 1032.0 | 1041.4 | 1041.4 | 1041.4 | 1041.4 | 1041.4 |
| 7 | 725.9 | 746.9 | 777.8 | 779.5 | 786.1 | 770.6 | 774.6 | 777.5 | 777.5 | 778.2 | 768.4 | 773.7 | 773.7 | 773.7 | 773.7 | 768.4 | 773.7 | 773.7 | 773.7 | 773.7 | 773.7 |
| 8 | 1088.9 | 1120.3 | 1166.7 | 1169.2 | 1179.1 | 1156.0 | 1161.8 | 1166.2 | 1166.3 | 1167.3 | 1152.7 | 1160.5 | 1160.5 | 1160.5 | 1160.5 | 1152.7 | 1160.5 | 1160.5 | 1160.5 | 1160.5 | 1160.5 |
| 9 | 679.1 | 740.5 | 848.7 | 841.0 | 856.6 | 794.6 | 804.4 | 809.6 | 811.5 | 810.2 | 831.0 | 843.3 | 843.3 | 843.3 | 843.3 | 831.0 | 843.3 | 843.3 | 843.3 | 843.3 | 843.3 |
| 10 | 950.7 | 1036.7 | 1188.1 | 1177.4 | 1199.2 | 1112.4 | 1126.2 | 1133.4 | 1136.1 | 1134.2 | 1163.4 | 1180.6 | 1180.6 | 1180.6 | 1180.6 | 1163.4 | 1180.6 | 1180.6 | 1180.6 | 1180.6 | 1180.6 |
| 11 | 685.6 | 830.5 | 857.1 | 857.1 | 857.1 | 844.5 | 857.1 | 857.1 | 857.1 | 857.1 | 845.1 | 857.1 | 857.1 | 857.1 | 857.1 | 845.1 | 857.1 | 857.1 | 857.1 | 857.1 | 857.1 |
| 12 | 959.8 | 1162.7 | 1200.0 | 1200.0 | 1200.0 | 1182.3 | 1200.0 | 1200.0 | 1200.0 | 1200.0 | 1200.0 | 1183.1 | 1200.0 | 1200.0 | 1200.0 | 1200.0 | 1200.0 | 1200.0 | 1200.0 | 1200.0 | 1200.0 |
| 13 | 862.0 | 961.8 | 1105.3 | 1088.5 | 1110.8 | 1029.0 | 1046.0 | 1051.1 | 1053.2 | 1051.5 | 1062.3 | 1081.6 | 1081.6 | 1081.6 | 1081.6 | 1062.3 | 1081.6 | 1081.6 | 1081.6 | 1081.6 | 1081.6 |
| 14 | 853.2 | 962.7 | 1100.8 | 1085.4 | 1105.8 | 1028.4 | 1045.5 | 1050.4 | 1052.3 | 1050.8 | 1059.3 | 1078.6 | 1078.6 | 1078.6 | 1078.6 | 1059.3 | 1078.6 | 1078.6 | 1078.6 | 1078.6 | 1078.6 |
| 15 | 850.4 | 958.0 | 1098.0 | 1081.2 | 1103.3 | 1022.1 | 1039.3 | 1044.5 | 1046.4 | 1044.8 | 1054.0 | 1073.5 | 1073.5 | 1073.5 | 1073.5 | 1054.0 | 1073.5 | 1073.5 | 1073.5 | 1073.5 | 1073.5 |
| Electric Node | Active power dispatch in gas-fired plants (pu) | | | | | | | | | | | | | | | | | | | | |
| 10 | 2.315 | 1.642 | 1.551 | 1.579 | 1.342 | 1.952 | 1.929 | 1.877 | 1.86 | 1.81 | 1.781 | 1.713 | 1.713 | 1.713 | 1.713 | 1.781 | 1.713 | 1.713 | 1.713 | 1.713 | 1.713 |
| 12 | 3.556 | 3.61 | 2.807 | 2.714 | 2.648 | 3.123 | 3.145 | 3.074 | 3.049 | 3.074 | 2.393 | 2.366 | 2.366 | 2.366 | 2.366 | 2.393 | 2.366 | 2.366 | 2.366 | 2.366 | 2.366 |
| 16 | 1.637 | 2.431 | 2 | 1.935 | 1.781 | 1.912 | 1.923 | 1.851 | 1.859 | 1.843 | 2.144 | 2.126 | 2.126 | 2.126 | 2.126 | 2.144 | 2.126 | 2.126 | 2.126 | 2.126 | 2.126 |
| 25 | 3.475 | 1.297 | 2.981 | 2.806 | 3.149 | 2.296 | 2.216 | 2.331 | 2.357 | 2.347 | 2.641 | 2.637 | 2.637 | 2.637 | 2.637 | 2.641 | 2.637 | 2.637 | 2.637 | 2.637 | 2.637 |
| 26 | 1.26 | 3.068 | 2.07 | 2.32 | 2.127 | 2.53 | 2.529 | 2.548 | 2.531 | 2.534 | 2.481 | 2.474 | 2.474 | 2.474 | 2.474 | 2.481 | 2.474 | 2.474 | 2.474 | 2.474 | 2.474 |
| 31 | 2.282 | 1.99 | 2.245 | 2.355 | 2.233 | 2.445 | 2.446 | 2.416 | 2.424 | 2.434 | 2.492 | 2.484 | 2.484 | 2.484 | 2.484 | 2.492 | 2.484 | 2.484 | 2.484 | 2.484 | 2.484 |

Table 4.9: Energy Balance for $\lambda = 0.001$, Case D

| Scenario | Gas System, MMSCF | | | Coal System, Ton | | | Electric System, MW | | |
|---|---|---|---|---|---|---|---|---|---|
| | Supply | Industrial Load | Generator's Load | Supply | Industrial Load | Generators' Load | Supply | Load | Losses |
| $S_1$ | 14.909 | 6.000 | 8.820 | 597.0 | 0 | 597.0 | 4374.2 | 4173.1 | 201.1 |
| $S_2$ | 14.858 | 6.000 | 8.770 | 454.1 | 0 | 454.1 | 4335.5 | 4173.1 | 162.4 |
| $S_3$ | 14.804 | 6.000 | 8.715 | 355.5 | 0 | 355.5 | 4315.6 | 4173.1 | 142.5 |
| $S_4$ | 14.791 | 6.000 | 8.702 | 288.6 | 0 | 288.6 | 4306.6 | 4173.1 | 133.5 |
| $S_5$ | 14.779 | 6.000 | 8.690 | 252.2 | 0 | 252.2 | 4303.2 | 4173.1 | 130.1 |

In Table 4.9, the energy balance of each energy network has been presented, for the case of the natural gas system, the difference between gas supplied and the total gas required by industrial and generators corresponds to the gas extracted by turbo-compressors installed in the system.

## 4.7 Study Case of the Belgian Natural Gas and Electricity Networks

In this case of study the integrated Belgian natural gas and electricity networks are considered to show the applicability of the proposed approach. The main components of the 20-nodes natural gas network are 24 pipelines, eight gas nonelectric loads, seven sources and two compressors. Data of these components and the gas network topology are reported in Appendix A. The electrical network is represented by an equivalent model composed of 32 buses, 16 loads, 25 transmission lines, 15 transformers and seven generation units, three of which are non-voltage regulating generators [Stubbe 1995]. For the purpose of this case of study, these three generators have been considered as wind power plants, while the rest of the power plants have been considered gas-fired thermal generators that connect both energy networks at those natural gas and electric nodes reported in Table 4.10. The parameters of the heat rate equations are also reported in Table 4.10 and have been selected considering that an efficiency close to 65% can be attained for the rated capacity of each generator. Lastly, the wind speed scenarios described in the previous case of study in section 4.6 are also considered for

this analysis.

Table 4.10: CIGRE-32 Belgium test system, generators

| Electric Node | Type | Primary energy bus | Rated power MW | $\alpha$ | $\beta$ | $\gamma$ |
|---|---|---|---|---|---|---|
| M1 | Gas | Gent | 850.0 | 450000 | 250 | 1.00 |
| M2 | Gas | Liege | 500.0 | 300000 | 150 | 1.60 |
| N10 | Gas | Mons | 2000.0 | 800000 | 550 | 0.25 |
| N15 | Gas | Blaregnies | 745.0 | 400000 | 250 | 1.30 |
| N105 | Wind | — | 175.0 | aw=1.070 | bw=-0.806 | cw=0.245 |
| N101 | Wind | — | 175.0 | dw=-0.043 | ew=5.09e-3 | fw=3.80e-4 |
| N103 | Wind | — | 150.0 | gw=1.66e-5 | hw=-3.85e-7 | iw=3.65e-9 |

The objective function to be minimized is the cost of natural gas consumed for thermal units, as given by the Equation (4.28).

$$\sigma = \sum_{i \in P_{gen,\,ng}} \left( NG^{k}_{cost\,x\,SCFH}\, MG^{k,i}_{load} \right) \tag{4.28}$$

The formulated RO counterpart consists of 83 variables, 102 equality constraints and 86 inequality constraints per wind scenario and penalizes the variance of this cost in order to set a similar operation cost for all wind speed scenarios. Therefore, the objective function of the robust model is defined by the following expression (4.29).

$$min \qquad \sum_{s \in \varsigma} p_s \sigma_s + \lambda \sum_{s \in \varsigma} p_s \left( \sigma_s - \sum_{s' \in \varsigma} p_{s'} \sigma_{s'} \right)^2 \tag{4.29}$$

Since the active power required to attain the load-generation balance for each wind speed scenario is supplied only by the gas-fired generators, the total active power delivered by these units for a given scenario remains almost constant for different values of $\lambda$ as shown in Figure 4.13. The consequence of this pattern of generation is that the standard deviation for the total active power is almost constant for every value of $\lambda$ as also shown in Figure 4.13. Finally, the existing difference of this power for different values of $\lambda$ is due to the transmission losses re-location, as a result of the penalization of the cost variance.

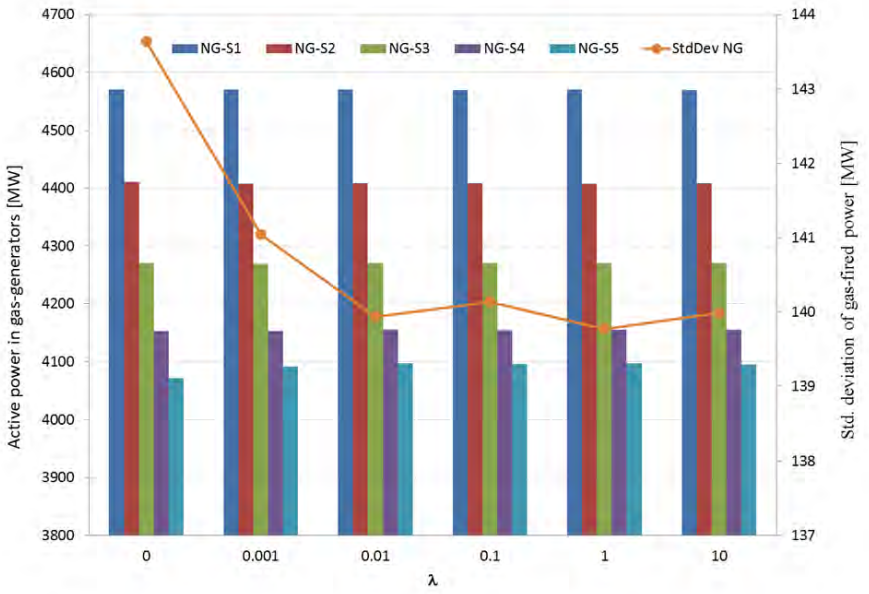


Figure 4.13: Active power and standard deviation of gas-fired units, Case 4.7

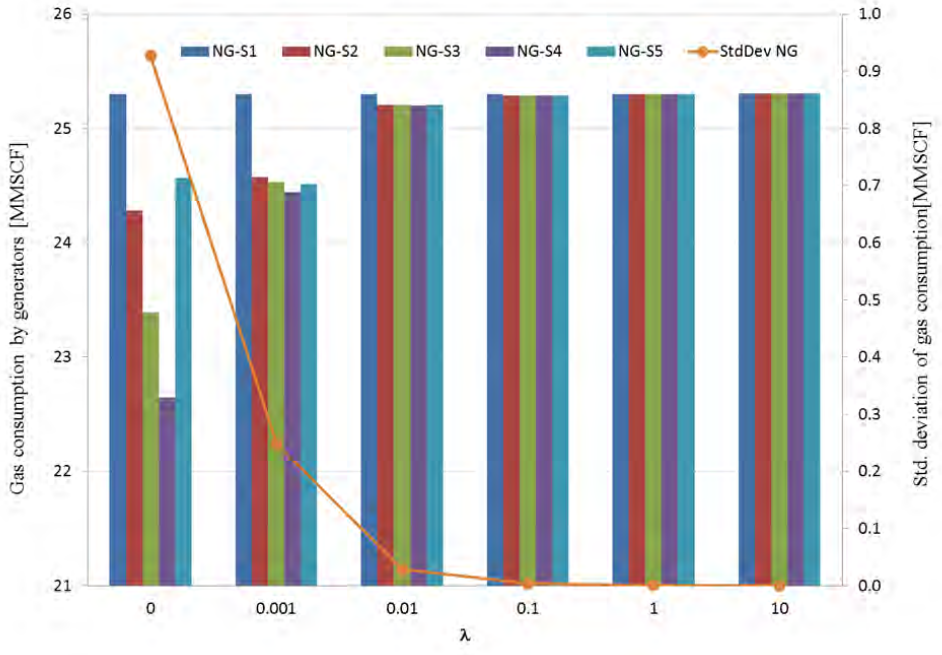


Figure 4.14: Natural gas consumption and standard deviation by generators, Case 4.7

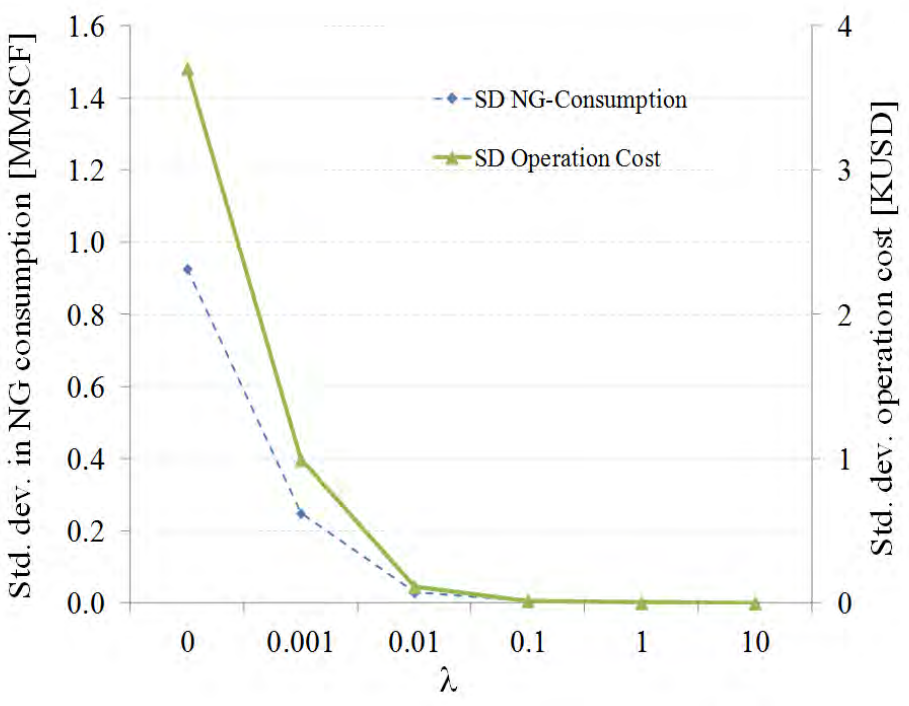


Figure 4.15: Natural gas consumption and standard deviation by generators, Case 4.7

On the other hand, since the gas used for electric generation is the only variable affecting the penalized cost, the reduction in the cost variance is achieved by reducing the variance of the total amount of natural gas consumed by all thermal generators at a given set of wind speed scenarios, as shown in Figure 4.14. Note that even though gas units have a constant production for all values of $\lambda$, the corresponding gas consumption follows a completely different profile because of the way in which these generators are dispatched for different values of $\lambda$: we can generate the same amount of active power considering different generation dispatches, which means a different consumption of natural gas. When a low value for the penalization factor is selected, thereby putting more weight on the total expected cost while there is a lower concerned about the cost variance, the balance in load-generation is attained through the most economic power generating schedule, which implies lower natural gas consumption. On the other hand, a higher value of $\lambda$ results in an increase in the active power dispatch of the most expensive generators, which means higher gas consumption.

In addition, the optimal results obtained for all wind speed scenarios and three different values of $\lambda$ are shown in Table 4.11 for the natural gas nodal pressures and for the active powers generated by thermal units. In order to show the prowess of the proposed approach to obtain an uncertainty-immunized solution, Table 4.12 reports the robust operation cost for each scenario and the total operation cost for each set of scenarios considering different values of the penalization factor $\lambda$.

Lastly, the correlation between the standard deviations of the natural gas consumed by thermal units and the total robust operation cost of the multi-energy system is shown in Figure 4.15.

Table 4.11: Belgian natural gas nodal pressure and active power generated by gas-fired plants

| Nodal Pressure (PSI) | | | | | | | | | | | | | | | | | | | | | |
|---|---|---|---|---|---|---|---|---|---|---|---|---|---|---|---|---|---|---|---|---|---|
| | $\lambda = 0$ | | | | | $\lambda = 0.001$ | | | | | | | | $\lambda = 10$ | | | | | | | |
| Node | $S_1$ | $S_2$ | $S_3$ | $S_4$ | $S_5$ | $S_1$ | $S_2$ | $S_3$ | $S_4$ | $S_5$ | $S_1$ | $S_2$ | $S_3$ | $S_4$ | $S_5$ | $S_1$ | $S_2$ | $S_3$ | $S_4$ | $S_5$ |
| Zeebugge | 950.0 | 950.0 | 950.0 | 950.0 | 950.0 | 950.0 | 950.0 | 950.0 | 950.0 | 950.0 | 950.0 | 950.0 | 950.0 | 950.0 | 950.0 | 950.0 | 950.0 | 950.0 | 950.0 | 950.0 | 950.0 |
| Dudzele | 947.9 | 948.0 | 948.1 | 948.2 | 948.0 | 947.9 | 948.0 | 948.0 | 948.0 | 948.0 | 947.9 | 947.9 | 947.9 | 947.9 | 947.9 | 947.9 | 947.9 | 947.9 | 947.9 | 947.9 | 947.9 |
| Brugge | 942.6 | 943.0 | 943.3 | 943.6 | 942.9 | 942.6 | 942.9 | 942.9 | 943.0 | 942.9 | 942.6 | 942.6 | 942.6 | 942.6 | 942.6 | 942.6 | 942.6 | 942.6 | 942.6 | 942.6 | 942.6 |
| Zomergem | 871.4 | 875.7 | 879.4 | 882.4 | 874.5 | 871.4 | 874.5 | 874.7 | 875.0 | 874.7 | 871.3 | 871.3 | 871.3 | 871.3 | 871.3 | 871.3 | 871.3 | 871.3 | 871.3 | 871.3 | 871.3 |
| Loenhout | 791.2 | 799.2 | 804.7 | 807.6 | 806.6 | 790.7 | 775.0 | 748.3 | 733.0 | 813.9 | 789.3 | 747.3 | 721.0 | 703.3 | 812.2 | 789.3 | 747.3 | 721.0 | 703.3 | 812.2 | 812.2 |
| Antwerpen | 790.9 | 798.9 | 804.5 | 807.4 | 806.4 | 790.4 | 774.7 | 748.0 | 732.7 | 813.6 | 789.1 | 747.0 | 720.7 | 703.0 | 812.0 | 789.1 | 747.0 | 720.7 | 703.0 | 812.0 | 812.0 |
| Gent | 807.5 | 815.3 | 820.7 | 823.6 | 822.6 | 807.0 | 791.6 | 765.5 | 750.5 | 829.7 | 805.6 | 764.5 | 738.8 | 721.5 | 828.1 | 805.6 | 764.5 | 738.8 | 721.5 | 828.1 | 828.1 |
| Voeren | 619.0 | 610.5 | 610.2 | 692.4 | 865.6 | 672.0 | 622.0 | 661.5 | 602.9 | 612.0 | 638.5 | 649.9 | 613.3 | 650.4 | 638.9 | 638.5 | 649.9 | 613.3 | 650.4 | 638.9 | 638.9 |
| Berneau | 897.4 | 903.1 | 911.1 | 920.6 | 869.7 | 897.0 | 913.0 | 925.4 | 934.1 | 905.9 | 897.0 | 921.3 | 926.6 | 934.0 | 897.1 | 897.0 | 921.3 | 926.6 | 934.0 | 897.1 | 897.1 |
| Liege | 869.2 | 875.1 | 883.4 | 893.1 | 840.5 | 868.8 | 885.3 | 898.1 | 907.1 | 877.9 | 868.8 | 893.9 | 899.3 | 906.9 | 868.9 | 868.8 | 893.9 | 899.3 | 906.9 | 868.9 | 868.9 |
| Warnand | 852.7 | 859.2 | 867.4 | 876.7 | 830.3 | 852.5 | 869.1 | 881.4 | 889.7 | 858.8 | 852.6 | 876.4 | 882.4 | 889.4 | 849.5 | 852.6 | 876.4 | 882.4 | 889.4 | 849.5 | 849.5 |
| Namur | 825.7 | 833.3 | 841.5 | 849.8 | 815.1 | 825.8 | 842.5 | 854.0 | 860.9 | 826.8 | 826.2 | 847.4 | 854.5 | 860.3 | 817.0 | 826.2 | 847.4 | 854.5 | 860.3 | 817.0 | 817.0 |
| Anderlues | 807.9 | 816.4 | 824.5 | 831.9 | 806.6 | 808.2 | 825.0 | 835.7 | 841.5 | 804.7 | 808.8 | 827.8 | 835.9 | 840.6 | 794.5 | 808.8 | 827.8 | 835.9 | 840.6 | 794.5 | 794.5 |
| Peronnes | 803.7 | 812.4 | 820.4 | 827.8 | 804.0 | 804.0 | 820.9 | 831.4 | 837.0 | 799.7 | 804.7 | 823.3 | 831.5 | 836.1 | 789.4 | 804.7 | 823.3 | 831.5 | 836.1 | 789.4 | 789.4 |
| Mons | 756.1 | 767.4 | 777.1 | 785.6 | 764.5 | 756.7 | 779.3 | 793.8 | 800.8 | 745.4 | 757.9 | 782.6 | 795.1 | 801.0 | 731.8 | 757.9 | 782.6 | 795.1 | 801.0 | 731.8 | 731.8 |
| Blaregnies | 724.0 | 736.0 | 746.8 | 755.7 | 728.0 | 724.7 | 749.7 | 765.2 | 772.7 | 718.1 | 725.7 | 754.0 | 766.2 | 773.1 | 704.5 | 725.7 | 754.0 | 766.2 | 773.1 | 704.5 | 704.5 |
| Wanze | 842.2 | 848.8 | 857.1 | 866.5 | 819.5 | 842.0 | 858.8 | 871.3 | 879.7 | 848.4 | 842.1 | 866.2 | 872.3 | 879.4 | 839.0 | 842.1 | 866.2 | 872.3 | 879.4 | 839.0 | 839.0 |
| Sinsin | 828.8 | 828.8 | 828.8 | 828.8 | 828.8 | 882.0 | 1007.5 | 892.5 | 828.8 | 828.8 | 828.8 | 1200.0 | 908.2 | 828.8 | 828.8 | 828.8 | 1200.0 | 908.2 | 828.8 | 828.8 | 828.8 |
| Arlon | 364.1 | 364.1 | 364.1 | 364.1 | 364.1 | 472.8 | 678.8 | 492.2 | 364.1 | 364.1 | 364.1 | 941.1 | 520.2 | 364.1 | 364.1 | 364.1 | 941.1 | 520.2 | 364.1 | 364.1 | 364.1 |
| Petange | 300.0 | 300.0 | 300.0 | 300.0 | 300.0 | 425.5 | 646.7 | 446.9 | 300.0 | 300.0 | 300.0 | 918.2 | 477.5 | 300.0 | 300.0 | 300.0 | 918.2 | 477.5 | 300.0 | 300.0 | 300.0 |
| Electric Node | Active power dispatch in gas-fired plants (pu) | | | | | | | | | | | | | | | | | | | | |
| M1 | 8.149 | 7.656 | 7.406 | 7.473 | 6.036 | 8.224 | 10.54 | 12.84 | 13.89 | 4.246 | 8.416 | 12.63 | 14.34 | 15.29 | 3.594 | 8.416 | 12.63 | 14.34 | 15.29 | 3.594 | 3.594 |
| M2 | 5.328 | 5.778 | 5.607 | 4.977 | 10.144 | 5.472 | 5.285 | 4.623 | 3.626 | 1.807 | 5.601 | 3.788 | 4.346 | 3.424 | 1.653 | 5.601 | 3.788 | 4.346 | 3.424 | 1.653 | 1.653 |
| N10 | 26.06 | 24.61 | 24.01 | 23.41 | 16.174 | 25.84 | 22.92 | 20.26 | 19.15 | 32.76 | 25.38 | 22.98 | 18.781 | 18.12 | 34.34 | 25.38 | 22.98 | 18.781 | 18.12 | 34.34 | 34.34 |
| N15 | 6.165 | 6.063 | 5.68 | 5.672 | 8.365 | 6.164 | 5.33 | 4.963 | 4.861 | 2.097 | 6.29 | 4.678 | 5.232 | 4.702 | 1.359 | 6.29 | 4.678 | 5.232 | 4.702 | 1.359 | 1.359 |

Table 4.12: Operation costs obtained by the RO approach

| $\lambda$ | Robust cost per scenario $\xi_s$ | | | | | Total RO cost |
|---|---|---|---|---|---|---|
| | $S_1$ | $S_2$ | $S_3$ | $S_4$ | $S_5$ | |
| 0 | 101192.4 | 97124.0 | 93556.9 | 90574.8 | 98263.2 | 93656.7 |
| 0.001 | 101188.1 | 98291.5 | 98120.8 | 97762.4 | 98045.4 | 99247.6 |
| 0.01 | 101191.3 | 100822.8 | 100831.6 | 100800.6 | 100822.5 | 100980.0 |
| 0.1 | 101207.4 | 101156.3 | 101153.4 | 101153.6 | 101148.4 | 101190.0 |
| 1 | 101195.7 | 101189.5 | 101189.2 | 101189.3 | 101189.0 | 101190.0 |
| 10 | 101215.8 | 101215.5 | 101215.5 | 101215.5 | 101215.5 | 101220.0 |

As a final remark, the concepts of RO are related to the practical operation of the multi-energy system as follows: the RO problem has been formulated in such a way that its RO solution is robust in terms of feasibility over all possible scenarios, independent of the value of the penalization factor $\lambda$, which means that the system operation robustness is ensured because all constraints imposed for each energy network are satisfied over all possible scenarios. On the other hand, a series of robust solutions have been reported with different values of the penalization factor $\lambda$. The solution to be selected in terms of solution robustness is based on the operator's preference or some preferable criteria. For this case, a criterion will be based on the desired trade-off between the total expected cost and the cost variance. If the operators want the total expected cost to be stable over all possible scenarios, the solution to be selected corresponds to the one where the cost variance is minimized, e.g. the solution corresponding to $\lambda = 10$ and a RO cost of 101220. Furthermore, for this selected RO solution, the power system operator has the information regarding how the generators must be dispatched for each wind speed scenario, as shown in Table 4.11, to satisfy the network operation conditions and to obtain the corresponding expected cost very close to the RO solution.

## 4.8 Conclusions and Remarks

The problem of considering wind power uncertainties within the context of the integrated optimization analysis of a multi-energy system composed by natural gas, coal

and electricity systems has been addressed in this chapter. A RO model has been derived from first principles and has been implemented to obtain an optimal operating point of the overall multi-energy system, taking into account the influence of uncertainties in the optimality and feasibility of the solution without making any distributional assumptions; therefore, an uncertainty-immunized solution is achieved for any realization of the wind power scenarios. Numerical examples have been reported to illustrate how the economic and secure operation of the multi-energy system is optimized over all wind power scenarios. The secure operation of the natural gas network is achieved by keeping the nodal gas pressures unchanged along the network for all possible variations of electric power flows. In all these analyzes, the model robustness has been prioritized in order to satisfy all physical and operation constraints associated with each network at the cost of losing optimality with respect to the best objective value.

In the daily real-time operation of power systems, the required power generation is recalculated and updated every specified period of time, based on a economic dispatch or a optimal power flow study, to achieve the power system balance for the corresponding estimated operating conditions. This is the background and justification of our decision to extrapolate this practice to the analysis of multi-energy systems focusing on the wind power randomness. In this context, the proposed approach allows us to fully understand and analyze how the variability in wind power generation affects the steady-state infrastructure interdependencies in a real-time, multi-energy operation environment. Since that study is performed at a specified instant of time, our proposed approach is also carried out for a single time period (snapshot).

The proposal of this chapter is framed in the assessment of the operation condition of a multi-energy infrastructure considering a single time period, where the fossil fuel prices are known in advanced for a daily time horizon. In this context, uncertainties of wind power outputs have the higher impact on the existing interdependency between multi-energy systems. Nevertheless, the proposed approach is completely general and could be extended to consider uncertainties in the supply of coal and gas or in the fossil-fuel prices in order to assess their impact in an energy market environment, which is

actually out of the scope of this thesis.

Lastly, The pros and cons of robust optimization have been described in Section 1.2 of Chapter 1, and can be listed as follows. The pros are: i) The formulation has flexibility for the construction of the penalized variance term in the objective function, ii) The problem can be formulated to get the desired trade-off between the robustness with respect to optimality and to feasibility, iii) The simple implementation of the algorithm benefits their application in different branches of engineering, and iv) The uncertainty model is not stochastic, but rather deterministic. On the other hand, the cons can be framed as: i) The selection of the representative scenarios for the uncertain parameter requires a pre-processing of the input data, ii) The dimension of the problem to be solved is a function of the number of scenarios considered in the study, such that the problem could be intractable for a large number of scenarios, iii) The number of scenarios to be analyzed must be reduced in order to get an equilibrium between accuracy and performance of the solution and, iv) The importance of the penalization factor in the robust optimization problem is that its value indicates the optimal robustness of the solution. High values of the penalization factor indicate that the optimal solution tends to be very close for all scenarios. The opposite applies to low values of this parameter. Hence, the penalization factor value has to be selected based on the operator´s intuition and knowledge of the problem according to the desired trade-off between the robust and the economic aspects of the model.

# Chapter 5

# Multi-Energy and Multi-Period Optimal Flow Under Wind Power Uncertainty

## 5.1 Introduction

Nowadays, wind energy conversion systems are one of the fastest growing type of renewable energy resources used in electric power systems for generating electricity. From the power system operation viewpoint, however, two of the major challenges in using wind as a source of power are associated with the unpredictable nature of wind speed, which translates into generation output variability, and with the possible unavailability of wind power when it is required. Consequently, the quantification of the impact that the high-level of penetration of wind turbine generation will cause on the operation of power systems is of paramount importance. On the other hand, this increasing penetration of wind generation in electric power systems has made evident the necessity of a integral energy network interdependency analysis, in order to explore the optimal use of fossil fuel-based generation and the security constraints associated with different energy networks.

In this context, the optimal generation dispatch of online generating units is impor-

tant in the daily operation planning. Hence, a multi-energy day-ahead optimal power flow (OPF) approach is proposed in this Chapter in order to assess the wind energy penetration in an electric power system and its impact on the fossil fuel-based generation management. The applicability of the proposed approach is demonstrated by integrating a 15-node natural gas network and a 4-node coal distribution system with the IEEE 118-bus power system.

## 5.2 Wind Speed Uncertainty

Unlike fossil-based generation where the rate of energy output is controllable, in the wind power it is variable, uncertain and therefore non-dispatchable. This creates new challenges for both system planners and operators in not only the electricity system, but also the fossil fuel industry [Wang 2008, Liu 2009, Monteiro 2009, Kaplan 2007]. Among these challenges has been the need to ensure a suitable generation dispatch strategy and to assess its impact on the existing interdependency between the primary energy supply and electricity systems, which will be affected by the uncertainty associated with non-dispatchable wind generators.

The assessment of this uncertainty in the energy production in all dispatchable generators as well as the operation conditions of each primary energy network requires new methodologies and formulations; in this context, several efforts have been made for developing software and models to forecast wind speed [Monteiro 2009, Kariniotakis 2006], which have an error around 10% in short-term predictions (24 hours in advance). Since the accuracy of wind forecasts depends on the forecasting horizon, a longer time wind-speed forecast would have larger errors than those of the short-term; in this chapter the impacts of wind forecast error and the amount of wind energy participation in the electric power system have been analyzed.

## 5.3 Multi-Energy and Multi-Period OPF Model

The mathematical models representing each energy network are integrated in a generic multi-time OPF formulation to assess the impact of wind energy penetration on the fuel scheduling of the integrated energy system.

### 5.3.1 Hydraulic Energy System

The hydraulic generators model presented in section 4.3 must be extended to consider intertemporal constraints associated to the water consumption at each subperiod of analysis.

The amount of energy available in one unit of water to electric energy is equal to the product of the mass of the water and the height that the water would fall [Wood 1984]. Figure 5.1 shows a typical representation of hydroelectric reservoirs and the corresponding height of the water falling to the group turbine-generator.

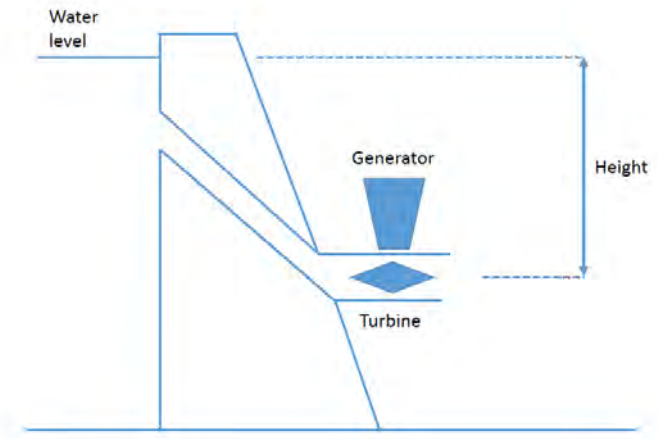


Figure 5.1: Hydraulic reservoir.

In real operation of power systems, the initial hydrological resource availability and the hourly inflow for each dam are considered to be known, and the height that the water would fall is computed as a function of the volume contained in the basin [Wood 1984].

During the water consumption the height of the water level in the reservoir changes as a function of the volume in the current subperiod $t$ of analysis; therefore, from the Equation (4.5), the ratio between the parameter $h^i_{rate}$ and the variable $h_i$ represents the impact of the water's height in the efficiency of energy conversion process. Based on the mentioned above, the water consumption must now be computed for each subperiod of analysis as

$$WR^t_i = \frac{h^i_{rate}}{h^t_i}\left[\alpha^i + \beta^i P^{i,t}_{gen,\,hy} + \gamma^i \left(P^{i,t}_{gen,\,hy}\right)^2\right] \tag{5.1}$$

The efficiency in the energy conversion process of hydraulic power plants is close to 90%, and these units have two important operational characteristics: they have a larger load ramp compared with thermal generators and they lose efficiency at light loads and the minimum active power for this units is frequently limited by mechanical vibrations, [Wood 1984]. A typical water consumption for these units is shown in Figure 5.2 for three different values of height ratio.

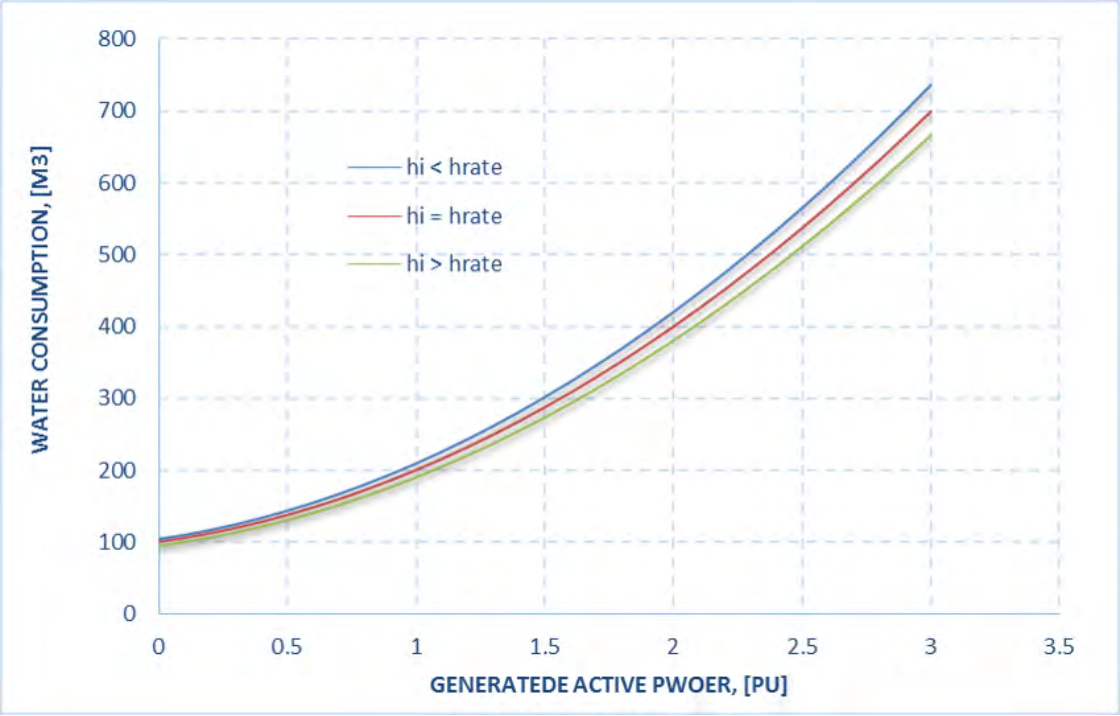


Figure 5.2: Water consumption.

Since the consumption of water is changing with time, the volume in the reservoir at the end of each subperiod of analysis shall be computed by the following linear function,

$$Vol_i^t = Vol_i^{t-1} + Inf_i^t - WR_i^t - Sp_i^t \tag{5.2}$$

where the parameter $inf_i^t$ represents the forecasted inflow of water at the subperiod $t$ for the reservoir $i^{th}$, and the parameter $Sp_i^t$ is the expected spill of water from the same reservoir and at the same subperiod.

Two variables are usually applied to quantify the status of each hydraulic resource, the volume and the water surface level. In this proposal, the second order function (5.3) considers the polynomial relationship between these two variables, and its coefficients are associated with the basin structure

$$h_i^t = \alpha_h^i + \beta_h^i \, Vol_i^t + \gamma_h^i \, \left(Vol_i^t\right)^2 \tag{5.3}$$

Finally, the level of the water shall be limited by the following security constraint:

$$h_i^{min} \leq h_i^t \leq h_i^{max} \tag{5.4}$$

### 5.3.2 General Formulation

The mathematical models representing each energy network are integrated in a generic multi-time OPF formulation to assess the impact of wind energy penetration on the fuel scheduling of the integrated energy system. The objective function could be settled to minimize electric losses, compression station energy consumption, train energy consumption, fossil fuel required by power generators or primary energy delivered by sources such as mines or natural gas deposits, among others; this is represented in a generic form as

$$min \quad \sum_{t}^{T} f_0\left(x_t\right) \quad \forall \, t \, \epsilon \, T \tag{5.5}$$

The set of equality constraints is defined by the following list:

- Nodal balance equation in coal system

$$\begin{aligned} \triangle MC_k^t &= \sum_{m \epsilon k} MC_r^{km,t} + MC_{source}^{k,t} - MC_l^{k,t} - MC_l^{k,i,t} = 0 \\ &\forall\, k \,\epsilon\, N_{co};\ \forall\, t \,\epsilon\, T \end{aligned} \tag{5.6}$$

- Nodal balance equation in natural gas system

$$\begin{aligned} \Delta G^{k,t} &= \sum_{i=1}^{N_{ng}} G_p^{ki,t} + \sum_{j=1}^{N_{ng}} G_c^{kj,t} + \sum_{x=1}^{N_c^k} \tau_k^{xi,t} - \sum_{y=1}^{N_s^k} G_{sk}^{y,t} + \sum_{z=1}^{N_l^k} G_{lk}^{z,t} = 0 \\ &\forall\, i \in N_p^k;\ \forall\, j \in N_c^k;\ \forall\, k \in (N_{ng} - 1)\,;\ \forall\, t \in T \end{aligned} \tag{5.7}$$

- Compression station energy consumption

$$\begin{aligned} BHP^{km,t} &= 0.0854\, Z_a \left[\frac{G_c^{km,t}\, T_k}{E_c\, \eta_c}\right] \left[\frac{c_k}{c_k - 1}\right] \left[\left(\frac{\Pi_{m,t}}{\Pi_{k,t}}\right)^{\frac{c_k - 1}{c_k}} - 1\right] \\ &\forall\, c \in N_c;\ \forall\, t \in T \end{aligned} \tag{5.8}$$

- Pressure compression ratio

$$\begin{aligned} \Pi_{k,t} R^{km} &= \Pi_{m,t} \\ &\forall\, k \wedge m \in N_{ng};\ \forall\, t \in T \end{aligned} \tag{5.9}$$

- Hydraulic reservoir volume, Equations (5.1), (5.2) and (5.3).

- Active and reactive electric power nodal balance equations

$$\begin{aligned} \triangle P_i^t &= P_{gen}^{i,t} - P_{load}^{i,t} \\ &- \sum_{j \in i} \left\{ V_{i,t}^2 G_{ii} + V_{i,t} V_{j,t} \left[ G_{ij} cos\left(\theta_{i,t} - \theta_{j,t}\right) + B_{ij} sin\left(\theta_{i,t} - \theta_{j,t}\right) \right] \right\} = 0 \\ &\forall\, i \in N_e;\ \forall\, t \in T \end{aligned} \tag{5.10}$$

$$\begin{aligned}\triangle Q_i^t &= Q_{gen}^{i,t} - Q_{load}^{i,t} \\ &- \sum_{j \in i} \left\{ -V_{i,t}^2 B_{ii} + V_{i,t} V_{j,t} \left[ G_{ij} sin\left(\theta_{i,t} - \theta_{j,t}\right) - B_{ij} cos\left(\theta_{i,t} - \theta_{j,t}\right) \right] \right\} = 0 \\ &\forall\, i \in \left(N_e - N_{PV}\right);\, \forall\, t \in T \end{aligned} \tag{5.11}$$

- Energy conversion equations

$$\begin{aligned} HR^{i,t} &= \alpha_g^i + \beta_g^i P_{gen}^{i,t} + \gamma_g^i \left(P_{gen}^{i,t}\right)^2 \\ G_{lk}^{i,t} &= \frac{HR^{i,t}}{GHV} \\ &\forall\, i \in Thermal\ generators;\, \forall\, t \in T \end{aligned} \tag{5.12}$$

The set of inequality constraints is defined by the following:

- Coal mine-mouth max. and min. supply limits

$$MC_{source}^{k-min} \leq \sum_{t}^{T} MC_{source}^{k,t} \leq MC_{source}^{k-max} \tag{5.13}$$

- Natural gas deposits max. and min. supply limits

$$G_{sk}^{y-min} \leq G_{sk}^{y,t} \leq G_{sk}^{y-max} \tag{5.14}$$

- Hydro-level surface, Equation (5.4).

The set of security constraints considered in this paper is defined by the following:

- Active power in each generator

$$\begin{aligned} P_{gen}^{i,min} &\leq P_{gen}^{i,t} \leq P_{gen}^{i,max} \\ &\forall\, P_{gen}^{i} \in \left\{ P_{gen,ng}^{i},\, P_{gen,co}^{i},\, P_{gen,hy}^{i},\, P_{gen,w}^{i} \right\};\, \forall\, t \in T \end{aligned} \tag{5.15}$$

- Up/down thermal generation ramps. These equations represent the dynamic behavior of the thermal process inside the power plant, in which the boiler temperature and vapor pressure cannot changed instantly to drive the generator from its minimum to its maximum capacity. Therefore a certain maximum change can be allowed for increasing and decreasing the active power capacity between successive subperiods of analysis in each generator. The mathematical model of these operative constraints are formulated as follows:

If $P_{gen}^{i,t} > P_{gen}^{i,t-1}$

$$R_{up} \geq P_{gen}^{i,t} - P_{gen}^{i,t-1} \tag{5.16}$$

If $P_{gen}^{i,t-1} > P_{gen}^{i,t}$

$$R_{up} \geq P_{gen}^{i,t-1} - P_{gen}^{i,t} \tag{5.17}$$

- The nodal voltage and pressure magnitude limits for the electric and natural gas, respectively, are represented by the following expressions

$$V_i^{min} \leq V_i^t \leq V_i^{max} \tag{5.18}$$

$$\Pi_i^{min} \leq \Pi_i^t \leq \Pi_i^{max} \tag{5.19}$$

## 5.4 Cases of Study

The suitability of the proposed approach to analyze the existing interactions between energy systems is tested on the electricity system related to the IEEE-118 bus test system, which is coupled to other energy networks via 21 generators according to Table 5.1. The cases of study have been formulated and analyzed utilizing CONOPT [Drud 1995], which is a nonlinear optimization solver for GAMS® [Brooke 1998].

Table 5.1: IEEE-118 Test system, generators.

| Electric Node | Type | Primary energy bus | Rated power | $\alpha$ | $\beta$ | $\gamma$ |
|---|---|---|---|---|---|---|
| E-10 | Gas | NG-4 | 197.0 | 200000 | 12 | 3 |
| E-12 | Gas | NG-5 | 204.4 | 200000 | 12 | 3 |
| E-16 | Gas | NG-8 | 179.2 | 200000 | 12 | 3 |
| E-25 | Gas | NG-12 | 183.1 | 200000 | 12 | 3 |
| E-26 | Gas | NG-13 | 187.0 | 200000 | 12 | 3 |
| E-31 | Gas | NG-15 | 169.9 | 200000 | 12 | 3 |
| E-40 | Coal | C-1 | 199.1 | 300000 | 120 | 3.5 |
| E-46 | Coal | C-2 | 186.5 | 300000 | 120 | 3.5 |
| E-49 | Coal | C-3 | 211.2 | 300000 | 120 | 3.5 |
| E-54 | Coal | C-3 | 225.9 | 300000 | 120 | 3.5 |
| E-59 | Coal | C-4 | 222.4 | 300000 | 120 | 3.5 |
| E-61 | Coal | C-4 | 138.7 | 300000 | 120 | 3.5 |
| E-80 | Hydro | — | 231.6 | 4000 | 480 | 0.2 |
| E-87 | Hydro | — | 218.2 | 4000 | 480 | 0.2 |
| E-89 | Hydro | — | 201.9 | 9000 | 450 | 0.2 |
| E100 | Hydro | — | 159.9 | 9000 | 450 | 0.2 |
| E-103 | Hydro | — | 217.0 | 9000 | 450 | 0.2 |
| E-111 | Hydro | — | 217.1 | 4000 | 480 | 0.2 |
| E-65 | Wind | — | 100.0 | a=1.070 | b=-0.806 | c=0.245 |
| E-66 | Wind | — | 100.0 | d=-0.043 | e=5.09e-3 | f=3.80e-4 |
| E-69 | Wind | — | 100.0 | g=1.66e-5 | h=-3.85e-7 | i=3.65e-9 |

The base power of the wind generators is assumed to be equal to their rated active power, and the limits for all the generators is defined by the following inequality constraints

$$20\,MW \leq P^{i,t}_{gen\,gas} \leq 300\,MW \tag{5.20}$$

$$40\,MW \leq P^{i,t}_{gen\,coal} \leq 300\,MW \tag{5.21}$$

$$0\,MW \leq P^{i,t}_{gen\,hydro} \leq 300\,MW \tag{5.22}$$

In addition, the security constraint for nodal voltage magnitudes is defined by Equa-

tion (5.23), while the surface level for hydraulic reservoirs is constrained according to Equation (5.24) considering $h_{rate} = 200\,mts$ for the six hydro reservoirs described in Table 5.1.

$$0.8\,pu \leq V_i^t \leq 1.2\,pu \tag{5.23}$$

$$0.85\,h_{rate}^i \leq h_i^t \leq 1.15\,h_{rate}^i \tag{5.24}$$

The parameters defined in Table 5.1 for hydraulic reservoirs correspond to the parameters of Equation (5.1). In addition, the following parameters are used in accordance with expression (5.3), $\alpha_h = 0.5$, $\beta_h = 2.5x10^{-6}$ and $\gamma_h = 7.9x10^{-8}$, in order to compute the height variation with respect to the volume of water in the reservoir. Finally, the parameters for heat rate curves of thermal units and water consumption for hydraulic generators are chosen to reflect the typical efficiency behavior of each unit in accordance with its best technology available.

The wind speed and load profiles values for 24 hours are shown in the Figure 5.3, where the wind speed profile has been adopted from [Kariniotakis 2006]. Each value in the curve defined as *"the load profile factor"* in Figure 5.3, corresponds to the factor affecting the load specified at each node of the electric and natural gas systems for each single period $t$ contained in $T$. All three wind-generators defined in Table 5.1 are exposed to the same wind-speed profile and are driven by the same wind power curve expressed in per unit of each wind-generators' rated power. This power curve is mathematically represented by a $8^{th}$ degree polynomial function given by Equation (4.8) with coefficients defined in Table 5.1; therefore, each wind-generator produces active power in accordance with the expression (4.9).

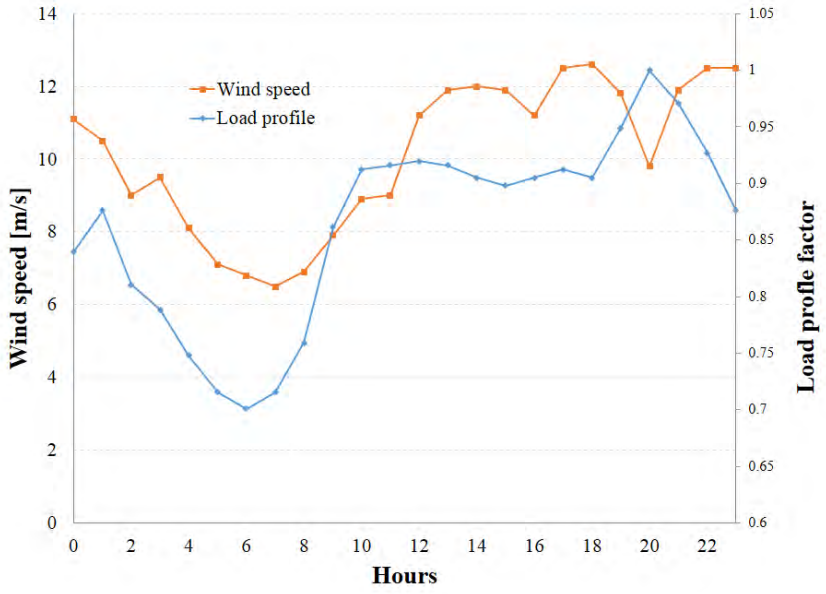


Figure 5.3: Forecast of wind speed and load profiles for 24 hours.

The natural gas system has three loads, two sources and four compressors driven by gas turbines supplied from the inlet node of the compressor station, as depicted in Figure 2.3, [An 2003]. The coal supply network depicted in Figure 4.3 has been considered for the reported cases of study, which consists of four nodes interconnected by three railways, two mines supplying coal at nodes 1 and 2, and two constant loads at nodes 2 (20 tons) and 4 (10 tons). The parameters for the train energy consumption for each railroad depicted in Figure 4.3 are $C_r = 0$, $K_r = 10$, $\eta = 80\%_r$ and $V_r = 60$.

The initial volume for each basin in the hydro-electric generators is 50,000 $Mm^3$, and an hourly inflow of 550 $m^3$ is considered. The cost function defined in Equation (5.25) is related to the cost of primary resources of fossil fuels (natural gas, coal, and diesel) delivered by all the sources at each single period $t$ contained in $T$ (coal, natural gas and diesel)

$$
\begin{aligned}
f_0^t &= \sum_{k_1=1}^{NG-sources} \left(NG_{cost\,x\,SCFH}\, G_s^{k_1,t}\right) \\
&+ \sum_{k_2=1}^{CO-sources} \left(CO_{cost\,x\,Ton}\, MC_s^{k_2,t}\right) \\
&+ DI_{cost\,x\,liter} \sum_{k_3=1}^{Railways} \left(DR_r^{k_3,t}\right)
\end{aligned} \tag{5.25}
$$

An important issue to be considered with this objective function is the impact of other natural gas and coal loads that are not associated with electric generation on the dispatch of electric generators: industrial natural gas (coal) loads can have an undesirable influence on the primary energy resources management, which could be avoided by changing the objective function to optimize the primary energy required by each electric generator. Lastly, the following assumptions are considered:

i) A 30 MW up/down ramp limit is considered for all thermal generators.

ii) Wind energy penetration from 0% to 25% is assumed.

iii) The reference prices are 1 USD/liter for diesel, 4 USD/MSCF for natural gas and 80.15 USD/Ton for coal "Gasoline and Diesel Fuel Update", February 2014, http://www.eia.gov/petroleum/gasdiesel/] and ["Coal", December 12, 2013, http://www.eia.gov/coal/data.cfm#prices].

iv) The coal is assumed to be extracted from Central Appalachia, which has a heating value of 12,500 Btu/lb and belongs to the category of sub-bituminous coal ["Coal", December 12, 2013, http://www.eia.gov/coal/data.cfm#prices].

### 5.4.1 Case of Study 5.A

A multi-time OPF simulation for 24 hours is performed considering the pressure profile in the natural gas network as a security constraint $400 \leq \Pi \leq 1800\, psia$, 0% of

penetration of wind generators and a price of diesel of 0 $/liter. The resulting electric power dispatch profile is shown in Figure 5.4, where it is possible to identify how the active power delivered by fossil fuel generators follow the hourly electric load behavior. For all the coal- and gas-generators the following thermal generation ramps have been considered, 30 MW limit for up ramp and 60 MW for down ramp.

Note that efficiencies of 60% and 44% (at rated power) have been assumed for the natural gas-fired and coal-fired generators, respectively. These efficiencies combined with the price of fossil fuels and the omission of the cost of coal transportation are the reasons for a higher participation of coal-fired generators in this study case, see Figure 5.4.

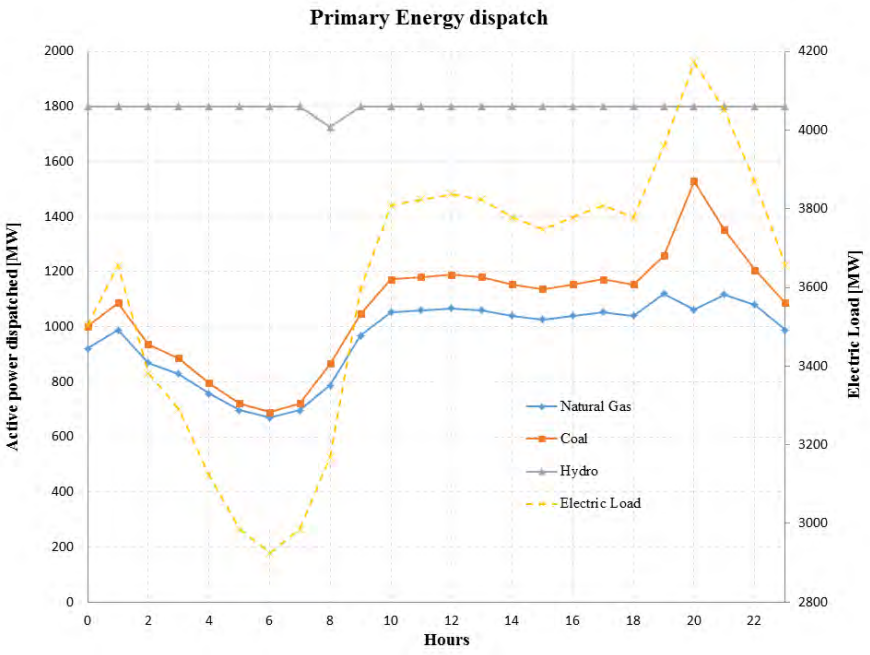


Figure 5.4: Power generation dispatch and electric load profiles, Case 5.A

Under the same operation conditions a wind-energy penetration variations from 0 to 25% of the electric installed capacity *(FWP)* and a wind-speed forecast error of ±10% *(DFW)* are considered to assess the impact of wind energy in fossil fuels management. Figures 5.5 and 5.6 show the energy production cost for natural gas and coal electric-generators, respectively.

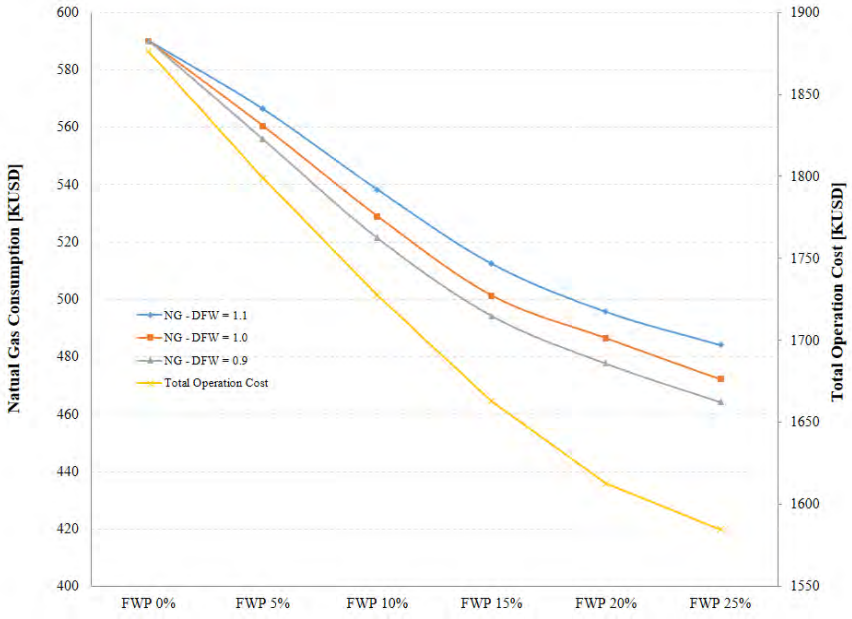


Figure 5.5: Cost of natural gas consumption and total operation as function of the wind-energy penetration, Case 5.A

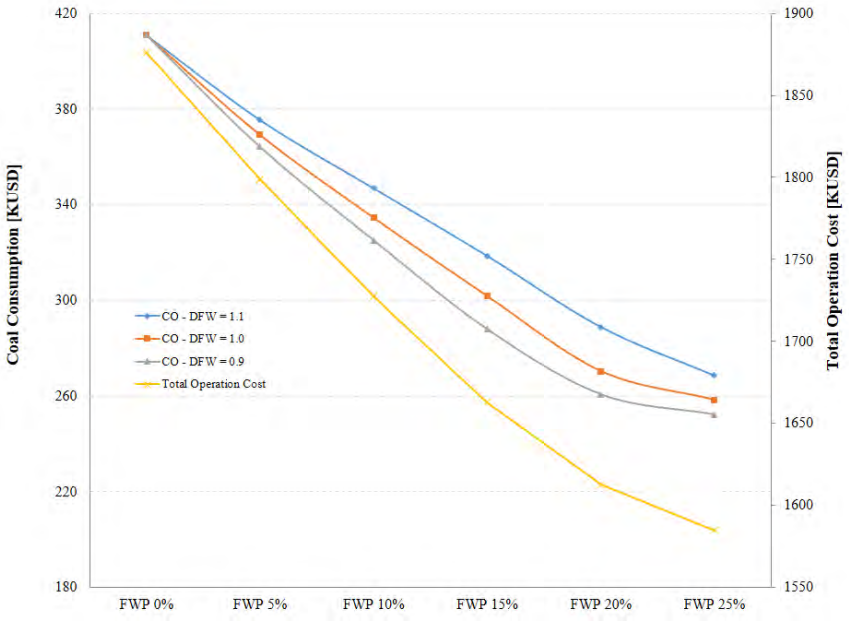


Figure 5.6: Cost of coal consumption and total operation as a function of the wind-energy penetration, Case 5.A

### 5.4.2 Case of Study 5.B

In this second study case the pressure profile in the natural gas system is constrained to $400 \leq \Pi \leq 1200 psia$, and the cost of diesel is assumed to be 1 \$/liter. A penetration of wind generators between 0%-25% (FWP) and a wind-speed forecast error of ±10% (DFW) are considered to assess the impact of wind energy in fossil fuels management. In Figure 5.7, the electric power dispatch profile associated with each type of primary energy examined in the study is shown for a null wind energy penetration. From Figure 5.7 it is possible to identify that coal-fired plants dispatch follow the load profile closer than gas-fired generators, which is opposite to the expected result.

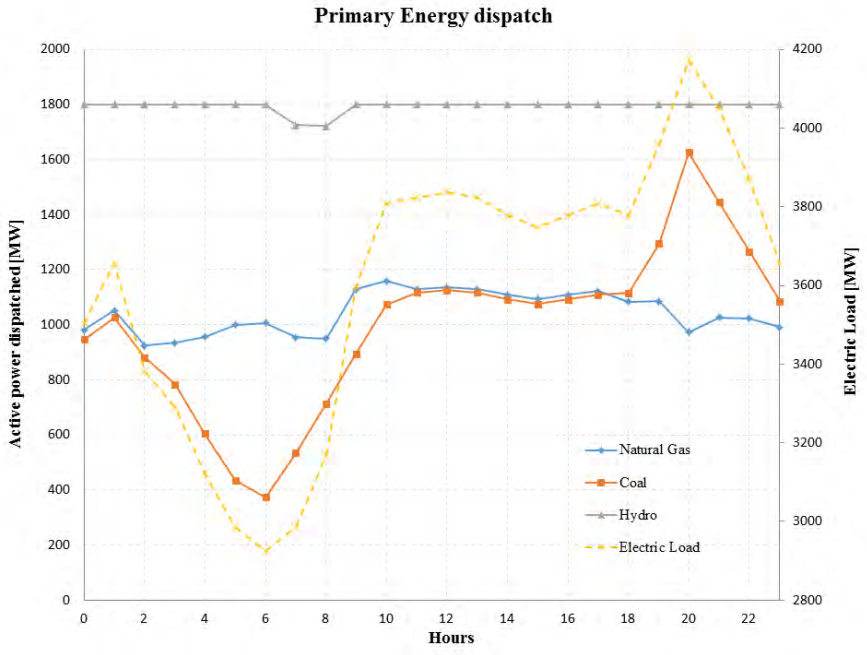


Figure 5.7: Power generation dispatch and electric load profiles for 24 hours, 0% of wind-energy penetration, Case 5.B

This behavior is caused by the combination of a poor efficiency conversion, the fossil fuel prices assumed, the gross heating value for the fossil fuels assumed, the cost associated with coal transportation by rail and the natural gas network security constrained with a pressure profile between 400 and 1200 PSIA. Note that the hourly variation of the active power in fossil fuel plants is limited by the up/down ramp.

The total operating cost of the multi-energy system and the cost of the natural gas consumption by electric generators are shown in Figure 5.8.

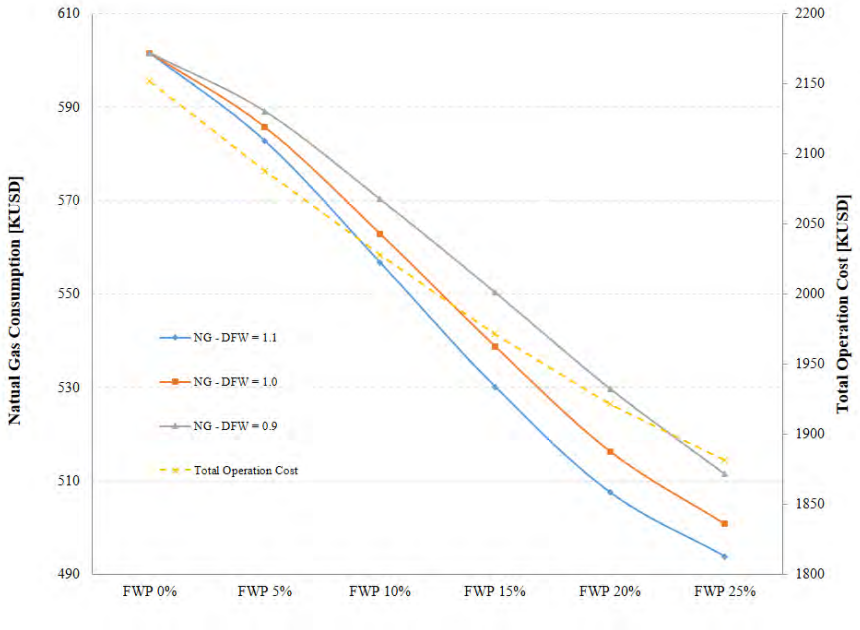


Figure 5.8: Cost of natural gas consumption and total operation as function of the wind-energy penetration, Case 5.B

Figure 5.8 demonstrates that the increase in wind-energy penetration will increase the uncertainty of natural gas consumption, given the existing gap between the corresponding curves associated with NG-DFW=1.1 and NG-DFW=0.9 due to wind forecast errors. By way of example, for the 25% of wind-energy penetration the difference in gas consumption is 17.7 KUSD caused by the wind-speed forecast error (approximately 0.94% of the total operation cost). Additionally, the increase of wind penetration results in a reduction of 100.7 KUSD in the cost of natural gas from the case with 0% to the 25% of wind energy, (this reduction is approximately 37.2% of the total operating cost reduction in the IEEE-118 nodes with a maximum load of approximately 4.173 GW).

The coal-fired cost reduction is illustrated in Figure 5.9. In this case, the maximum difference caused by the wind-speed forecast error is 28.99 KUSD (approximately 1.5% of the total operation cost) when the 25% of wind-energy participation is considered,

and a 149.1 KUSD of reduction in cost of coal from the case with 0% to the 25% of wind energy, (this reduction is approximately 55.1% of the total operation cost reduction).

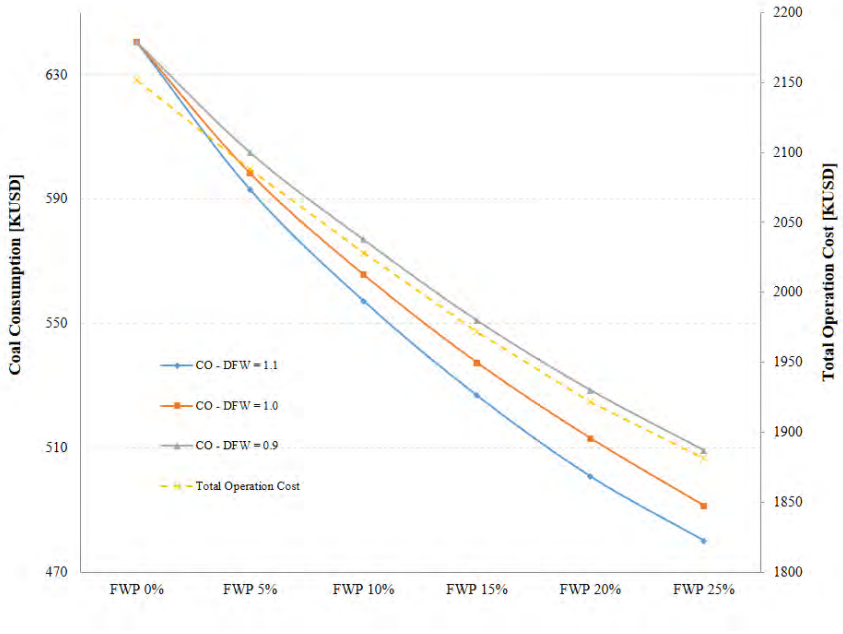


Figure 5.9: Cost of coal consumption and total operation as a function of the wind-energy penetration, 5.B

In order to summarize the results for fossil fuels consumption, Figure 5.10 shows level curves for a variation of FWP and of DFW from 0 to 25% and from 0.8 to 1.2, respectively. Note that the higher wind energy penetration factor, the higher non-linearity of fossil fuel consumption uncertainty considering the forecast wind-speed error. By way of example when the FWP is 5%, the fossil fuel consumption remains almost constant in approximately 1200 KUSD independently of wind-speed forecast error, nevertheless in the case of 20% of FWP, the difference in fossil fuel consumption is approximately 97.3 KUSD.

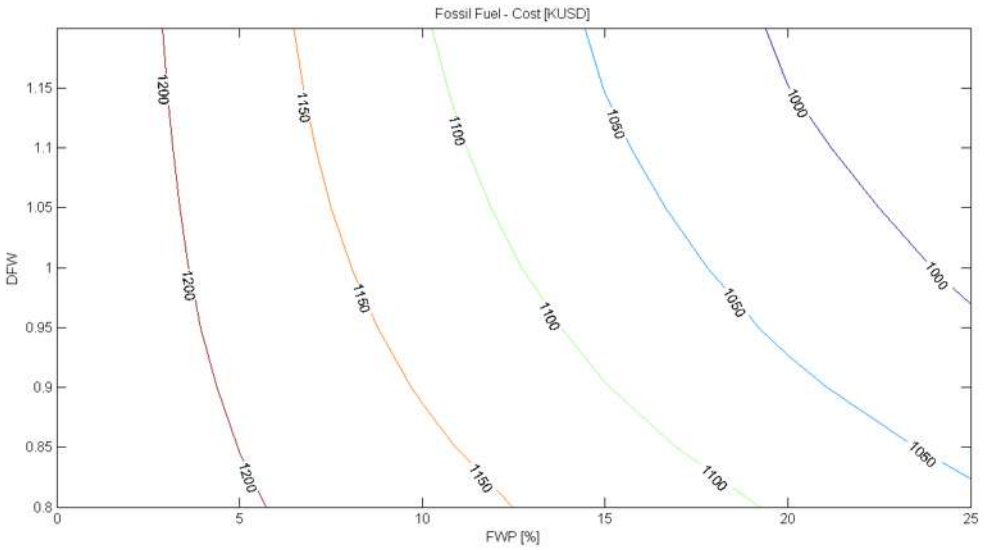


Figure 5.10: Fossil fuels consumption in KUSD, considering different wind penetration factor and wind-speed forecast error, Case 5.B

### 5.4.3 Case of Study 5.C

Owing to the fact that the wind power production is uncorrelated with the level of electric demand, the case study reported in the last section has been newly analyzed but considering the profiles of wind power production and electric load variation, as a function of time, as shown in Figure 5.11. Note that there exists an opposite variation between these two profiles in the time period between 4 and 9 hours. Besides the thermal up and down ramps for generation have been modified to 40/60 MW for up-ramp/down-ramp, respectively, in gas fired power plants, and to 10/10 MW for up-ramp/down ramp in coal-generators. The resulting electric power dispatch for each type of generators is shown in Figures 5.12 and 5.13 considering 0% and 20% of wind-energy penetration in the power system, respectively.

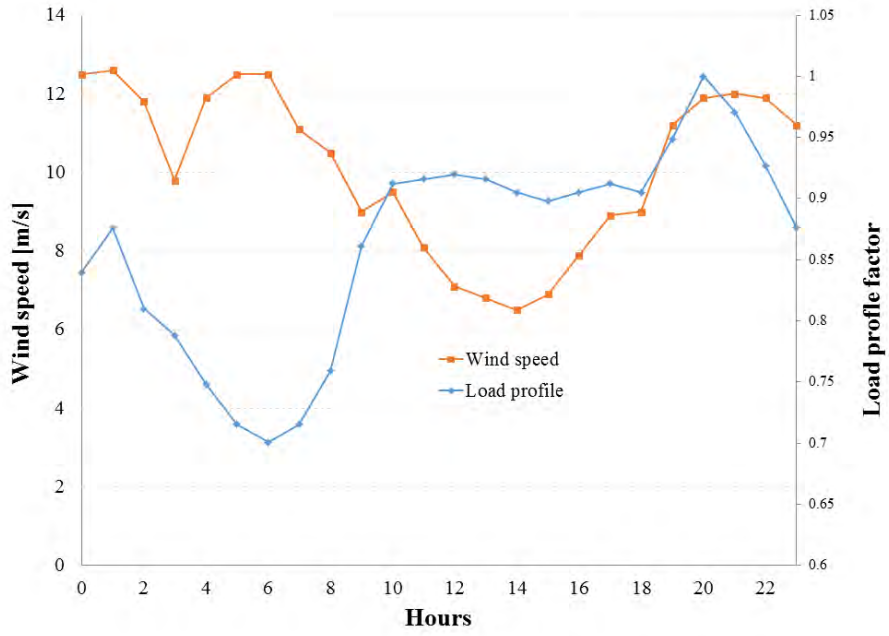


Figure 5.11: Forecast of wind speed and load profiles for 24 hours, Case 5.C

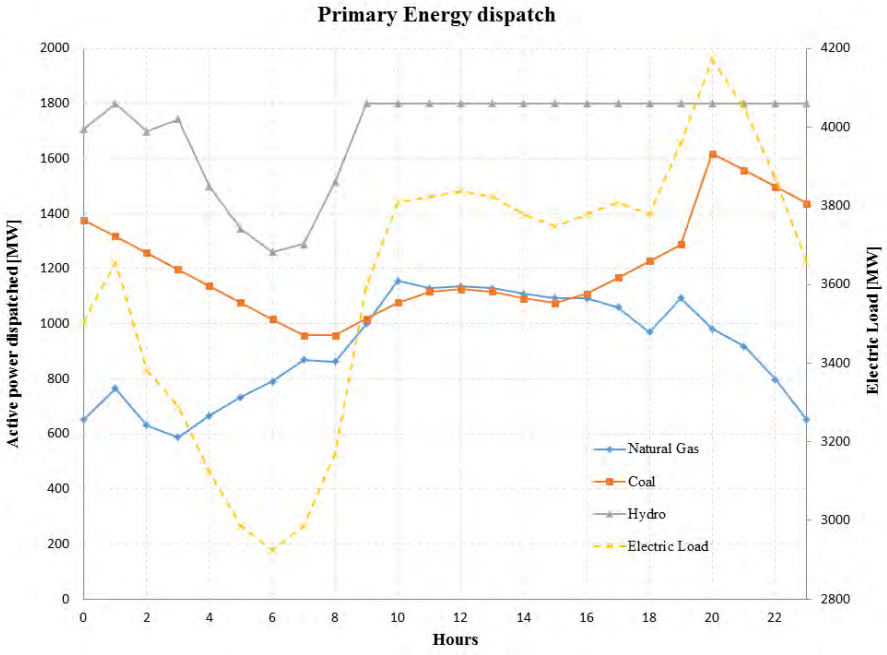


Figure 5.12: Power generation dispatch and electric load profiles for 24 hours, 0% of wind-energy penetration, Case 5.C

From Figure 5.12 it is possible to identify that in the first hours of analysis the

rate of change in the active power delivered by the thermal generators is constrained by their corresponding thermal generation ramps. Hence, the decrement in the electric power load is mainly compensated by regulating the active power produced by hydro-generators.

On the other hand, the effect of the wind-energy penetration on the power dispatch of thermal-based units is clearly observed in Figure 5.13. In this case, these fossil fuel generators have a smaller participation in the load dispatch than when wind generators are not embedded in the system. Besides, the hydro-generators have a larger variation in their active power delivered to the electric power system, compensating the small changes in the thermal generators active power caused by their corresponding ramps constraints and the wind-energy contribution.

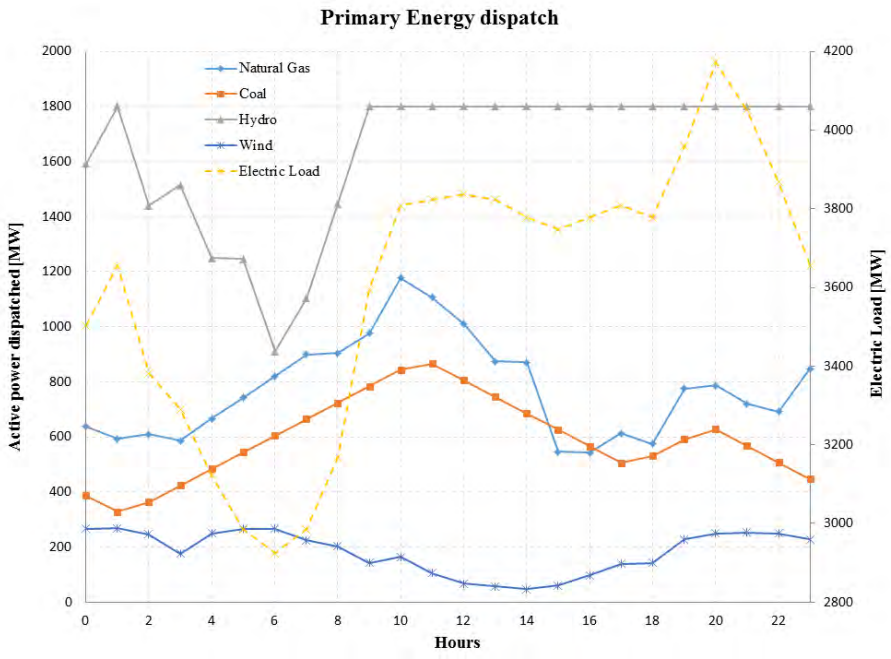


Figure 5.13: Power generation dispatch and electric load profiles for 24 hours, 20% of wind-energy penetration, Case 5.C

## 5.5 Conclusions and Remarks

A nonlinear multi-energy OPF approach has been proposed in order to assess the interactions among different energy networks. As shown in the cases studied, gas-fired generators supply base load and coal-fired generators following the electric load profile as intermittent units, which is the opposite of the typical case. These results are caused mainly by five important parameters assumed in these study cases: 1) the heat rate curves considering the maximum efficiency available for each technology, 2) the gross heating value for each fossil fuel, 3) the price of each fossil fuel, 4) the cost associated with coal transportation by rail, and lastly 5) the natural gas network security constraints for the pressure profile between 400 and 1200 PSI, which could be observed in the nonlinear network formulation.

The study cases reflect the importance of the integral formulation of the different primary energy systems in order to assess their interactions, in this chapter the impact of the forecast error in the wind speed prediction has been remarked and how this becomes more relevant in electric power systems with high wind power penetration factor due to the impact of forecast error increases polynomially and not linearly has happens for systems with low penetrations of wind energy.

# Chapter 6

# Short-Term Operation Planning in Multi-Energy Systems

## 6.1 Introduction

In the daily optimal operation planning of electric power systems, the restrictions associated with the primary energy systems are implicitly considered through the active power generation limits of the dispatchable electric generators, which are set below their rated power. These operating limits intend to approximate the physical constraints associated with each generator as well as those restrictions caused by their corresponding primary energy system that supplies its mechanical torque. In order to avoid this simplistic way of managing the constraints of primary energy systems, this chapter describes a integral formulation of the mathematical models for each primary energy system to assess the short-term optimal operation planning of the electric plants' commitment in multi-energy systems. Simulations are then performed on benchmark systems to achieve an optimal operation condition for all the energy systems while satisfying their corresponding security and operation constraints.

## 6.2 Short-Term Operation Planning

Short-term operation planning for electric power systems is defined in this thesis as the process to economically determine a schedule of what generation units, involving the turn-on and turn-off times and the active power production for each generator, will be used on a day-ahead basis to meet the forecast demand as well as operating constraints. The problem is, therefore, to determine which power plant units should be kept online and which should not, in order to achieve maximum economy.

The solution of this optimization problem involves two separate but mutually connected subproblems: i) the unit commitment or pre-dispatch consisting of the selection of units to be placed in operation and the determination of when they start-up and shut-down in a given period of time, and ii) the economic dispatch, which deals with the most economic allocation of the forecast demand in the same given period of time among the generation units that have been scheduled. For this analysis mixed integer formulations for the optimization problem are commonly utilized, in which the solution gives the scheduled on/off status and the active power contribution of the committed generators for the whole time period of study, which is usually divided into discrete subperiods of one hour [Wood 1984].

This Unit Commitment problem has been approached by a wide group of methodologies and mathematical formulations, in [Narayana 2004] a good bibliographical research has been presented. Based on the information mentioned above, the UC model formulated in this chapter is considering the variable duplication method, explored in [Beltran 2001] and [Murillo 2000]. This formulation proposes a duplication of state variables: the variables associated with only one single time subperiod (*static variables*) and the variables that are part of multiple time subperiods (*dynamic variables*). In order to split the original problem into two subproblems, the first one deals with the integer variables to attain the optimal scheduling of generators, the dynamic variables and the intertemporal constraints.

The solution of this subproblem through a dynamic programming *(DP)* technique is proposed in [Murillo 2000, Beltran 2001], which works on one generator at a time and

for all the subperiods composing the entire time period of study. The second subproblem addresses the static variables and the constraints dependent on static variables, and it is solved by using a nonlinear optimal power flow (OPF) formulation, which solves for the optimal operation condition of one subperiod at a time and for all the subperiods in the study term.

## 6.3 Unit Commitment Formulation

The conventional UC problem can be formulated as an optimization problem with an objective function given by the following equation:

$$\min_{U,P} \left\{ K(U) + \sum_{t=1}^{T} \sum_{i=1}^{N_g} u^{i,t} F^i \left( P_{gen}^{i,t} \right) \right\}. \tag{6.1}$$

The first term in (6.1) describes the minimization of the start-up costs, which is a function of the amount of time that a given generator has been offline or banking [Rajan 2009], while the second term corresponds to the production energy cost of all the online units for all the subperiods in the study term. On the other hand, the constraints of the most basic formulation of the UC problem consist of the power balance equations neglecting losses and the operative limits of committed generators, which are expressed by Equations (6.2) and (6.3), respectively:

$$P_D^t - \sum_{i=1}^{N_g} u^{i,t} P_{gen}^{i,t}; \qquad \forall\, t \in T \tag{6.2}$$

$$u^{i,t} P_{gen}^{i-min} \leq P_{gen}^{i,t} \leq u^{i,t} P_{gen}^{i-max}; \qquad \forall\, i \in N_g. \tag{6.3}$$

### 6.3.1 Unit Commitment by the Variable Duplication Technique

In this section the UC process is described considering the variable duplication technique [Murillo 2000, Beltran 2001]. The basic algorithm is detailed in [Murillo 2000], where the decision variables corresponding to the dynamic $d$ and the static $s$ processes are

first defined as follows:

- Dynamic variables
  - $u^{i,t}$ is the commitment status $\{0, 1\}$ for generator $i$ at time $t$
  - $d_p^{i,t}$ is the active power output for generator $i$ at time $t$
  - $d_q^{i,t}$ is the reactive power output for generator $i$ at time $t$
  - $U$ is the set of commitment statuses $u^{i,t}$, $\forall i \in N_{gen} \wedge \forall t \in T$
  - $D_p$ is the set of generated active powers $d_p^{i,t}$, $\forall i \in N_{gen} \wedge \forall t \in T$
  - $D_q$ is the set of generated reactive powers $d_q^{i,t}$, $\forall i \in N_{gen} \wedge \forall t \in T$
  - $D$ is the set of generated active and reactive powers $\{D_p, D_q\}$
- Static variables
  - $s_p^{i,t}$ is the active power output for generator $i$ at time $t$
  - $s_q^{i,t}$ is the reactive power output for generator $i$ at time $t$
  - $S_p$ is the set of generated active powers $s_p^{i,t}$, $\forall i \in N_{gen} \wedge \forall t \in T$
  - $S_q$ is the set of generated reactive powers $s_q^{i,t}$, $\forall i \in N_{gen} \wedge \forall t \in T$
  - $S$ is the set of generated active and reactive powers $\{S_p, S_q\}$

The Equation (6.1) is then defined in terms of the dynamic and static variables as

$$\min_{D,U,S} \sum_{t=1}^{T} \sum_{i=1}^{N_{gen}} \left[ u^{i,t} F^i \left( d_p^{i,t} \right) + K^{i,t} \left( u^{i,t} \right) \right] \tag{6.4}$$

where $F^i \left( d_p^{i,t} \right)$ corresponds to the operation cost of the $i^{th}$ generator delivering $d_p$ active power in the subperiod $t$, and the term $K^{i,t} \left( u^{i,t} \right)$ is the start-up cost of the $i^{th}$ generator which depends on the time that the unit has been *offline* or *banking*. In addition, the change in the status of one generator is subjected to minimum up/down constraints,

which describe the physical characteristics of the thermal processes in the power plants: if one generator is online, it must remain in this status for a certain quantity of hours before it can be turned off.

Similarly, if one unit is offline, its status must remain the same for a certain number of hours before it can be turned on. On the other hand, the set of equations that constrain the feasible solution space of the optimization problem is

- Dynamic subset of constraints:

$$u^{i,t} P^i_{min} \leq d^{i,t}_p \leq u^{i,t} P^i_{max} \tag{6.5}$$

$$u^{i,t} Q^i_{min} \leq d^{i,t}_q \leq u^{i,t} Q^i_{max} \tag{6.6}$$

$$\{U \mid MDT \wedge MUT\} \tag{6.7}$$

- Static subset of constraints:

$$0 \leq s^{i,t}_p \leq P^i_{max} \tag{6.8}$$

$$Q^i_{min} \leq s^{i,t}_q \leq Q^i_{max} \tag{6.9}$$

$$\left\{S_p \wedge S_q \mid \triangle P^t_i = 0 \wedge \triangle Q^t_i = 0\right\} \forall i \in N_e; \forall t \in T \tag{6.10}$$

where the power flow constraints correspond to the following power flow mismatch equations defined for the $i^{th}$ node and the subperiod $t$:

$$\begin{aligned} \triangle P_i^t &= P_{gen}^{i,t} - P_{load}^{i,t} \\ &- \sum_{j \in i} \left\{ V_{i,t}^2 G_{ii} + V_{i,t} V_{j,t} \left[ G_{ij} cos\left(\theta_{i,t} - \theta_{j,t}\right) + B_{ij} sin\left(\theta_{i,t} - \theta_{j,t}\right) \right] \right\} = 0 \\ &\forall\, i \in N_e;\, \forall\, t \in T \end{aligned} \tag{6.11}$$

$$\begin{aligned} \triangle Q_i^t &= Q_{gen}^{i,t} - Q_{load}^{i,t} \\ &- \sum_{j \in i} \left\{ -V_{i,t}^2 B_{ii} + V_{i,t} V_{j,t} \left[ G_{ij} sin\left(\theta_{i,t} - \theta_{j,t}\right) - B_{ij} cos\left(\theta_{i,t} - \theta_{j,t}\right) \right] \right\} = 0 \\ &\forall\, i \in \left(N_e - N_{PV}\right);\, \forall\, t \in T. \end{aligned} \tag{6.12}$$

Additionally, in order to reach the same active and reactive power solution obtained by the DP (dynamic variables) and the OPF (static variables), the following equality constraints shall be included in the problem formulation:

$$s_p^{i,t} - u^{i,t} d_p^{i,t} = 0,\ \forall i \in N_{gen}\ \wedge\ \forall t \in T \tag{6.13}$$

$$s_q^{i,t} - u^{i,t} d_q^{i,t} = 0,\ \forall i \in N_{gen}\ \wedge\ \forall t \in T. \tag{6.14}$$

The equality constraints defined by (6.13) and (6.14) permit the application of the variable duplication technique to converge to the same values for both sets of optimization variables. Furthermore, these constraints are included through Lagrangian multipliers to formulate the constrained optimization problem (6.4) as an unconstrained optimization problem in the following function:

$$\begin{aligned}\mathcal{L}\left(U,\, D,\, \lambda\right) &= \sum_{t=1}^{T}\sum_{i=1}^{N_{gen}}\left[u^{i,t}F^{i}\left(d_{p}^{i,t}\right)+K^{i,t}\left(u^{i,t}\right)\right] \\ &+ \sum_{t=1}^{T}\sum_{i=1}^{N_{gen}}\lambda_{p}^{i,t}\left[s_{p}^{i,t}-u^{i,t}d_{p}^{i,t}\right] \\ &+ \sum_{t=1}^{T}\sum_{i=1}^{N_{gen}}\lambda_{q}^{i,t}\left[s_{q}^{i,t}-u^{i,t}d_{q}^{i,t}\right]. \end{aligned} \tag{6.15}$$

Reordering terms is possible to split the Lagrangian function into two terms depending only on static and dynamic variables, respectively.

$$\begin{aligned}\mathcal{L}\left(U,\, D,\, \lambda\right) &= \sum_{t=1}^{T}\sum_{i=1}^{N_{gen}}\left[u^{i,t}F^{i}\left(d_{p}^{i,t}\right)+K^{i,t}\left(u^{i,t}\right)-\lambda_{p}^{i,t}u^{i,t}d_{p}^{i,t}-\lambda_{q}^{i,t}u^{i,t}d_{q}^{i,t}\right] \\ &+ \sum_{t=1}^{T}\sum_{i=1}^{N_{gen}}\left(\lambda_{p}^{i,t}s_{p}^{i,t}+\lambda_{q}^{i,t}s_{q}^{i,t}\right) \\ &= \mathcal{L}_{1}\left(U,D,\lambda\right)+\mathcal{L}_{2}\left(S,\lambda\right) \end{aligned} \tag{6.16}$$

where $\lambda = \left\{\lambda_{p}^{i,t},\, \lambda_{q}^{i,t}\right\}$ are the corresponding multipliers to the relaxed equality constraints (6.13) and (6.14). It is important to note the separable nature in Equation (6.16) for the static and dynamic variables.

According to the algorithm proposed in [Murillo 2000], this last Lagrangian function can produce convergence problems towards the feasible solution because the cost reflected in the reactive power outputs for the dynamic subproblems is linear (not strictly convex). To circumvent this potential problem, it has been proposed to augment the Lagrangian function (6.15) by including two convexification terms as follows:

$$
\begin{aligned}
\mathcal{L}(U,D,\lambda) &= \sum_{t=1}^{T}\sum_{i=1}^{N_{gen}}\left[u^{i,t}F^{i}\left(d_{p}^{i,t}\right)+K^{i,t}\left(u^{i,t}\right)\right] \\
&+ \sum_{t=1}^{T}\sum_{i=1}^{N_{gen}}\lambda_{p}^{i,t}\left[s_{p}^{i,t}-u^{i,t}d_{p}^{i,t}\right] \\
&+ \sum_{t=1}^{T}\sum_{i=1}^{N_{gen}}\lambda_{q}^{i,t}\left[s_{q}^{i,t}-u^{i,t}d_{q}^{i,t}\right] \\
&+ \sum_{t=1}^{T}\sum_{i=1}^{N_{gen}}\frac{c_{p}}{2}\left[s_{p}^{i,t}-u^{i,t}d_{p}^{i,t}\right]^{2} \\
&\quad \sum_{t=1}^{T}\sum_{i=1}^{N_{gen}}\frac{c_{q}}{2}\left[s_{q}^{i,t}-u^{i,t}d_{q}^{i,t}\right]^{2}. \qquad (6.17)
\end{aligned}
$$

Despite the solution for the non-convexity problem is achieved by the convexification terms, we have newly a non-separable Lagrangian function where the static and dynamic variables of the same subperiod are mixed in the perfect square trinomial that arises from the convexification terms.

The above mentioned problem has been solved by using the auxiliary problem principle, which consists of substituting the convexification terms for the set of terms given in Equation (6.18) at the $k^{th}$ iteration of the iterative solution process of the optimization problem without affecting the convergence process in the algorithm. For details, please refer to [Murillo 2000].

$$
\begin{aligned}
&+ \sum_{t=1}^{T}\sum_{i=1}^{N_{gen}} c_p \left(s_{p,\,k-1}^{i,t} - u_{k-1}^{i,t} d_{p,\,k-1}^{i,t}\right)\left(s_p^{i,t} - u^{i,t} d_p^{i,t}\right) \\
&+ \sum_{t=1}^{T}\sum_{i=1}^{N_{gen}} \frac{b_p}{2}\left\{\left(s_p^{i,t} - s_{p,\,k-1}^{i,t}\right)^2 + \left(u^{i,t} d_p^{i,t} - u_{k-1}^{i,t} d_{p,\,k-1}^{i,t}\right)^2\right\} \\
&+ \sum_{t=1}^{T}\sum_{i=1}^{N_{gen}} c_q \left(s_{q,\,k-1}^{i,t} - u_{k-1}^{i,t} d_{q,\,k-1}^{i,t}\right)\left(s_q^{i,t} - u^{i,t} d_q^{i,t}\right) \\
&+ \sum_{t=1}^{T}\sum_{i=1}^{N_{gen}} \frac{b_q}{2}\left\{\left(s_q^{i,t} - s_{q,\,k-1}^{i,t}\right)^2 + \left(u^{i,t} d_q^{i,t} - u_{k-1}^{i,t} d_{q,\,k-1}^{i,t}\right)^2\right\}
\end{aligned}
\tag{6.18}
$$

In Equation (6.18) $u_{k-1}^{i,t}$, $d_{p,\,k-1}^{i,t}$, $d_{q,\,k-1}^{i,t}$, $s_{p,\,k-1}^{i,t}$ and $s_{q,\,k-1}^{i,t}$ correspond to the values obtained at the $(k-1)^{th}$iteration in the solution process, and the new constants $b_p$ and $b_q$ are the weights used in the auxiliary problem principle against the original objective function. Lastly, the terms in (6.18) are now separable in such a way that for the $k^{th}$ iteration the Lagrangian function is expressed as

$$
\begin{aligned}
& \mathcal{L}\left(U,\, D,\, S,\, \lambda_{k-1},\, U_{k-1},\, D_{k-1},\, S_{k-1}\right) \\
= \;& \sum_{t=1}^{T}\sum_{i=1}^{N_{gen}}\{u^{i,t}F^{i}\left(d_{p}^{i,t}\right)+K^{i,t}\left(u^{i,t}\right) \\
+ \;& \frac{b_p}{2}u^{i,t}\left(d_{p}^{i,t}\right)^{2}+\frac{b_q}{2}u^{i,t}\left(d_{q}^{i,t}\right)^{2} \\
+ \;& \left[-\lambda_{p,\,k-1}^{i,t}-c_p\left(s_{p,\,k-1}^{i,t}-u_{k-1}^{i,t}d_{p,\,k-1}^{i,t}\right)-b_p u_{k-1}^{i,t}d_{p,\,k-1}^{i,t}\right]u^{i,t}d_{p}^{i,t} \\
+ \;& \left[-\lambda_{q,\,k-1}^{i,t}-c_q\left(s_{q,\,k-1}^{i,t}-u_{k-1}^{i,t}d_{q,\,k-1}^{i,t}\right)-b_q u_{k-1}^{i,t}d_{q,\,k-1}^{i,t}\right]u^{i,t}d_{q}^{i,t}\} \\
+ \;& \sum_{t=1}^{T}\sum_{i=1}^{N_{gen}}\{\frac{b_p}{2}\left(s_{p}^{i,t}\right)^{2}+\frac{b_q}{2}\left(s_{q}^{i,t}\right)^{2} \\
+ \;& \left[\lambda_{p,\,k-1}^{i,t}+c_p\left(s_{p,\,k-1}^{i,t}-u_{k-1}^{i,t}d_{p,\,k-1}^{i,t}\right)-b_p s_{p,\,k-1}^{i,t}\right]s_{p}^{i,t} \\
+ \;& \left[\lambda_{q,\,k-1}^{i,t}+c_q\left(s_{q,\,k-1}^{i,t}-u_{k-1}^{i,t}d_{q,\,k-1}^{i,t}\right)-b_q s_{q,\,k-1}^{i,t}\right]s_{q}^{i,t}\} \\
+ \;& \sum_{t=1}^{T}\sum_{i=1}^{N_{gen}}\{\frac{b_p}{2}\left[\left(s_{p,\,k-1}^{i,t}\right)^{2}+\left(u_{k-1}^{i,t}d_{p,\,k-1}^{i,t}\right)^{2}\right] \\
+ \;& \frac{b_q}{2}\left[\left(s_{q,\,k-1}^{i,t}\right)^{2}+\left(u_{k-1}^{i,t}d_{q,\,k-1}^{i,t}\right)^{2}\right]\} \\
= \;& \mathcal{L}_1\left(U,\, D,\, \lambda_{k-1},\, U_{k-1},\, D_{k-1},\, S_{k-1}\right)+\mathcal{L}_2\left(S,\, \lambda_{k-1},\, U_{k-1},\, D_{k-1},\, S_{k-1}\right).
\end{aligned}
\tag{6.19}
$$

Currently, the Equation (6.19) has the same separable structure as Equation (6.16) for the static and dynamic variables, and the following algorithm proposed in [Murillo 2000] can be used to solve the optimization process associated with the unit commitment problem:

1. Iteration $k = 1$

2. Initialize the vector of Lagrangian multipliers $\lambda$ by running $t$ OPF subproblems considering all the units committed.

3. Solve $t$ OPFs in which all generators are committed and their generation ranges are expanded to include $P_{min}^{i} = 0$, and the special cost $\mathcal{L}_2$ is used.

4. Solve $N_{gen}$ single generator dynamic programming problems:

$$\min_{D,U} \mathcal{L}_1 (U,\, D,\, \lambda_{k-1},\, U_{k-1},\, D_{k-1},\, S_{k-1}) \tag{6.20}$$

5. If the commitment schedule $U_k$ obtained in the previous step is not in a data base of tested commitments, perform a cheap primal feasibility test. If the results are not encouraging, store the schedule in the database labeled as *"infeasible"* and go to step 8; otherwise continue to step 6.

6. Perform another primal feasibility test by running $t$ OPFs with the original $P_{min}$ constraints. If all OPFs are successful, store the commitment in the database labeled as *"feasible,"* and go to step 8.

7. If the mismatch between the two sets of variables (dynamic and static) is small enough, stop.

8. Update all multipliers using subgradient techniques, with a step size no larger than $c_p$ or $c_q$ times the corresponding subgradient, and let $k = k + 1$.

9. Go to step 3.

This previous algorithm has been proposed in [Murillo 2000] as a means to obtain a suitable solution for the unit commitment problem, by solving for $\mathcal{L}_1$ through a dynamic programming technique which is detailed in Section 6.3.2 and for $\mathcal{L}_2$ by an OPF formulation in a separable manner. The update of all multipliers using subgradient techniques is one of many existing methodologies for solving UC problems. In the Lagrangian Relaxation algorithms there are three main updating methods: i) The subgradient method which is the one used in this work, ii) The cutting plane method in which a linear subproblem must be solved to determine the multipliers update, and iii) The bundle method which is a more sophisticated method which updates the multipliers solving a quadratic subproblem; see [Bertsekas 1982, Hiriart 1996].

In the context of this work, the OPF must be solved considering the constraints associated with the primary energy networks involved in the conversion energy process as defined in Section 6.3.3. Figure 6.1 shows a flow chart of this optimization process.

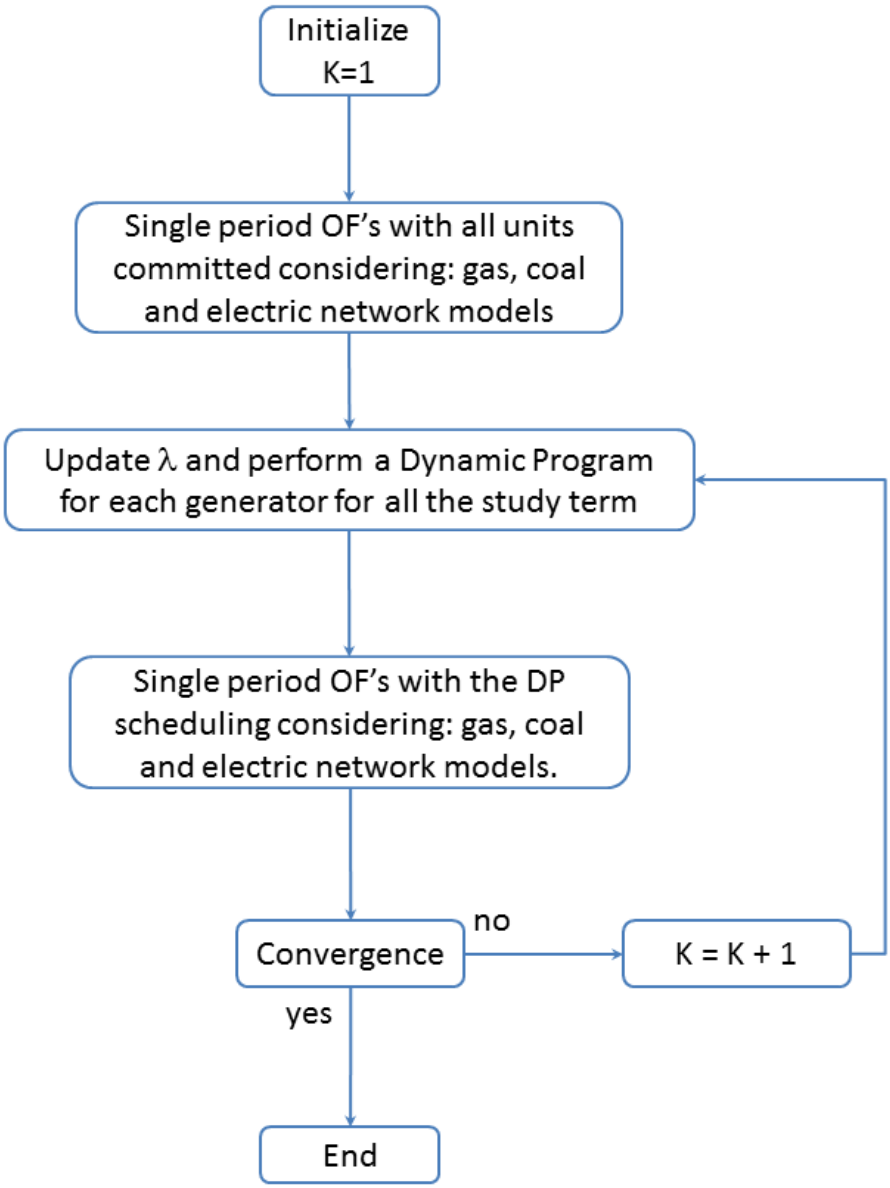


Figure 6.1: Unit Commitment flow chart.

The first step of the algorithm solves $t$ individual OPFs with a nonlinear programming formulation named modified barrier-augmented Lagrangian [Goldfarb 1999]. This

optimization method, which is detailed in Section (6.3.3), is considered an interior-exterior point approach because of the treatment of inequality constraints with a modified barrier term and the equality constraints with a penalization term included in the Lagrangian function.

Once the OPFs have been solved, these results provide the initial condition for the Lagrange multipliers, and one dynamic programming (DP) study is then performed for each thermal-generator to set the plant operation condition. The detailed dynamic programming algorithm is presented in Section 6.3.2.

In the case of hydro-generators, their active/reactive power levels are determined considering that these units are always committed and that their water consumption over the entire time period of analysis shall be less than or equal to the total resource available in their corresponding dam.

Note that under certain operation conditions, the optimization process could lead to one solution where some generators are offline but consuming a certain quantity of fuel to keep the boiler ready to start over in the following subperiods of analysis. The power plants operating in this regime are referred to as *"banking units"* [Murillo 2000] and [Rajan 2009]. After the operating conditions of all dispatchable generators have been established by the dynamic programming module, a new set of $t$ single period OPFs studies is performed considering only the units committed for each subperiod of study. The algorithm is stopped when the difference between the active/reactive powers obtained from DP (dynamic variables) and OPF (static variables) for each subperiod is below a predefined tolerance [Murillo 2000].

### 6.3.2 Dynamic Programming Module

This module determines the status *on, off, or banking* for each generator and for all the subperiods of analysis based on the comparison of its individual cost and the system's cost.

The initial state for each generator must be specified: the initial operative status

for each generator in the subperiod $t-1$ with its corresponding number of hours that the unit has been in this condition.

Figure 6.2 shows a typical dynamic programming graph for one generator where its operating status between two consecutive subperiods is illustrated. In this case, the operation parameters are defined as follows: the *Minimum Down Time (MDT)* corresponds to four hours, the *Minimum Up Time (MUT)* is three hours, and the *Downtime Cold Start (DCSA)* corresponds to eight hours. The numbers inside the circles indicate the number of subperiods of time that the generator has been operating in either *on* or *off* status. The positive numbers indicate the number of subperiods that the generator has been *online*; otherwise, the generator has been *offline* by $n$ subperiods.

If the generator has been in *"on"* status, the unit must remain online for a minimum of $MUT$ hours: if the generator has been *online* one or two hours, this unit must remain *online* for a least the next subperiod of analysis (the unit cannot be turned off). On the other hand, if the unit has been *online* for at least three hours, now the generator has two options: remain *online* or be turned off depending on its individual cost with respect to the system's operation cost. In these cases where the unit is already *online,* the transition cost is represented by the operation cost $c$.

Based on the operating parameters described in the last paragraph, if the generator has been in *"off"* status, the unit must remain offline for at least $MDT$ subperiods: if the generator has been *offline* one, two or three subperiods, it must remain *offline* for a least one extra subperiod (the unit cannot be turned on) to satisfy the minimum of four subperiods defined by $MUT$. On the other hand, if the generator has been *offline* by four subperiods or more, it has two options: to remain offline or change its operating status to online depending on the comparison of its individual cost with respect to the system's operation cost. In this case, the cost of turning on the unit is represented in Figure 6.2 by $SC4$, $SC5$, etc., which is a function of the operating cost plus the start-up cost.

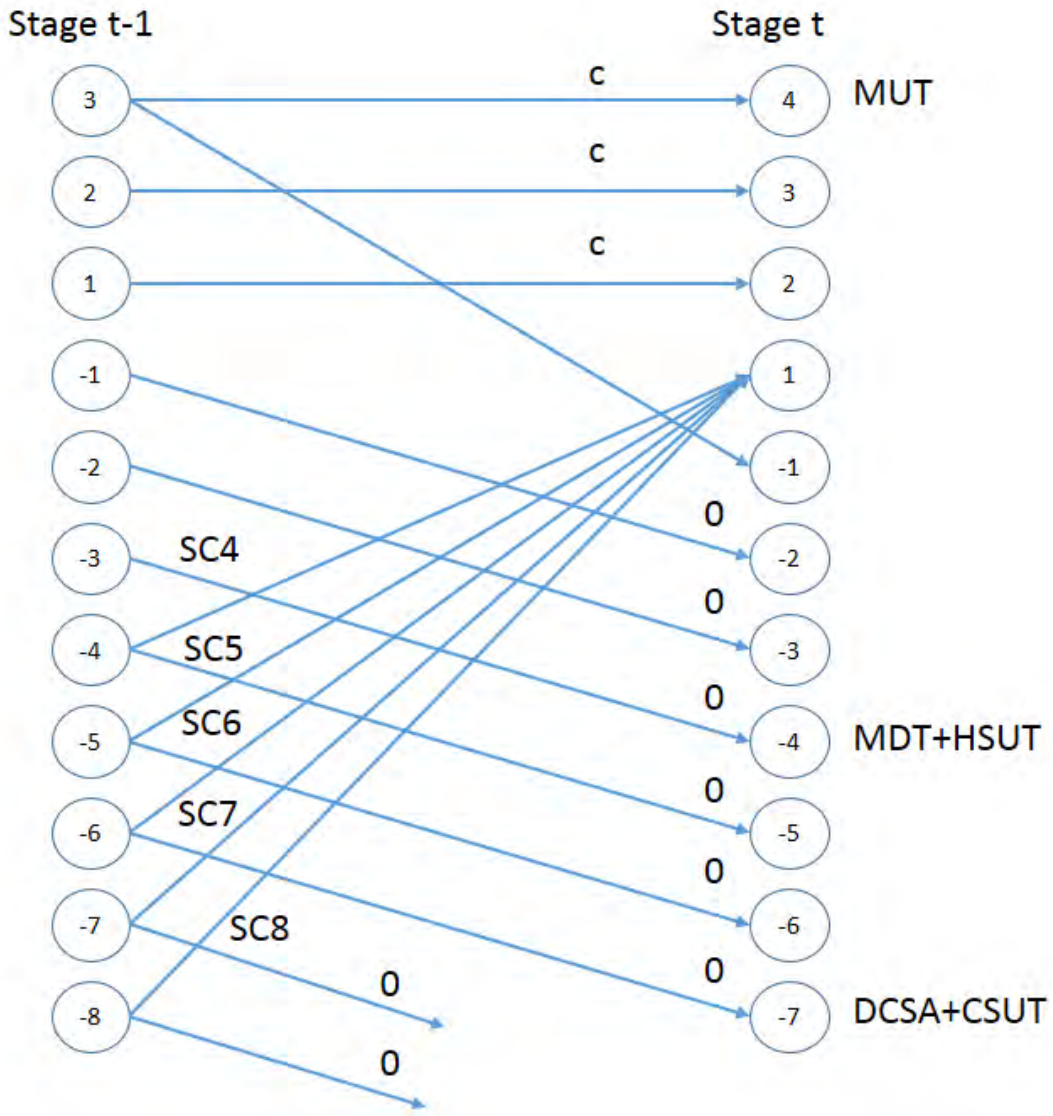


Figure 6.2: Dynamic programming graph for a single generator.

Based on the parameters defined above, Figure 6.2 shows the possibilities for change or remain the status for the generator between consecutive subperiods. The first column of circles represent different options of hours that the variable $n$ can take, for example:

- If $n = 1$, this means the unit has been *online* for one subperiod and in accordance with the parameters defined for this single unit where $MUT = 3$, the unit must remain *online* for at least three subperiods before it can be turned off. Because of

this constraint, the unit cannot change its status and shall remain online in the next subperiod as it is represented in Figure 6.2 with the transition from $n = 1$ in the subperiod $t - 1$ to $n = 2$ in the subperiod $t$.

- If $n = 2$, the unit has not been online enough time to satisfy the $MUT = 3$ constraint, therefore, the unit must remain online for another subperiod.

- If $n = 3$, the unit has been enough time *online*, and the generator now has two operating options: if its marginal operation cost is less than the system's marginal cost, the unit shall remain *online*; otherwise the unit must be turned off.

- If $n > 3$, the same logic must be applied to determine the operating status of the thermal-generator in the next subperiod of analysis.

- In the case where $n = -1$, this means that the unit is *offline* in the stage $t - 1$, and the unit has not been *offline* enough time to be switched on given that the minimum down time has been defined by $MDT = 4$. Therefore, this unit must remain *offline* as indicated by the transition state in Figure 6.2.

- If $n = -2$ or $n = -3$, the unit still has not been enough time *offline* to be switched on.

- If $n = -4$, the unit has two operating options: remain *offline* if its marginal operation cost is higher than the system's marginal cost, otherwise the unit must be turned on.

- Once the unit has been *offline* for $n \geq MDT$ subperiods, the start-up cost considers the residual temperature in the boiler of the thermal-generator which becomes exponentially colder as a function of $n$. This means that if the unit has been *offline* for a large number of subperiods $n > DCSA$, the unit is considered to be starting up with a down time cold start $DCSA$ plus an additional cold start-up cost $CSUT$. On the other hand, if $MDT < n < DCSA$, the unit takes advantage of the residual temperature in the boiler, and less fuel is required for the start-up

of the generator, since the unit is turned on at the hot start-up time $HSUT$ plus minimum down time $MDT$.

Lastly, the following intertemporal constraints must be satisfied in this dynamic programming module:

1. Ramp up/down of thermal power generators, per Equations (5.16) and (5.17).

If $P_{gen}^{i,t} > P_{gen}^{i,t-1}$

$$R_{up} \geq P_{gen}^{i,t} - P_{gen}^{i,t-1} \tag{6.21}$$

If $P_{gen}^{i,t-1} > P_{gen}^{i,t}$

$$R_{up} \geq P_{gen}^{i,t-1} - P_{gen}^{i,t} \tag{6.22}$$

2. Maximum and minimum limits for thermal generators, according to Equation (5.15).

$$\begin{aligned} P_{gen}^{i,min} \quad &\leq \quad P_{gen}^{i,t} \leq P_{gen}^{i,max} \\ &\forall\, P_{gen}^{i} \in \left\{ P_{gen,ng}^{i},\, P_{gen,co}^{i},\, P_{gen,hy}^{i},\, P_{gen,w}^{i} \right\};\, \forall\, t \in T \end{aligned} \tag{6.23}$$

3. The constraints associated with the thermal process in the power plant:

   *3.1.* The minimum up time $MUT$ that the generator must remain *online* before being able to be turned *off*.

   *3.2.* The minimum down time $MDT$ that the generator must remain *offline* before being able to be turned *on*.

   *3.3.* The must run constraint, $MR$, which indicates that the unit must remain online $\forall t \in T$.

Regarding the start-up cost, which is a function of the time that the unit has been *offline*, it can be computed by

$$Start^{i}_{cost} = Start^{i}_{cost\,max}\left(1 - e^{-\gamma^{i}_{b}t}\right) \tag{6.24}$$

where $\gamma^{i}_{b}$ represents the time constant associated with the thermal processes inside the boiler for $i^{th}$ power plant. In addition, $Start^{i}_{cost\,max}$ is the cost for the starting process considering that the unit is completely cold: the unit has been *offline* for a number of subperiods higher than the *Down time cold start applies (DCSA).*

The algorithm for the dynamic programming modules applied to each dispatchable generator in the system is described as follow:

1. Determine the current status of each generator and the number of hour that the unit has been in this status or if the unit has and declaration of *"Must Run"*.

2. Determine if the unit is able to change its current status, based on the $MUT$ or $MDT$ parameters defined for each generator.

3. Compute $d^{i,t}_{p}$ for each generator and for each subperiod of analysis.

$$d^{i,t}_{p} = \frac{\left(\lambda^{i,t}_{p} - \beta^{i}_{p} + c_{p}\left(s^{i,t}_{p} - u^{i,t}d^{i,t}_{p}\right) + b_{p}u^{i,t}d^{i,t}_{p}\right)}{(2c_{p} + b_{p})}$$

4. Compare the dynamic active power with respect to the load ramp constraints of each generator.

5. Compare the marginal cost of the unit with respect to the operative cost of the system for one subperiod of analysis at the time, and determine if the unit must change its status.

6. Continue to the next subperiod for the complete analysis term.

7. Use this schedule of the units in the next Optimal Flow step.

### 6.3.3 Optimal Power Flow Module

The optimal power flow solution method adopted in this chapter is based on the *Modified Barrier - Augmented Lagrangian (MBAL)* formulation presented in [Goldfarb 1999]. In which, departing from the classical OPF formulation given by

$$\begin{aligned} minimize \quad & f_0(x) & \\ s.t. \quad & f_i(x) & \geq 0 \; i = 1, ...., p \\ & g_j(x) & = 0 \; i = j, ...., q \end{aligned} \tag{6.25}$$

where $x \in \mathbb{R}^n$, and $f_o$, $f_1$, ... , $f_p$ and $g_1$, $g_2$, ..., $g_q$ correspond to the inequality and equality constraints sets, respectively, defined by $C^2$ functions from the mapping $\mathbb{R}^n \to \mathbb{R}$. Transforming the original constrained optimization problem (6.25) to an unconstrained optimization problem, the Lagrangian function defining the latter problem is given by

$$\mathcal{L}(x, u, v) = f_o(x) - u^T f(x) - v^T g(x) \tag{6.26}$$

where $u \in \mathbb{R}^p_+$, $v \in \mathbb{R}^q$, $f(x) = [f_1(x), \cdots, f_p(x)]$ and $g(x) = [g_1(x), \cdots, g_q(x)]$ are column vectors. $\mathbb{R}^p_+$ denotes the nonnegative orthant of $\mathbb{R}^p$. Let $x^*$ be a strict local minimum of problem (6.25), and $I^* = \{i : f_i(x^*) = 0\}$ where $i \in \{1, \cdots, r\}$ is the set of indices of the active inequality constraints in the optimal solution. Assuming that the second-order sufficient conditions for an isolated local minimum hold at $x^*$ and given that $\nabla f_i(x^*)$ and $\nabla g_j(x^*)$ are linearly independent, there exists a unique Lagrange multiplier vector $w* = (u^*, v^*) \in \mathbb{R}^p_+ \times \mathbb{R}^q$ such that

$$\nabla_x \mathcal{L}(x^*, u^*, v^*) = \nabla f_0(x^*) - \sum_{i=1}^{p} u_i^* \nabla f_i(x^*) - \sum_{j=1}^{q} v_j^* \nabla g_j(x^*) = 0 \tag{6.27}$$

Hence, the Hessian of the Lagrangian function with respect to $x$ at $(x^*, u^*, v^*)$ is

given by

$$\nabla_{xx}^2 \mathcal{L}\left(x^*,\, u^*,\, v^*\right) = \nabla^2 f_0\left(x^*\right) - \sum_{i=1}^{p} u_i^* \nabla^2 f_i\left(x^*\right) - \sum_{j=1}^{q} v_j^* \nabla^2 g_j\left(x^*\right) \tag{6.28}$$

which is positive definite on the affine subspace tangent to the feasible set at $x^*$.

Lastly, strong complementary slackness holds for the $p$ inequality constraints:

$$u_i^* f_i\left(x^*\right) = 0,\; i = 1, \cdots,\, p \tag{6.29}$$

$$u_i^* > 0,\; i = 1, \cdots, r;\; f_i\left(x^*\right) > 0,\; i = r+1, \cdots,\, p$$

where $\{1, \cdots,\, r\}$ represents the active set of inequality constraints.

Based on the theoretical description reported above, the *modified barrier-augmented Lagrangian function (MBAL)* is defined as follows:

$$F\left(x,\, u,\, v,\, k\right) = \begin{cases} f_0\left(x\right) - k^{-1} \sum_{i=1}^{p} u_i \, ln\left(k f_i\left(x\right) + 1\right) \\ - \sum_{j=1}^{q} v_j g_j\left(x\right) + \frac{k}{2} \sum_{j=1}^{q} g_j^2\left(x\right), & if\; x \in int\, \Omega_k \\ \infty, & if\; x \notin int\, \Omega_k \end{cases} \tag{6.30}$$

where $\Omega_k = \{x : f_i\left(x\right) \geq -k^{-1},\, i = 1, \cdots,\, p\}$ represents the solution space.

Note that $F\left(x,\, u,\, v,\, k\right)$ contains the penalty-barrier parameter $k$ which shall be large enough (typically $k > 10000$), which is used in the modified barrier terms for the inequality constraints and augmented Lagrangian terms for the equality constraints in (6.25).

If the complementary slackness condition (6.29) holds at the point $(x^*,\, u^*,\, v^*)$, then for any $k > 0$

$$F\left(x^*,\, u^*,\, v^*,\, k\right) = f_0\left(x^*\right) \tag{6.31}$$

with its corresponding gradient

$$\begin{aligned}\nabla_x F(x^*, u^*, v^*, k) &= \nabla f_0(x^*) \\ &- \sum_{i=1}^{p} \frac{u_i^*}{k f_i(x^*) + 1} \nabla f_i(x^*) - \sum_{j=1}^{q} \left(v_j^* - k g_j(x^*)\right) \nabla g(x^*)\end{aligned} \tag{6.32}$$

furthermore, the corresponding Hessian term is given by

$$\begin{aligned}\nabla_{xx}^2 F(x^*, u^*, v^*, k) &= \nabla_{xx}^2 \mathcal{L}(x^*, u^*, v^*) \\ &+ k \nabla f^T(x^*) U^* \nabla f(x^*) + k \nabla g^T(x*) \nabla g(x^*)\end{aligned} \tag{6.33}$$

where $\nabla f(x)$ and $\nabla g(x)$ are the Jacobian matrices of the vector functions $f$ and $g$ respectively. In addition, $U^*$ is a diagonal matrix with diagonal entries $u_i^*$, $i = 1, \cdots, p$. Contrary to the classical OPF mathematical models where the state variables' vector is composed of the set $\{x, u, v\}$, in the MBAL model this state variables vector is composed only by $x$.

The MBAL formulation detailed in [Goldfarb 1999] shows that if the vector of Lagrange multipliers $w = (u, v) \in \mathbb{R}_+^p \times \mathbb{R}^q$ is close enough to $w^* = (u^*, v^*)$, then $\hat{x}$ is a good approximation of $x^*$ if $\hat{x} = \hat{x}(u, v, k) = argmin\{F(x, u, v, k) \mid x \in \mathbb{R}^n\}$. The minimizer $\hat{x}$ can then be used to improve the approximation of $w = (u, v)$ to the optimal Lagrange multipliers $w^* = (u^*, v^*)$ given that the fixed penalty-barrier parameter $k > 0$ is sufficiently large. Hence, the sequential minimization of $F(x, u, v, k)$ and the corresponding updating of the Lagrange multipliers $(u, v)$ make possible to get a globally convergent method by solving the problem 6.25 with any initial condition $(x, w)$, where $x \in int\,\Omega_k$ and $w = (u, v) \in \mathbb{R}_+^p \times \mathbb{R}^q$ with a parameter $k$ large enough.

When the optimal power flow module is only applied to the analysis of an electricity

system, the nonlinear constraints associated with the power flow mismatch Equations (6.34) and (6.35) must be satisfied $\forall t \in T$, and this formulation is referred to as the generalized unit commitment GUC problem [Beltran 2001];

$$\begin{aligned} \triangle P_i^t &= P_{gen}^{i,t} - P_{load}^{i,t} - \sum_{j \in i} \left\{ V_{i,t}^2 G_{ii} + V_{i,t} V_{j,t} \left[ G_{ij} cos\left(\theta_{i,t} - \theta_{j,t}\right) + B_{ij} sin\left(\theta_{i,t} - \theta_{j,t}\right) \right] \right\} = 0 \\ & \forall\, i \in N_e;\, \forall\, t \in T \end{aligned} \tag{6.34}$$

$$\begin{aligned} \triangle Q_i^t &= Q_{gen}^{i,t} - Q_{load}^{i,t} - \sum_{j \in i} \left\{ -V_{i,t}^2 B_{ii} + V_{i,t} V_{j,t} \left[ G_{ij} sin\left(\theta_{i,t} - \theta_{j,t}\right) - B_{ij} cos\left(\theta_{i,t} - \theta_{j,t}\right) \right] \right\} = 0 \\ & \forall\, i \in \left(N_e - N_{PV}\right);\, \forall\, t \in T \end{aligned} \tag{6.35}$$

In the context of multi-energy systems optimization, however, the physical and operating constraints related to each network must also be included in the OPF formulation in order to obtain a feasible solution. Hence, the following equality constraints shall be included:

- Nodal balance equation in coal system

$$\begin{aligned} \triangle MC_k^t &= \sum_{m \epsilon k} MC_r^{km,t} + MC_{source}^{k,t} - MC_l^{k,t} - MC_l^{k,i,t} = 0 \\ & \forall\, k \,\epsilon\, N_{co};\, \forall\, t \,\epsilon\, T \end{aligned} \tag{6.36}$$

- Nodal balance equation in natural gas system

$$\begin{aligned} \Delta G^{k,t} &= \sum_{i=1}^{N_{ng}} G_p^{ki,t} + \sum_{j=1}^{N_{ng}} G_c^{kj,t} + \sum_{x=1}^{N_c^k} \tau_k^{xi,t} - \sum_{y=1}^{N_s^k} G_{sk}^{y,t} + \sum_{z=1}^{N_l^k} G_{lk}^{z,t} = 0 \\ & \forall\, i \in N_p^k;\, \forall\, j \in N_c^k;\, \forall\, k \in \left(N_{ng} - 1\right);\, \forall\, t \in T \end{aligned} \tag{6.37}$$

- Dynamic behavior of natural gas in pipelines

$$\frac{G_p^{km,\,out} - G_p^{km,\,in}}{L^{km}} + A\frac{z_0 T_0}{\Pi_0 T}\frac{\frac{\Pi_m(t)}{z(\Pi_m(t))} - \frac{\Pi_m(t-\Delta t)}{z(\Pi_m(t-\Delta t))}}{\Delta t} = 0 \tag{6.38}$$

$$\begin{aligned} &\frac{\Pi_m\left(t\right) - \Pi_k\left(t\right)}{L^{km}} + g\frac{\rho_0 z_0 T_0}{\Pi_0 T}\frac{\partial h}{\partial x}\frac{\Pi_m\left(t\right)}{z\left(\Pi_m\left(t\right)\right)} \\ &\quad + \frac{\lambda}{2D}\frac{\rho_0 \Pi_0 T}{A^2 z_0 T_0}\frac{G_p^{km,\,out}\left(t\right)^2 z\left(\Pi_m\left(t\right)\right)}{\Pi_m\left(t\right)} \\ &\quad + \frac{\rho_0}{A}\frac{G_p^{km,\,out}\left(t\right) - G_p^{km,\,out}\left(t-\Delta t\right)}{\Delta t} \\ &+ \frac{\rho_0 \Pi_0 T}{A^2 z_0 T_0}\frac{\frac{G_p^{km,\,out}(t)^2 z(\Pi_m(t))}{\Pi_m(t)} - \frac{G_p^{km,\,in}(t)^2 z(\Pi_k(t))}{\Pi_k(t)}}{L^{km}} \quad = \quad 0 \end{aligned} \tag{6.39}$$

- Compression station energy consumption

$$\begin{aligned} BHP^{km,t} \quad &= \quad 0.0854\, Z_a \left[\frac{G_c^{km,t}\, T_k}{E_c\, \eta_c}\right]\left[\frac{c_k}{c_k - 1}\right]\left[\left(\frac{\Pi_{m,t}}{\Pi_{k,t}}\right)^{\frac{c_k-1}{c_k}} - 1\right] \\ &\quad \forall\, c \in N_c;\, \forall\, t \in T \end{aligned} \tag{6.40}$$

- Pressure compression ratio. In our firsthand experience, for multi-period studies it is better to use the compression stations to regulate the reception node's pressure within a specified range more than setting a compression ratio to a fixed value. The reason behind this recommendation is that high load variations can lead to undesirable pressure values:

$$\Pi_i^{min} \leq \Pi_i^t \leq \Pi_i^{max} \tag{6.41}$$

- Energy conversion equation

$$\begin{aligned} HR^{i,t} &= \alpha_g^i + \beta_g^i P_{gen}^{i,t} + \gamma_g^i \left(P_{gen}^{i,t}\right)^2 \\ G_{lk}^{i,t} &= \frac{HR^{i,t}}{GHV} \\ & \forall\, i \in Thermal\ generators;\ \forall\, t \in T \end{aligned} \tag{6.42}$$

On the other hand, the set of inequality constraints is defined by the following equations:

- Coal mine-mouth maximum and minimum supply limits

$$MC_{source}^{k-min} \leq \sum_{t}^{T} MC_{source}^{k,t} \leq MC_{source}^{k-max} \tag{6.43}$$

- Natural gas deposits maximum and minimum supply limits

$$G_{sk}^{y-min} \leq G_{sk}^{y,t} \leq G_{sk}^{y-max} \tag{6.44}$$

Lastly, the set of security constraints considered in this paper is defined by the following:

- Active power in each generator

$$\begin{aligned} P_{gen}^{i,min} &\leq P_{gen}^{i,t} \leq P_{gen}^{i,max} \\ & \forall\, P_{gen}^{i} \in \left\{P_{gen,ng}^{i},\, P_{gen,co}^{i},\, P_{gen,hy}^{i},\, P_{gen,w}^{i}\right\};\ \forall\, t \in T \end{aligned} \tag{6.45}$$

- Nodal magnitude voltage profile in an electric system

$$V_i^{min} \leq V_i^t \leq V_i^{max} \tag{6.46}$$

- Nodal pressure profile in a natural gas system

$$\Pi_i^{min} \leq \Pi_i^t \leq \Pi_i^{max} \tag{6.47}$$

## 6.4 Case Studies

### 6.4.1 Case Study A

In this case of study, the proposed Multi-Energy Unit Commitment *(MEGUC)* is applied to a multi-energy system composed by the following networks: a 5 nodes electrical system with a maximum load of 165 MW [Stagg 1968], a 3 nodes natural gas network with a maximum load of 216.7 MSCM [Tao 1998], and a 4 nodes coal supply network [Martinez-Mares 2013]. The network's topologies are shown in Figures 6.3, 6.4 and 6.5 for the electricity, natural gas and coal networks, respectively, while the generator's parameters are reported in Table 6.1.

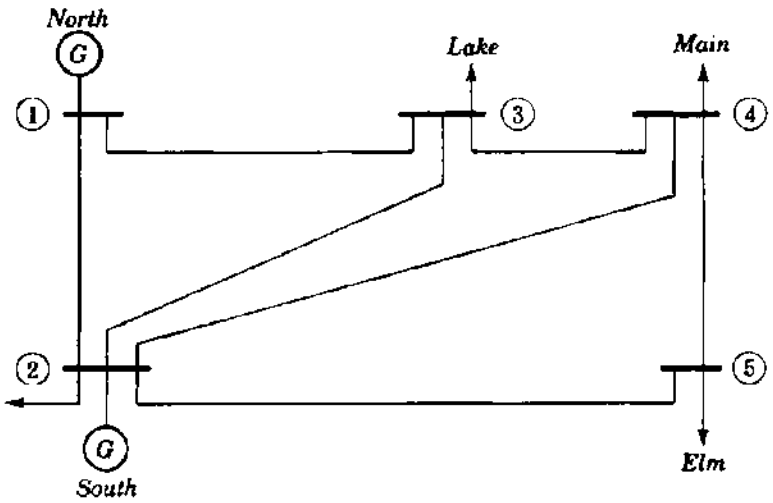


Figure 6.3: Electrical system, 5 nodes benchmark system

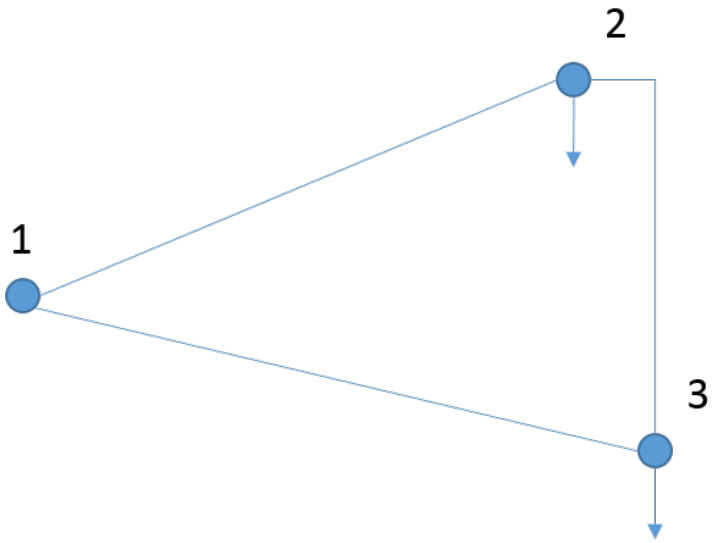


Figure 6.4: Natural gas system, 3 nodes benchmark system.

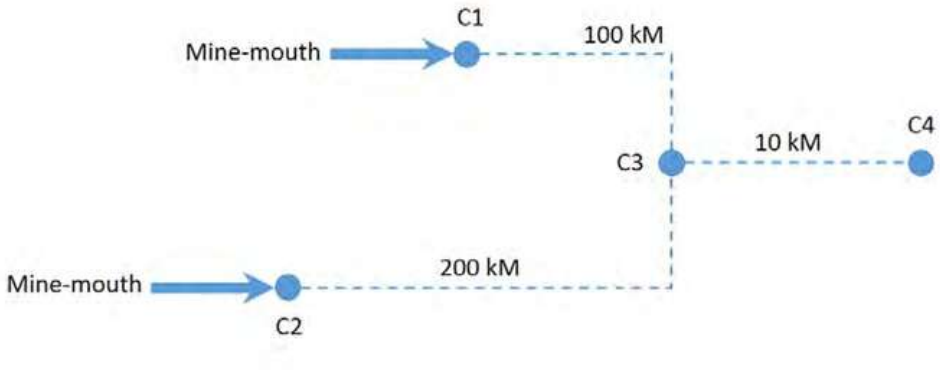


Figure 6.5: Coal supply network, 4 nodes benchmark system.

Table 6.1: 5 nodes benchmark system, generators

| *Electric Node* | *Energy bus* | *MWmax* | *MWmin* | $\alpha$ | $\beta$ | $\gamma$ | $\sum$*Hours* | *HSUT&MDT* | *MUT* | *DCS&CST* | *K* | *R* | $\tau$ | *UR* | *LR* | *MR* |
|---|---|---|---|---|---|---|---|---|---|---|---|---|---|---|---|---|
| North | NG-3 | 200.0 | 0.3 | 150000 | 12 | 4 | 3 | 4 | 3 | 8 | 10e3 | 35e3 | 2 | 0.3 | 0.3 | 0 |
| South | C-4 | 65 | 0.3 | 140000 | 120 | 4 | 1 | 4 | 3 | 8 | 20e3 | 35e3 | 2 | 0.3 | 0.3 | 0 |

In order to assess the interdependencies between energy networks, a wind-generator

is connected at the "MAIN" node of the electric power system. For the sake of simplicity, the same load variation profile has been considered in all the energy networks in such a way that the load at each node of the multi-energy network is computed by Equation (6.48). Figure 6.6 depicts the load and wind speed variation profiles as a function of time:

$$Load_i\,(t) = Load_i^{max}\; f_{load}\,(t) \tag{6.48}$$

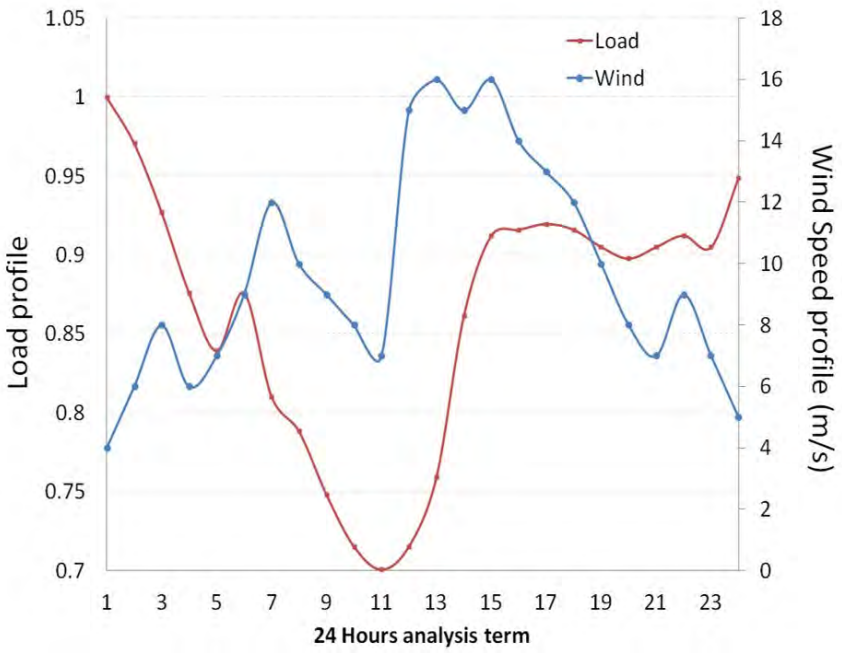


Figure 6.6: Load and wind speed profiles for the analysis term.

According to Equation (6.48), the load at each node of the multi-energy system is always expressed as a fraction of the maximum load $Load_i^{max}$, and the corresponding factor is determined by the function $f_{load}\,(t)$. On the other hand, the wind energy profile shown in Figure 6.6 together with expressions (4.8) and (4.9) permit determining the active power delivered from the wind generator to the electric power system at each subperiod of analysis.

A *MEGUC* analysis for 24 hours in advance is performed in the multi-energy system described above, where the security constraints for nodal pressure and voltage magni-

tude profiles are defined as $60 \leq \Pi \leq 30\,MPa$ and $1.4 \leq V \leq 0.7\,pu$, respectively. The production cost considered in this study is 100 USD/MSCM for natural gas, 80 USD/Ton for coal and 1 USD/liter for diesel. Lastly, Figure 6.7 shows the active powers produced by coal- and natural gas-fired generators.

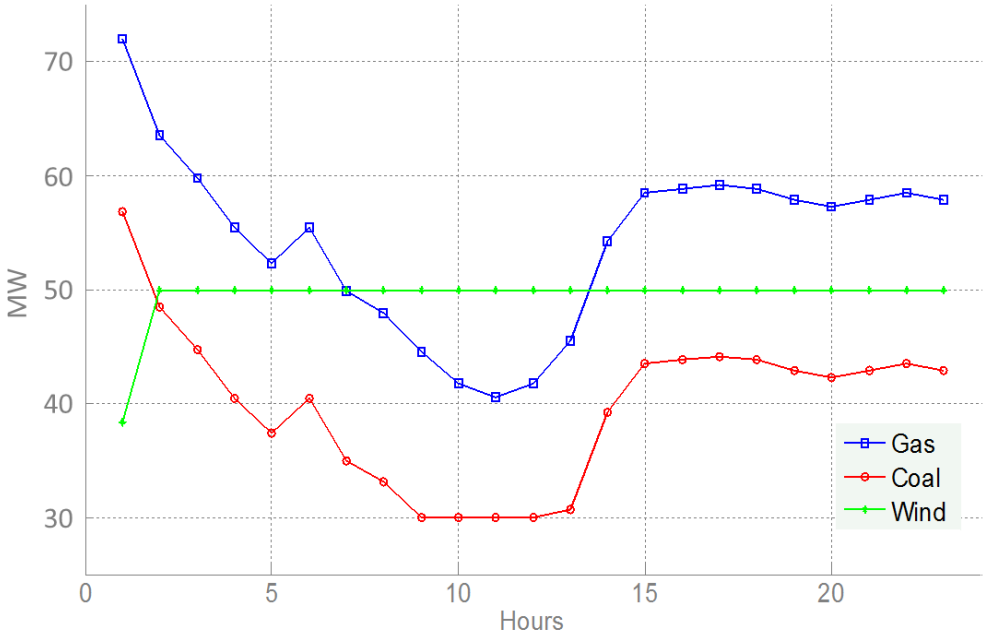


Figure 6.7: Generated active powers for 24 hours of study, Case 6.A.

From Figure 6.6, clearly the wind speed in the first hour of analysis is not sufficient to produce the maximum capacity of the wind generator, as shown in Figure 6.7; however, the natural gas-fired generators' capacity is enough to supply the load during the entire period of study. Despite these observations, though, that may indicate how the demand can be satisfied, the operation of the whole multi-energy system is subjected to security constraints that determine how the optimization process looks for the most economical combination of generators to satisfy the load at every subperiod of the study term. In this case study, the response of the natural gas and the coal generators to the load demand could be identified, as shown in Figure 6.7, where in between 9 and 12 hours of study the coal generator is delivering its minimum capacity (only 0.3 pu). Hence, there are two options for the *MEGUC* algorithm: to keep the unit running at its minimum capacity or turn it off during these hours. The reasons to chose the first condition could

include the following:

- In the analysis of the entire period of study the algorithm identifies the most economical operation condition with the unit running at its minimum with respect to the case where the unit is turned off during the referred period of time. Furthermore, it is turned *"on"* few hours after the minimum load scenario has occurred.

- The security operative constraints associated with the voltage magnitude profile along the electrical system is satisfied when the two coal-fired units are active.

- Lastly, the number of subperiods requiring the units off are lower than the minimum number of subperiods where the unit shall remain in an off status before it is turned on because of the thermal constraints involved in the energy conversion process.

Figure 6.8 shows the results of analyzing only the first 12 hours involving the same load and wind speed profiles depicted in Figure 6.6. From this Figure results evidence emerge that the coal-generator will not be used beyond the seventh hour, and therefore the most economical operation condition, which also satisfies all the security constraints, is achieved when the coal unit is offline.

The dynamic behavior of the natural gas flows is shown in Figures 6.9 and 6.10, which was obtained by using the dynamic model approach described in Section 2.2.1. The maximum load of this multi-energy systems occurs at the first hour of analysis and is reduced to approximately 70% of this value after 10 hours. This load behavior is reflected in the reduction of natural gas flowing in the pipelines, as shown in Figure 6.9 and the increment of nodal pressures, as shown in Figure 6.10.

Lastly, the sudden change in the nodal voltage magnitude occurs after the ninth hour in which the coal-generator has been turned off, and therefore the reactive power

support in the electrical power system has been reduced. Nevertheless, the nodal voltage magnitude constraints are satisfied and the active power demand is supplied only with the natural gas and the wind generators remaining online in the electric power system.

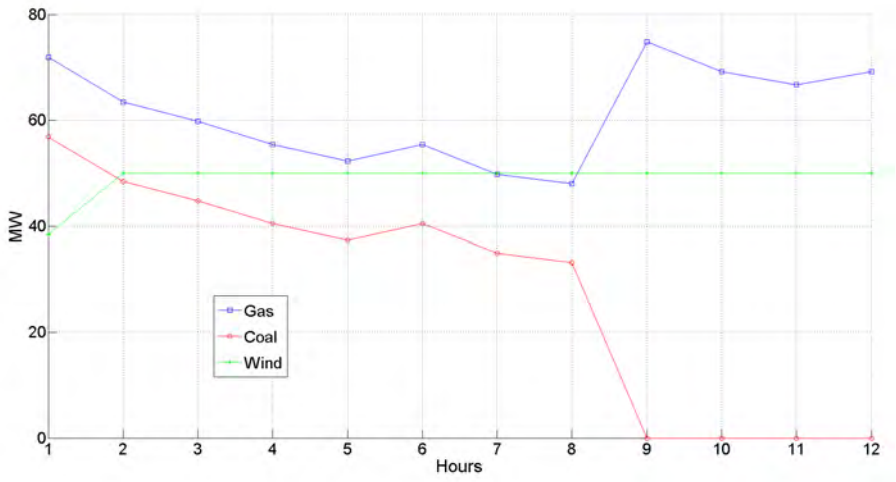


Figure 6.8: Generated active power for 12 hours of study for Case 6.A.

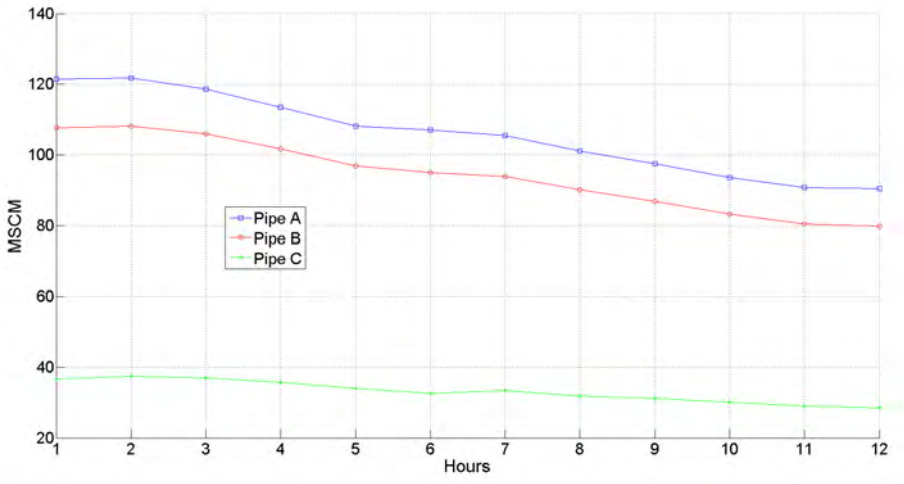


Figure 6.9: Dynamic behavior of natural gas in pipelines for Case 6.A.

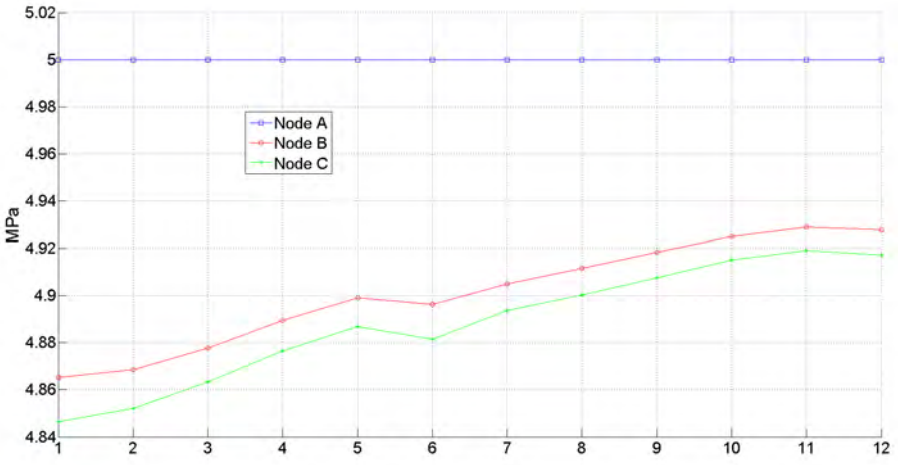


Figure 6.10: Dynamic behavior of nodal pressure for Case 6.A.

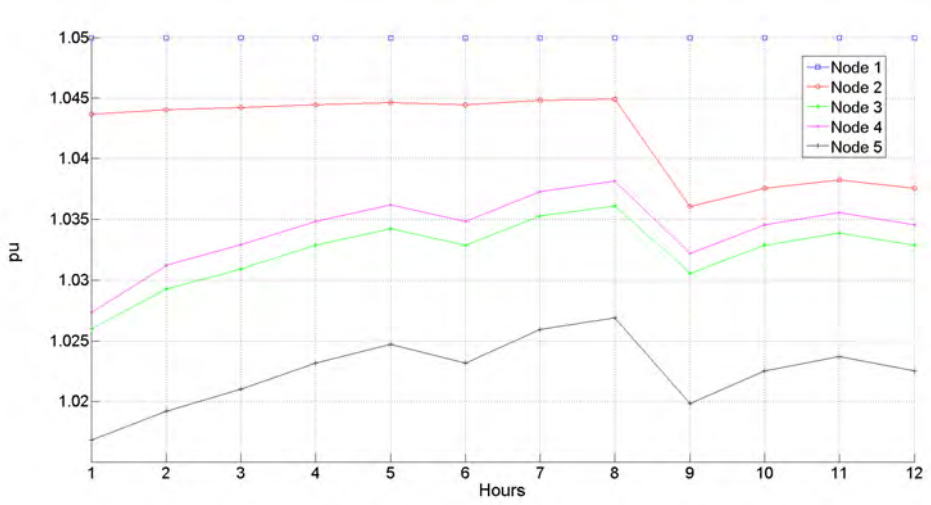


Figure 6.11: Nodal voltage of electric system for Case 6.A.

Figure 6.12 correspond to the active power delivered by the generators considering an increment in the reactive power load at the electric node 2 of 15 MVAR. This change in the operation conditions causes the coal-generator to remain on-line for another hour with respect to its operation without an increment in the rective power load, shown in Figure 6.8, in order to satisfy the security constraints. This results is very important because shows that even when the active power demand can be supplied by the gas and wind generators, the increment of the reactive power demand requires the coal unit to

remain online. The resulting voltage magnitudes are shown in Figure 6.13.

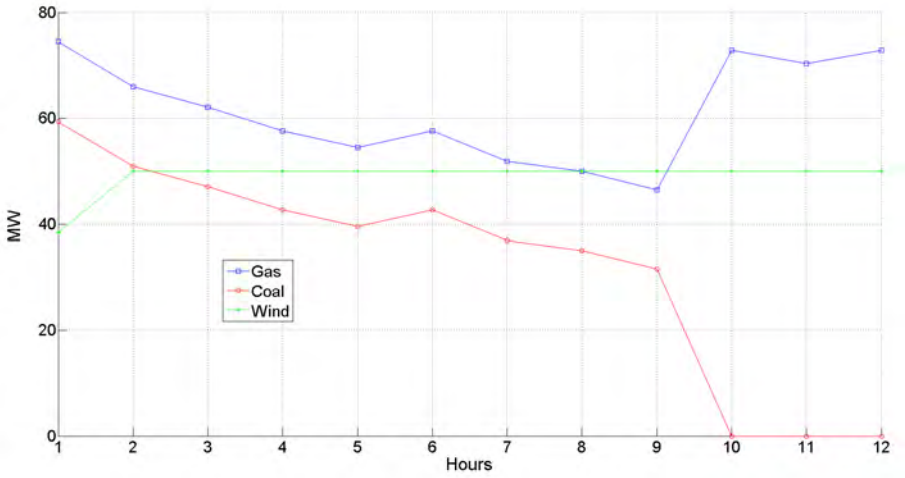


Figure 6.12: Generated active power for 12 hours for additional 15 MVAR at node 2.

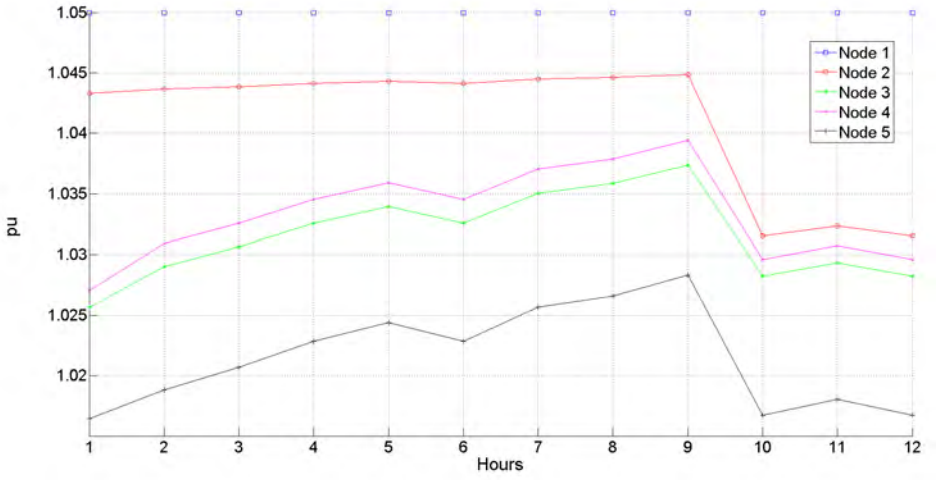


Figure 6.13: Nodal voltage of electric system for additional 15 MVAR at node 2.

### 6.4.2 Case Study B

An increment of 20% in the installed wind energy capacity is noted in this study case, and the impact of this increment on the unit commitment is shown in Figure 6.14. Note the earlier shut-down of the coal-fired generator with respect to the previous analysis (Figure 6.8). Another important difference with respect to the previous study case is

that the nodal voltage magnitude at node 5 of the electric power system has dropped below 1.02 pu because of the reduction of online units, as shown in Figure 6.15.

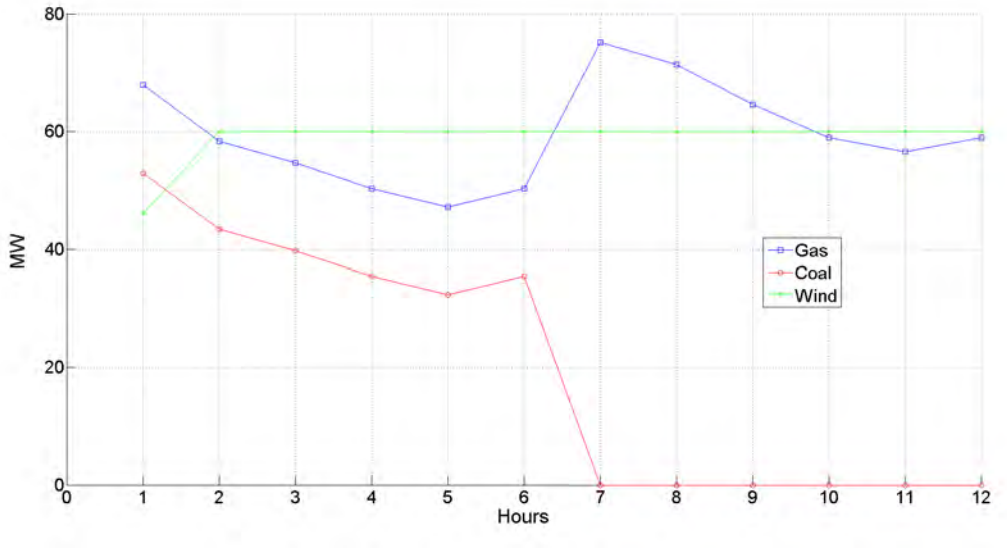


Figure 6.14: Generated active powers for 12 hours of study for Case 6.B.

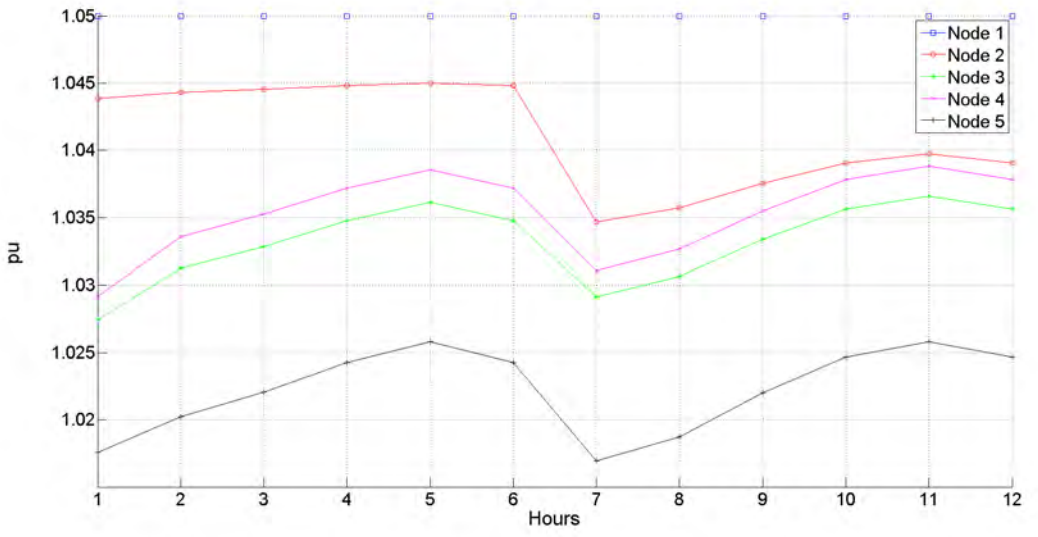


Figure 6.15: Nodal voltage of electric power system for Case 6.B.

In this case of study, the same load ramps have been considered for the gas and coal units, such that the dynamic behavior of both units is very similar with the main

difference associated with the efficiency in the conversion energy process, which makes the coal generator a more expensive unit than the gas-generator.

### 6.4.3 Case Study C

In this case of study, the well-known IEEE 118 nodes benchmark system ["Power Systems Test Case Archive", http://www.ee.washington.edu/research/pstca/] is coupled to the 15 nodes natural gas system depicted in Figure 2.3 [An 2003], and to the four nodes coal system shown in Figure 6.5. The type of primary energy driving the electric generators and their corresponding parameters are reported in Table 6.2, while the load and wind speed variation profiles are those reported in Figure 6.6.

Table 6.2: IEEE-118 Test system, generators.

| Electric node | Primary energy | Primary energy node | $P_{max}$, [pu] | $P_{min}$, [pu] | $\alpha$ | $\beta$ | $\gamma$ |
|---|---|---|---|---|---|---|---|
| 10 | Natural gas | 1 | 6 | 0.5 | 150000 | 12 | 4 |
| 12 | Natural gas | 3 | 6 | 0.5 | 150000 | 12 | 4 |
| 16 | Natural gas | 6 | 6 | 0.5 | 140000 | 14 | 5 |
| 25 | Natural gas | 8 | 6 | 0.5 | 140000 | 14 | 5 |
| 26 | Natural gas | 10 | 6 | 0.5 | 140000 | 14 | 5 |
| 31 | Natural gas | 12 | | 0.5 | 140000 | 14 | 5 |
| 40 | Coal | 3 | 6 | 0.5 | 150000 | 12 | 7 |
| 46 | Coal | 3 | 6 | 0.5 | 150000 | 12 | 7 |
| 49 | Coal | 3 | 6 | 0.5 | 150000 | 12 | 7 |
| 54 | Coal | 4 | 6 | 0.5 | 150000 | 12 | 7 |
| 59 | Coal | 4 | 6 | 0.5 | 180000 | 12 | 7 |
| 61 | Wind | — | 1.7 | 0 | a=1.070 | b=-0.806 | c=0.245 |
| 65 | Wind | — | 1.7 | 0 | | | |
| 66 | Wind | — | 1.7 | 0 | d=-0.043 | e=5.09e-3 | f=3.80e-4 |
| 69 | Wind | — | 1.7 | 0 | | | |
| 80 | Wind | — | 1.7 | 0 | g=1.66e-5 | h=-3.85e-7 | i=3.65e-9 |
| 87 | Hydro | — | 2.5 | 0 | 4000 | 480 | 0.2 |
| 89 | Hydro | — | 2.5 | 0 | 9000 | 450 | 0.2 |
| 100 | Hydro | — | 2.5 | 0 | 9000 | 450 | 0.2 |
| 113 | Hydro | — | 2.5 | 0 | 9000 | 450 | 0.2 |
| 111 | Hydro | — | 2.5 | 0 | 4000 | 480 | 0.2 |

In order to perform this study, the parameters related to gas loads and compressor's parameters have been changed with respect to the base case, as reported in Table 6.3.

Table 6.3: Load's and compressor's parameters for case study C.

| Natural gas node | Load, [MMSCF] |
|---|---|
| 2 | 1.25 |
| 3 | 0.75 |
| 12 | 1.58 |
| 13 | 1.66 |
| 14 | 1.75 |
| **Compressor** | **Ratio** |
| 1 | 1.2 |
| 2 | 1.2 |
| 3 | 1.5 |
| 4 | 1.5 |

The initial condition in $t_0$ for the natural gas system is reported in Table 6.4, which has been determined by a gas flow study based on the steady-state formulation reported in Section 2.2.1.

Table 6.4: Initial condition for state variables in the natural gas system.

| Natural gas node | Pressure, [PSIA] | Natural gas node | Pressure, [PSIA] |
|---|---|---|---|
| 1 | 1000 | 9 | 650 |
| 2 | 1000 | 10 | 975 |
| 3 | 844 | 11 | 835 |
| 4 | 856 | 12 | 1252 |
| 5 | 662 | 13 | 820 |
| 6 | 794 | 14 | 806 |
| 7 | 777 | 15 | 814 |
| 8 | 932 | — | — |
| **Compressor** | **Horse Power** | **Gas flow, [MMSCF]** | |
| 1 | 1282 | 5.6096 | |
| 2 | 835 | 3.6970 | |
| 3 | 2370 | 4.5360 | |
| 4 | 1341 | 2.5975 | |

Lastly, the following parameters have been used: $K = 10000$ for Equation (6.30), and $c_p = 1x10^6$, $c_q = 1x10^5$, $b_p = 1.5x10^6$ and $b_q = 1.5x10^5$ for the parameters in

Equation (6.19). For purposes of this simulation, a constant active power generation has also been considered for the hydro-generators.

#### 6.4.3.1 Base Case

The results of this study are reported in Table 6.5 and correspond to the schedule and active powers for generators considering the first 12 hours of the load and wind variation profiles depicted in Figure 6.6. In this case, the primary energies costs have been considered as follows: 141.3 USD/MSCM for natural gas, 65 USD/Ton for coal and 1 USD/liter for diesel. For this study case the no ramp constraints have been considered for the power generators.

Table 6.5: Active power generated for 12 hours of simulation for the base case.

| Generator | Active power generated in hour, [pu] | | | | | | | | | | | |
|---|---|---|---|---|---|---|---|---|---|---|---|---|
| | 1 | 2 | 3 | 4 | 5 | 6 | 7 | 8 | 9 | 10 | 11 | 12 |
| 10 | 3.528 | 3.196 | 2.452 | 2.808 | 2.394 | 2.241 | 1.971 | 1.882 | 1.718 | 1.584 | 1.828 | 1.584 |
| 12 | 3.574 | 3.243 | 2.504 | 2.851 | 2.438 | 2.289 | 2.015 | 1.923 | 1.756 | 1.620 | 1.864 | 1.620 |
| 16 | 2.721 | 2.477 | 1.925 | 2.188 | 1.878 | 1.764 | 1.558 | 1.489 | 1.362 | 1.258 | 1.445 | 1.258 |
| 25 | 2.873 | 2.591 | 1.970 | 2.271 | 1.927 | 1.798 | 1.579 | 1.506 | 1.373 | 1.265 | 1.466 | 1.265 |
| 26 | 2.888 | 2.603 | 1.977 | 2.280 | 1.933 | 1.804 | 1.583 | 1.510 | 1.376 | 1.267 | 1.469 | 1.267 |
| 31 | 2.868 | 2.597 | 1.995 | 2.280 | 1.945 | 1.823 | 1.603 | 1.530 | 1.397 | 1.288 | 1.484 | 1.288 |
| 40 | 3.643 | 3.251 | 2.418 | 2.833 | 2.378 | 2.202 | 1.927 | 1.836 | 1.671 | 1.537 | 1.797 | 1.537 |
| 46 | 3.623 | 3.214 | 2.359 | 2.797 | 2.332 | 2.146 | 1.875 | 1.786 | 1.624 | 1.493 | 1.758 | 1.493 |
| 49 | 4.071 | 3.552 | 2.516 | 3.048 | 2.494 | 2.272 | 1.968 | 1.869 | 1.691 | 1.547 | 1.845 | 1.547 |
| 54 | 4.122 | 3.609 | 2.576 | 3.099 | 2.544 | 2.326 | 2.015 | 1.913 | 1.730 | 1.583 | 1.882 | 1.583 |
| 59 | 4.289 | 3.712 | 2.586 | 3.165 | 2.567 | 2.328 | 2.008 | 1.904 | 1.718 | 1.569 | 1.882 | 1.569 |
| 61 | 0.000 | 0.484 | 1.700 | 0.484 | 1.052 | 1.700 | 1.700 | 1.700 | 1.700 | 1.700 | 1.052 | 1.700 |
| 65 | 0.000 | 0.484 | 1.700 | 0.484 | 1.052 | 1.700 | 1.700 | 1.700 | 1.700 | 1.700 | 1.052 | 1.700 |
| 66 | 0.000 | 0.484 | 1.700 | 0.484 | 1.052 | 1.700 | 1.700 | 1.700 | 1.700 | 1.700 | 1.052 | 1.700 |
| 69 | 0.000 | 0.484 | 1.700 | 0.484 | 1.052 | 1.700 | 1.700 | 1.700 | 1.700 | 1.700 | 1.052 | 1.700 |
| 80 | 0.000 | 0.484 | 1.700 | 0.484 | 1.052 | 1.700 | 1.700 | 1.700 | 1.700 | 1.700 | 1.052 | 1.700 |
| 87 | 1.417 | 1.407 | 1.407 | 1.407 | 1.407 | 1.407 | 1.407 | 1.407 | 1.407 | 1.407 | 1.407 | 1.407 |
| 89 | 1.417 | 1.407 | 1.407 | 1.407 | 1.407 | 1.407 | 1.407 | 1.407 | 1.407 | 1.407 | 1.407 | 1.407 |
| 100 | 1.417 | 1.407 | 1.407 | 1.407 | 1.407 | 1.407 | 1.407 | 1.407 | 1.407 | 1.407 | 1.407 | 1.407 |
| 113 | 1.417 | 1.407 | 1.407 | 1.407 | 1.407 | 1.407 | 1.407 | 1.407 | 1.407 | 1.407 | 1.407 | 1.407 |
| 111 | 1.417 | 1.407 | 1.407 | 1.407 | 1.407 | 1.407 | 1.407 | 1.407 | 1.407 | 1.407 | 1.407 | 1.407 |
| TOTAL | 45.285 | 43.5 | 40.813 | 39.075 | 37.125 | 38.528 | 35.637 | 34.683 | 32.951 | 31.546 | 31.015 | 31.546 |

From Table 6.5, the coal-fired generators clearly supply more of the electric load than the gas-fired generators; in addition, these thermal-generators have a behavior in accordance with the load profile depicted in Figure 6.6. Note that no generator has

been turned off, which means that all the units remain *online* for the 12 subperiods of analysis. Lastly, Figure 6.16 shows the convergence towards the *MEGUC´s* feasible solution. The nodal pressure for the natural gas system is presented in Table 6.6.

Table 6.6: Nodal pressure in Natural Gas System for 12 hours of simulation for the base case.

| Node | Nodal pressure in hour, [BARS] | | | | | | | | | | | |
|---|---|---|---|---|---|---|---|---|---|---|---|---|
| | 1 | 2 | 3 | 4 | 5 | 6 | 7 | 8 | 9 | 10 | 11 | 12 |
| 1 | 68.95 | 68.95 | 68.95 | 68.95 | 68.95 | 68.95 | 68.95 | 68.95 | 68.95 | 68.95 | 68.95 | 68.95 |
| 2 | 68.95 | 68.95 | 68.95 | 68.95 | 68.95 | 68.95 | 68.95 | 68.95 | 68.95 | 68.95 | 68.95 | 68.95 |
| 3 | 58.54 | 58.54 | 58.53 | 58.53 | 58.53 | 58.53 | 58.53 | 58.52 | 58.52 | 58.52 | 58.53 | 58.53 |
| 4 | 59.31 | 59.32 | 59.33 | 59.33 | 59.32 | 59.32 | 59.32 | 59.31 | 59.30 | 59.29 | 59.28 | 59.27 |
| 5 | 44.36 | 43.29 | 42.77 | 41.97 | 41.44 | 40.93 | 40.60 | 40.30 | 40.08 | 39.93 | 39.64 | 39.43 |
| 6 | 55.89 | 55.67 | 54.97 | 55.22 | 55.01 | 54.85 | 54.84 | 54.91 | 55.08 | 55.27 | 55.63 | 55.78 |
| 7 | 53.13 | 52.77 | 52.32 | 51.74 | 51.04 | 50.20 | 49.20 | 48.05 | 46.74 | 45.26 | 43.64 | 41.87 |
| 8 | 69.78 | 66.62 | 62.95 | 63.71 | 62.35 | 62.98 | 63.00 | 64.19 | 65.51 | 67.33 | 69.82 | 72.05 |
| 9 | 44.04 | 43.49 | 43.43 | 43.22 | 43.27 | 43.46 | 43.81 | 44.26 | 44.81 | 45.45 | 46.06 | 46.84 |
| 10 | 64.76 | 65.35 | 66.92 | 66.25 | 66.89 | 67.22 | 67.52 | 67.55 | 67.56 | 67.53 | 67.08 | 67.20 |
| 11 | 55.85 | 54.79 | 54.90 | 54.78 | 55.38 | 56.25 | 57.66 | 59.36 | 61.43 | 63.81 | 66.18 | 68.83 |
| 12 | 86.37 | 86.37 | 86.37 | 86.37 | 86.37 | 86.37 | 86.37 | 86.37 | 86.37 | 86.37 | 86.37 | 86.37 |
| 13 | 56.28 | 56.17 | 56.21 | 56.19 | 56.32 | 56.44 | 56.62 | 56.81 | 57.04 | 57.30 | 57.54 | 57.79 |
| 14 | 55.38 | 55.28 | 55.33 | 55.41 | 55.56 | 55.65 | 55.88 | 56.11 | 56.39 | 56.69 | 56.97 | 57.21 |
| 15 | 55.96 | 55.79 | 55.75 | 55.77 | 55.87 | 56.01 | 56.15 | 56.36 | 56.59 | 56.87 | 57.14 | 57.40 |

From Table 6.6, it is observed that the change of nodal pressures, at nodes eight and ten, between consecutive subperiods of analysis could be an important constraint in the operation of gas fired power plants if the variation of these pressures is an operative constraint in the coupling point between the gas and electricity systems..

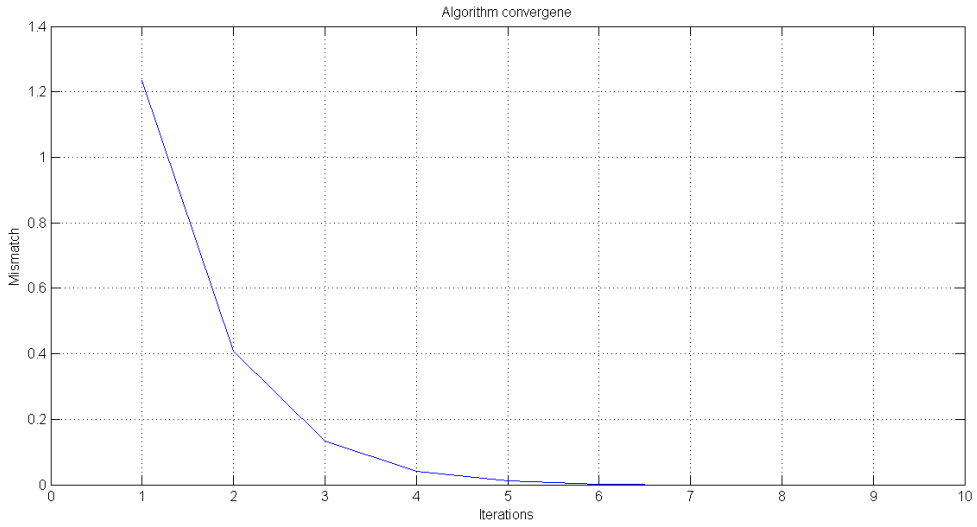


Figure 6.16: Algorithm convergence for case base C.

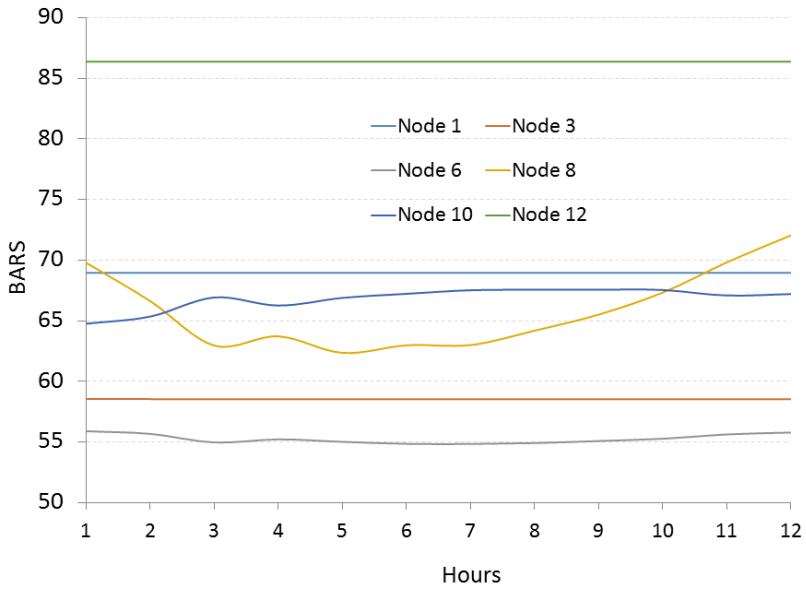


Figure 6.17: Nodal pressure in gas system, case C.

In Figure 6.17 the variation of nodal pressure for the nodes delivering gas to thermal generators are presented, the nodes one, three and twelve correspond to pressure controlled nodes, the curve corresponding to the node eight presents large variations during the period of study, these variations must be considered in the operation limits

associated to the inlet gas controls for each particular power-plant.

#### 6.4.3.2 Heat Rate Curves Modification for gas-generators

In this case of study the parameters corresponding to the heat rate curves for generators 12, 16 and 25 have been changed as reported in Table 6.7; in addition, the active power limit of $P_{max} = 2.8\,pu$ has been considered for all the wind power generators and of $P_{min} = 0.8\,pu$ for all thermal generators.

Table 6.7: Heat rate parameters for generators 12, 16 and 25.

| Generator | $\alpha$ | $\beta$ | $\gamma$ |
|---|---|---|---|
| 12 | 30000 | 12 | 4 |
| 16 | 30000 | 14 | 5 |
| 25 | 30000 | 14 | 5 |

The active power and schedule results are shown in Table 6.8.

Table 6.8: Active power generated for 12 hours of simulation.

| Generator | Active power generated in hour, [pu] | | | | | | | | | | | |
|---|---|---|---|---|---|---|---|---|---|---|---|---|
| | 1 | 2 | 3 | 4 | 5 | 6 | 7 | 8 | 9 | 10 | 11 | 12 |
| 10 | 3.528 | 3.196 | 2.439 | 2.808 | 2.394 | 1.893 | 1.670 | 1.567 | 1.561 | 1.789 | 2.082 | 1.545 |
| 12 | 3.574 | 3.243 | 2.490 | 2.851 | 2.438 | 1.940 | 0.000 | 0.000 | 0.000 | 0.000 | 0.000 | 0.000 |
| 16 | 2.721 | 2.477 | 1.914 | 2.188 | 1.878 | 1.499 | 1.343 | 1.261 | 1.255 | 1.434 | 1.662 | 0.000 |
| 25 | 2.873 | 2.591 | 1.959 | 2.271 | 1.927 | 1.511 | 1.308 | 1.227 | 1.224 | 1.406 | 1.640 | 0.000 |
| 26 | 2.888 | 2.603 | 1.966 | 2.280 | 1.933 | 1.515 | 1.311 | 1.230 | 1.227 | 1.410 | 1.646 | 1.221 |
| 31 | 2.868 | 2.597 | 1.984 | 2.280 | 1.945 | 1.542 | 1.338 | 1.256 | 1.251 | 1.428 | 1.656 | 1.234 |
| 40 | 3.643 | 3.251 | 2.403 | 2.833 | 2.378 | 1.829 | 1.552 | 1.455 | 1.457 | 1.687 | 1.982 | 1.392 |
| 46 | 3.623 | 3.214 | 2.344 | 2.797 | 2.332 | 1.768 | 1.480 | 1.387 | 1.394 | 1.626 | 1.923 | 1.310 |
| 49 | 4.071 | 3.552 | 2.498 | 3.048 | 2.494 | 1.842 | 1.524 | 1.424 | 1.433 | 1.692 | 2.028 | 1.340 |
| 54 | 4.122 | 3.609 | 2.558 | 3.099 | 2.544 | 1.892 | 1.563 | 1.460 | 1.468 | 1.727 | 2.063 | 1.369 |
| 59 | 4.289 | 3.712 | 2.566 | 3.165 | 2.567 | 1.871 | 1.537 | 1.434 | 1.446 | 1.717 | 2.072 | 1.346 |
| 61 | 0.000 | 0.484 | 1.729 | 0.484 | 1.052 | 2.451 | 2.800 | 2.800 | 2.451 | 1.729 | 1.052 | 2.800 |
| 65 | 0.000 | 0.484 | 1.729 | 0.484 | 1.052 | 2.451 | 2.800 | 2.800 | 2.451 | 1.729 | 1.052 | 2.800 |
| 66 | 0.000 | 0.484 | 1.729 | 0.484 | 1.052 | 2.451 | 2.800 | 2.800 | 2.451 | 1.729 | 1.052 | 2.800 |
| 69 | 0.000 | 0.484 | 1.729 | 0.484 | 1.052 | 2.451 | 2.800 | 2.800 | 2.451 | 1.729 | 1.052 | 2.800 |
| 80 | 0.000 | 0.484 | 1.729 | 0.484 | 1.052 | 2.451 | 2.800 | 2.800 | 2.451 | 1.729 | 1.052 | 2.800 |
| 87 | 1.417 | 1.407 | 1.407 | 1.407 | 1.407 | 1.407 | 1.407 | 1.407 | 1.407 | 1.407 | 1.407 | 1.407 |
| 89 | 1.417 | 1.407 | 1.407 | 1.407 | 1.407 | 1.407 | 1.407 | 1.407 | 1.407 | 1.407 | 1.407 | 1.407 |
| 100 | 1.417 | 1.407 | 1.407 | 1.407 | 1.407 | 1.407 | 1.407 | 1.407 | 1.407 | 1.407 | 1.407 | 1.407 |
| 113 | 1.417 | 1.407 | 1.407 | 1.407 | 1.407 | 1.407 | 1.407 | 1.407 | 1.407 | 1.407 | 1.407 | 1.407 |
| 111 | 1.417 | 1.407 | 1.407 | 1.407 | 1.407 | 1.407 | 1.407 | 1.407 | 1.407 | 1.407 | 1.407 | 1.407 |
| TOTAL | 45.285 | 43.5 | 40.801 | 39.075 | 37.125 | 38.392 | 35.661 | 34.736 | 33.006 | 31.596 | 31.049 | 31.792 |

Table 6.8 clearly shows how the generator connected to the electrical node 12 is disconnected from the seventh subperiod of analysis, and the generators connected to the electrical nodes 16 and 25 are turned off in the last subperiod of analysis. Note that the heat rate curves corresponding to these three generators are those that were intentionally modified in accordance to Table 6.7. On the other hand, it is important to compare the total active power generated between Tables 6.5 and 6.8, in the second one a smaller number of online generators causes a redistribution of active power flowing on the transmission elements causing different losses in the electric power system. The convergence of the proposed *MEGUC* algorithm based on the variable duplication technique is shown in Figure 6.18.

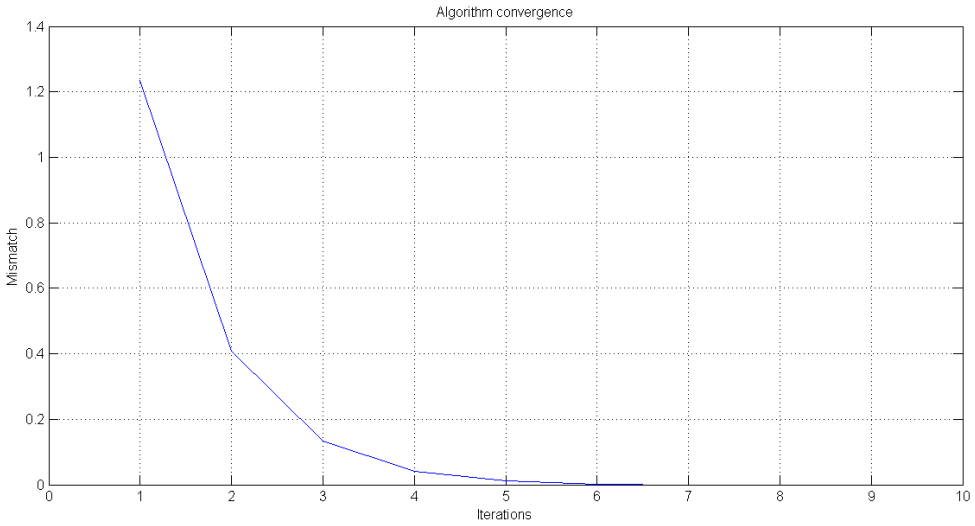


Figure 6.18: Algorithm convergence.

Lastly, the dynamic behavior of the natural gas flowing in pipelines and the nodal pressures at the gas network are reported in Tables 6.9 and 6.10, respectively.

Table 6.9: Natural gas in the reception node of the pipelines.

| Pipeline | From | To | Gas flow in hour, [MSCM] | | | | | | | | | | | |
|---|---|---|---|---|---|---|---|---|---|---|---|---|---|---|
| | | | 1 | 2 | 3 | 4 | 5 | 6 | 7 | 8 | 9 | 10 | 11 | 12 |
| 1 | 1 | 3 | 170.2 | 170.2 | 170.2 | 170.2 | 170.2 | 170.2 | 170.2 | 170.1 | 170.1 | 170.1 | 170.0 | 170.0 |
| 2 | 2 | 4 | 165.6 | 165.6 | 165.6 | 165.6 | 165.6 | 165.6 | 165.6 | 165.7 | 165.7 | 165.8 | 165.8 | 165.9 |
| 3 | 4 | 3 | 56.1 | 56.3 | 56.4 | 56.4 | 56.4 | 56.4 | 56.0 | 55.6 | 55.1 | 54.6 | 53.9 | 53.1 |
| 4 | 3 | 5 | 157.1 | 158.5 | 158.9 | 159.6 | 159.8 | 159.7 | 157.0 | 153.2 | 147.9 | 140.4 | 129.3 | 111.7 |
| 5 | 4 | 7 | 120.3 | 122.4 | 124.7 | 127.2 | 130.0 | 132.9 | 136.0 | 139.0 | 142.1 | 145.1 | 147.9 | 150.5 |
| 6 | 6 | 9 | 118.6 | 121.0 | 116.1 | 117.6 | 117.3 | 114.8 | 114.6 | 113.1 | 114.4 | 115.5 | 117.5 | 115.5 |
| 7 | 8 | 11 | 100.5 | 91.7 | 75.6 | 79.7 | 70.9 | 65.4 | 59.5 | 57.4 | 55.6 | 56.5 | 59.4 | 53.9 |
| 8 | 10 | 13 | 75.4 | 76.6 | 83.7 | 81.7 | 83.8 | 87.2 | 87.9 | 88.8 | 88.0 | 86.8 | 84.8 | 86.6 |
| 9 | 13 | 14 | 26.4 | 26.5 | 26.3 | 25.0 | 24.5 | 25.1 | 24.6 | 23.9 | 23.2 | 22.4 | 21.8 | 22.2 |
| 10 | 13 | 15 | 14.2 | 17.0 | 19.0 | 18.2 | 18.9 | 18.5 | 20.4 | 19.6 | 19.8 | 19.3 | 18.7 | 18.9 |
| 11 | 15 | 14 | 23.2 | 21.6 | 19.6 | 18.4 | 17.1 | 18.3 | 15.5 | 15.2 | 13.8 | 13.0 | 12.9 | 13.2 |

Table 6.10: Natural gas nodal pressure.

| Node | Pressure in hour, [BARS] | | | | | | | | | | | |
|---|---|---|---|---|---|---|---|---|---|---|---|---|
| | 1 | 2 | 3 | 4 | 5 | 6 | 7 | 8 | 9 | 10 | 11 | 12 |
| 1 | 68.95 | 68.95 | 68.95 | 68.95 | 68.95 | 68.95 | 68.95 | 68.95 | 68.95 | 68.95 | 68.95 | 68.95 |
| 2 | 68.95 | 68.95 | 68.95 | 68.95 | 68.95 | 68.95 | 68.95 | 68.95 | 68.95 | 68.95 | 68.95 | 68.95 |
| 3 | 54.86 | 54.86 | 54.86 | 54.86 | 54.86 | 54.86 | 54.86 | 54.87 | 54.87 | 54.88 | 54.89 | 54.90 |
| 4 | 55.92 | 55.93 | 55.93 | 55.93 | 55.93 | 55.93 | 55.92 | 55.91 | 55.90 | 55.89 | 55.87 | 55.86 |
| 5 | 35.85 | 34.99 | 34.74 | 34.23 | 34.05 | 34.14 | 35.92 | 37.81 | 39.87 | 42.17 | 44.79 | 47.92 |
| 6 | 45.36 | 45.64 | 44.31 | 44.51 | 44.37 | 43.76 | 43.75 | 43.40 | 43.65 | 43.72 | 43.84 | 43.24 |
| 7 | 46.91 | 46.52 | 46.06 | 45.52 | 44.89 | 44.17 | 43.37 | 42.49 | 41.52 | 40.47 | 39.35 | 38.17 |
| 8 | 64.17 | 60.54 | 55.93 | 56.79 | 54.80 | 54.31 | 54.27 | 55.27 | 56.51 | 58.21 | 60.11 | 62.32 |
| 9 | 30.49 | 29.77 | 29.59 | 29.21 | 29.04 | 29.14 | 29.23 | 29.28 | 29.14 | 28.66 | 27.67 | 27.55 |
| 10 | 44.15 | 44.57 | 47.55 | 46.57 | 47.53 | 49.07 | 49.43 | 49.91 | 49.59 | 49.06 | 48.27 | 49.14 |
| 11 | 47.48 | 46.25 | 46.23 | 45.91 | 46.28 | 47.22 | 48.58 | 50.15 | 51.90 | 53.61 | 55.18 | 58.54 |
| 12 | 74.05 | 74.05 | 74.05 | 74.05 | 74.05 | 74.05 | 74.05 | 74.05 | 74.05 | 74.05 | 74.05 | 74.05 |
| 13 | 29.32 | 29.14 | 29.09 | 28.90 | 28.91 | 28.99 | 29.15 | 29.26 | 29.45 | 29.64 | 29.84 | 30.14 |
| 14 | 27.52 | 27.31 | 27.28 | 27.27 | 27.35 | 27.36 | 27.59 | 27.80 | 28.08 | 28.38 | 28.65 | 28.92 |
| 15 | 28.87 | 28.48 | 28.25 | 28.12 | 28.09 | 28.20 | 28.19 | 28.37 | 28.55 | 28.79 | 29.05 | 29.34 |

#### 6.4.3.3 Heat Rate Curves Modification for coal-generators

The previous exercise is repeated from the case base with the modification of the parameters corresponding to the heat rate curves for generators 40, 46 and 49 in accordance with Table 6.11.

Table 6.11: Heat rate parameters for generators 40, 46 and 49.

| Generator | $\alpha$ | $\beta$ | $\gamma$ |
|---|---|---|---|
| 40 | 50000 | 24 | 9 |
| 46 | 50000 | 24 | 9 |
| 49 | 50000 | 24 | 9 |

The active power and schedule results are shown in Table 6.12.

Table 6.12: Active power generated for 12 hours of simulation.

| Generator | Active power generated in hour, [pu] | | | | | | | | | | | |
|---|---|---|---|---|---|---|---|---|---|---|---|---|
| | 1 | 2 | 3 | 4 | 5 | 6 | 7 | 8 | 9 | 10 | 11 | 12 |
| 10 | 3.724 | 3.378 | 2.583 | 2.972 | 2.537 | 2.006 | 2.022 | 1.896 | 1.897 | 2.192 | 2.568 | 1.758 |
| 12 | 3.765 | 3.422 | 2.633 | 3.013 | 2.579 | 2.054 | 2.064 | 1.937 | 1.935 | 2.226 | 2.597 | 0.000 |
| 16 | 2.862 | 2.610 | 2.022 | 2.309 | 1.985 | 1.586 | 1.595 | 1.499 | 1.498 | 1.721 | 2.002 | 1.409 |
| 25 | 3.037 | 2.743 | 2.077 | 2.407 | 2.044 | 1.603 | 1.615 | 1.513 | 1.515 | 1.759 | 2.071 | 1.377 |
| 26 | 3.054 | 2.757 | 2.085 | 2.418 | 2.052 | 1.608 | 1.620 | 1.517 | 1.520 | 1.766 | 2.081 | 1.382 |
| 31 | 3.023 | 2.741 | 2.099 | 2.410 | 2.058 | 1.633 | 1.639 | 1.537 | 1.537 | 1.771 | 2.071 | 1.400 |
| 40 | 3.122 | 2.775 | 2.034 | 2.410 | 2.013 | 1.538 | 0.000 | 0.000 | 0.000 | 0.000 | 0.000 | 0.000 |
| 46 | 3.138 | 2.770 | 1.997 | 2.399 | 1.988 | 1.494 | 0.000 | 0.000 | 0.000 | 0.000 | 0.000 | 0.000 |
| 49 | 3.463 | 3.010 | 2.101 | 2.576 | 2.099 | 1.541 | 0.000 | 0.000 | 0.000 | 0.000 | 0.000 | 0.000 |
| 54 | 4.449 | 3.890 | 2.748 | 3.338 | 2.736 | 2.029 | 2.070 | 1.924 | 1.941 | 2.329 | 2.848 | 1.686 |
| 59 | 4.626 | 3.998 | 2.755 | 3.406 | 2.758 | 2.005 | 2.020 | 1.876 | 1.898 | 2.298 | 2.838 | 1.643 |
| 61 | 0.000 | 0.484 | 1.729 | 0.484 | 1.052 | 2.451 | 2.800 | 2.800 | 2.451 | 1.729 | 1.052 | 2.800 |
| 65 | 0.000 | 0.484 | 1.729 | 0.484 | 1.052 | 2.451 | 2.800 | 2.800 | 2.451 | 1.729 | 1.052 | 2.800 |
| 66 | 0.000 | 0.484 | 1.729 | 0.484 | 1.052 | 2.451 | 2.800 | 2.800 | 2.451 | 1.729 | 1.052 | 2.800 |
| 69 | 0.000 | 0.484 | 1.729 | 0.484 | 1.052 | 2.451 | 2.800 | 2.800 | 2.451 | 1.729 | 1.052 | 2.800 |
| 80 | 0.000 | 0.484 | 1.729 | 0.484 | 1.052 | 2.451 | 2.800 | 2.800 | 2.451 | 1.729 | 1.052 | 2.800 |
| 87 | 1.417 | 1.407 | 1.407 | 1.407 | 1.407 | 1.407 | 1.407 | 1.407 | 1.407 | 1.407 | 1.407 | 1.407 |
| 89 | 1.417 | 1.407 | 1.407 | 1.407 | 1.407 | 1.407 | 1.407 | 1.407 | 1.407 | 1.407 | 1.407 | 1.407 |
| 100 | 1.417 | 1.407 | 1.407 | 1.407 | 1.407 | 1.407 | 1.407 | 1.407 | 1.407 | 1.407 | 1.407 | 1.407 |
| 113 | 1.417 | 1.407 | 1.407 | 1.407 | 1.407 | 1.407 | 1.407 | 1.407 | 1.407 | 1.407 | 1.407 | 1.407 |
| 111 | 1.417 | 1.407 | 1.407 | 1.407 | 1.407 | 1.407 | 1.407 | 1.407 | 1.407 | 1.407 | 1.407 | 1.407 |
| TOTAL | 45.347 | 43.546 | 40.815 | 39.111 | 37.145 | 38.385 | 35.679 | 34.733 | 33.031 | 31.743 | 31.372 | 31.689 |

Table 6.12 shows a higher participation of the gas-fired generators because the increment in the heat rate curves of the coal power plants. Lastly, the dynamic behavior of the nodal pressures at the gas network are reported in Table 6.13.

Table 6.13: Natural gas nodal pressure.

| Node | Pressure in hour, [BARS] | | | | | | | | | | | |
|---|---|---|---|---|---|---|---|---|---|---|---|---|
| | 1 | 2 | 3 | 4 | 5 | 6 | 7 | 8 | 9 | 10 | 11 | 12 |
| 1 | 68.948 | 68.948 | 68.948 | 68.948 | 68.948 | 68.948 | 68.948 | 68.948 | 68.948 | 68.948 | 68.948 | 68.948 |
| 2 | 68.948 | 68.948 | 68.948 | 68.948 | 68.948 | 68.948 | 68.948 | 68.948 | 68.948 | 68.948 | 68.948 | 68.948 |
| 3 | 58.543 | 58.537 | 58.532 | 58.529 | 58.526 | 58.523 | 58.522 | 58.521 | 58.521 | 58.521 | 58.520 | 58.524 |
| 4 | 59.312 | 59.323 | 59.330 | 59.329 | 59.330 | 59.327 | 59.320 | 59.313 | 59.304 | 59.295 | 59.286 | 59.273 |
| 5 | 44.149 | 42.884 | 42.232 | 41.243 | 40.551 | 40.127 | 39.707 | 39.339 | 38.966 | 38.407 | 37.556 | 38.140 |
| 6 | 56.19 | 55.84 | 54.97 | 55.28 | 55.02 | 54.62 | 54.76 | 54.88 | 55.14 | 55.56 | 56.06 | 55.70 |
| 7 | 53.13 | 52.77 | 52.30 | 51.72 | 51.00 | 50.14 | 49.12 | 47.94 | 46.60 | 45.10 | 43.44 | 41.64 |
| 8 | 70.86 | 67.19 | 62.79 | 63.64 | 61.86 | 61.58 | 62.30 | 63.40 | 64.90 | 67.02 | 69.35 | 70.15 |
| 9 | 43.89 | 43.22 | 43.11 | 42.83 | 42.83 | 43.16 | 43.54 | 44.01 | 44.53 | 44.95 | 45.22 | 45.89 |
| 10 | 64.35 | 64.94 | 66.67 | 65.95 | 66.68 | 67.66 | 67.56 | 67.63 | 67.46 | 66.91 | 66.26 | 67.39 |
| 11 | 55.52 | 54.18 | 54.14 | 53.80 | 54.25 | 55.37 | 56.76 | 58.48 | 60.44 | 62.34 | 64.02 | 66.62 |
| 12 | 86.37 | 86.37 | 86.37 | 86.37 | 86.37 | 86.37 | 86.37 | 86.37 | 86.37 | 86.37 | 86.37 | 86.37 |
| 13 | 56.24 | 56.11 | 56.14 | 56.11 | 56.23 | 56.40 | 56.57 | 56.76 | 56.99 | 57.20 | 57.39 | 57.69 |
| 14 | 55.36 | 55.23 | 55.27 | 55.33 | 55.48 | 55.59 | 55.83 | 56.06 | 56.34 | 56.61 | 56.84 | 57.10 |
| 15 | 55.94 | 55.75 | 55.69 | 55.70 | 55.79 | 55.95 | 56.09 | 56.31 | 56.55 | 56.80 | 57.03 | 57.29 |

## 6.5 Conclusions and Remarks

The integration of different energy networks in a integral model permits the assessment of the interdependencies between the different types of energy used for electricity generation considering the impact that constraints associated with the different primary energy systems has in the operating condition of the multi-energy system. These constraints represent the integrated physical characteristics of each system and their security operation conditions which must be satisfied. Furthermore, these operative and security constraints modeling the different primary energy systems are represented by equality and inequality constraints.

The unit commitment problem formulated by the variable duplication method has a modular structure, which is an important characteristic that permits the addition of equality and inequality constraints modeling the physical characteristics associated with the primary energy systems in the OPF module without altering the basic structure of the *MEGUC* algorithm.

# Chapter 7

# Final Remarks and Suggestions for Future Research Work

## 7.1 General conclusions

The integration of the primary energy systems under a single formulation permits the identification and analysis of the existing interdependencies between networks. Currently, there are many tools and techniques for the independent analysis of the natural gas, coal and electricity systems composing an entire energy system, and these techniques can be extended to perform the study of a multi-energy system in which the existing interactions between subsystems can be straightforwardly analyzed. This integral study in a single frame of reference leads to superior integral solutions and proposals for the operative conditions of the different energy networks.

In this thesis a integral formulation of natural gas and electricity has been presented for steady-state operation conditions, in which the concepts of distributed slacks and primary frequency regulation have been explored in order to better represent the physical interaction between the natural gas and electric networks. The mathematical connection between both systems is modeled through the *"heat rate curve"* which quantifies the fuel extracted from the natural gas network to produce a certain quantity of active power delivered in the electric power system. The regulated generation

of active power by gas-fired power plants causes variations in the operating conditions of the natural gas system, which are directly assessed under the same integral study without the necessity of sequential simulations between the electricity and the natural gas networks. Furthermore, the gas temperature changes caused by the heat exchange between the gas inside the pipeline and the soil have been modeled in the proposed approach. This general modeling permits the assessment of the steady-state operation of a natural gas system based on both the nodal gas pressures and gas temperature and has the remarkable characteristic of determining the possible generation of hydrates inside pipelines. This formation of hydrates can block the pipeline's cross section causing important technical and economic issues.

On the other hand, the assessment of the uncertainty associated with the wind energy production causes a high volatility in the fossil fuel consumption; therefore, a scenario-based robust optimization (RO) approach has been formulated to immunize the fossil fuel consumption with respect to this uncertainty. The usefulness of the proposed RO has also been demonstrated in the reduction of the variation of operative conditions in the natural gas system for different levels of wind power production. As mentioned above, the RO has proven itself to be a reliable technique in the treatment of uncertainties associated with energy system's operation.

The integral formulation proposed in this thesis for the short-term operation planning of multi-energy systems permits the quantification of the impact of the wind generation forecast error and the level of wind energy penetration in the existing interdependency between energy networks. The proposed approach allow us to determine the quantity of the fossil fuels required to supply the demand in different networks, while the dynamic behavior of gas flowing in pipelines has been included in a unit commitment along with the physical and operation constraints associated with all networks composing the entire energy system.

In summary, the main objective of this thesis has been achieved: the development of a general mathematical modeling and analysis of energy networks in a integral frame of reference in order to assess the existing interdependency between these networks in

terms of the most common studies performed in the operation of electric power systems: power flows, optimal power flows and unit commitment studies.

## 7.2 Future Work

Departing from the integral formulation proposed in this work and the understanding of the interdependencies between energy networks, new proposals for future research work are detailed below.

1. *Analysis of Interdependencies Between Energy networks Considering Contingencies.* In this subject the idea is to assess the impact that contingencies which occur in one energy network have in other networks. The nonlinear models presented in this thesis can be used to identify secure operation conditions for the multi-energy system. In [Brown 2004] the importance of this subject has been discussed.

2. *Energy Reserve Quantification.* The active power reserve in an electric power system is typically considered the difference between the current active power delivered by generators and their corresponding maximum allowable limit of active power generation $P_{max}$; nevertheless, in a multi-energy context the energy stored in pipelines or coal deposits shall be considered for the reserve market.

3. *Reliability in Multi-Energy Systems.* The classical reliability techniques, which are used to determine the expected cost of load not supplied under forced outages of primary equipment in the electric power system, can be extended by considering the equipment of other energy networks. In this case, the derating of power generators considering the security and operative constraints associated with their energy networks and the maintenance cost of the multi-energy system can be quantified in economic terms.

4. *Pollutant Emissions Policies Assessment.* Based on the increasing concern

in global warming, governments around the world are also increasingly willing to implement limitations of pollutants into the power generation. The production of greenhouse gases as a function of the energy conversion technology and its corresponding penalization discourages the development of coal-fired technologies, which recently have adopted $CO_2$ capture and storage systems. Nevertheless, the increase in their operation cost has been increased in such a way that the power produced by these generators is less competitive in the energy market. Even when the natural gas technology has a most clean conversion process, the volatility of its price in the market can be a factor working against the gas-fired generators. The assessment of these factors can help to define the most suitable policies in this field.

5. *Short-term Operation Planning Considering Wind Power Uncertainty.* The impact of the wind power variability in the unit commitment under the context of multi-energy systems can improve the primary energy management for the short-term planning. The RO formulation applied to multi-energy systems presented in this thesis can be extended to the unit commitment problem. Currently, the scenario with the highest probability of occurrence is the only one examined for each subperiod of the Unit Commitment analysis (load, wind-power, fossil-fuel prices, etc.). Contrary to this way of analysis, the proposed robust unit commitment analysis must satisfy intertemporal constraints for this scenario with the highest probability of occurrence, and the robustness of each subperiod can improve the fuel management and the operative conditions of the entire energy system as demonstrated in in Chapter 4 of this thesis.

6. *Expansion Planning of Energy networks.* The integral formulation for primary energy networks presented in this thesis can be employed to assess different expansion scenarios for the different networks involved in the multi-energy system. The expansion of the electric power system linked to the expansion of the other networks can increase the reliability of the whole

multi-energy system.

7. *Energy Control Device's Assessment.* The assessment of energy control devices in one network can have undesirable effects in other networks; for example, the use of FACTS devices in the electric power system allows the control of power flows but can reduce the reliability in the gas network or even worse lead it to an operation condition beyond its limits. In addition, the natural gas system has flow control devices, which will affect the operation condition in the electricity system. These interdependencies can be analyzed under a integral multi-energy formulation as proposed in this thesis.

8. *Sensitivities analysis.* The sensitivity analysis is a widely used technique to assess the influence that one variable or parameter has on the electric power system. Under a multi-energy context, this technique can be extended to analyze the influence of any parameter or variable in the whole multi-energy system. Furthermore, this technique has been employed for expansion purposes or location of energy control devices.

9. *Uncertainty Models.* Work with uncertainty models in order to attain a suitable mathematical representation of physical phenomena in order to develop better models, programs, methodologies and techniques to assess parametric uncertainty in the operation of electric power systems and the impact in other primary energy networks caused by the inherent interdependnecies.

10. *Energy Markets Models Integration.* The addition of bids models for the industrial loads in the different primary energy networks can help to understand the behavior of the energy markets, identify risks and improve the integral solutions since a financial and technical points of view.

# Appendix A

# Appendix: Systems Data

Table A.1: 3 Nodes natural gas network.

| NODES | | | | | | | |
|---|---|---|---|---|---|---|---|
| Number | Type | $\Pi$ (PSI) | $\Pi^{max}$ (PSI) | $\Pi^{min}$ (PSI) | Temperature ($^{o}$R) | Load (MMSCF) | Source (MMSCF) |
| 1 | 0 | 725.188 | 1200 | 0.00 | 520 | 0.00 | 10.0 |
| 2 | 1 | 708.668 | 1200 | 0.00 | 520 | 2.54 | 0.00 |
| 3 | 1 | 707.036 | 1200 | 0.00 | 520 | 5.08 | 0.00 |

| PIPELINES | | | | | |
|---|---|---|---|---|---|
| From | To | Length (Mi) | Diameter (in) | Efficiency (%) | Temperature ($^{o}$R) |
| 1 | 3 | 49.72 | 23.622 | 100 | 520 |
| 1 | 2 | 55.93 | 23.622 | 100 | 520 |
| 2 | 3 | 62.15 | 23.622 | 100 | 520 |

Table A.2: 15 Nodes natural gas network.

| NODES | | | | | | | |
|---|---|---|---|---|---|---|---|
| Number | Type | Π (PSI) | $\Pi^{max}$ (PSI) | $\Pi^{min}$ (PSI) | Temperature (ºR) | Load (MMSCF) | Source (MMSCF) |
| 1 | 0 | 1000.0 | 1200 | 0.00 | 520 | 0.00 | 10.0 |
| 2 | 0 | 1000.0 | 1200 | 0.00 | 520 | 1.25 | 6.87 |
| 3 | 1 | 729.7 | 1200 | 0.00 | 520 | 3.75 | 0.00 |
| 4 | 1 | 737.3 | 1200 | 0.00 | 520 | 0.00 | 0.00 |
| 5 | 1 | 575.5 | 1200 | 0.00 | 520 | 0.00 | 0.00 |
| 6 | 1 | 1035.0 | 1200 | 0.00 | 520 | 0.00 | 0.00 |
| 7 | 1 | 607.6 | 1200 | 0.00 | 520 | 0.00 | 0.00 |
| 8 | 1 | 1154.4 | 1200 | 0.00 | 520 | 0.00 | 0.00 |
| 9 | 1 | 918.6 | 1200 | 0.00 | 520 | 0.00 | 0.00 |
| 10 | 1 | 951.0 | 1200 | 0.00 | 520 | 0.00 | 0.00 |
| 11 | 1 | 932.8 | 1200 | 0.00 | 520 | 0.00 | 0.00 |
| 12 | 1 | 933.8 | 1200 | 0.00 | 520 | 4.58 | 0.00 |
| 13 | 1 | 601.6 | 1200 | 0.00 | 520 | 1.66 | 0.00 |
| 14 | 1 | 600.8 | 1200 | 0.00 | 520 | 3.75 | 0.00 |
| 15 | 1 | 600.0 | 1200 | 0.00 | 520 | 0.00 | 8.00 |

| PIPELINES | | | | | |
|---|---|---|---|---|---|
| From | To | Length (Mi) | Diameter (in) | Efficiency (%) | Temperature (ºR) |
| 1 | 3 | 80.5 | 19.56 | 90 | 520 |
| 2 | 4 | 80.3 | 19.56 | 90 | 520 |
| 3 | 4 | 55.9 | 19.56 | 90 | 520 |
| 3 | 5 | 81.1 | 19.62 | 90 | 520 |
| 4 | 7 | 87.9 | 19.62 | 90 | 520 |
| 6 | 9 | 93.5 | 19.62 | 90 | 520 |
| 8 | 11 | 99.7 | 16.69 | 90 | 520 |
| 10 | 13 | 93.5 | 16.69 | 90 | 520 |
| 12 | 14 | 97.9 | 16.69 | 85 | 520 |
| 13 | 14 | 86.6 | 16.69 | 90 | 520 |
| 13 | 15 | 79.7 | 16.69 | 90 | 520 |
| 14 | 15 | 83.5 | 16.69 | 85 | 520 |

| COMPRESSORS | | | | |
|---|---|---|---|---|
| From | To | Efficiency (%) | Compression ratio | Temperature (ºR) |
| 5 | 6 | 83 | 1.6 | 520 |
| 7 | 8 | 84 | 1.8 | 520 |
| 9 | 10 | 83 | 1.3 | 520 |
| 11 | 12 | 84 | 1.8 | 520 |

Table A.3: Belgian natural gas network.

NODES

| Number | Type | Π (PSI) | $\Pi^{max}$ (PSI) | $\Pi^{min}$ (PSI) | Temperature ($^{o}$R) | Load (MMSCF) | Source (MMSCF) |
|---|---|---|---|---|---|---|---|
| 1 | 1 | 809.6 | 1200 | 0.00 | 520 | 0.00 | 16.1 |
| 2 | 1 | 809.2 | 1200 | 0.00 | 520 | 0.00 | 12.3 |
| 3 | 1 | 807.2 | 1200 | 0.00 | 520 | 5.76 | 0.00 |
| 4 | 1 | 784.8 | 1200 | 0.00 | 520 | 0.00 | 0.00 |
| 5 | 1 | 769.1 | 1200 | 0.00 | 520 | 0.00 | 4.14 |
| 6 | 1 | 758.2 | 1200 | 0.00 | 520 | 5.93 | 0.00 |
| 7 | 1 | 759.6 | 1200 | 0.00 | 520 | 7.73 | 0.00 |
| 8 | 1 | 868.1 | 1200 | 0.00 | 520 | 0.00 | 32.4 |
| 9 | 1 | 861.6 | 1200 | 0.00 | 520 | 0.00 | 0.00 |
| 10 | 1 | 835.3 | 1200 | 0.00 | 520 | 9.36 | 0.00 |
| 11 | 1 | 818.3 | 1200 | 0.00 | 520 | 0.00 | 0.00 |
| 12 | 1 | 790.7 | 1200 | 0.00 | 520 | 3.11 | 0.00 |
| 13 | 1 | 771.4 | 1200 | 0.00 | 520 | 0.00 | 1.76 |
| 14 | 1 | 768.4 | 1200 | 0.00 | 520 | 0.00 | 1.41 |
| 15 | 1 | 749.2 | 1200 | 0.00 | 520 | 10.1 | 0.00 |
| 16 | 0 | 725.2 | 1200 | 0.00 | 520 | 22.9 | 0.00 |
| 17 | 1 | 806.7 | 1200 | 0.00 | 520 | 0.00 | 0.00 |
| 18 | 1 | 913.7 | 1200 | 0.00 | 520 | 0.00 | 0.00 |
| 19 | 1 | 518.4 | 1200 | 0.00 | 520 | 0.32 | 0.00 |
| 20 | 1 | 490.8 | 1200 | 0.00 | 520 | 2.82 | 0.00 |
| 21 | 1 | 861.6 | 1200 | 0.00 | 520 | 0.00 | 0.00 |
| 22 | 1 | 707.6 | 1200 | 0.00 | 520 | 0.00 | 0.00 |

PIPELINES

| From | To | Length (Mi) | Diameter (in) | Efficiency (%) | Temperature ($^{o}$R) |
|---|---|---|---|---|---|
| 1 | 2 | 3.7 | 35.0394 | 100 | 520 |
| 1 | 2 | 3.7 | 35.0394 | 100 | 520 |
| 2 | 3 | 5.6 | 35.0394 | 100 | 520 |
| 2 | 3 | 5.6 | 35.0394 | 100 | 520 |
| 3 | 4 | 24.3 | 35.0394 | 100 | 520 |
| 5 | 6 | 40.2 | 23.2323 | 100 | 520 |
| 6 | 7 | 27.1 | 23.2323 | 100 | 520 |
| 7 | 4 | 17.8 | 23.2323 | 100 | 520 |
| 4 | 14 | 51.5 | 35.0394 | 100 | 520 |
| 8 | 21 | 4.7 | 35.0394 | 100 | 520 |
| 8 | 21 | 4.7 | 15.5709 | 100 | 520 |
| 9 | 10 | 18.7 | 35.0394 | 100 | 520 |
| 9 | 10 | 18.7 | 15.5709 | 100 | 520 |
| 10 | 11 | 23.4 | 35.0394 | 100 | 520 |
| 10 | 11 | 23.4 | 15.5709 | 100 | 520 |
| 11 | 12 | 39.3 | 35.0394 | 100 | 520 |
| 12 | 13 | 37.4 | 35.0394 | 100 | 520 |
| 13 | 14 | 4.7 | 35.0394 | 100 | 520 |
| 14 | 15 | 9.4 | 35.0394 | 100 | 520 |
| 15 | 16 | 23.4 | 35.0394 | 100 | 520 |
| 11 | 17 | 9.8 | 15.5709 | 100 | 520 |
| 17 | 22 | 24.3 | 12.4213 | 100 | 520 |
| 18 | 19 | 91.7 | 12.4213 | 100 | 520 |
| 19 | 20 | 5.6 | 12.4213 | 100 | 520 |

COMPRESSORS

| From | To | Efficiency (%) | Compression ratio | Temperature ($^{o}$R) |
|---|---|---|---|---|
| 21 | 9 | 100 | 1.0 | 520 |
| 22 | 18 | 100 | 1.3 | 520 |

Table A.4: 4 Nodes coal network.

| NODES | | | | | |
|---|---|---|---|---|---|
| Number | Type | Source (PSI) | Load (Ton) | $MC^{max}$ (Ton) | $MC^{min}$ (Ton) |
| 1 | 0 | 0.00 | 0.00 | 500 | 0.00 |
| 2 | 1 | 10.0 | 0.00 | 500 | 0.00 |
| 3 | 1 | 0.00 | 0.00 | 0.00 | 0.00 |
| 4 | 1 | 0.00 | 0.00 | 0.00 | 0.00 |

| RAILROADS | | | | | | |
|---|---|---|---|---|---|---|
| From | To | $l_r^{km}$(Mi) | $V_r^{km}$ (Mi/hr) | $C_r^{km}$ | $K_r^{km}$ | Efficiency (%) |
| 1 | 3 | 100 | 60 | 0.00 | 10 | 80 |
| 2 | 3 | 200 | 60 | 0.00 | 10 | 80 |
| 3 | 4 | 10 | 60 | 0.00 | 10 | 80 |

Table A.5: 14 Nodes electric power system.

| NODES | | | | | | | | | | | | |
|---|---|---|---|---|---|---|---|---|---|---|---|---|
| Number | Name | Type | Voltage (pu) | Angle (grad) | Load | | Generation | | MVAR | | Shunts | |
| | | | | | MW | MVAR | MW | MVAR | Max | Min | G | B |
| 1 | Bus 1 | 3 | 1.06 | 0 | 0 | 0 | 232.4 | -16.9 | 0 | 0 | 0 | 0 |
| 2 | Bus 2 | 2 | 1.045 | -4.98 | 21.7 | 12.7 | 40 | 42.4 | 50 | -40 | 0 | 0 |
| 3 | Bus 3 | 2 | 1.01 | -12.72 | 94.2 | 19 | 0 | 23.4 | 40 | 0 | 0 | 0 |
| 4 | Bus 4 | 0 | 1.019 | -10.33 | 47.8 | -3.9 | 0 | 0 | 0 | 0 | 0 | 0 |
| 5 | Bus 5 | 0 | 1.02 | -8.78 | 7.6 | 1.6 | 0 | 0 | 0 | 0 | 0 | 0 |
| 6 | Bus 6 | 2 | 1.07 | -14.22 | 11.2 | 7.5 | 0 | 12.2 | 24 | -6 | 0 | 0 |
| 7 | Bus 7 | 0 | 1.062 | -13.37 | 0 | 0 | 0 | 0 | 0 | 0 | 0 | 0 |
| 8 | Bus 8 | 2 | 1.09 | -13.36 | 0 | 0 | 0 | 17.4 | 24 | -6 | 0 | 0 |
| 9 | Bus 9 | 0 | 1.056 | -14.94 | 29.5 | 16.6 | 0 | 0 | 0 | 0 | 0 | 0.19 |
| 10 | Bus 10 | 0 | 1.051 | -15.1 | 9 | 5.8 | 0 | 0 | 0 | 0 | 0 | 0 |
| 11 | Bus 11 | 0 | 1.057 | -14.79 | 3.5 | 1.8 | 0 | 0 | 0 | 0 | 0 | 0 |
| 12 | Bus 12 | 0 | 1.055 | -15.07 | 6.1 | 1.6 | 0 | 0 | 0 | 0 | 0 | 0 |
| 13 | Bus 13 | 0 | 1.05 | -15.16 | 13.5 | 5.8 | 0 | 0 | 0 | 0 | 0 | 0 |
| 14 | Bus 14 | 0 | 1.036 | -16.04 | 14.9 | 5 | 0 | 0 | 0 | 0 | 0 | 0 |

| TRANSMISSION ELEMENTS | | | | | |
|---|---|---|---|---|---|
| From | To | R | X | B/2 | TAP |
| 1 | 2 | 0.01938 | 0.05917 | 0.0528 | 0 |
| 1 | 5 | 0.05403 | 0.22304 | 0.0492 | 0 |
| 2 | 3 | 0.04699 | 0.19797 | 0.0438 | 0 |
| 2 | 4 | 0.05811 | 0.17632 | 0.034 | 0 |
| 2 | 5 | 0.05695 | 0.17388 | 0.0346 | 0 |
| 3 | 4 | 0.06701 | 0.17103 | 0.0128 | 0 |
| 4 | 5 | 0.01335 | 0.04211 | 0 | 0 |
| 4 | 7 | 0 | 0.20912 | 0 | 0.978 |
| 4 | 9 | 0 | 0.55618 | 0 | 0.969 |
| 5 | 6 | 0 | 0.25202 | 0 | 0.932 |
| 6 | 11 | 0.09498 | 0.1989 | 0 | 0 |
| 6 | 12 | 0.12291 | 0.25581 | 0 | 0 |
| 6 | 13 | 0.06615 | 0.13027 | 0 | 0 |
| 7 | 8 | 0 | 0.17615 | 0 | 0 |
| 7 | 9 | 0 | 0.11001 | 0 | 0 |
| 9 | 10 | 0.03181 | 0.0845 | 0 | 0 |
| 9 | 14 | 0.12711 | 0.27038 | 0 | 0 |
| 10 | 11 | 0.08205 | 0.19207 | 0 | 0 |
| 12 | 13 | 0.22092 | 0.19988 | 0 | 0 |
| 13 | 14 | 0.17093 | 0.34802 | 0 | 0 |

Table A.6: 118 Nodes electric power system.

| NODES | | | | | | | | | | | | |
|---|---|---|---|---|---|---|---|---|---|---|---|---|
| Number | Name | Type | Voltage (pu) | Angle (grad) | Load | | Generation | | MVAR | | Shunts | |
| | | | | | MW | MVAR | MW | MVAR | Max | Min | G | B |
| 1 | Riverside | 2 | 0.955 | 10.67 | 51 | 27 | 0 | 0 | 15 | -5 | 0 | 0 |
| 2 | Pokagon | 0 | 0.971 | 11.22 | 20 | 9 | 0 | 0 | 0 | 0 | 0 | 0 |
| 3 | HickryCk | 0 | 0.968 | 11.56 | 39 | 10 | 0 | 0 | 0 | 0 | 0 | 0 |
| 4 | NwCarlsl | 2 | 0.998 | 15.28 | 30 | 12 | -9 | 0 | 300 | -300 | 0 | 0 |
| 5 | Olive | 0 | 1.002 | 15.73 | 0 | 0 | 0 | 0 | 0 | 0 | 0 | -0.4 |
| 6 | Kankakee | 2 | 0.99 | 13 | 52 | 22 | 0 | 0 | 50 | -13 | 0 | 0 |
| 7 | JacksnRd | 0 | 0.989 | 12.56 | 19 | 2 | 0 | 0 | 0 | 0 | 0 | 0 |
| 8 | Olive | 2 | 1.015 | 20.77 | 0 | 0 | -28 | 0 | 300 | -300 | 0 | 0 |
| 9 | Bequine | 0 | 1.043 | 28.02 | 0 | 0 | 0 | 0 | 0 | 0 | 0 | 0 |
| 10 | Breed | 2 | 1.05 | 35.61 | 0 | 0 | 450 | 0 | 200 | -147 | 0 | 0 |
| 11 | SouthBnd | 0 | 0.985 | 12.72 | 70 | 23 | 0 | 0 | 0 | 0 | 0 | 0 |
| 12 | TwinBrch | 2 | 0.99 | 12.2 | 47 | 10 | 85 | 0 | 120 | -35 | 0 | 0 |
| 13 | Concord | 0 | 0.968 | 11.35 | 34 | 16 | 0 | 0 | 0 | 0 | 0 | 0 |
| 14 | GoshenJt | 0 | 0.984 | 11.5 | 14 | 1 | 0 | 0 | 0 | 0 | 0 | 0 |
| 15 | FtWayne | 2 | 0.97 | 11.23 | 90 | 30 | 0 | 0 | 30 | -10 | 0 | 0 |
| 16 | N. E. | 0 | 0.984 | 11.91 | 25 | 10 | 0 | 0 | 0 | 0 | 0 | 0 |
| 17 | Sorenson | 0 | 0.995 | 13.74 | 11 | 3 | 0 | 0 | 0 | 0 | 0 | 0 |
| 18 | McKinley | 2 | 0.973 | 11.53 | 60 | 34 | 0 | 0 | 50 | -16 | 0 | 0 |
| 19 | Lincoln | 2 | 0.963 | 11.05 | 45 | 25 | 0 | 0 | 24 | -8 | 0 | 0 |
| 20 | Adams | 0 | 0.958 | 11.93 | 18 | 3 | 0 | 0 | 0 | 0 | 0 | 0 |
| 21 | Jay | 0 | 0.959 | 13.52 | 14 | 8 | 0 | 0 | 0 | 0 | 0 | 0 |
| 22 | Randolph | 0 | 0.97 | 16.08 | 10 | 5 | 0 | 0 | 0 | 0 | 0 | 0 |
| 23 | CollCrnr | 0 | 1 | 21 | 7 | 3 | 0 | 0 | 0 | 0 | 0 | 0 |
| 24 | Trenton | 2 | 0.992 | 20.89 | 0 | 0 | -13 | 0 | 300 | -300 | 0 | 0 |
| 25 | TannrsCk | 2 | 1.05 | 27.93 | 0 | 0 | 220 | 0 | 140 | -47 | 0 | 0 |
| 26 | TannrsCk | 2 | 1.015 | 29.71 | 0 | 0 | 314 | 0 | 1000 | -1000 | 0 | 0 |
| 27 | Madison | 2 | 0.968 | 15.35 | 62 | 13 | -9 | 0 | 300 | -300 | 0 | 0 |
| 28 | Mullin | 0 | 0.962 | 13.62 | 17 | 7 | 0 | 0 | 0 | 0 | 0 | 0 |
| 29 | Grant | 0 | 0.963 | 12.63 | 24 | 4 | 0 | 0 | 0 | 0 | 0 | 0 |
| 30 | Sorenson | 0 | 0.968 | 18.79 | 0 | 0 | 0 | 0 | 0 | 0 | 0 | 0 |
| 31 | DeerCrk | 2 | 0.967 | 12.75 | 43 | 27 | 7 | 0 | 300 | -300 | 0 | 0 |
| 32 | Delaware | 2 | 0.964 | 14.8 | 59 | 23 | 0 | 0 | 42 | -14 | 0 | 0 |
| 33 | Haviland | 0 | 0.972 | 10.63 | 23 | 9 | 0 | 0 | 0 | 0 | 0 | 0 |
| 34 | Rockhill | 2 | 0.986 | 11.3 | 59 | 26 | 0 | 0 | 24 | -8 | 0 | 0.14 |
| 35 | WestLima | 0 | 0.981 | 10.87 | 33 | 9 | 0 | 0 | 0 | 0 | 0 | 0 |
| 36 | Sterling | 2 | 0.98 | 10.87 | 31 | 17 | 0 | 0 | 24 | -8 | 0 | 0 |
| 37 | EastLima | 0 | 0.992 | 11.77 | 0 | 0 | 0 | 0 | 0 | 0 | 0 | -0.25 |
| 38 | EastLima | 0 | 0.962 | 16.91 | 0 | 0 | 0 | 0 | 0 | 0 | 0 | 0 |
| 39 | NwLibrty | 0 | 0.97 | 8.41 | 27 | 11 | 0 | 0 | 0 | 0 | 0 | 0 |
| 40 | West End | 2 | 0.97 | 7.35 | 20 | 23 | -46 | 0 | 300 | -300 | 0 | 0 |
| 41 | S.Tiffin | 0 | 0.967 | 6.92 | 37 | 10 | 0 | 0 | 0 | 0 | 0 | 0 |
| 42 | Howard | 2 | 0.985 | 8.53 | 37 | 23 | -59 | 0 | 300 | -300 | 0 | 0 |
| 43 | S.Kenton | 0 | 0.978 | 11.28 | 18 | 7 | 0 | 0 | 0 | 0 | 0 | 0 |
| 44 | WMVernon | 0 | 0.985 | 13.82 | 16 | 8 | 0 | 0 | 0 | 0 | 0 | 0.1 |
| 45 | N.Newark | 0 | 0.987 | 15.67 | 53 | 22 | 0 | 0 | 0 | 0 | 0 | 0.1 |
| 46 | W.Lancst | 2 | 1.005 | 18.49 | 28 | 10 | 19 | 0 | 100 | -100 | 0 | 0.1 |
| 47 | Crooksvl | 0 | 1.017 | 20.73 | 34 | 0 | 0 | 0 | 0 | 0 | 0 | 0 |
| 48 | Zanesvll | 0 | 1.021 | 19.93 | 20 | 11 | 0 | 0 | 0 | 0 | 0 | 0.15 |
| 49 | Philo | 2 | 1.025 | 20.94 | 87 | 30 | 204 | 0 | 210 | -85 | 0 | 0 |
| 50 | WCambrdg | 0 | 1.001 | 18.9 | 17 | 4 | 0 | 0 | 0 | 0 | 0 | 0 |

| NODES | | | | | | | | | | | | |
|---|---|---|---|---|---|---|---|---|---|---|---|---|
| Number | Name | Type | Voltage (pu) | Angle (grad) | Load | | Generation | | MVAR | | Shunts | |
| | | | | | MW | MVAR | MW | MVAR | Max | Min | G | B |
| 51 | Newcmrst | 0 | 0.967 | 16.28 | 17 | 8 | 0 | 0 | 0 | 0 | 0 | 0 |
| 52 | SCoshoct | 0 | 0.957 | 15.32 | 18 | 5 | 0 | 0 | 0 | 0 | 0 | 0 |
| 53 | Wooster | 0 | 0.946 | 14.35 | 23 | 11 | 0 | 0 | 0 | 0 | 0 | 0 |
| 54 | Torrey | 2 | 0.955 | 15.26 | 113 | 32 | 48 | 0 | 300 | -300 | 0 | 0 |
| 55 | Wagenhls | 2 | 0.952 | 14.97 | 63 | 22 | 0 | 0 | 23 | -8 | 0 | 0 |
| 56 | Sunnysde | 2 | 0.954 | 15.16 | 84 | 18 | 0 | 0 | 15 | -8 | 0 | 0 |
| 57 | WNwPhil1 | 0 | 0.971 | 16.36 | 12 | 3 | 0 | 0 | 0 | 0 | 0 | 0 |
| 58 | WNwPhil2 | 0 | 0.959 | 15.51 | 12 | 3 | 0 | 0 | 0 | 0 | 0 | 0 |
| 59 | Tidd | 2 | 0.985 | 19.37 | 277 | 113 | 155 | 0 | 180 | -60 | 0 | 0 |
| 60 | SWKammer | 0 | 0.993 | 23.15 | 78 | 3 | 0 | 0 | 0 | 0 | 0 | 0 |
| 61 | W.Kammer | 2 | 0.995 | 24.04 | 0 | 0 | 160 | 0 | 300 | -100 | 0 | 0 |
| 62 | Natrium | 2 | 0.998 | 23.43 | 77 | 14 | 0 | 0 | 20 | -20 | 0 | 0 |
| 63 | Tidd | 0 | 0.969 | 22.75 | 0 | 0 | 0 | 0 | 0 | 0 | 0 | 0 |
| 64 | Kammer | 0 | 0.984 | 24.52 | 0 | 0 | 0 | 0 | 0 | 0 | 0 | 0 |
| 65 | Muskngum | 2 | 1.005 | 27.65 | 0 | 0 | 391 | 0 | 200 | -67 | 0 | 0 |
| 66 | Muskngum | 2 | 1.05 | 27.48 | 39 | 18 | 392 | 0 | 200 | -67 | 0 | 0 |
| 67 | Summerfl | 0 | 1.02 | 24.84 | 28 | 7 | 0 | 0 | 0 | 0 | 0 | 0 |
| 68 | Sporn | 0 | 1.003 | 27.55 | 0 | 0 | 0 | 0 | 0 | 0 | 0 | 0 |
| 69 | Sporn | 3 | 1.035 | 30 | 0 | 0 | 516.4 | 0 | 300 | -300 | 0 | 0 |
| 70 | Portsmth | 2 | 0.984 | 22.58 | 66 | 20 | 0 | 0 | 32 | -10 | 0 | 0 |
| 71 | NPortsmt | 0 | 0.987 | 22.15 | 0 | 0 | 0 | 0 | 0 | 0 | 0 | 0 |
| 72 | Hillsbro | 2 | 0.98 | 20.98 | 0 | 0 | -12 | 0 | 100 | -100 | 0 | 0 |
| 73 | Sargents | 2 | 0.991 | 21.94 | 0 | 0 | -6 | 0 | 100 | -100 | 0 | 0 |
| 74 | Bellefnt | 2 | 0.958 | 21.64 | 68 | 27 | 0 | 0 | 9 | -6 | 0 | 0.12 |
| 75 | SthPoint | 0 | 0.967 | 22.91 | 47 | 11 | 0 | 0 | 0 | 0 | 0 | 0 |
| 76 | Darrah | 2 | 0.943 | 21.77 | 68 | 36 | 0 | 0 | 23 | -8 | 0 | 0 |
| 77 | Turner | 2 | 1.006 | 26.72 | 61 | 28 | 0 | 0 | 70 | -20 | 0 | 0 |
| 78 | Chemical | 0 | 1.003 | 26.42 | 71 | 26 | 0 | 0 | 0 | 0 | 0 | 0 |
| 79 | CapitlHl | 0 | 1.009 | 26.72 | 39 | 32 | 0 | 0 | 0 | 0 | 0 | 0.2 |
| 80 | CabinCrk | 2 | 1.04 | 28.96 | 130 | 26 | 477 | 0 | 280 | -165 | 0 | 0 |
| 81 | Kanawha | 0 | 0.997 | 28.1 | 0 | 0 | 0 | 0 | 0 | 0 | 0 | 0 |
| 82 | Logan | 0 | 0.989 | 27.24 | 54 | 27 | 0 | 0 | 0 | 0 | 0 | 0.2 |
| 83 | Sprigg | 0 | 0.985 | 28.42 | 20 | 10 | 0 | 0 | 0 | 0 | 0 | 0.1 |
| 84 | BetsyLne | 0 | 0.98 | 30.95 | 11 | 7 | 0 | 0 | 0 | 0 | 0 | 0 |
| 85 | BeaverCk | 2 | 0.985 | 32.51 | 24 | 15 | 0 | 0 | 23 | -8 | 0 | 0 |
| 86 | Hazard | 0 | 0.987 | 31.14 | 21 | 10 | 0 | 0 | 0 | 0 | 0 | 0 |
| 87 | Pinevlle | 2 | 1.015 | 31.4 | 0 | 0 | 4 | 0 | 1000 | -100 | 0 | 0 |
| 88 | Fremont | 0 | 0.987 | 35.64 | 48 | 10 | 0 | 0 | 0 | 0 | 0 | 0 |
| 89 | ClinchRv | 2 | 1.005 | 39.69 | 0 | 0 | 607 | 0 | 300 | -210 | 0 | 0 |
| 90 | Holston | 2 | 0.985 | 33.29 | 78 | 42 | -85 | 0 | 300 | -300 | 0 | 0 |
| 91 | HolstonT | 2 | 0.98 | 33.31 | 0 | 0 | -10 | 0 | 100 | -100 | 0 | 0 |
| 92 | Saltvlle | 2 | 0.993 | 33.8 | 65 | 10 | 0 | 0 | 9 | -3 | 0 | 0 |
| 93 | Tazewell | 0 | 0.987 | 30.79 | 12 | 7 | 0 | 0 | 0 | 0 | 0 | 0 |
| 94 | Switchbk | 0 | 0.991 | 28.64 | 30 | 16 | 0 | 0 | 0 | 0 | 0 | 0 |
| 95 | Caldwell | 0 | 0.981 | 27.67 | 42 | 31 | 0 | 0 | 0 | 0 | 0 | 0 |
| 96 | Baileysv | 0 | 0.993 | 27.51 | 38 | 15 | 0 | 0 | 0 | 0 | 0 | 0 |
| 97 | Sundial | 0 | 1.011 | 27.88 | 15 | 9 | 0 | 0 | 0 | 0 | 0 | 0 |
| 98 | Bradley | 0 | 1.024 | 27.4 | 34 | 8 | 0 | 0 | 0 | 0 | 0 | 0 |
| 99 | Hinton | 2 | 1.01 | 27.04 | 0 | 0 | -42 | 0 | 100 | -100 | 0 | 0 |
| 100 | Glen Lyn | 2 | 1.017 | 28.03 | 37 | 18 | 252 | 0 | 155 | -50 | 0 | 0 |
| 116 | KygerCrk | 2 | 1.005 | 27.12 | 0 | 0 | -184 | 0 | 1000 | -1000 | 0 | 0 |
| 117 | Corey | 0 | 0.974 | 10.67 | 20 | 8 | 0 | 0 | 0 | 0 | 0 | 0 |
| 118 | WHuntngd | 0 | 0.949 | 21.92 | 33 | 15 | 0 | 0 | 0 | 0 | 0 | 0 |

NODES

| Number | Name | Type | Voltage (pu) | Angle (grad) | Load | | Generation | | MVAR | | Shunts | |
|---|---|---|---|---|---|---|---|---|---|---|---|---|
| | | | | | MW | MVAR | MW | MVAR | Max | Min | G | B |
| 101 | Wythe | 0 | 0.993 | 29.61 | 22 | 15 | 0 | 0 | 0 | 0 | 0 | 0 |
| 102 | Smythe | 0 | 0.991 | 32.3 | 5 | 3 | 0 | 0 | 0 | 0 | 0 | 0 |
| 103 | Claytor | 2 | 1.001 | 24.44 | 23 | 16 | 40 | 0 | 40 | -15 | 0 | 0 |
| 104 | Hancock | 2 | 0.971 | 21.69 | 38 | 25 | 0 | 0 | 23 | -8 | 0 | 0 |
| 105 | Roanoke | 2 | 0.965 | 20.57 | 31 | 26 | 0 | 0 | 23 | -8 | 0 | 0.2 |
| 106 | Cloverdl | 0 | 0.962 | 20.32 | 43 | 16 | 0 | 0 | 0 | 0 | 0 | 0 |
| 107 | Reusens | 2 | 0.952 | 17.53 | 28 | 12 | -22 | 0 | 200 | -200 | 0 | 0.06 |
| 108 | Blaine | 0 | 0.967 | 19.38 | 2 | 1 | 0 | 0 | 0 | 0 | 0 | 0 |
| 109 | Franklin | 0 | 0.967 | 18.93 | 8 | 3 | 0 | 0 | 0 | 0 | 0 | 0 |
| 110 | Fieldale | 2 | 0.973 | 18.09 | 39 | 30 | 0 | 0 | 23 | -8 | 0 | 0.06 |
| 111 | DanRiver | 2 | 0.98 | 19.74 | 0 | 0 | 36 | 0 | 1000 | -100 | 0 | 0 |
| 112 | Danville | 2 | 0.975 | 14.99 | 25 | 13 | -43 | 0 | 1000 | -100 | 0 | 0 |
| 113 | Deer Crk | 2 | 0.993 | 13.74 | 0 | 0 | -6 | 0 | 200 | -100 | 0 | 0 |
| 114 | WMedford | 0 | 0.96 | 14.46 | 8 | 3 | 0 | 0 | 0 | 0 | 0 | 0 |
| 115 | Medford | 0 | 0.96 | 14.46 | 22 | 7 | 0 | 0 | 0 | 0 | 0 | 0 |
| 116 | KygerCrk | 2 | 1.005 | 27.12 | 0 | 0 | -184 | 0 | 1000 | -1000 | 0 | 0 |
| 117 | Corey | 0 | 0.974 | 10.67 | 20 | 8 | 0 | 0 | 0 | 0 | 0 | 0 |
| 118 | WHuntngd | 0 | 0.949 | 21.92 | 33 | 15 | 0 | 0 | 0 | 0 | 0 | 0 |

TRANSMISSION ELEMENTS

| From | To | R | X | B/2 | TAP | From | To | R | X | B/2 | TAP | From | To | R | X | B/2 | TAP |
|---|---|---|---|---|---|---|---|---|---|---|---|---|---|---|---|---|---|
| 1 | 2 | 0.0303 | 0.0999 | 0.0254 | 0 | 46 | 47 | 0.038 | 0.127 | 0.0316 | 0 | 79 | 80 | 0.0156 | 0.0704 | 0.0187 | 0 |
| 1 | 3 | 0.0129 | 0.0424 | 0.01082 | 0 | 46 | 48 | 0.0601 | 0.189 | 0.0472 | 0 | 68 | 81 | 0.00175 | 0.0202 | 0.808 | 0 |
| 4 | 5 | 0.00176 | 0.00798 | 0.0021 | 0 | 47 | 49 | 0.0191 | 0.0625 | 0.01604 | 0 | 81 | 80 | 0 | 0.037 | 0 | 0.935 |
| 3 | 5 | 0.0241 | 0.108 | 0.0284 | 0 | 42 | 49 | 0.0715 | 0.323 | 0.086 | 0 | 77 | 82 | 0.0298 | 0.0853 | 0.08174 | 0 |
| 5 | 6 | 0.0119 | 0.054 | 0.01426 | 0 | 42 | 49 | 0.0715 | 0.323 | 0.086 | 0 | 82 | 83 | 0.0112 | 0.03665 | 0.03796 | 0 |
| 6 | 7 | 0.00459 | 0.0208 | 0.0055 | 0 | 45 | 49 | 0.0684 | 0.186 | 0.0444 | 0 | 83 | 84 | 0.0625 | 0.132 | 0.0258 | 0 |
| 8 | 9 | 0.00244 | 0.0305 | 1.162 | 0 | 48 | 49 | 0.0179 | 0.0505 | 0.01258 | 0 | 83 | 85 | 0.043 | 0.148 | 0.0348 | 0 |
| 8 | 5 | 0 | 0.0267 | 0 | 0.985 | 49 | 50 | 0.0267 | 0.0752 | 0.01874 | 0 | 84 | 85 | 0.0302 | 0.0641 | 0.01234 | 0 |
| 9 | 10 | 0.00258 | 0.0322 | 1.23 | 0 | 49 | 51 | 0.0486 | 0.137 | 0.0342 | 0 | 85 | 86 | 0.035 | 0.123 | 0.0276 | 0 |
| 4 | 11 | 0.0209 | 0.0688 | 0.01748 | 0 | 51 | 52 | 0.0203 | 0.0588 | 0.01396 | 0 | 86 | 87 | 0.02828 | 0.2074 | 0.0445 | 0 |
| 5 | 11 | 0.0203 | 0.0682 | 0.01738 | 0 | 52 | 53 | 0.0405 | 0.1635 | 0.04058 | 0 | 85 | 88 | 0.02 | 0.102 | 0.0276 | 0 |
| 11 | 12 | 0.00595 | 0.0196 | 0.00502 | 0 | 53 | 54 | 0.0263 | 0.122 | 0.031 | 0 | 85 | 89 | 0.0239 | 0.173 | 0.047 | 0 |
| 2 | 12 | 0.0187 | 0.0616 | 0.01572 | 0 | 49 | 54 | 0.073 | 0.289 | 0.0738 | 0 | 88 | 89 | 0.0139 | 0.0712 | 0.01934 | 0 |
| 3 | 12 | 0.0484 | 0.16 | 0.0406 | 0 | 49 | 54 | 0.0869 | 0.291 | 0.073 | 0 | 89 | 90 | 0.0518 | 0.188 | 0.0528 | 0 |
| 7 | 12 | 0.00862 | 0.034 | 0.00874 | 0 | 54 | 55 | 0.0169 | 0.0707 | 0.0202 | 0 | 89 | 90 | 0.0238 | 0.0997 | 0.106 | 0 |
| 11 | 13 | 0.02225 | 0.0731 | 0.01876 | 0 | 54 | 56 | 0.00275 | 0.00955 | 0.00732 | 0 | 90 | 91 | 0.0254 | 0.0836 | 0.0214 | 0 |
| 12 | 14 | 0.0215 | 0.0707 | 0.01816 | 0 | 55 | 56 | 0.00488 | 0.0151 | 0.00374 | 0 | 89 | 92 | 0.0099 | 0.0505 | 0.0548 | 0 |
| 13 | 15 | 0.0744 | 0.2444 | 0.06268 | 0 | 56 | 57 | 0.0343 | 0.0966 | 0.0242 | 0 | 89 | 92 | 0.0393 | 0.1581 | 0.0414 | 0 |
| 14 | 15 | 0.0595 | 0.195 | 0.0502 | 0 | 50 | 57 | 0.0474 | 0.134 | 0.0332 | 0 | 91 | 92 | 0.0387 | 0.1272 | 0.03268 | 0 |
| 12 | 16 | 0.0212 | 0.0834 | 0.0214 | 0 | 56 | 58 | 0.0343 | 0.0966 | 0.0242 | 0 | 92 | 93 | 0.0258 | 0.0848 | 0.0218 | 0 |
| 15 | 17 | 0.0132 | 0.0437 | 0.0444 | 0 | 51 | 58 | 0.0255 | 0.0719 | 0.01788 | 0 | 92 | 94 | 0.0481 | 0.158 | 0.0406 | 0 |
| 16 | 17 | 0.0454 | 0.1801 | 0.0466 | 0 | 54 | 59 | 0.0503 | 0.2293 | 0.0598 | 0 | 93 | 94 | 0.0223 | 0.0732 | 0.01876 | 0 |
| 17 | 18 | 0.0123 | 0.0505 | 0.01298 | 0 | 56 | 59 | 0.0825 | 0.251 | 0.0569 | 0 | 94 | 95 | 0.0132 | 0.0434 | 0.0111 | 0 |
| 18 | 19 | 0.01119 | 0.0493 | 0.01142 | 0 | 56 | 59 | 0.0803 | 0.239 | 0.0536 | 0 | 80 | 96 | 0.0356 | 0.182 | 0.0494 | 0 |
| 19 | 20 | 0.0252 | 0.117 | 0.0298 | 0 | 55 | 59 | 0.04739 | 0.2158 | 0.05646 | 0 | 82 | 96 | 0.0162 | 0.053 | 0.0544 | 0 |
| 15 | 19 | 0.012 | 0.0394 | 0.0101 | 0 | 59 | 60 | 0.0317 | 0.145 | 0.0376 | 0 | 94 | 96 | 0.0269 | 0.0869 | 0.023 | 0 |
| 20 | 21 | 0.0183 | 0.0849 | 0.0216 | 0 | 59 | 61 | 0.0328 | 0.15 | 0.0388 | 0 | 80 | 97 | 0.0183 | 0.0934 | 0.0254 | 0 |
| 21 | 22 | 0.0209 | 0.097 | 0.0246 | 0 | 60 | 61 | 0.00264 | 0.0135 | 0.01456 | 0 | 80 | 98 | 0.0238 | 0.108 | 0.0286 | 0 |
| 22 | 23 | 0.0342 | 0.159 | 0.0404 | 0 | 60 | 62 | 0.0123 | 0.0561 | 0.01468 | 0 | 80 | 99 | 0.0454 | 0.206 | 0.0546 | 0 |
| 23 | 24 | 0.0135 | 0.0492 | 0.0498 | 0 | 61 | 62 | 0.00824 | 0.0376 | 0.0098 | 0 | 92 | 100 | 0.0648 | 0.295 | 0.0472 | 0 |
| 23 | 25 | 0.0156 | 0.08 | 0.0864 | 0 | 63 | 59 | 0 | 0.0386 | 0 | 0.96 | 94 | 100 | 0.0178 | 0.058 | 0.0604 | 0 |
| 26 | 25 | 0 | 0.0382 | 0 | 0.96 | 63 | 64 | 0.00172 | 0.02 | 0.216 | 0 | 95 | 96 | 0.0171 | 0.0547 | 0.01474 | 0 |
| 25 | 27 | 0.0318 | 0.163 | 0.1764 | 0 | 64 | 61 | 0 | 0.0268 | 0 | 0.985 | 96 | 97 | 0.0173 | 0.0885 | 0.024 | 0 |
| 27 | 28 | 0.01913 | 0.0855 | 0.0216 | 0 | 38 | 65 | 0.00901 | 0.0986 | 1.046 | 0 | 98 | 100 | 0.0397 | 0.179 | 0.0476 | 0 |
| 28 | 29 | 0.0237 | 0.0943 | 0.0238 | 0 | 64 | 65 | 0.00269 | 0.0302 | 0.38 | 0 | 99 | 100 | 0.018 | 0.0813 | 0.0216 | 0 |
| 30 | 17 | 0 | 0.0388 | 0 | 0.96 | 49 | 66 | 0.018 | 0.0919 | 0.0248 | 0 | 100 | 101 | 0.0277 | 0.1262 | 0.0328 | 0 |
| 8 | 30 | 0.00431 | 0.0504 | 0.514 | 0 | 49 | 66 | 0.018 | 0.0919 | 0.0248 | 0 | 92 | 102 | 0.0123 | 0.0559 | 0.01464 | 0 |
| 26 | 30 | 0.00799 | 0.086 | 0.908 | 0 | 62 | 66 | 0.0482 | 0.218 | 0.0578 | 0 | 101 | 102 | 0.0246 | 0.112 | 0.0294 | 0 |
| 17 | 31 | 0.0474 | 0.1563 | 0.0399 | 0 | 62 | 67 | 0.0258 | 0.117 | 0.031 | 0 | 100 | 103 | 0.016 | 0.0525 | 0.0536 | 0 |
| 29 | 31 | 0.0108 | 0.0331 | 0.0083 | 0 | 65 | 66 | 0 | 0.037 | 0 | 0.935 | 100 | 104 | 0.0451 | 0.204 | 0.0541 | 0 |

| TRANSMISSION ELEMENTS | | | | | | | | | | | | | | | | | |
|---|---|---|---|---|---|---|---|---|---|---|---|---|---|---|---|---|---|
| From | To | R | X | B/2 | TAP | From | To | R | X | B/2 | TAP | From | To | R | X | B/2 | TAP |
| 23 | 32 | 0.0317 | 0.1153 | 0.1173 | 0 | 66 | 67 | 0.0224 | 0.1015 | 0.02682 | 0 | 103 | 104 | 0.0466 | 0.1584 | 0.0407 | 0 |
| 31 | 32 | 0.0298 | 0.0985 | 0.0251 | 0 | 65 | 68 | 0.00138 | 0.016 | 0.638 | 0 | 103 | 105 | 0.0535 | 0.1625 | 0.0408 | 0 |
| 27 | 32 | 0.0229 | 0.0755 | 0.01926 | 0 | 47 | 69 | 0.0844 | 0.2778 | 0.07092 | 0 | 100 | 106 | 0.0605 | 0.229 | 0.062 | 0 |
| 15 | 33 | 0.038 | 0.1244 | 0.03194 | 0 | 49 | 69 | 0.0985 | 0.324 | 0.0828 | 0 | 104 | 105 | 0.00994 | 0.0378 | 0.00986 | 0 |
| 19 | 34 | 0.0752 | 0.247 | 0.0632 | 0 | 68 | 69 | 0 | 0.037 | 0 | 0.935 | 105 | 106 | 0.014 | 0.0547 | 0.01434 | 0 |
| 35 | 36 | 0.00224 | 0.0102 | 0.00268 | 0 | 69 | 70 | 0.03 | 0.127 | 0.122 | 0 | 105 | 107 | 0.053 | 0.183 | 0.0472 | 0 |
| 35 | 37 | 0.011 | 0.0497 | 0.01318 | 0 | 24 | 70 | 0.00221 | 0.4115 | 0.10198 | 0 | 105 | 108 | 0.0261 | 0.0703 | 0.01844 | 0 |
| 33 | 37 | 0.0415 | 0.142 | 0.0366 | 0 | 70 | 71 | 0.00882 | 0.0355 | 0.00878 | 0 | 106 | 107 | 0.053 | 0.183 | 0.0472 | 0 |
| 34 | 36 | 0.00871 | 0.0268 | 0.00568 | 0 | 24 | 72 | 0.0488 | 0.196 | 0.0488 | 0 | 108 | 109 | 0.0105 | 0.0288 | 0.0076 | 0 |
| 34 | 37 | 0.00256 | 0.0094 | 0.00984 | 0 | 71 | 72 | 0.0446 | 0.18 | 0.04444 | 0 | 103 | 110 | 0.03906 | 0.1813 | 0.0461 | 0 |
| 38 | 37 | 0 | 0.0375 | 0 | 0.935 | 71 | 73 | 0.00866 | 0.0454 | 0.01178 | 0 | 109 | 110 | 0.0278 | 0.0762 | 0.0202 | 0 |
| 37 | 39 | 0.0321 | 0.106 | 0.027 | 0 | 70 | 74 | 0.0401 | 0.1323 | 0.03368 | 0 | 110 | 111 | 0.022 | 0.0755 | 0.02 | 0 |
| 37 | 40 | 0.0593 | 0.168 | 0.042 | 0 | 70 | 75 | 0.0428 | 0.141 | 0.036 | 0 | 110 | 112 | 0.0247 | 0.064 | 0.062 | 0 |
| 30 | 38 | 0.00464 | 0.054 | 0.422 | 0 | 69 | 75 | 0.0405 | 0.122 | 0.124 | 0 | 17 | 113 | 0.00913 | 0.0301 | 0.00768 | 0 |
| 39 | 40 | 0.0184 | 0.0605 | 0.01552 | 0 | 74 | 75 | 0.0123 | 0.0406 | 0.01034 | 0 | 32 | 113 | 0.0615 | 0.203 | 0.0518 | 0 |
| 40 | 41 | 0.0145 | 0.0487 | 0.01222 | 0 | 76 | 77 | 0.0444 | 0.148 | 0.0368 | 0 | 32 | 114 | 0.0135 | 0.0612 | 0.01628 | 0 |
| 40 | 42 | 0.0555 | 0.183 | 0.0466 | 0 | 69 | 77 | 0.0309 | 0.101 | 0.1038 | 0 | 27 | 115 | 0.0164 | 0.0741 | 0.01972 | 0 |
| 41 | 42 | 0.041 | 0.135 | 0.0344 | 0 | 75 | 77 | 0.0601 | 0.1999 | 0.04978 | 0 | 114 | 115 | 0.0023 | 0.0104 | 0.00276 | 0 |
| 43 | 44 | 0.0608 | 0.2454 | 0.06068 | 0 | 77 | 78 | 0.00376 | 0.0124 | 0.01264 | 0 | 68 | 116 | 0.00034 | 0.00405 | 0.164 | 0 |
| 34 | 43 | 0.0413 | 0.1681 | 0.04226 | 0 | 78 | 79 | 0.00546 | 0.0244 | 0.00648 | 0 | 12 | 117 | 0.0329 | 0.14 | 0.0358 | 0 |
| 44 | 45 | 0.0224 | 0.0901 | 0.0224 | 0 | 77 | 80 | 0.017 | 0.0485 | 0.0472 | 0 | 75 | 118 | 0.0145 | 0.0481 | 0.01198 | 0 |
| 45 | 46 | 0.04 | 0.1356 | 0.0332 | 0 | 77 | 80 | 0.0294 | 0.105 | 0.0228 | 0 | 76 | 118 | 0.0164 | 0.0544 | 0.01356 | 0 |

Table A.7: 32 Nodes, Belgian electric power system.

| NODES | | | | | | | | | | | | |
|---|---|---|---|---|---|---|---|---|---|---|---|---|
| Number | Name | Type | Voltage (pu) | Angle (grad) | Load | | Generation | | MVAR | | Shunts | |
| | | | | | MW | MVAR | MW | MVAR | Max | Min | G | B |
| 1 | N16 | 0 | 1.0 | 0.0 | 0 | 0 | 0 | 0 | – | – | 0 | 0 |
| 2 | N11 | 0 | 1.0 | 0.0 | 98 | 32 | 0 | 0 | – | – | 0 | 0 |
| 3 | N6 | 0 | 1.0 | 0.0 | 0 | 0 | 0 | 0 | – | – | 0 | 0 |
| 4 | N13 | 0 | 1.0 | 0.0 | 600 | 200 | 0 | 0 | – | – | 0 | 0 |
| 5 | N8 | 0 | 1.0 | 0.0 | 237 | 78 | 0 | 0 | – | – | 0 | 0 |
| 6 | N9 | 0 | 1.0 | 0.0 | 223 | 73 | 0 | 0 | – | – | 0 | 0 |
| 7 | N1 | 0 | 1.0 | 0.0 | 0 | 0 | 0 | 0 | – | – | 0 | 0 |
| 8 | M1 | 2 | 1.0 | 0.0 | 48 | 40 | 850 | 346 | – | – | 0 | 0 |
| 9 | M2 | 2 | 1.0 | 0.0 | 54 | 45 | 500 | 178 | – | – | 0 | 0 |
| 10 | N10 | 2 | 1.0 | 0.0 | 580 | 100 | 2800 | 498 | – | – | 0 | 0 |
| 11 | N14 | 0 | 1.0 | 0.0 | 300 | 75 | 0 | 0 | – | – | 0 | 0 |
| 12 | N5 | 0 | 1.0 | 0.0 | 0 | 0 | 0 | 0 | – | – | 0 | 0 |
| 13 | N4 | 0 | 1.0 | 0.0 | 0 | 0 | 0 | 0 | – | – | 0 | 0 |
| 14 | N7 | 0 | 1.0 | 0.0 | 0 | 0 | 0 | 0 | – | – | 0 | 0 |
| 15 | N3 | 0 | 1.0 | 0.0 | 0 | 0 | 0 | 0 | – | – | 0 | 0 |
| 16 | N2 | 0 | 1.0 | 0.0 | 0 | 0 | 0 | 0 | – | – | 0 | 0 |
| 17 | N104 | 0 | 1.0 | 0.0 | 0 | 0 | 0 | 0 | – | – | 0 | 75 |
| 18 | N203 | 0 | 1.0 | 0.0 | 300 | 167 | 0 | 0 | – | – | 0 | 45 |
| 19 | N106 | 0 | 1.0 | 0.0 | 0 | 0 | 0 | 0 | – | – | 0 | 0 |
| 20 | N206 | 0 | 1.0 | 0.0 | 300 | 167 | 0 | 0 | – | – | 0 | 45 |
| 21 | N102 | 0 | 1.0 | 0.0 | 0 | 0 | 0 | 0 | – | – | 0 | 75 |
| 22 | N202 | 0 | 1.0 | 0.0 | 300 | 167 | 0 | 0 | – | – | 0 | 45 |
| 23 | N105 | 2 | 1.0 | 0.0 | 0 | 0 | 175 | 30 | – | – | 0 | 75 |
| 24 | N205 | 0 | 1.0 | 0.0 | 300 | 167 | 0 | 0 | – | – | 0 | 45 |
| 25 | N101 | 2 | 1.0 | 0.0 | 0 | 0 | 175 | 30 | – | – | 0 | 75 |
| 26 | N201 | 0 | 1.0 | 0.0 | 300 | 167 | 0 | 0 | – | – | 0 | 45 |
| 27 | N107 | 0 | 1.0 | 0.0 | 0 | 0 | 0 | 0 | – | – | 0 | 75 |
| 28 | N207 | 0 | 1.0 | 0.0 | 300 | 167 | 0 | 0 | – | – | 0 | 45 |
| 29 | N103 | 2 | 1.0 | 0.0 | 0 | 0 | 150 | 20 | – | – | 0 | 0 |
| 30 | N204 | 0 | 1.0 | 0.0 | 300 | 167 | 0 | 0 | – | – | 0 | 45 |
| 31 | N12 | 0 | 1.0 | 0.0 | 319 | -100 | 0 | 0 | – | – | 0 | 0 |
| 32 | N15 | 3 | 1.0 | 0.0 | 0 | 0 | -64.8 | 38.8 | – | – | 0 | 0 |

| TRANSMISSION ELEMENTS | | | | | |
|---|---|---|---|---|---|
| From | To | R | X | B/2 | TAP |
| N11 | N10 | 0.00079 | 0.00838 | 0.09860 | 0.0000 |
| N6 | N8 | 0.00100 | 0.01000 | 0.12200 | 0.0000 |
| N6 | N9 | 0.00094 | 0.00995 | 0.12210 | 0.0000 |
| N6 | N4 | 0.00084 | 0.00708 | 0.08640 | 0.0000 |
| N6 | N7 | 0.00084 | 0.00708 | 0.08640 | 0.0000 |
| N13 | N10 | 0.00095 | 0.01004 | 0.11810 | 0.0000 |
| N8 | N10 | 0.00150 | 0.01600 | 0.20000 | 0.0000 |
| N9 | N10 | 0.00150 | 0.01600 | 0.20000 | 0.0000 |
| N1 | N4 | 0.00054 | 0.00464 | 0.05670 | 0.0000 |
| N1 | N4 | 0.00049 | 0.00522 | 0.06410 | 0.00000 |
| N1 | N4 | 0.00049 | 0.00522 | 0.06410 | 0.0000 |
| N1 | N2 | 0.00014 | 0.00145 | 0.01620 | 0.0000 |
| N10 | N14 | 0.00087 | 0.00969 | 0.11570 | 0.0000 |
| N4 | N3 | 0.00073 | 0.00772 | 0.09480 | 0.0000 |
| N5 | N4 | 0.00046 | 0.00490 | 0.05450 | 0.0000 |
| N5 | N4 | 0.00046 | 0.00490 | 0.05450 | 0.0000 |
| N102 | N103 | 0.00100 | 0.01140 | 0.00200 | 0.0000 |
| N102 | N101 | 0.01700 | 0.06320 | 0.01150 | 0.0000 |
| N106 | N103 | 0.00550 | 0.02500 | 0.00400 | 0.0000 |
| N106 | N105 | 0.00800 | 0.04300 | 0.00700 | 0.0000 |
| N104 | N105 | 0.00620 | 0.03000 | 0.00500 | 0.0000 |
| N104 | N103 | 0.00620 | 0.03000 | 0.00500 | 0.0000 |
| N15 | N14 | 0.00219 | 0.02309 | 0.14430 | 0.0000 |
| N11 | N12 | 0.00126 | 0.01331 | 0.13550 | 0.0000 |
| N3 | N16 | 0.00126 | 0.01331 | 0.13550 | 0.0000 |

# Bibliography


[Aalto 2008] Aalto H. "Transfer functions for natural gas pipelines systems," Proceedings of the 17th world congress, The International Federation of Automatic Control, Seoul, Korea, July 6-11, 2008.

[Abdolahi 2007] F. Abdolahi, A. Mesbah, R. B. Boozarjomehry and W. Y. Svrcek, "The effect of major parameters on simulations results of gas pipelines," Int. jorunal of Mechanical Soc., vol. 49, no. 8, pp. 989-1000, Aug. 2007.

[Acha 2004] E. Acha, C. R. Fuerte-Esquivel, H. Ambriz-Perez and C. Angeles-Camacho, *FACTS: Modeling and Simulation in Power Networks*, John Wiley & Sons, 2004.

[Ackermann 2005] T. Ackermann, Wind Power in Power Systems, John Wiley & Sons, Inc., 1st edition, 2005.

[An 2003] An. S., Li Q. and Gedra T., "Natural gas and electricity optimal power flow," Trans. and Dist. Conference and Exposition, 2003 IEEE PES, Vol. 1, Pages 138-143.

[Behbahani-Nejad 2008] Behbahani-Nejad M. and Bagheri A., "A MATLAB Simulink library for transient flow simulation of gas networks," World Academy od Science, Engineering and Technology 43, 2008.

[Beltran 2001] C. Beltran Arroyo, Generalized unit commitment by the radar multiplier method, Ph.D. Thesis, Universitat Politecnica de Catalunya, 2001.

[Ben-Tal 2009] Ben-Tal, A., El Ghaoui, L., Nemirovski, A. Robust Optimization, Princeton University Press, 2009.

[Bertsekas 1982] D. P. Bertsekas, *Contrained Optimization and Lagrange Multiplier Methods*, Computer Science and Applied Mathematics. Academic Press, USA, 1982.

[Breeze 2005] Breeze Paul, *Power Generation Technologies*, Newnes, Elsevier, 2005.

[Brooke 1998] A. Brooke, D. Kendrick, A. Meeraus and R. Raman, GAMS a user's guide, GAMS Development co., 1998.

[Brown 2004] T. Brown, W. Beyeler and D. Barton, "Assessing network interdependencies: the challenge of risk analysis for complex adaptive systems," International Journal of Critical networks, Vol. 1, No. 1, pp. 86-99, 2004.

[Burton 2005] T. Burton, D. Sharpe, N. Jenkins and E. Bossanyi, Wind Energy Handbook, John Wiley & Sons, 2005.

[Carroll 2003] Carroll John J., *Natural Gas Hydrates: A guide for Engineers*, Gulf Professional Publishing, Elsevier, 2003

[Castro 2012] L.M. Castro, C.R. Fuerte-Esquivel, and J.H. Tovar-Hernández, "Solution of power flow with automatic load-frequency control devices including wind farms," IEEE Trans. Power Syst., vol. 27, no. 4, pp. 2186-2195, Nov. 2012.

[Chaudry 2008] Chaudry M., Jenkins N. and Strbac G., "Multi-period combined gas and electricity network optimisation," Electric Power System Research 78 (2008), 1265-1279, ELSEVIER.

[Coelho 2007] Coelho P. M. and Pinho C., "Considerations about equations for steady-state flow in natural gas pipelines," J. of the Braz. Soc. of Mech. Sci. & Eng., Vol. XXIX, No. 3, 2007.

[Coulson 1999] Coulson J. M., Richardson J. F., Backhurst J. R. and Harker J. H., *Fluid Flow Heat Transfer and Mass Transfer*, Coulon & Richardson, Chemical Engineering, vol. 1, ELSEVIER, 1999.

[Coutler 1979] Coutler T. L. and Bardon M. F., "Revised equation improves flowing gas temperature prediction," Oil & Gas Journal, vol. 26, pp. 107-108, 1979.

[Drud 1995] A. Drud, CONOPT solver for GAMS, available at www.gams.com/solvers/conopt.pdf.

[Erdogan 2006] E. Erdogan and G. Iyengar, "Ambiguous chance constrained problems and robust optimization," Math. Progr., vol. 107, no. 1, pp. 37-61, June 2006.

[Freris 2008] L. Freris and D. Infield, Renewable Energy in Power Systems, John Wiley & Sons, Ltd., 2008.

[Geidl 2007] M.Geidl and G. Andersson, "Optimal power flow of multiple energy carriers," IEEE Trans. Power Syst., vol. 22, no. 1, pp. 145-155, Feb. 2007.

[Giebel 2002] G. Giebel, 'The state-of-the-art in short-term prediction of wind power – A literature overview,' Project ANEMOS, funded by the European Comission under the 5th (EC) RTD, Contract No. ENK5-CT-2002-00665, 2002.

[Goldfarb 1999] D. Goldfarb, R. Polyak, K, Sheinberg and I. Yuzefovich, "A modified barrier-augmented lagrangian method for constrained minimization," Computational Optimization and Applications 14, 55-74 (1999), Kluwer Academic Publishers, Netherlands.

[Greyvenstein 2002] G. P. Greyvenstein, "An implicit method for the analysis of transient flows in pipe networks," Int. Journal for Numerical Methods in Engineering, Vol. 53, 2002.

[Guoyu 1985] X. Guoyu, F. D. Galiana and S. Low, "Decoupled economic dispatch using the participation factors load flow," IEEE Tran. Power Apparatus and Syst., vol. PAS-104, no. 6, pp. 1377-1384, Jun. 1985.

[Hajimiragha 2007] A.H. Hajimiragha, C.A. Cañizares, M.W. Fowler, S. Moazeni, and A. Elkamel, "A Robust Optimization Approach for Planning the Transition to Plug-in Hybrid Electric Vehicles," IEEE Trans. Power Syst., vol. 26, no. 2, pp. 829-836, Feb. 2007.

[Hetzer 2008] J. Hetzer, D.C. Yu, and K. Bhattarai, "An economic dispatch model incorporating wind power," IEEE Trans. Energy Conv., vol. 23, no. 2, pp. 603-611, June 2008.

[Hickman 1999] J. Hickman, D. Hassel, R. Joumard, Z. Samaras, and S. Sorenson, "Methodology for Calculating Transport Emissions and Energy Consumption," Transport Research Laboratory, Project Report SE/491/98, 1999.

[Hiriart 1996] J. B. Hiriart-Urruty and C. Lemarechál. *Convex Analysis and minimization Algorithms*, Volume I and II. Springer-Verlag, Berlin, 1996.

[IEA 2012] International Energy Agency, Golden Rules for a Golden Age of Gas, Worl Energy Outlook: Special Report on Unconventional Gas, OECD/IEA, 2012

[Kaplan 2007] S. M. Kaplan, Rail Transportation of Coal for Power Plants: Reliability Issues, CRS Report for Congress, Specialists in Energy and Environmental Policy Resources, Science, and Industry Division; Order Code RL34186, September 2007.

[Kaplan 2010] S. M. Kaplan, Displacing Coal with Generation from Existing Natural Gas-Fired power Plants, CRS Report for Congress, Specialists in Energy and Environmental Policy Resources, Science, and Industry Division; Order Code R41027, January 2010.

[Kariniotakis 2006] G. N. Kariniotakis, I. Marti, T. S. Nielsen, G. Giebel, J. Tambke, I. Waldl, J. Usaola, R. Brownsword, G. Kallos, U. Focken, I. Sanchez, N. Hatziargyriou, A. M. Palomares and P. Frayssinet, "Advanced short-term forecasting of wind generations -Anemos," IEEE Trans. On Power Syst. – invited paper to Special Section on Power System Performance Issues Associates with Wind Energy, 2006.

[Kehlhofer 2009] R. Kehlhofer, B. Rukes, F. Hannemann and F. Stirnimann, Combined-Cycle Gas & Steam Turbine Power Plants, PennWell, 3rd edition, 2009.

[Kralik 2008] Kralik J., Stiegler P., Vostry S. and Zavorka J., "Modeling the dynamics of flow in gas pipelines," IEEE Trans. on Systems, Man. and cybernetics, Vol. SMC-14, No. 4, 1984.

[Kremens 2000] Z. B. Kremens & M. Labuzek, Load flow analysis incorporating frequency as state vector variable, 9th International Conference on Harmonics and Quality of Power, 2000.

[Kundur 1994] P. Kundur, *Power System Stability and Conrol*, EPRI Power System Engineering Series, Mc. Graw-Hill, Inc., 1994.

[Liptak 2009] B. Liptak, *Post-oil Energy Technology: the first solar-hydrogen demonstration plant*, CRC Press, 2009.

[Liu 2009] C. Liu, M. Shahidehpour, Y. Fu and Z. Li, "Security-Constrained unit commitment with natural gas transmission constraints," IEEE Trans. on Power Systems, Vol. 24, No. 3, pp. 1523-1536, August 2009.

[Liu 2011] Lui C., Shahidehpour M. and Wang J., "Coordinated scheduling of electricity and natural gas infrastrusctures with a transient model for natural gas flow,"AIP CHaos 21, 025102 (2011), doi: 10.1063/1.3600761

[Malcom 1994] S. A. Malcom and S. A. Zenios, "Robust optimization for power systems capacity expansion under uncertainty," J. Opl. Res. Soc., vol. 45, no. 9, pp. 1040-1049, Sept. 1994.

[Martinez-Mares 2011] Martinez-Mares A. and Fuerte-Esquivel C. R., "Integrated energy flow analysis in natural gas and electricity coupled system," North American Power Symposium, 2011.

[Martinez-Mares 2012A] A. Martinez-Mares, C. R. Fuerte-Esquivel, Lei Wu, and T. Ortmeyer, "Wind Energy Impact in Fossil Fuel management: A Multi-Energy OPF Approach," 2012 IEEE PES General Meeting, July 2012.

[Martinez-Mares 2012B] A. Martínez-Mares and C.R. Fuerte-Esquivel, "A unified gas and power flow analysis in natural gas and electricity coupled networks, " IEEE Trans. Power Syst., vol. 27, no. 4, pp. 2156-2166, Nov. 2012.

[Martinez-Mares 2013] A. Martinez-Mares and C. R. Fuerte-Esquivel, "A robust optimization approach for the interdependency analysis of integrated energy system considering uncertainty," IEEE Trans. On Power Syst., Vol. PP, May. 2013.

[Mohtashami 2009] S. Mohtashami and H. R. Mashhadi, "Power generation scheduling of thermal units considering gas pipelines constraints," World Academy of Science, Engineering and Technology 49, 2009.

[Mokhatab 2006] S. Mokhatab, W. A. Poe and J. G. Speight, *Handbook of Natural Gas Transmission and Processing*, Gulf Professional Publishing, ELSEVIER, 2006.

[Monteiro 2009] C. Monteiro, R. Bessa, V. Miranda, A. Botterud, J. Wang and G. Conzelmann, "Wind power forecasting: state-of-the-art 2009," Argonne National Laboratory, ANL/DIS-10-1, Decision and Information Sciences Division, November 2009.

[Moritz 2007] Moritz S., A mixed integer approach for the transient case of gas network optimization, Ph. D. Thesis, Technischen Universitat Darmstadt, 2007.

[Mulvey 1995] J. M. Mulvey, R. J. Vanderbei, and S. A. Zennios, "Robust optimization of large-scale systems," Operations Research, vol. 43, no. 2, pp. 264-281, March-April 1995.

[Munoz 2003] J. Munoz, N. Jimenez-Redondo, J. Perez-Ruiz, and J. Barquin, "Natural gas network modeling for power systems relia-

bility studies," in 2003 IEEE Bologna Power Tech Conference, vol. 4, 8 pages.

[Murillo 2000] C. E. Murillo-Sanchez, On the integration of unit commitment and optimal power flow, Ph.D. Thesis, Cornell University, 2000.

[Narayana 2004] N. Prasad Padhy, "A bibliographical survey," IEEE Transactions on Power Systems, Vol. 19, No. 2, May 2004.

[Network Rail 2008] Network Rail U.K., "Network Rail - consultation on traction electricity consumption rates methodology for freight operating companies," Consultation on Consumption Rates for FOCs, 2008.

[Oadrdan 2010] M. Qadrdan, M. Chaudry, J. Wu, N. Jenkins and J. Ekanayake, "Impact of a large penetration of wind generation on the GB gas network," Energy Policy, vol. 38, no. 10, pp. 5684-5695, Oct. 2010.

[Okamura 1975] M. Okamura, Y. O-ura, S. Hayashi, K. Uemura and F. Ishiguro, "A new power flow model and solution method - Including load and generator characteristics and effects of system control devices," IEEE Transactions on Power Apparatus and Systems, vol. PAS-94, No. 3, May/June 1975.

[Olajumoke 2010] Olajumoke O. C., Comparative study of pressure drop model equations for fluid flow in pipes, Master of Sciende Thesis, University of Oklahoma, 2010.

[Ortega 2000] J. M. Ortega and W. C. Rheinboldt, "Iterative solutions of nonlinear equation in several variables," SIAM, Philadelphia, 2000.

[Osiadacz 1990] Osiadacz A., "Different transient models - limitations, advantages and disadvantages," Warsaw University of Technology, Intitute of Heating and Ventilation, Poland, www.psig.org/papers/1990/9606.pdf

[Outcalt 2009] D. M. Outcalt, "Probabilistic load flow for high wind penetrated power systems based on a five point estimation method," Ph.D. dissertation, Dept. Elec. Eng. and Comp. Sc., University of Wisconsin-Milwaukee, 2009.

[Parisio 2012] A. Parisio, C. Del Vecchio, and A. Vaccaro, "A robust optimization approach to energy hub management," Int. J. of Elec. Power and Energy Syst., vol. 42, no. 1, pp. 98-104, Nov. 2012.

[Ping 1998] Y. Ping, "A fast load flow model for a dispatcher training simulator considering frequency deviation effects," ELSEVIER, Electric Power & Energy Systems, vol. 20, No. 3, pp. 177-182, 1998.

[Qadrdan 2010] M. Qadrdan, M. Chaudry, J. Wu, N. Jenkins and J. Ekanayake, "Impact of a large penetratios of wind generation on the GB gas network," Energy Policy, vol. 38, no. 10, pp. 5684-5695, Oct. 2010.

[Quelhas 2006] A. M. Quelhas Alves de Freitas, Economic efficiencies of the energy flows from the primary energy resource suppliers to the electric load centers, Ph. D Thesis, Iowa State university, 2006.

[Rajan 2009] C. A. Rajan, "Genetic algorithm based tabu search method for solving UC problem with cooling - banking constraints," Journal of Electrical Engineering, Vol. 60, No. 2, 2009, 69-78.

[Restrepo 2005] J. Restrepo and F. D. Galiana, "Unit commitment with primary frequency regulation contraints," IEEE Trans. on Power Sys. vol. 20, No. 4, pp. 1836-1842, (2005).

[Rinaldi 2001] S. M. Rinaldi, J.P. Peerenboom, and T.K. Kelly, "Identifying, understanding, and analyzing critical network interdependencies," IEEE Control Syst. Mag., vol. 21, no. 6, pp. 11-25, Dec. 2001.

[Sadanandan 1983] N. D. Sadanandan, M.E. Needham, D.W. Hilson, K.W. Morris, and M. Sendaula, "Impact assessment of wind generation on the operations of a power system, " IEEE Trans. Power App. and Syst., vol. PAS-102, no. 9, pp. 2905-2911, Sep. 1983.

[Schroeder 2000] Schroeder D. W., A tutorial on pipe flow equations, Stoner Associates, Ic., Carlisle, Pennsylvania, www.psig.org/papers/2000/0112.pdf, 2001.

[Shahidehpour 2005] M. Shahidehpour, Y. Fu, and T. Wiedman, "Impact of natural gas network on electric power systems," Proc. of the IEEE, vol. 93, no. 5, pp. 1042-1056, May 2005.

[Soares 2007] C. Soares, *Microturbines*, Academic Publishing, ELSEVIER, 2007.

[Soder 2011] L. Soder and L. Bertling, "Different time scales for studies of power system performance," North European Power Perspectives, NEPP Fact Sheets, September 2011.

[Sorensen 2007] P. Sorensen, N.A. Cutululis, A. Vigueras-Rodriguez, L.E. Jensen, J. Hjerrild, M. Donovan, and H. Madsen, "Power fluctuations from large wind farms," IEEE Trans. Power Syst., vol. 22, no. 3, pp. 958-965, Aug. 2007.

[Stagg 1968] Stagg and El-Abiad, "Computer Methods in Power System Analysis," McGraw-Hill, 1968.

[Sttot 1971] B. Sttot, "Effective starting process for Newton-Raphson load flows," Proceedings of IEEE, Vol. 118, No. 8, Aug. 1971, pp. 983-987.

[Stubbe 1995] M. Stubbe, M. Amorouayeche, M. Brown, R.Craven, J.L. Jardim, A. Johannensen, P. Kundur, R. Marconato, K. Maslo, F. McNamara, B. Meyer, J.V. Mitsche, Y. Nakanishi, W.W. Price, J.L. Sancha, K. Walve, D. Xia, and R. Yokoyama "Long Term Dynamics Phase II Final Report," CIGRE Task Force 38-02-08, Belgium, March 1995.

[Tao 1998] Tao W. Q. and Ti H. C., "Transient analysis of gas pipeline network,"Chemical Engineering Journal 69 (1998), 47-52, ELSEVIER.

[Thresher 2007] R. Thresher, M. Robinson, and P. Veers, "To capture de wind," IEEE Power and Energy Mag., vol. 5, no. 6, pp. 34-46, Nov.-Dec. 2007.

[Unsihuay 2007] [24] C. Unsihuay, J. W. Marangon Lima and A. C. Zambroni de Souza, "Modeling the integrated natural gas and electricity optimal power flow," in 2007 Proc. of IEEE PES General Meeting, pp. 24-28.

[Wang 2008] J. Wang, M. Shahidehpour, Z. Li, "Security-Constrained unit commitment with volatile wind power generation," IEEE Trans. on Power Systems, Vol. 23, No.3, pp.1319-1327, August 2008.

[WCI 2005] World Coal Institute, The coal resource - a comprehensive overview of coal, UK, May 2005.

[Wolf 2000] D. Wolf and Y. Smeers, "The gas transmission problem solved by an extension of the simplex algorithm", Management Science, vol. 46, no. 11, pp. 1454-1465, Nov. 2000.

[Wood 1984] A. J. Wood & B. Wollenberg, *Power Generation Operation & Control*, John Wiley & Sons, Inc. 1984.

[Zack 2006] J. W. Zack, "An analysis of the errors and uncertainty in wind power production forecasts," WINDPOWER 2006, AWTruewind, Pittsburgh, PA, 2006.

[Zammerilli 2010] A. M. Zammerilli, "Investment decisions for baseload power plants," National Energy Technology Laboratory, Final Report 402/012910, 2010.